17-AAG and sihsp90α combinational therapy as a novel anti-cancer approach

By

Adi B. Mehta

A thesis submitted to the University of Central Lancashire in partial fulfilment of the requirements for the degree of Doctor of Philosophy.

Month Year submitted: September 2012

Student Declaration

Concurrent registration for two or more academic awards

I declare that while registered as a candidate for the research degree, I have not been a registered candidate or enrolled student for another award of the University or other academic or professional institution

---

Material submitted for another award

I declare that no material contained in the thesis has been used in any other submission for an academic award and is solely my own work

---

Collaboration

Where a candidate's research programme is part of a collaborative project, the thesis must indicate in addition clearly the candidate's individual contribution and the extent of the collaboration. Please state below:
The extent of collaboration has been specified in the thesis.

Signature of Candidate 

Type of Award **Doctor of Philosophy (PhD)**

School **Pharmacy and Biomedical Sciences**

Abstract

Heat Shock Protein 90 (Hsp90) is a molecular chaperone which plays an active role in maintaining protein homeostasis. Hsp90 is known to be highly expressed in tumour cells where it regulates stability and function of several key oncogenic client proteins including Akt kinase, EGFR, CDK and PDGFR. These client proteins are mutated or overexpressed in tumours and are involved in tumour progression and metastasis due to their roles in signalling pathways, cell cycle and apoptosis.

Hsp90 has two isoforms, namely Hsp90α and Hsp90β and share 85% sequence homology. Hsp90β is the constitutive isoform, however, Hsp90α is highly induced in many cancers and is responsible for tumourigenesis. Previous studies from our laboratory established Hsp90α mRNA and protein to be highly expressed in glioma cell lines and tissues compared to normal tissue and cells. In a follow up study, Hsp90α was silenced using predesigned small interfering RNA (sihsp90α) with high target specificity and it showed a clinical impact on the chemosensitivity to Temozolomide (TMZ). Thus, Hsp90α could be a therapeutic target for the treatment of glioma.

This study utilized a Hsp90-inhibitor 17-AAG and *hsp90α*-specific siRNA (sihsp90α), either as single agent or in combination, to inhibit Hsp90 function in glioblastoma. Hsp90α mRNA and protein expression levels post treatment were evaluated using qRT-PCR and confocal microscopy. To determine if Hsp90α inhibition influenced Akt kinase activity, a Hsp90 client protein, Akt activity was examined in treated and control cells using a Akt Kinase activity kit. Novel results from the study revealed that Hsp90α was significantly down-regulated at both the mRNA and protein levels which were associated with reduced cell viability. Hsp90α inhibition resulted in loss of Akt kinase

activity which validated the role of Hsp90α in chaperoning tumour progression. The use of 17-AAG concomitant with si*hsp90α* did not demonstrate synergistic anti-tumour effects in glioblastoma *in vitro*.

Furthermore, the application of siRNA as an alternative to small-molecule inhibitors in the treatment of human disease has shown therapeutic potential. However, a major hurdle to its utility has been the difficulty in delivering these anionic macromolecules *in vivo*. In this study, the ability of Tat peptide to enhance siRNA-mediated knockdown of *hsp90α* and siRNA stability in serum was investigated. In glioblastoma, Tat-mediated sihsp90α transfection concomitant with 17-AAG exhibited significant downregulation of Hsp90α mRNA and protein levels with increased peptide concentrations. Hsp90α suppression was associated with reduced Akt kinase activity and cell viability. The sihsp90α/Tat complex significantly improved sihsp90α stability in human serum for up to 36 h post serum exposure.

Finally, the combination therapy induced *hsp90α* knockdown and reduced Akt kinase activity *in vivo*. Although these results are preliminary and requires further validation, the anti-cancer activity is promising. These results suggest that the combination treatment with sihsp90α and 17-AAG may have therapeutic potential in GBM.

The novel work of this thesis has been published in:

Mehta A, Shervington L, Munje C, & Shervington A (2011). A Novel Therapeutic Strategy for the Treatment of Glioma, Combining Chemical and Molecular Targeting of Hsp90α. *Cancers* **3**, 4228-4244.

Table of Contents

List of Figures

List of Tables

Acknowledgements

I would like to show my sincere gratitude to all the people in my life that have supported me throughout this research.

I would like to thank Dr Amal Shervington for her constant guidance and encouraging nature that increased my confidence. She has been a great inspiration and her critical thinking has contributed tremendously to this project. A big thank you to Dr Leroy Shervington for all the support and guidance I have received from him. For everything they have done for me, I am truly grateful. I would like to thank Dr Robert Lea and the School of Pharmacy for the research grants.

This would not have been possible if it was not for my family's love and support that was a huge motivation for me. Words cannot describe how grateful I am for all that my parents have done for me. Behram Mehta (Father) and Zarin Mehta (Mother) have been there for when I needed them, they have encouraged me to get through tough times and helped me realise the true meaning of life. I would like to thank all my brothers Neville, Rustom and Jehangir for their belief in me gave me strength. I have appreciated both their emotional and financial support throughout my entire life, for this I am greatly indebted and always will be.

I would like to take this opportunity to say special thanks to my research colleagues Dr Chinmay Munje, Dr Zarine Khan, Dr Chris Platt, Shraddha Aptekar, Seema Jaiswal, Harshada Patil, Robin Moll and Dr Glenda Melling for their help and making the lab a friendly and fun environment. Dr Julie Shorrocks and Dr Sarah Dennison have been very helpful during my research for which I show my deepest gratitude.

Last few years have been very tough trying to accommodate part-time work with PhD responsibilities. But, Paul Cuff, Tim Butler, James Butler, Paddy McElroy, Ben Copley and Phil Morton for being more than just friends and being there for me. Special thanks to Paul Cuff and Charlene Welsby for all their support and guidance.

I would also like to thank Professor Ulo Langel for giving me the opportunity to conduct *in vivo* work at the University of Tartu. Dr Kaido Kurrikoff who supervised the work in Tartu, showed tremendous commitment to my project and for all your time and effort, I thank you.

I have been actively involved in Ten-pin bowling at Lakeside Superbowl which is where I have worked part-time for the past 5 years. I have made good friends and to a certain extent bowling helped ease the pressure of being a full-time PhD student. With this in mind I thank everyone at the bowling alley for sharing the good and bad moments of life.

Abbreviations

17-AAG	17-allylamino-17-demethoxygeldanamycin
17-DMAG	17-dimethylaminoethylamino-17-demethoxygeldanamycin
ACDP	Advisory Committee on Dangerous Pathogens
Ago2,	Argonaute 2
AHA1	Activator of Hsp90 ATPase homologue 1
AIC	5-Aminoimidazole-4-carboxamide
AMV	Avian myeloblastosis virus
ATCC	American type culture collection
ATP	Adenosine-5-triphosphate
BBB	Blood brain barrier
BCNU	1,3-bis (2-Chloroethyl)-1-nitrosourea
Bp	Base pair
BSA	Bovine serum albumin
CDK4	Cyclin-dependant kinase 4
cDNA	Complementary DNA
CENUs	Chloroethylnitrosoureas
CNS	Central nervous system
CPP	Cell-penetrating peptide
CSF	Cerebrospinal fluid
CT	Chemotherapy
Ct	Cycle threshold
C-terminal	Carboxyl-terminal
DMEM	Dulbecco's modified Eagle's medium
DMSO	Dimethyl sulfoxide
DNA	Deoxyribonucleic acid
dsRNA	Double stranded RNA
ECACC	European collection of cell cultures
EDTA	Ethylenediaminetetraacetic acid
EGFR	Epithelial growth factor receptor

ELISA	Enzyme-linked immuno-absorbent assay
EMEM	Eagle's minimum essential medium
EMBL	European molecular biology laboratory
FACS	Fluorescence activated cell sorting
FBS	Foetal bovine serum
FITC	Fluorescein isothiocyanate
GA	Geldanamycin
GAGs	Glycosaminoglycan chains
GAPDH	Glyceraldehyde-3-phosphate dehydrogenase
GBM	Glioblastoma multiforme
HA2	Hemagglutinin-2
HCl	Hydrochloric acid
HIF-1α	Hypoxia inducible factor 1α
HIV	Human immunodeficiency virus
Hop	Hsp70/Hsp90 organising protein
HRP	Horseradish peroxidase
HSEs	Heat shock elements
HSF1	Heat shock factor 1
Hsp70	Heat shock protein 70 kDa
Hsp90	Heat shock protein 90 kDa
hTERT	Human telomerase reverse transcriptase
IC_{50}	50% inhibition concentration
LDH	Lactate dehydrogenase
LiCl	Lithium chloride
MAPK	Mitogen-activated protein kinase
MGMT	O^6-methlyguanine-DNA-methyltransferase
miRNA	Micro RNA
MMP2	Matrix metalloproteinase 2
MTIC	Methyltriazen-1-yl imidazole-4-carboxamide
mTOR	Mammalian target of rapamycin
MTS	3-(4,5-dimethylthiazol-2-yl)-5-(3-carboxymethoxyphenyl)-2-(4-sulfophenyl)-2H-tetrazolium

NAD	Nicotinamide adenine dinucleotide
NADH	Reduced form of NAD
NaOAc	Sodium acetate
NaOH	Sodium Hydroxide
NCBI	National centre for biotechnology information
NEAA	Non-essential amino acid
NPC	Nuclear pore complex
p53	protein 53
PAGE	polyacrylamide gel electrophoresis
PBS	Phosphate buffer saline
PCI	Photochemical internalisation
PCNA	Proliferating cell nuclear antigen
PCR	Polymerase chain reaction
PDGF	Platelet derived growth factor
PDGFR	Platelet derived growth factor receptor
PF6	PepFect 6 peptide
PI3K	Phosphatidly-inositol 3'-kinsae
PIP	PCNA interacting protein
PKB	Protein kinase B
PNA	Peptide nucleic acid
PTEN	Phosphatase and tensin homolog gene
RA	Radicicol
Rb	Retinoblastoma
RISC	RNA induced silencing complex
RNA	Ribonucleic acid
RNAi	RNA interference
RT	Radiotherapy
RVG	Rabies virus glycoprotein
SD	Standard deviation
SDS	Sodium dodecyl sulphate
sihsp90α	*hsp90α*-specific siRNA
siRNA	Small interfering RNA

si-FAM	*Silencer*® FAM™ fluorescently labelled negative control siRNA
SMPs	Streptavidin magnetic particles
TAE	Tris/Acetic acid/EDTA
TBE	Tris/Boric acid/EDTA
Tat	HIV-1 Tat_{48-60} peptide (Amino acid sequence 48-60)
TMB	Tetramethylbenzidine
TMZ	Temozolomide
VEGFR	Vascular endothelial growth factor receptor
WHO	World health organisation

CHAPTER 1

INTRODUCTION

1.1 Glioma

There are several distinct cancers that are currently recognised of which those affecting the central nervous system (CNS) are amongst the most uncommon. In the UK, approximately 4500 people are diagnosed with malignant brain tumours every year corresponding to around 2 out of a 100 cancers diagnosed (Cancer Research UK). Of all the benign and malignant brain and CNS tumours, gliomas are the most common and accounts for approximately 45-50% of all those diagnosed, and are most common in people aged 60 years or over (Figure 1.1.1). In 2008, a total of 9337 individuals were diagnosed with brain tumours in the UK, of which ~52% confer malignant and progressive forms of the disease, with 41.5% of men and women likely to survive for at least 1 year and a five-year survival rate of ~15% in both men and women (Cancer Research UK). The following year, brain tumours caused 3674 deaths in the UK which account for more than 2% of all cancer deaths (Cancer Research UK).

The different glioma grade classification currently available as established by the World Health Organisation (WHO) assigns gliomas a grade on a scale of I-IV to reflect the degree of malignancy with grade IV being most malignant (Table 1.1.1). The most common, metastatic and malignant histological type of brain tumour which accounts for 65% of all gliomas is glioblastoma multiforme (GBM) (Ohgaki & Kleihues, 2005). Although other gliomas with astrocytic, oligodendroglial origin account for 70% of all brain tumours. Malignant gliomas belong to the hypervascular neoplasms, mostly responsible for rapid growth and poor prognosis of the tumour (Harada *et al.*, 2003). GBM is more predominant in elderly patients where diagnosis at late stages of the

disease has been reported to be a major prognostic factor of poor survival (Ohgaki *et al.*, 2004).

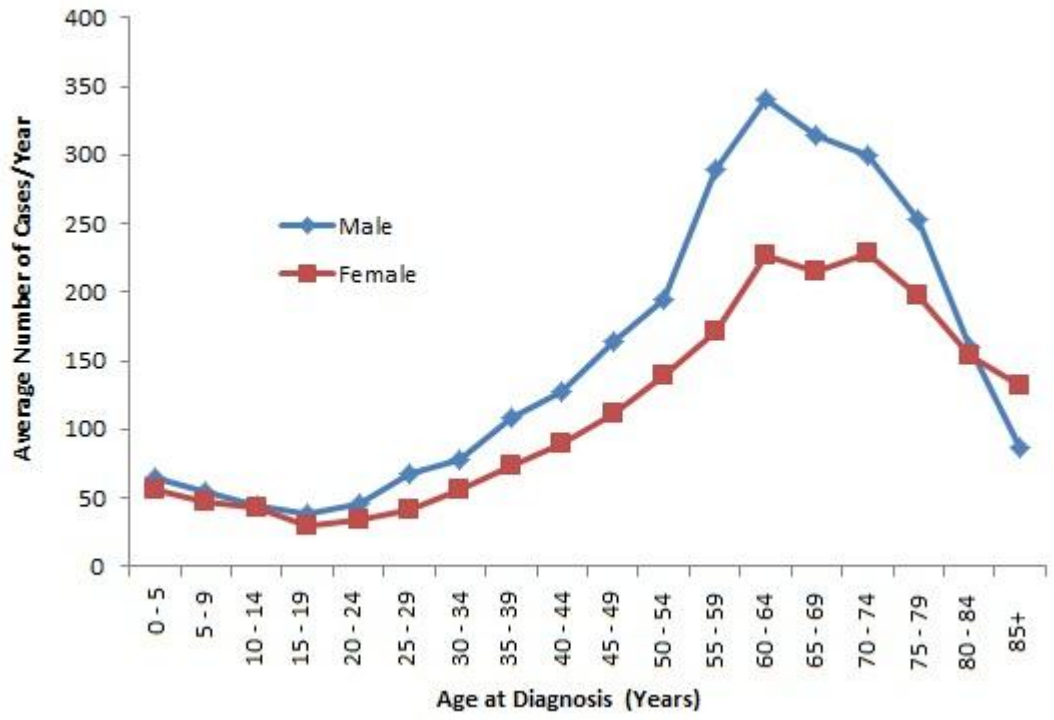

Figure 1.1.1: Latest malignant brain tumours incidence statistics (Cancer Research UK).

Table 1.1.1: WHO grading and survival rates of gliomas (Liu *et al.*, 2012).

WHO Grade	Glioma	Survival
I	Pilocytic astrocytoma	10 years +
II	Diffuse astrocytoma/ oligodendroglioma/ oligoastrocytoma	5-10 years
III	Anaplastic astrocytoma / oligodendroglioma/ oligoastrocytoma	2-5 years
IV	Glioblastoma multiforme (GBM)	9-12 months

1.2 Treatment for malignant gliomas

Despite recent technological advancement the treatment of malignant gliomas remains adamant. At present, the standard treatment for GBM involves surgical resection of the tumour followed by radiotherapy, and concomitant and adjuvant chemotherapy, which up till now has failed to improve the prognosis and quality of life in patients affected. Treatment options for recurrent GBM include chemotherapy, reirradiation, surgery, best supportive care with corticosteroids or gene therapy (Thumma *et al.*, 2012).

1.2.1 Surgical resection

Surgical resection is a vital aspect of the management of patients with GBM and the extent of resection is strongly associated with longer survival (Lanzetta & Minniti, 2010; Mueller & Chang, 2009). Upon initial diagnosis, maximal surgical resection is critical and has been correlated with survival (Gerstein *et al.*, 2010). However, this is compromised by the fact that gliomas are normally in close proximity to vital anatomical structures and often lack a defined tumour edge thus negating the possibility of surgical resection in patients with recurrent tumours. Although, studies suggest that surgery prolongs survival, the reported maximum survival advantage is less than 6 months in patients without residual tumour (Lanzetta & Minniti, 2010).

1.2.2 Radiotherapy

Radiation therapy has been the standard procedure of care for many years for patients with GBM. Radiotherapy (RT) (standard dose of 60 Gray (Gy); absorbed radiation dose) is given as a postoperative clinical course to ensure removal of any residual tumour that has remained after surgery with progression-free survival of 14.9 weeks (Lanzetta & Minniti, 2010; Siu *et al.*, 2012). However, radiation therapy is not without risk with radiation induced injuries occurring in a certain proportion of patients which further complicates the treatment course and can compromise care. Although, survival rate is significantly longer in patients subjected to radiotherapy than non-irradiated patients (10.6 months *vs* 1.9 months) (Lanzetta & Minniti, 2010), reirradiation produces only a modest benefit in patients with recurrent GBM (Thumma *et al.*, 2012).

1.2.3 Chemotherapy

Chemotherapy (CT) has been a part of the standard treatment against GBM since the 1970's. The most common systemically administered chemotherapeutic drugs include 1,3-bis (2-Chloroethyl)-1-nitrosourea (BCNU or carmustine), procarbazine, vincristine and lomustine, or temozolomide (Table 1.2.1). BCNU is one of the oldest drugs used to treat GBM. The BCNU wafer (Gliadel®), a synthetic biodegradable polymer, impregnated with carmustine is a clinically approved chemotherapeutic agent for the treatment of newly diagnosed and recurrent GBM (Cohen *et al.*, 2009). Although, BCNU is lipophilic in nature, substantial body toxicity has limited its treatment efficacy. BCNU wafer implants are associated with complications such as cerebrospinal fluid (CSF) leakage, hydrocephalus, seizures, cerebral edema, intracranial infection and cyst formation (Bock *et al.*, 2010).

Table 1.2.1: Summary of the commonly used chemotherapeutic agents for the treatment of brain tumours.

Class of agent	Commonly employed agents	Mechanism of action	Reference
Alkylating agents /Chloroethylnitroso-ureas (CENUs)	Temozolomide, Carboplatin, Procarbazine, Chlorambucil / BCNU (carmustine) CCNU (lomustine)	Addition of methyl group to DNA residues, DNA cross linking agents / DNA cross linking agents, alkylating and carbamoylating agents	(Liu *et al.*, 2012; Quiros *et al.*, 2011)
Antimicrotubule agents	Vincristine, Vinblastin	Blocks formation of microtubules resulting in cell cycle arrest in metaphase	(Mabeta & Pepper, 2009)
Topoisomerase I inhibitors	Irinotecan	Inhibit action of DNA repair enzyme topoisomerase I	(Jaeckle *et al.*, 2010)
Anti-angiogenic agents	Bevacizumab	Inhibit formation of new tumour blood vessels	(Lai *et al.*, 2011)
Platinum compounds	Cisplatin, carboplatin	DNA cross linkers	(Tallen *et al.*, 2008)

Temozolomide (TMZ) a second generation imidazotetrazine alkylating agent is the commonly used chemotherapeutic agent which mainly targets tumour recurrence following surgical removal of the tumour due to its ability to cross the blood brain barrier (Lanzetta & Minniti, 2010; Quiros *et al.*, 2011; Siu *et al.*, 2012). TMZ (Figure 1.2.1) was first synthesized in the early 1980s at Aston University and was effective against a broad range of tumours including gliomas (Friedman *et al.*, 2000). Characteristics that justified the use of TMZ for clinical evaluation in patients with cancer included wide drug distribution into the mouse brain, its lipophilic nature, complete (100%) bioavailability of the drug after dosing and no additional requirement

of enzymatic conversion into active anti-tumour component (Cohen *et al.*, 2009). In 2005, a study by Stupp *et al.* showed that TMZ supplemented with radiotherapy had significant survival benefit in patients with primary glioblastoma compared to patients treated with radiotherapy alone (Stupp *et al.*, 2005). TMZ (commercially known as Temodar®/Temodal®) coupled with radiation therapy showed modest improvement in the median survival from 12-15 months (Minniti *et al.*, 2009). These encouraging results led TMZ plus radiotherapy to be globally accepted as a standard therapy for glioblastoma multiforme. Clinical studies with TMZ revealed further details about its pharmacokinetics. The blood half-life of TMZ ranges between 1.6-1.8 h with peak plasma concentration attained within 0.33 and 2 h after drug administration (Wesolowski *et al.*, 2010).

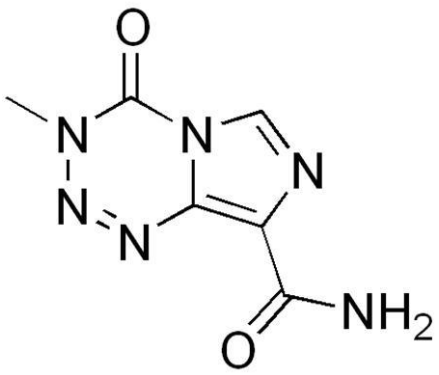

Figure 1.2.1: Molecular structure of TMZ (Fukushima et al., 2009).

1.2.3.1 TMZ: Mechanism of action

The cytotoxic effect of TMZ is exerted by methylation of the O^6 position of guanine which deters the next replication cycle due to the formation of G:T mispair eventually leading to cell death (Fukushima *et al.*, 2009). TMZ initiates G2/M cell cycle arrest in the glioma cells which leads to cell death by autophagy (Kanzawa *et al.*, 2004). TMZ undergoes non-catalytic conversion into methyltriazen-1-yl imidazole-4-carboxamide (MTIC) at a pH above 7.44 (physiological pH) (Friedman *et al.*, 2000). After drug ingestion the C^4 position of the tetrazinone ring of the TMZ undergoes hydrolysation whereby loss of carbon dioxide results in MTIC. MTIC rapidly degrades into 5-amino-imidazole-4-carboxamide (AIC), an inactive carboxylic acid derivative, and a highly reactive methyldiazonium ion at physiological conditions (Friedman *et al.*, 2000) (Figure 1.2.2). This highly reactive ion spontaneously transfers methyl group to the DNA nucleotide at the O^6 and N^7 positions of guanine, N^1 and N^3 or adenine and N^3 of cytosine to form a methylated-DNA adduct (Fukushima *et al.*, 2009).

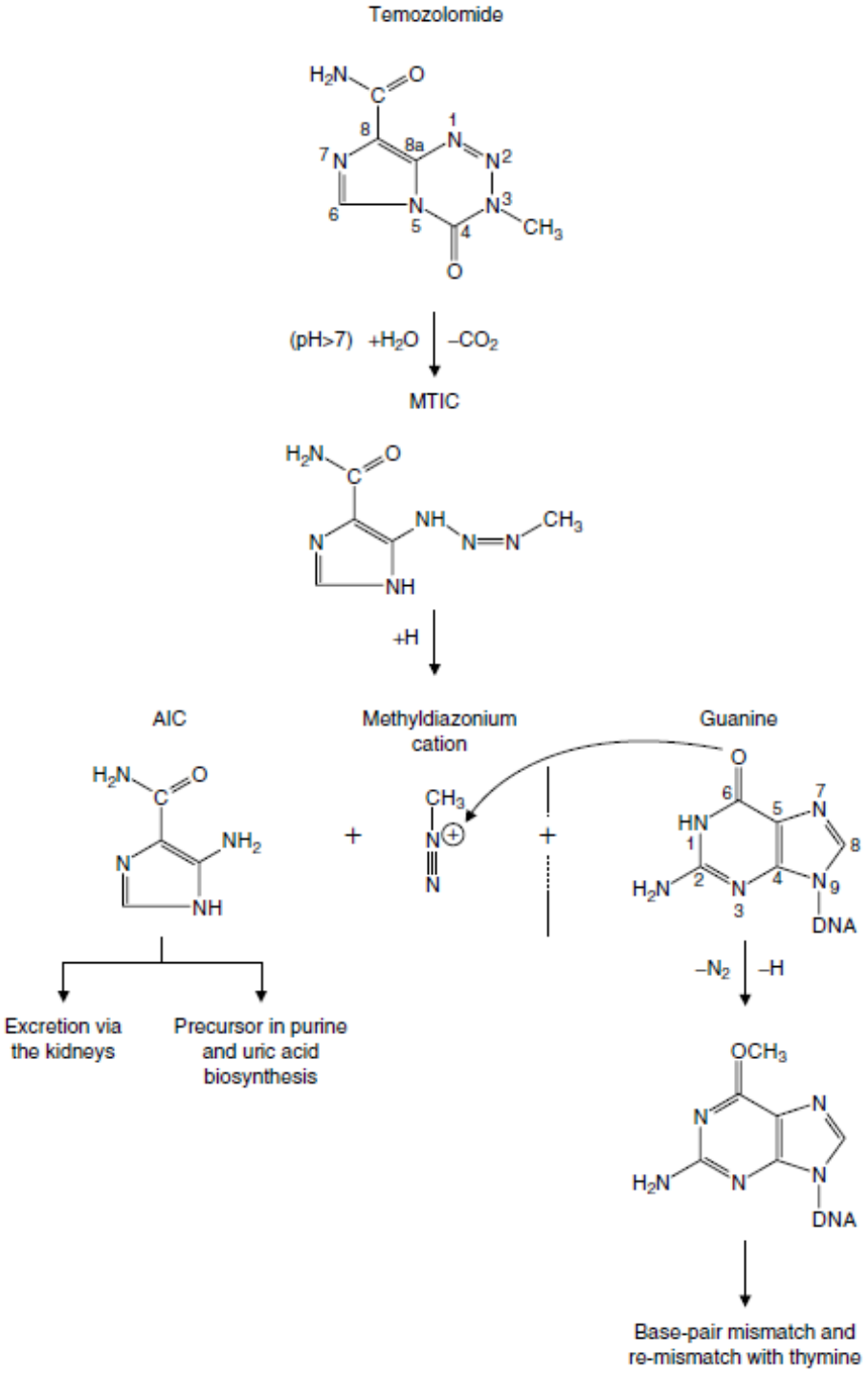

Figure 1.2.2: Mechanism of action of TMZ. The half-life of TMZ is approximately 1.8 h, but the half-life of the active component MTIC is slightly longer. Figure modified from (Friedman *et al.*, 2000).

1.2.3.2 Chemotherapy: its advantages and disadvantages

Cytotoxic chemotherapeutic drugs targets cancer cells over normal cells due to their enhanced proliferation rate. However, effects of chemotherapy are prevalent in normal cells due to the lack of site/cell specific treatment approaches. Taking this into account, chemotherapy is an effective treatment for lower grade gliomas resulting in high survival expectancy (Stupp & Baumert, 2003). There is a growing concern about increased chemo-resistance with higher grade gliomas including GBM and overcoming this hurdle has been the priority in order to improve treatment therapy against this fatal disease (Sarkaria *et al.*, 2008).

The efficacy of chemotherapy in patients is very low and only a handful of patients treated are cured of the disease (Quiros *et al.*, 2011). Moreover, treatment options are very limited for recurrent GBM with a median overall survival in patients of only 25 weeks (Minniti *et al.*, 2009). The expression of DNA repair enzyme O^6-methyl-guanine-DNA-methyltransferase (MGMT) in most glioblastomas has been attributed as the main reason for treatment resistance to TMZ (Esteller *et al.*, 2000). Side effects observed in patients treated with alkylating agents such as TMZ include thrombocytopenia, anaemia, fatigue and mild nausea, with rare occurrence of stomach ache and headache. Dose reduction is often required in patients illustrating hematologic complications due to the short blood half-life of TMZ which constrain the accumulation of drug at therapeutically effective concentrations in the tumour area, thus limiting the use of TMZ for chemotherapy (Ekeblad *et al.*, 2007; Sarin *et al.*, 2008).

Although it is hard to predict the cost effectiveness of the treatment of malignant gliomas, a few studies have assessed the total cost of the treatment therapy (Lamers *et al.*, 2008; Mabasa & Taylor, 2006). The estimated total cost of care for the treatment of

a patient with GBM is £36,000 per life-year gained mostly attributed to the high acquisition costs of TMZ (Linz, 2008). Despite its modest effects there is an urgent need to replace the present TMZ based standard post resection glioblastoma chemotherapy with other more stable and cost effective treatments.

Surprisingly, glioblastomas treated with concomitant chemotherapy and radiotherapy tend to accumulate considerable amounts of genetic mutations over a period of time which leads to tumour recurrence. For instance, loss of the *MSH6* gene (gene encoding mismatch repair protein) is the consequence of X-ray therapy and TMZ treatments which eventually leads to progressive tumour growth and recurrence (Cahill *et al.*, 2007). Furthermore, the expression level of O^6-methlyguanine-DNA-methyltransferase (MGMT) determines the effectiveness of TMZ since MGMT removes the methyl adducts from the O^6 position of the guanine and hence acts to reverse the cytotoxic effects induced by TMZ (Hegi *et al.*, 2005).

Although, TMZ combined with radiotherapy has been shown to improve survival times in patients with GBM, the 5-year survival for GBM remains dismal (Stupp *et al.*, 2009). The low therapeutic index of this combination treatment is attributed to the acquired drug resistance in glioblastoma (de Groot & Gilbert, 2007). Thus, identifying and understanding the processes responsible for the effectiveness of the TMZ plus radiotherapy may help improve treatment therapy for GBM. In recent years information has revealed a genetic and molecular basis of resistance, unregulated proliferation and anti-apoptotic mechanisms which remains the major obstacle to the successful treatment of brain tumours (Sarkaria *et al.*, 2008). This has led to the discovery of novel chemotherapeutic drugs that inhibit key molecular targets which have crucial roles in assisting signalling pathways responsible for malignancy (Mercer *et al.*, 2009; Ziegler *et al.*, 2008). In contrast, the effectiveness of anti-cancer drugs targeting individual protein

or signalling pathways have been low and in some cases completely lost, due to accumulation of mutations and variations in tumour cells considered as a major concern in cancer therapy (Wong *et al.,* 2007; Xiao *et al.*, 2006).

1.2.4 Present and Future perspectives: Gene therapy

GBM is characterised by several genetic and signalling abnormalities, including several growth factors such as epidermal growth factor receptor (EGFR), platelet-derived growth factor receptor (PDGFR) and vascular endothelial growth factor receptor (VEGFR), that ultimately lead to the irrepressible growth, angiogenesis, survival and differentiation (Minniti *et al.*, 2009). The molecular characterisation of GBM could contribute towards identification of optimal therapeutic targets, however, the major challenge in the use of targeted therapies is to select novel agents which have the potential to yield survival benefit in patients with GBM (Cloughesy & Mischel, 2011). Several phase I/II clinical trials have evaluated the treatment efficacy of inhibitors of growth factor receptor transduction pathway and angiogenesis (Cohen *et al.*, 2009; Jaeckle *et al.*, 2010; Lai *et al.*, 2011; Uhm *et al.*, 2011).

Gefitinib (Iressa, AstraZeneca) and erlotinib (Tarceva, Osi Pharmaceuticals), two main EGFR tyrosine kinases inhibitors, have been previously utilized as single agents in patients with recurrent GBM but the survival response observed was dismal (Prados *et al.*, 2008). EGFR is a 170-kDa receptor tyrosine kinase which activates several signalling pathways such as the phosphatidyl-inositol 3'-kinase (PI3K)/Akt and Ras/mitogen-activated protein kinase (MAPK), subsequent to phosphorylation which contributes towards several biological processes including cell proliferation, angiogenesis, survival and differentiation (Holsken *et al.*, 2011). No survival benefits of

combining erlotinib with RT and TMZ were observed compared to RT and TMZ alone and has been discontinued from clinical practice (Minniti *et al.*, 2009).

Imatinib (Gleevec, Novartis) is a PDGFR inhibitor which when used as a single agent has demonstrated limited activity in patients with recurrent GBM (Holdhoff *et al.*, 2010). PDGF signal through the alpha and beta receptor tyrosine kinase, whereby binding of ligand induces phosphorylation and subsequent activation of PI3K, MAPK and Akt signalling pathways. Modest survival benefits of imatinib have been accompanied with toxicity including neutropenia, thrombocytopenia and edema (Timotheadou, 2011). To enhance survival benefits in patients with GBM, regimens incorporating imatinib and TMZ have showed encouraging results with low side-effects.

Bevacizumab (Avastin, Genentech), a recombinant monoclonal antibody that selectively binds and blocks the VEGF, has previously shown significant survival benefits in patients with recurrent malignant glioma (Pope *et al.*, 2011). VEGF is a key factor responsible for angiogenetic processes which stimulate endothelial cell proliferation, extracellular matrix degradation and cell migration. Bevacizumab prevents VEGF from binding to its receptors on the surface of endothelial cells thereby reducing tumour vascularisation and subsequent reduction in tumour growth. A phase II trial of bevacizumab and irinotecan has shown encouraging response in patients with recurrent GBM (Kang *et al.*, 2008; Reardon *et al.*, 2012). A combination of bevacizumab with conventional RT and CT has shown promising anti-tumour effects with improved progression-free and overall survival, and moderate toxicity in patients with newly diagnosed GBM (Lai *et al.*, 2011; Narayana *et al.*, 2012; Vredenburgh *et al.*, 2011).

1.3 Heat Shock Protein 90 (Hsp90)

The molecular chaperone Hsp90 is highly abundant molecular chaperone (Workman *et al.*, 2007), and constitutes 1-2% of total cellular proteins under non-stressed conditions (Taipale *et al.*, 2010). While the amino acid sequence of a protein dictates its native conformation, most proteins fail to fold efficiently in the highly concentrated and complex environment of the cell without the help of heat shock molecular chaperone proteins (Bagatell & Whitesell, 2004) (Figure 1.3.1). Since its discovery in the 1960s, study of chaperone structure and function has been the active area of research due to its essential house-keeping functions including protein folding and translocation across membranes, and most importantly the post-translational regulation of cell signalling molecules (Whitesell & Lindquist, 2005). Hsp90 is unique since it is not required for the *de novo* synthesis of most polypeptides but it is required for folding of particular subset of proteins that have difficulty in reaching the active conformation. Alternatively, most but not all of its client proteins are conformationally labile signal transducers and have vital role in growth and survival processes (Whitesell & Lindquist, 2005).

Over the past decade, Hsp90 has emerged as an important biomolecule responsible for cancer cell survival under obnoxious conditions (Kang *et al.*, 2011). Although, Hsp90 is present in all cells, Hsp90 protein level is induced by heat shock, oxidative stress and nutritional deficiencies in many cancers including glioma but not in normal human brain tissue (Shervington *et al.*, 2006). This over-expression has been attributed to the hostile conditions and stressful environment prevalent in tumours (Price *et al.*, 2005; Shervington *et al.*, 2008).

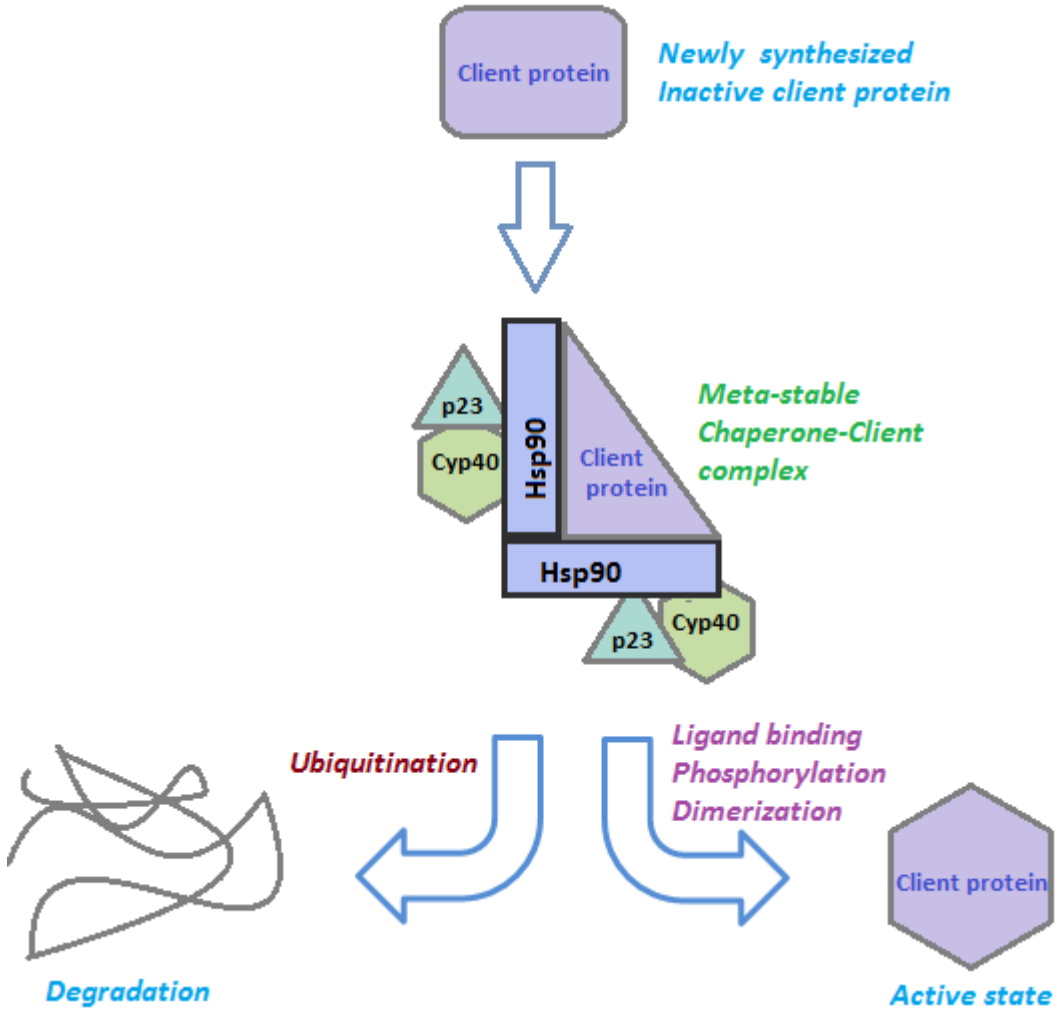

Figure 1.3.1: Hsp90 regulates the stability and activity of client proteins shown here to function as a vital component of a multi-protein complex. Hsp90 mediated conformational stabilisation functions as a multi-protein complex consisting of Hsp90, its co-chaperone proteins and accessory proteins that assist in client protein activation. The co-chaperone components of the Hsp90 complex are dependent on specific client proteins, most commonly include p23, Hsp70 and p60/Hop (Shervington *et al.*, 2006). In this case, p23 and immunophilin Cyp40 associate with the Hsp90 complex and maintains client proteins in a stable and non-aggregated form, which in the presence of specific signals such as ligand binding, phosphorylation permits activation of the client protein. Client proteins are degraded via the ubiquitin-proteasome pathway in the absence of appropriate stimulus. Figure modified from (Bagatell & Whitesell, 2004).

1.3.1 Glioma: Role of Hsp90

An increased expression of heat shock protein seen in cancer cells, in addition to the levels seen in normal cells, is common among solid tumours including gliomas (Whitesell & Lindquist, 2005). Molecular chaperones act as biochemical buffers for the molecular and genetic instability commonly observed in solid tumours. In addition, chaperones also permit tolerance to genetic alterations including mutations of fundamental signalling molecules which would otherwise be fatal (Bagatell & Whitesell, 2004). This exemplifies the vital role of Hsp90 in maintaining cellular homeostasis in the hostile environment imminent in gliomas. Moreover, gliomas have induced levels of Hsp90α (inducible isoform of Hsp90) protein as compared to its normal counterpart which has minimal or no presence of the chaperone protein (Shervington *et al.*, 2008). Furthermore, oncogenic client proteins of Hsp90 such as Akt kinase, C-RAF, MET oncogene, CDK4, hypoxia inducible factor 1α (HIF-1α), human telomerase reverse transcriptase (hTERT), PDGFR, EGFR and mutant p53 hugely contribute to the pathogenesis of glioblastomas (Powers & Workman, 2006) (Figure 1.3.2). The pharmacologic inhibition of Hsp90 in tumour cells has also been reported to cause client protein degradation via the ubiquitin-proteasome pathway (Holmes *et al.*, 2008). The ability to achieve multiple effects via a single drug target may potentially prove to be remarkably promising in the treatment of cancer. CDK4 is a serine/ threonine kinase that plays a pivotal role in cell cycle progression from G1 to S phase whose function is reliant on active Hsp90 and inhibition of Hsp90 causes destabilisation and degradation of CDK4 which further leads to cell cycle halt at G1 phase (Shervington *et al.*, 2006).

Recently, an overwhelming array of Hsp90 client proteins have been identified (Table 1.3.1). Hsp90 mainly involved in protein chaperoning of client proteins that actively

participate in glioma progression include CDK4, EGFR, FAK, Akt, hTERT, p53, PDGFR, MAPK, MMP2, PI3K, EF-2 kinase, and HIF-1α and appear to play vital roles in cell cycle regulation and signal transduction (Sauvageot *et al.*, 2009; Graner & Bigner, 2005).

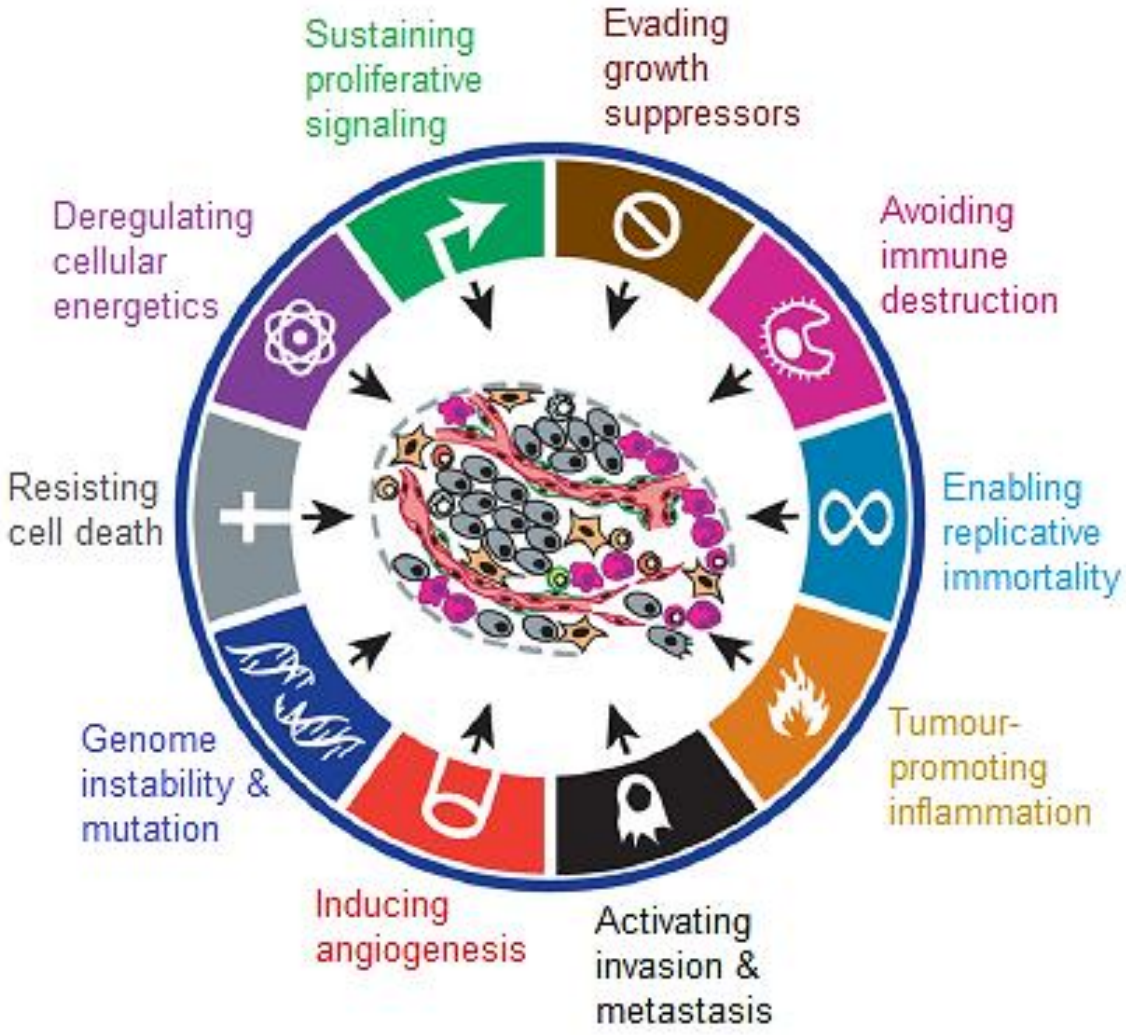

Figure 1.3.2: Hsp90 is essential for the stability and function of several oncogenic client proteins in glioblastoma. The roles of various client proteins in glioblastoma have been listed. Inhibition of Hsp90 could consequently interfere with the 10 hallmarks of cancer. Figure modified from (Hanahan & Weinberg, 2011).

Table 1.3.1 A list of Hsp90 client proteins (Zuehlke & Johnson, 2010).

Transcription factors	Eml4-Alk	Raf-1, B-Raf, Ste11
12(S)-HETE receptor	EphA2	RET
AF9/MLLT3	ErbB2	RET/PTC1
BCL-6	ERK5	Ron
CAR	FGFR3, -4	Ryk
Cytoplasmic v-erbA	FOP2-FGFR1	SGK-1
EcR	GRK2 and GRK6	Slt2
Nanog	GSK3β	SRPK1
PPARα (PPARβ)	HER3	SSCMK1
PXR	IκB kinases α, β, γ, ε	SSTK
Hap1	Insulin receptor	TAK1
HSF-1	IGFR1	TBK1
IRF3	Integrin-linked kinase	TGFβ receptors I and II
Mal63	IP6K2	TrkB
Oct4	IRAK-1	TrkAI and III
p53	Ire1α	Tyk2
AhR	JAK1	Ulk1
HIF-1α	JNK	VEGFR1, VEGFR2
HIF-2α	c-Kit	Wee1, Swe1
HIF-3α	KSR	ZAP-70
Sp1	LATS1, LATS2	**Others**
Stat3	Lkb1	α2C adrenergic receptor
Stat5	LRRK2	AID
TDP-43	MAPK6	Annexin II
TonEBP/OREBP	MEK	ANP receptor
Ure2	MEKK1 and MEKK3	Apaf-1
VDR	Mik1	ApoB
WT1	MLK3	Argonaute-1 (Ago1)
Kinases	MOK, MAK, MRK	Argonaute 2 , 4
Akt/PKB	c-Mos	ATG8 (GABARAP) proteins
ALK1, ALK5	mTOR	Axin 1
AMPKα, AMPKγ	NIK	Bcl-2
ASK1	p38	Bcl-xL
Aurora B	p90RSK	Beclin 1
Bcr-Abl	PDGFRα	Bid
BTK	PDK1	BLM helicase
c-Abl	PI4KIIβ	Bms1
Cdc2	Pim-1	BRCA1
Cdk2, -4, -6, -9, -11	Pink1	BRCA2
Chk1	PKCλ, PKCε and other PKCs	BRMS1
Tpl-2	Plk1	Cna2
DDR1	Pnck	Calmodulin
DAPK1, -2, -3	pp60v-src, c-src	Calponin
eEF-2 kinase	PRKD2	CARM1
EGF receptor	PRKDC	β-catenin
ElF2-α kinases HRI, Perk	PTK6	CB2 cannabinoid receptor

Continued from previous page

CD91	KSHV K1	R2TP complex through Pih1
Cdc13	Kir6.2	Rab-αGDI
Cdc25a and Cdc25c	LAMP-2A	Rab11a
Cdk5 activator p35	LAP	Rac/Rop GTPase Rac1 (rice)
Clostridium toxin CDT	LIS1	Rac1
CFTR	tRNA	Ral-binding protein 1
Chronophin	Synthetase complex	Rapsyn
ClC-2 chloride channel	Macrophage receptor	Raptor
Cineole synthase 1	Mdm2	Reovirus protein σ1
COG complex	MMP2, MMP9	REV1
CTA1	MRE11/Rad50/NBS1 (MRN)	Reverse transcriptase HBV
Ctf13/Skp1	Msps/XMAP215/ch-TOG	Ribosomal proteins S3 &S6
Cup	MTG8	Ribosomal protein L2
Cyclin B	MUC1	Ricin catalytic A chain
Cyclophilin D	NadA	RIG-I
Cyr1	Na+-K+-Cl- cotransporter 1	RNA-dep.
Actin, tubulin	RPM1 and RPS2	Rpb1
DEDD	Nod1, Nod2, NALP2, NALP3	R-protein I-2
Diphtheria toxin	NALP4, NALP12, IPAF	SENP3
Dengue virus protein E	NELF-E	SIR2
DNA polymerase α	Neuropeptide Y	SKP2 complexes
DNA polymerase η	NRDG1	SMYD1, SMYD2, SMYD3
DNMT1	Nox1, Nox2, Nox3, Nox5	snoRNP complexes
Dsn1	Nsl1	SREC-I
eNOS, nNOS	NS1	DNA helicase Ssl2
F1F0-ATP synthase	NSP3	SUR1
FLIPS and FLIPL	Nup62	Survivin
Gα0, Gα12	N-WASP	SV40 large T-antigen
Free βγ subunit of G protein	OGT	α-synuclein
Glutathione S-transferase	OsCERK1	Tab2/3
Guanylate cyclase, soluble	P1	Tau protein
HDAC6	P300	Telomerase
Hepatitis B core protein	P450 CYP2E1	Thiopurine S-methyltrans.
Hepatitis C protein NS3	P2X7 purinergic receptor	Thrombin receptor (PAR-1)
Hepatitis E capsid protein	PARK7 (DJ-1)	Thromboxane synthase
HERG	PB1/2 influenza RNA pol.	Tissue plasminogen activator
Histones 1,2A, 2B, 3 & 4	PCNA	Titin
Huntingtin	Perilipin	TLR4/MD-2 complex
c-IAP1	PIDD	TOM40
Importin β1	Piwi	TRIM8
IPO4	PIWIL2	Triosephosphate isomerase
Importin-α6 (KPNA5)	Mg-dependent phosphatidate	Trithorax
PIP3	Phosphohydrolase	Tyrosine hydroxylase
INrf2 (=Keap1)	Polysomal ribonuclease 1	UCH-L1
Clostridium toxin iota	PRMT5	URI complex
IRS-2	Prolactin receptor	Vaccinia core protein 4a
Encephalitis virus E protein	Prostacyclin synthase	Vimentin
JlpA	Proteasome	WASF3

Akt is a serine/threonine protein kinase (also known as protein kinase B, PKB) activated by growth factor stimuli such as insulin and PDGF (Miyata, 2005). Akt is present in the cell as an enzymatically active complex in association with Hsp90 (Figure 1.3.3). Hsp90 prevents Akt inactivation by evading its dephosphorylation by phosphatases. Association with functional Hsp90 is essential for Akt stability and binding of inhibitors to Hsp90 results in its destabilisation and is subsequently targeted for proteasomal degradation (Won *et al.*, 2009). Additionally, the ability of Hsp90 to bind to hTERT is crucial for assembly of telomerase complexes responsible for cancer cell immortalisation (Patel *et al.*, 2008). The anti-apoptotic signalling is regulated by the association of hTERT and Akt with Hsp90, and subsequent phosphorylation of both the client proteins (Shervington *et al.*, 2006).

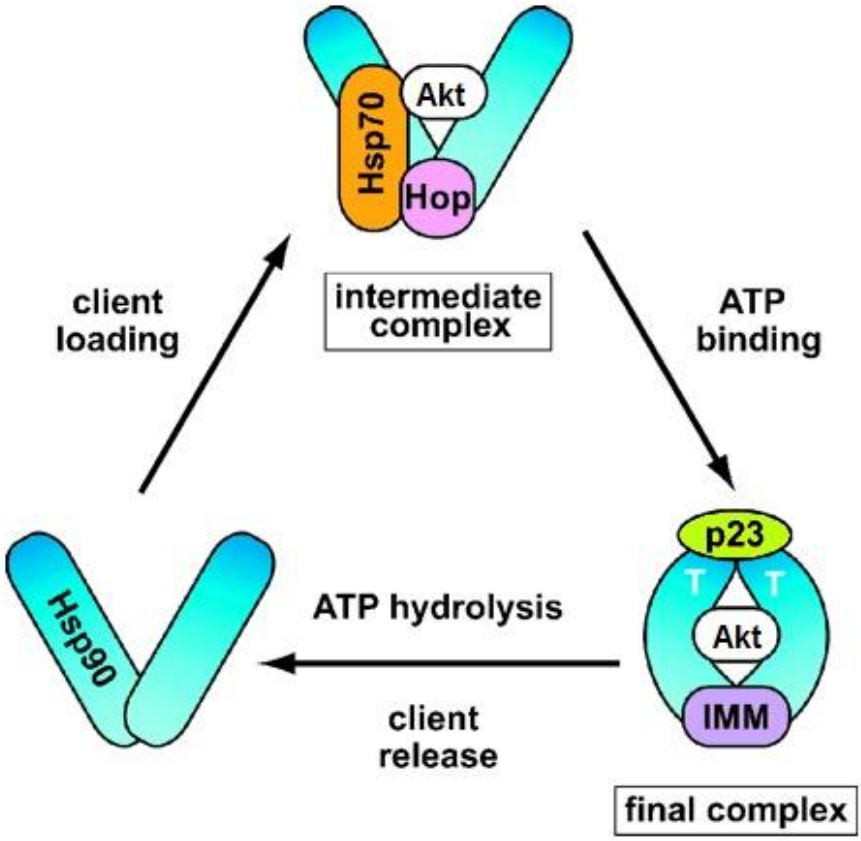

Figure 1.3.3: The role of Hsp90 in regulating cellular apoptosis by modulating the function and stability of Akt. The low-affinity interaction between the Hsp90, co-chaperones and the client protein, in this case Akt, maintains it in a latent but readily activated state. However, oncogenic mutations of client protein Akt result in higher requirements of Hsp90 function. Figure modified from (Terasawa *et al.*, 2005).

1.3.2 Structure and functions of Hsp90 protein

Hsp90 belongs to a family of molecular chaperones known to be highly conserved from prokaryotes to eukaryotes (Brown *et al.*, 2007). Hsp90 mainly resides in the cytoplasm and exists predominantly as a homodimer (Whitesell & Lindquist, 2005). It has three domains: N-terminal domain with ability to bind ATP, middle domain and C-terminal domain which facilitates the homo-dimerization of Hsp90 monomers (Xiao *et al.*, 2006) (Figure 1.3.4). The N-terminal ATP binding domain requires the binding and hydrolysis

of the ATP to execute and maintain the proper chaperoning of its client proteins. The conformational change in Hsp90 as a result of the phosphorylation at the N-terminal domain of Hsp90 further assists the conformational activation of its client proteins (Goetz *et al.*, 2003). In eukaryotes, a versatile, highly charged linker sequence connects the N-terminal domain to the middle domain (Brown *et al.*, 2007). The length and composition of this linker region is variable among the different organisms. Structural analysis of the N-terminal domain of Hsp90 shows the existence of an ATP-binding site. Moreover, biochemical studies of this domain also suggest that the intermolecular interaction between the two N-terminal domains of the Hsp90 homodimer occur in an ATP-dependent manner which gives Hsp90 characteristic ATP-driven chaperoning activity (Brown *et al.*, 2007). Inhibition of ATPase dependent Hsp90 activity using inhibitors such as radicicol and geldanamycin that binds to the N-terminal domain of Hsp90 was one of the important findings of the 20^{th} century in anticancer research (Roe *et al.*, 1999). For the past decade, Hsp90 has been considered as primary therapeutic target for the treatment of cancer.

The middle domain is proteolytically resistant and contains a catalytic loop that accepts the terminal phosphate of ATP bound to the N-terminal ATP binding pocket of Hsp90 (also called the γ-phosphate) (Brown *et al.*, 2007). Structural studies of Hsp90 indicate that the middle domain is involved in the interface of many client proteins including p53 and Akt (Fontana *et al.*, 2002; Muller *et al.*, 2004). Also, a recently discovered co-chaperone AHA1 (activator of Hsp90 ATPase homologue 1) interacts with Hsp90 and accelerates ATP hydrolysis by promoting association between the N-terminal and the middle domains (Meyer *et al.*, 2004). The middle domain and the C-terminal domain of the Hsp90 are associated via another versatile linker region that drastically facilitates the ATPase activity of Hsp90 (Whitesell & Lindquist, 2005). C-terminal truncations of

Hsp90 eliminate its ability to hydrolyze ATP, therefore signifying the importance of the dimeric nature of C-terminal domain for Hsp90 activity (Prodromou *et al.*, 2000). More importantly, the C-terminal domain contains the MEEVD motif (highly conserved pentapeptide) which is responsible for recruiting several co-chaperones containing the tetratricopeptide repeats, such as immunophilins and Hsp90 organizing protein (Hop), which corroborates the C-terminal domain as an essential subunit for Hsp90/co-chaperone complex formation (Scheufler *et al.*, 2000).

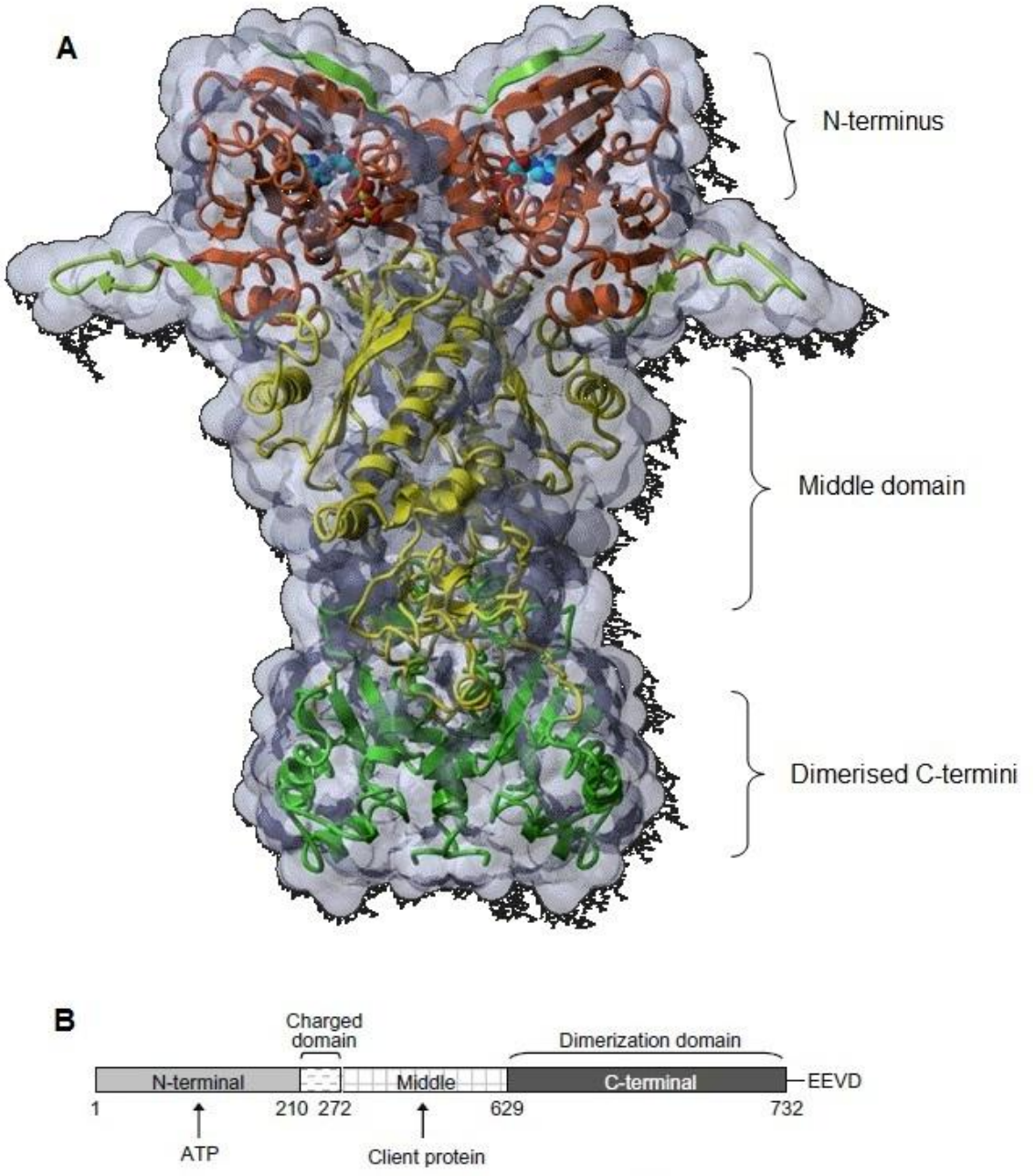

Figure 1.3.4: Structure of Hsp90 showing the different domains in the homodimer. A: The crystal structure of Hsp90 illustrates the N-terminus (red) that holds the ATP binding site essential for the binding and hydrolysis of ATP. Middle domain (yellow) has a critical role of interacting with many client proteins. The C-terminal domain (green) contains the MEEVD motif which recruits several co-chaperones essential for Hsp90 chaperone activity. B. Schematic structure of Hsp90. The numbers signify the position of amino acids. Figure modified from (Ali *et al.*, 2006; Fukuyo *et al.*, 2010).

The structural mechanism adapted by Hsp90 for its chaperone activity resembles a 'molecular clamp'. In the absence of ATP, the N-terminal domain of the Hsp90 homodimer binds its client proteins by maintaining an open-state (Figure 1.3.5) (Brown *et al.*, 2007). Once bound to ATP, Hsp90 homodimer undergoes conformational changes that permit transitory interaction between the N-terminal domains of the homodimer which ultimately leads to the formation of the closed-form of Hsp90 homodimer and clamping of the substrate protein. Ultimately, the client proteins are activated through this ATPase-driven cycle involving Hsp90/co-chaperone complex (Voellmy & Boellmann, 2007).

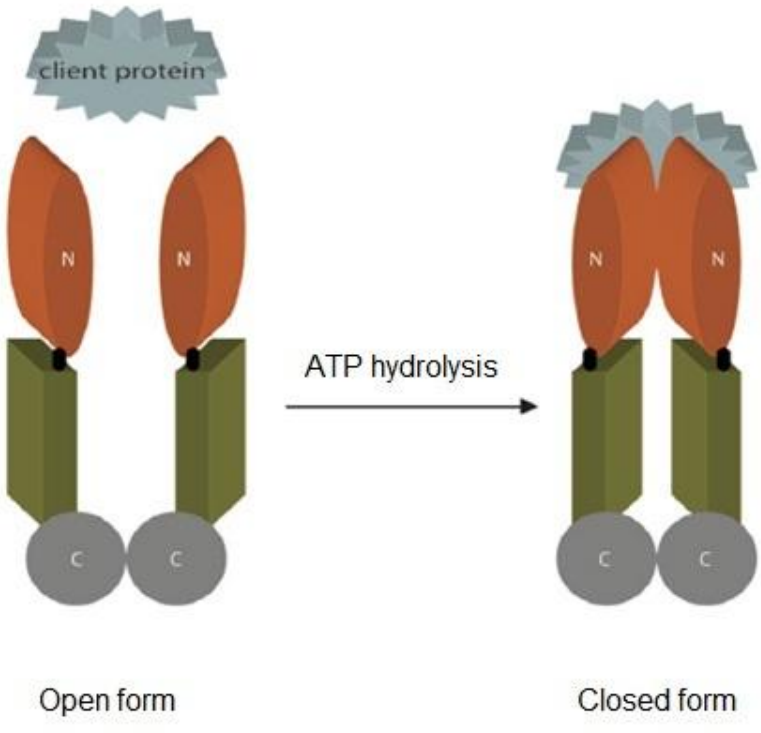

Figure 1.3.5: ATPase driven Hsp90 dependent activation of client protein. The Hsp90 homodimer maintains an open state which facilitates capture of client proteins. Once associated with ATP, Hsp90 homodimer undergoes conformational changes including transitory interaction between the two N-terminal domains with concomitant activation of the captured client protein. Figure modified from (Brown *et al.*, 2007).

Two cytoplasmic isoforms of Hsp90 exists in humans, namely Hsp90*α* (inducible expression) and Hsp90*β* (constitutively expressed), who share sequence homology of 85% (Shervington *et al.*, 2008). Hsp90 is mainly a homodimer, but monomers (*α* or β) and heterodimers can also exist (Sreedhar *et al.*, 2004). The α isoform readily forms dimers, whereas β isoform dimerizes with less efficiency. The C terminal of Hsp90 is mainly responsible for dimerization (Figure 1.3.4). Another distinctive isoform, Hsp90N is associated with cellular transformation. Hsp90N shares sequence homology with Hsp90α, but it lacks the N-terminal domain which is a mandatory requirement for the ATP-driven Hsp90 chaperoning (Grammatikakis *et al.*, 2002). Gene sequencing experiments identified *hsp90α* cDNA sequence in chromosome 14 and *hsp90β* cDNA sequence in chromosome 6 at the genomic locations at 14q32-33 and 6p21 for *hsp90α* and *hsp90β*, respectively, have been documented as functional (Sreedhar *et al.*, 2004).

1.3.3 Transcriptional regulation of *hsp90α*

The transcription of human *hsp90α* gene is regulated by the 5' upstream promoter sequences bearing the heat shock elements (HSEs) known to regulate gene expression of *hsp90α* (Sreedhar *et al.*, 2004). The heat shock factor 1 (HSF1) binds to the HSEs and marks the initiation of *hsp90α* gene transcription. Under normal conditions, HSF1 is bound to cytosolic Hsp90 and Hsp70 and hence avoids transcription of heat shock genes. However, under stress, or upon inhibition of Hsp90, the Hsp90 chaperone refolds partially denatured client proteins which liberates HSF1 consequently resulting in its translocation to the nucleus where it initiates transcription of *hsp90* gene (Kamal *et al.*, 2004). Hence, through a feedback mechanism, Hsp90 regulates its own gene expression whereby under normal conditions, HSF1 binds to Hsp90 and prompts gene transcription

to a halt (Westerheide & Morimoto, 2005). The exact mechanism responsible for the dissociation of Hsp90 from HSF1 under stress or in response to its inhibition of Hsp90 inhibitors is still unclear. However, under stressful conditions it may alter protein stability by increasing the concentration of partially folded proteins which compete for Hsp90, consequently increasing the concentration of the active HSF1 (Powers & Workman, 2007). Figure 1.3.6 illustrates the negative feedback mechanism between Hsp90/Hsp70 and HSF1 which regulates transcription of the *hsp90* genes.

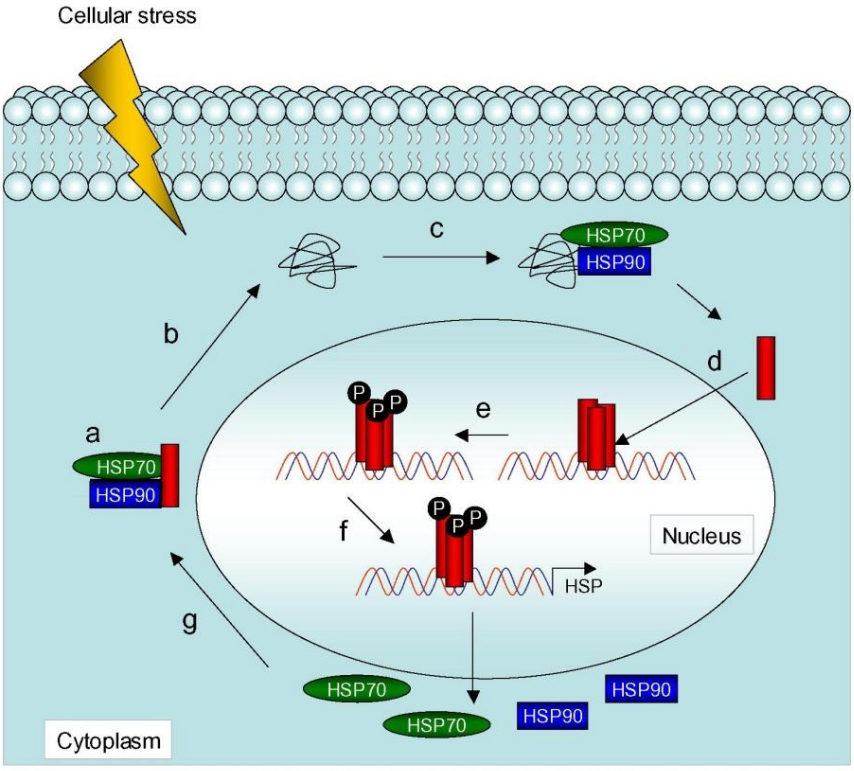

Figure 1.3.6: Transcriptional regulation of Hsp90. a) Under normal condition, HSF1 exists as a complex with Hsp90 and Hsp70. b) Under stress, Hsp90/Hsp70 dissociates from HSF1 to stabilise denatured proteins (c). d) Monomeric HSF1 now translocates to the nucleus where it can trimerize. e) HSF1 undergoes a series of post-translational phosphorylation events before it activates *hsp90* gene transcription (f). g) HSF1 is inactivated when cellular concentrations of Hsp90 and Hsp70 increases. Figure adapted from (Powers & Workman, 2007).

1.3.4 Rationale for targeting the Hsp90α protein

Hsp90 is involved in cell survival and signalling pathways that regulate cell proliferation. High levels of Hsp90 protein has been reported in several cancers including gliomas and has been correlated with tumour progression in glioma (Ohba *et al.*, 2010; Porter *et al.*, 2010). In addition, Hsp90 client proteins including PDGFR, EGFR and Akt play central role in survival and growth signalling pathways in glioma which validates targeting Hsp90 as an anti-cancer approach (Sauvageot *et al.*, 2009). The inducible isoform Hsp90α is highly expressed in brain tumours and is known to be involved in cell cycle progression, apoptosis, malignant invasiveness and metastasis (Gaspar *et al.*, 2009; Shervington *et al.*, 2008). Furthermore, not only does Hsp90 facilitate tumour cell survival in noxious tumour environments, but in its presence tumour cells tolerate genetic alterations to vital signalling molecules that would otherwise be fatal (Westerheide & Morimoto, 2005). Therefore, down regulation of Hsp90α mRNA and protein levels in glioblastoma may induce tumour cell death.

A recent study on glioma cell lines showed that *hsp90α* was elevated (27-fold increase) in 3/3 glioma cell lines and 8/8 glioma tissue specimens as compared to extremely low or absent in normal brain cell lines and tissue specimens analysed (Shervington *et al.*, 2008). The inducible isoform, Hsp90α has also been reported to be released into the extracellular matrix surrounding tumour cells where it assists in activation of MMP2, in addition to contributing to tumour metastasis (Eustace *et al.*, 2004). Due to the important role played by Hsp90α in tumour survival and progression as discussed above, and its induced protein levels in glioblastoma validates Hsp90α as an important therapeutic molecular target in glioblastoma, whose etiology is so multifaceted.

Various methods exist to silence/downregulate Hsp90 levels *in vitro*. Established approaches involve the use of Hsp90 inhibitors such as geldanamycin (GA), radicicol (RA) and 17-allylamino-17-demethoxygeldanamycin (17-AAG) that target the Hsp90 protein. These inhibitors bind to the N-terminal domain of Hsp90 and interfere with its heat shock chaperoning by eradicating its ability to hydrolyse ATP (Fukuyo *et al.*, 2010; Porter *et al.*, 2010). Another approach using small interfering RNA (siRNA) has emerged as an effective silencing tool for post-transcriptional down regulation of target gene since the discovery of RNA interference (RNAi) pathway in invertebrates (Fire *et al.*, 1998). RNAi mediated down regulation of *hsp90α* gene in glioblastoma *in vitro* using siRNA has been shown to induce chemosensitivity in glioblastoma (Cruickshanks *et al*., 2010).

1.4 Silencing Hsp90 protein

Benzoquinone ansamycins, represented by 17-AAG and GA (Figure 1.4.1), were the first class of Hsp90 inhibitors known to have potent anti-cancer effects *in vitro* and *in vivo* (Li *et al.*, 2009). These benzoquinone antibiotics bind to the N-terminal nucleotide binding pocket of Hsp90 thereby blocking the activation/maturation of client proteins (Figure 1.4.2), by inhibiting the crucial Hsp90 ATPase activity, primarily required during tumour growth (Graner & Bigner, 2005). In doing so, they induce ubiquitination and proteasomal degradation of aforementioned client proteins by the 26S proteasome (Taldone *et al.*, 2008). Radicicol is another macrocyclic antibiotic isolated from fungus *Monocillium nordinii* and *Monosporium bonorden* (Figure 1.4.1), and targets the ATP binding site on the N-terminal domain of Hsp90 illustrated in Figure 1.4.2 (Duerfeldt & Blagg, 2010). Hsp90 inhibitors like GA and RA have been used in pre-clinical settings and have shown potent tumour inhibitory ability; however, its anti-cancer potential has been condemned mainly due to hepatotoxicity in animal models and has thus led to the development of GA derivatives with similar anti-cancer function but with considerably low toxicity profile (Li *et al.*, 2009). This led to the discovery of 17-AAG which entered phase I clinical trials in 1999 and its intravenous formulations have shown encouraging results in more than 30 clinical trials with signs of therapeutic activity observed in melanoma, breast cancer, prostate cancer, and multiple myeloma (Gaspar *et al.*, 2010; Li *et al.*, 2009; Porter *et al.*, 2010). Presently, 17-AAG is in phase II/phase III clinical trials in adults with advanced solid tumour malignancies (Gaspar *et al.*, 2009; Siegel *et al.*, 2012). Several clinical trials evaluating the combination of 17-AAG with other

targeted agents have demonstrated anti-tumour activity in patients with solid tumours (Holzbeierlein *et al.*, 2010; Hubbard *et al.*, 2011; Iyer *et al.*, 2012).

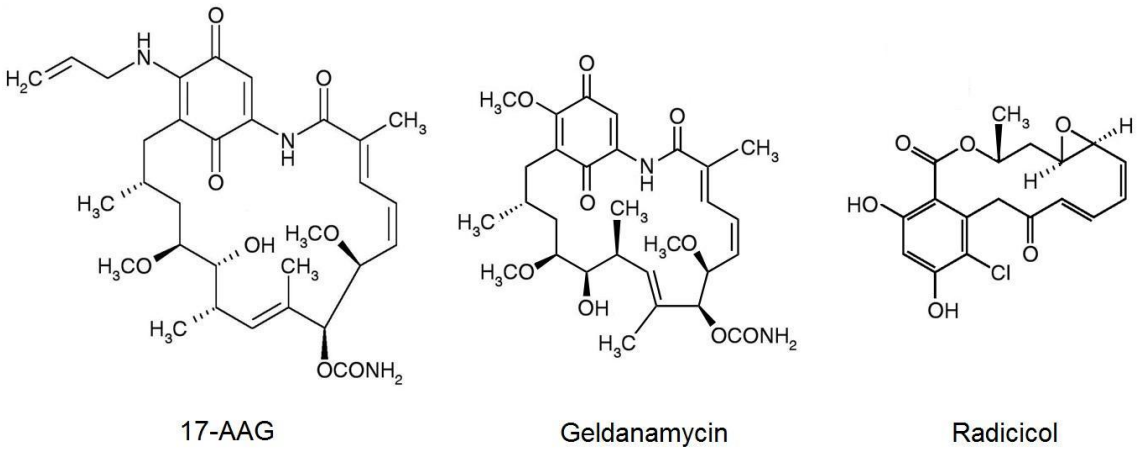

Figure 1.4.1: Chemical structures of Hsp90 inhibitors. Figure modified from (Fukuyo *et al.*, 2010).

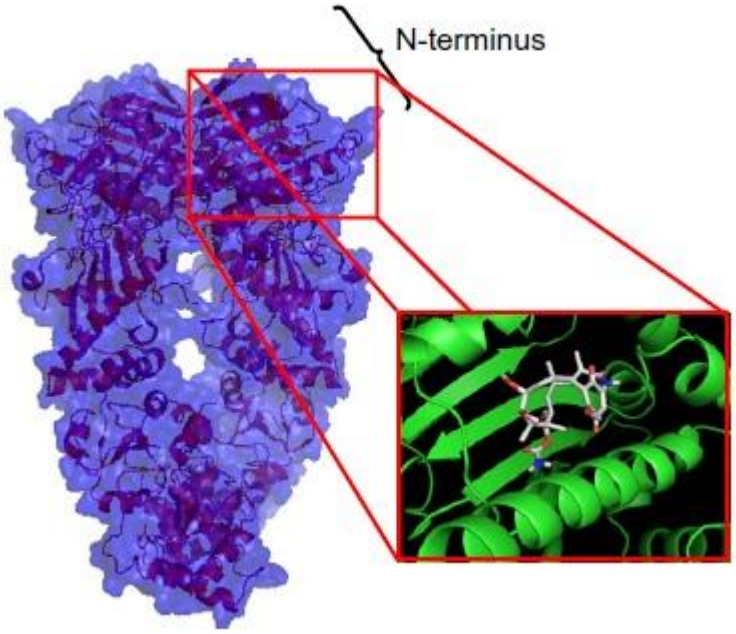

Figure 1.4.2: Crystal structure of Hsp90 with insert showing the bound GA on the N-terminal domain. Figure adapted from (Duerfeldt & Blagg, 2010).

A study in 2003 demonstrated that Hsp90 in cancer cells binds to 17-AAG with >100-fold higher binding affinity in comparison to Hsp90 in normal cells (Kamal *et al.*, 2003), which could suggest that the enhanced binding affinity may be due to the presence of Hsp90 in a multiprotein complex (active) state in tumour cells (Bagatell & Whitesell, 2004; Whitesell & Lindquist, 2005). Not only does 17-AAG have enhanced binding affinity for Hsp90 but only a small dose of it is required to inhibit tumour growth in glioma cell lines as compared to the dose required to inhibit growth in non-tumourigenic cells (Sauvageot *et al.*, 2009). Although, a high level of Hsp90 is present in most cells, 17-AAG selectively binds and kills tumour cells compared to normal cells (Kamal *et al.*, 2003). Under clinical settings, the ability of 17-AAG to target tumour cells over normal cells can be used to establish a therapeutic window of dosing where only the glioma cells are specifically targeted.

17-AAG is lipophilic in nature, which facilitates its passage through the blood brain barrier (BBB) (Sauvageot *et al.*, 2009). In addition, 17-AAG has an improved toxicity profile making it an ideal therapeutic candidate in GBM (Schulte & Neckers, 1998). The ability of 17-AAG to inhibit tumour growth when used in combination with another drug was recently realised when 17-AAG was administered with trastuzumab in patients with metastatic breast cancer and demonstrated promising anti-cancer activity with tolerable levels of toxicity (Modi *et al.*, 2007). Also, 17-AAG was experimentally shown to induce radiosensitization in glioma cell lines, however, 17-AAG failed to synergize with TMZ treatment (Ohba *et al.*, 2010; Sauvageot *et al.*, 2009).

Although 17-AAG has demonstrated promising anti-tumour activity *in vitro* and *in vivo*, several drawbacks including low water-solubility, instability in solution and low oral bioavailability limits its use in further clinical development (Porter *et al.*, 2010). In order to address this issue, Kosan Biosciences developed 17-dimethylaminoethyl-amino-17-demethoxygeldanamycin (17-DMAG) which retained Hsp90 inhibitory properties with improved water solubility and oral bioavailability profile compared with 17-AAG (Li *et al.*, 2009).

1.5 Silencing *hsp90α* using siRNA

RNA interference (RNAi) is an evolutionarily conserved genetic silencing mechanism used to achieve sequence-specific post-transcriptional downregulation of target genes (Lee & Kumar, 2009;Siomi, 2009). The process of RNAi was first reported by Fire and Mello in the invertebrate nematode *Caenorhabditis elegans* but soon after RNAi was encountered in plants and vertebrates (Fire *et al.*, 1998;Kim *et al.*, 2009). RNAi can be induced by endogenously encoded microRNAs (miRNAs) or exogenously administered small interfering RNAs (siRNAs) but in either case the 21-23 base pair long oligonucleotides associate with a protein complex called the RNA induced silencing complex (RISC) in the cytoplasm to drive the sequence-specific degradation of the target mRNA (Shan, 2010). Long precursor dsRNA is spliced into short siRNAs, a duplex with anti-sense strand (guide strand) and a sense strand (passenger strand), by an enzyme called Dicer (an RNA III-family endonuclease). Following the Dicer cleavage, mature siRNAs associate with Argonaute family of proteins, namely Argonaute 2 (Ago2), which functions as a core component of the RISC, to form the active RISC (Sashital & Doudna, 2010). In doing so, Ago2 retains the guide stand of the mature siRNA, crucial for the sequence-specific siRNA-mediated silencing of the complementary mRNA, while the passenger strand is removed (Figure 1.5.1). Finally, the guide strand binds to the target mature mRNA triggering mRNA degradation and subsequent inhibition of protein production (Sashital & Doudna, 2010).

Post-transcriptional gene silencing using siRNA results in rapid reduction in mature mRNA levels; however, stable proteins require a longer period of time for depletion. Further, the effects of siRNA are temporary and only lasts for up to 3-5 doubling times

which can be attributed to the gradual dilution of siRNA through cell duplication (Kim, 2003). siRNAs designed to specifically target *hsp90α* in glioma cannot only reduce mRNA levels but may have tumour inhibitory effects through down-regulation of Hsp90 protein level and consequently sensitise glioma cells to apoptosis (Chen *et al.*, 2009).

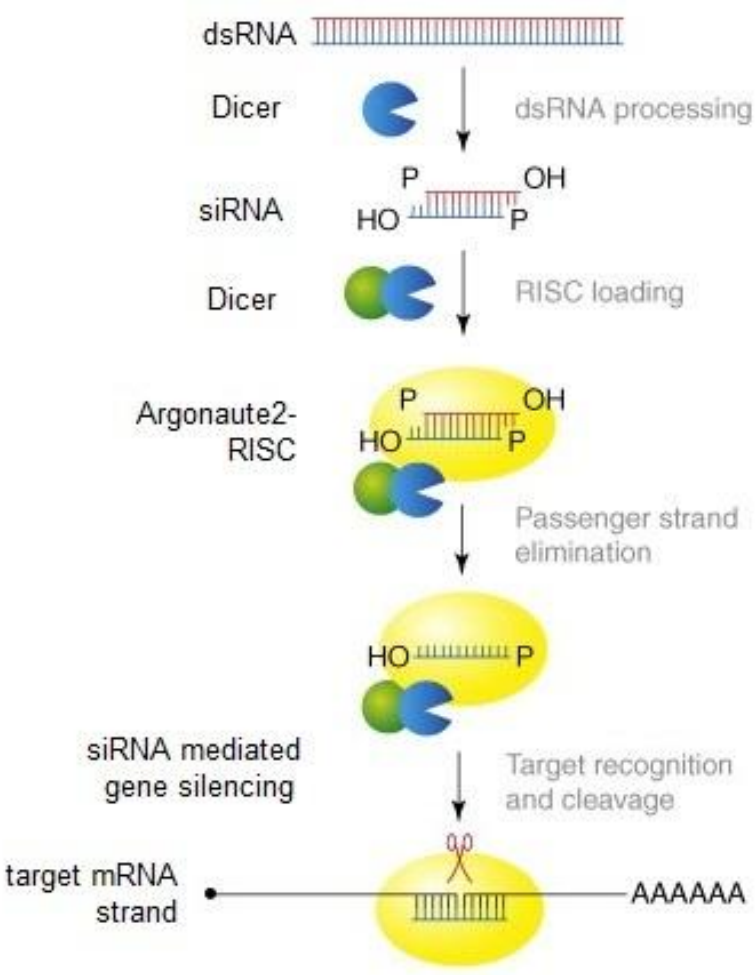

Figure 1.5.1: The schematic of RNA interference mechanism. The precursor dsRNA is cleaved into siRNA duplex by the Dicer enzyme which then forms the RISC in association with Ago2 protein. Being the effector of RISC, Ago2 retains the guide strand (anti-sense) and negates the passenger strand from the RISC complex. The active single-stranded siRNA formed as a result of this then targets the mRNA subsequently inhibiting protein synthesis. Figure modified from (Kim *et al.*, 2009).

A functional siRNAs which mediates gene silencing are 21 base pairs in length and are generated from longer dsRNA by the Dicer enzyme (Tran *et al.,* 2003). Previously, it was established that both Hsp90 mRNA and protein levels are induced in glioma cell line and tissue (Shervington *et al.,* 2008). Recent publication from our laboratory employed three sets of siRNAs, each sequence being target-specific at different regions on *hsp90α* gene (Cruickshanks *et al.,* 2010). Exon 5 of *hsp90α* is targeted by both siRNA 1 and 2 while siRNA 3 targets *hsp90α* exon 9. The results demonstrated that siRNA treatment of glioma cells significantly reduced *hsp90α* expression after 24 h and completely silenced its expression 48 h after sihsp90α transfection (Cruickshanks *et al.,* 2010). In contrast, normal cells showed no signs of sihsp90α mediated gene silencing.

An *in vitro* experiment on glioblastoma cell line (U87-MG) assessed the ability of sihsp90α targeting *hsp90α* to induce TMZ chemosensitivity when treated concomitantly. The study reported that the use of sihsp90α with TMZ considerably reduced the TMZ dose (by 13-fold) required to attain a comparable inhibitory effect on glioma cells as compared to when TMZ was used independently (Cruickshanks *et al.*, 2010). However, novel treatment regimens are now emerging fundamentally based on molecular targets and utilizing various advanced gene delivery systems.

1.6 Cell-penetrating peptides as delivery vehicles

The brain is the most delicate organ in the body and is protected by the blood brain barrier from potentially toxic molecules circulating in the blood which includes molecules of therapeutic activity (Patel *et al.*, 2009) (Figure 1.6.1). Despite recent advances in the treatment of neurological disorders, disorders related to the central nervous system including brain cancers by far outnumber the fatalities from all other types of systemic cancer or cardiovascular diseases. The poor prognosis in terminally ill patients with malignant glioma has been attributed largely to a lack of effective drug delivery systems (Patel *et al.*, 2009).

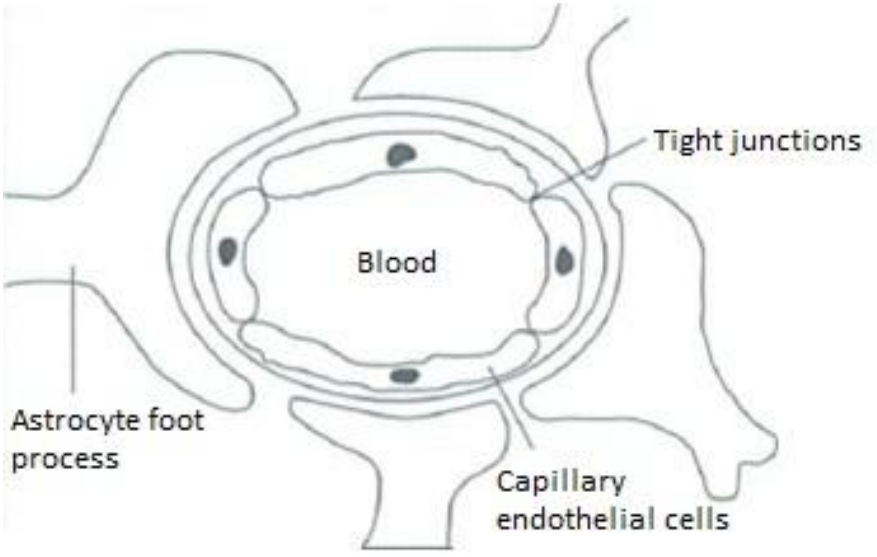

Figure 1.6.1: Blood brain barrier restrains entry of toxic substances (Patel *et al.*, 2009).

Malignant gliomas remain to be one of the most critical and life threatening cancers without a cure (Sathornsumetee *et al.*, 2007). Despite recent technological advances in surgical tumour resection, chemotherapy and radiation therapy, the disease progression is rapid after recurrence and prognosis is poor with a median survival of patients not more than 2 years (Sauvageot *et al.*, 2009). Therefore, it is important to develop more effective therapies for the treatment of malignant gliomas.

While the cellular origins of GBMs still remain firmly unidentified, there is increasing evidence that the malignant phenotype is driven by a subset of cells with stem-like qualities (Sauvageot *et al.*, 2009). The origin of these glioma stem cells is widely debated whereby it could arise from endogenous stem cells or from more differentiated glioma cells which have accrued multiple mutations that confer stem cell-like characteristics (Sauvageot *et al.*, 2007). At a molecular level, GBMs exhibit several mutational aberrations and signalling abnormalities which eventually results in uncontrolled proliferation, invasion and angiogenesis. Phosphatase and tensin homologue (PTEN) is a lipid phosphatase which restricts growth and survival signals mediated by the phophoinositide-3 kinase /Akt/mammalian target of rapamycin (mTOR) pathway. Loss of functional PTEN has been noted in approximately 30-40% of GBMs caused by mutational deletion within the PTEN on the chromosome 10 tumour suppressor gene (Wang *et al.*, 1997; Sansal & Sellers, 2004), which leads to uncontrolled growth due to constitutive Akt activation.

About 40% of GBMs exhibit amplified EGFR which results in induced proliferation, increased angiogenesis and inhibition of apoptosis. Additionally, 40% of GBMs express constitutively autophosphorylated variant of the EGFR known as EGFR variant III

known to increase proliferation and inhibit apoptosis in brain tumours by activating the Ras/Raf/MAPK and the PI3K-Akt signalling pathways (Sauvageot *et al.*, 2009). GBMs also show aberrations in the platelet-derived growth factor (PDGF) signal transduction pathway due to the coexpression of PDGF-A and -B ligands and PDGF-α and -β in most glioma cells and endothelial cells creating an autocrine loop which can initiate cell transformation processes. Also, PDGF receptor (PDGFR) expression is upregulated in endothelial cells of tumour vasculature, which is undetected in blood vessels in normal brain, may suggest that PDGF produced by glioma cells may induce angiogenesis by binding to neighbouring endothelial cells (Sauvageot *et al.*, 2009).

Hsp90 plays a vital role in regulating cellular processes such as protein folding and degradation, and signal transduction; through its association with a list of well-characterised client proteins, Hsp90 regulates their stability, phosphorylation states and function (Premkumar *et al.*, 2006; Karkoulis *et al.*, 2010). The client proteins that are overexpressed or mutated in GBM include EGFR, Raf, MEK, PDGFR, Cdk-4, -6 and -9, Akt and p53 (Pratt & Toft, 2003). With a diverse list of oncogenic clients, inhibiting Hsp90 could promote simultaneous shutdown of multiple signal transduction pathways involved in cell survival and proliferation, thus offering a better prognosis than single targeted agents.

The discovery of RNAi for knockdown of protein expression through gene silencing using siRNA has revolutionised the area of functional genomics (Moschos *et al.*, 2007a; Arthanari *et al.*, 2010). The elucidation of the function of several genes using RNAi has led to a widespread interest amongst academic groups and biotechnology companies to investigate the therapeutic potential of RNAi using siRNA in the treatment of cancer (Mahanthappa, 2005; Karagiannis & El-Osta, 2005; Pu *et al.*, 2006). Gene silencing using siRNA has been shown to significantly reduce Hsp90α mRNA levels in

glioblastoma (Cruickshanks *et al.*, 2010). Although, transfection is relatively straight forward *in vitro*, achieving high transfection *in vivo* is challenging since electroporation is not practical for use *in vivo* (Meng *et al.*, 2009).

1.6.1 Challenges faced in siRNA-mediated gene shutdown

Targeting Hsp90 *in vitro* is successful and straight forward (Sauvageot *et al.*, 2009), whereas gene silencing utilizing target-specific siRNA is rather difficult to achieve *in vivo* without using delivery vehicles (Arthanari *et al.*, 2010). Cancer siRNA therapy using neat siRNA in xenograft models is challenging due to low serum stability attributed to the rapid degradation of the dsRNA by the nucleases, non-specific immune stimulation and poor cellular uptake (Boado, 2005; Lundberg *et al.*, 2007; Schiffelers *et al.*, 2004). Thus, the major hurdle for glioma therapy is to improve drug/oligonucleotide delivery to the target site to achieve a more efficient and prolonged therapeutic effect. Under the circumstances, therapeutic approaches need to consider siRNA delivery in a manner that will not only ensure complete integrity of the cargo but will also permit sustained siRNA release for prolonged effects. The delivery of mature siRNAs benefits RNAi significantly since its action is mediated in the cytosol which thus eliminates the physiological barrier of the nuclear membrane (Grunweller *et al.*, 2003).

There have been numerous attempts to overcome the limited access of therapeutic molecules to the brain. siRNA is an anionic macromolecule whose cellular internalisation is rather difficult since it does not enter the cell by a passive diffusion mechanism (Shim & Kwon, 2010). An ideal siRNA delivery system would therefore enhance its cellular uptake, reduce enzymatic degradation and improve pharmacokinetics (i.e. longer half-life). Delivery of siRNA to various cell types has

been performed using cell-penetrating peptides (CPPs) which can stretch up to 30 amino acids long (Jarver & Langel, 2004).

1.6.2 Approaches to enhance oligonucleotide/drug delivery into the brain

1.6.2.1 Intracellular siRNA delivery using carrier peptides

Exploring peptides as cell delivery agents for oligonucleotides has received much of the impetus from the discovery of protein transduction domains, also known as CPPs, such as *Drosophila melanogaster* homeobox protein helix 3 peptide (Penetratin) (Coursindel *et al.,* 2012).Carrier peptides are short cationic peptides, with lengths of no more than 30 amino acids, that have been widely used for its enhanced intracellular cargo delivering ability (Meade & Dowdy, 2007) (Figure 1.6.2). The positive charge of the CPPs facilitates electrostatic bond formation with the negative charged phosphate backbone of the nucleic acids to form stable complexes which protect siRNA from degradation (Morris *et al.,* 2008). These peptides, together with the carrier siRNA, bind to the anionic cell membrane and prompt cellular internalisation through a endocytosis-mediated process (Meade & Dowdy, 2008). Carrier peptide mediated transport of siRNA into the cells can be via covalent or a non-covalent binding (Figure 1.6.3).

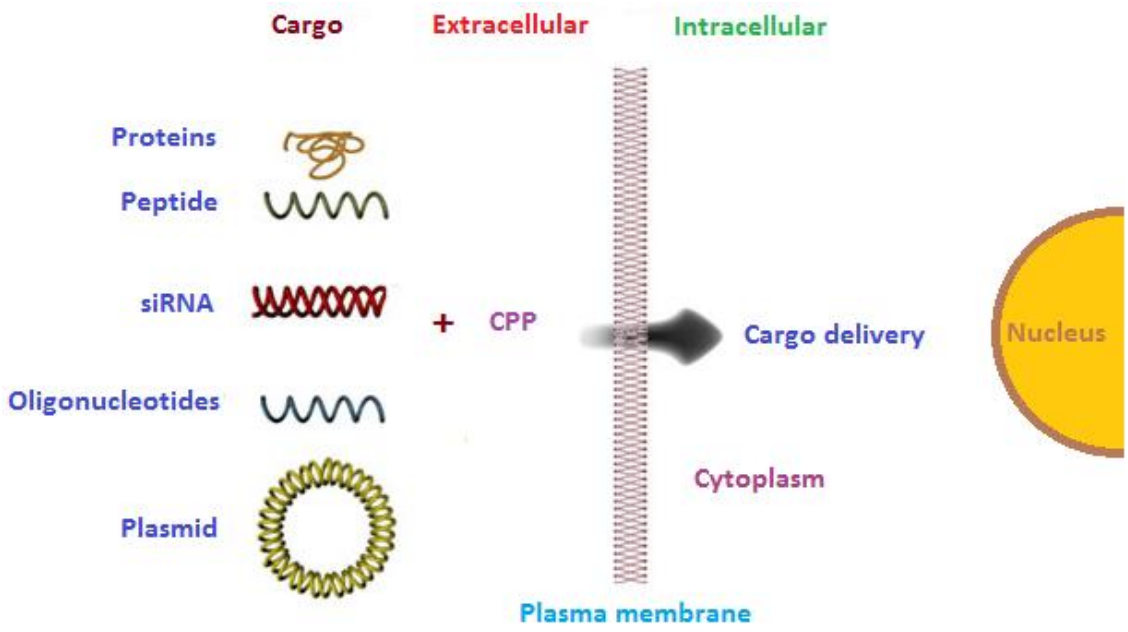

Figure 1.6.2: Cell penetrating peptides have been used for the delivery of various cargos. CPPs facilitate delivery of hydrophilic macromolecules across the plasma membrane but their internalisation mechanism is widely debated and is suggested to be influenced by the cell type and cargo. Figure modified from (Mae & Langel, 2006).

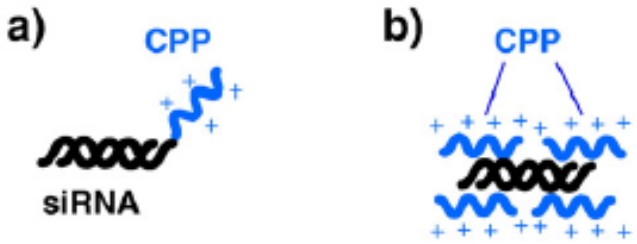

Figure 1.6.3: CPP-mediated siRNA delivery (Endoh & Ohtsuki, 2009). A) Covalent attachment of the CPP to siRNA. B) Non-covalent complex formed between CPP and siRNA by electrostatic interactions.

1.6.2.2 Cellular Internalisation of CPPs

The exact mechanism of cellular uptake of the CPPs remains elusive and is still extensively debated. Although it has been suggested that the uptake mechanism for different CPPs may vary influenced by the kind of CPP, cell type and size of the cargos (El-Andaloussi *et al.*, 2005). Previous studies suggested that the Tat_{48-60} CPP (derived from HIV-1 *trans*-activator protein) internalisation did not involve endocytosis as indicated by receptor-, energy- and temperature-independent uptake (Patel *et al.*, 2007). The studies designed a model of Tat peptide uptake, according to which the highly positively charged basic residues of the peptides have the ability to strongly adsorb to the negatively charged phospholipids of the cell membrane through electrostatic interactions which leads to local invagination of the cell membrane with subsequent formation of inverted micelles and, ultimately, release of the peptide inside the cell. Similar studies on live cells demonstrated that the uptake of Tat_{48-60} was inhibited at low temperatures which implicate endocytosis as a major mechanism for peptide uptake by the cells (Console *et al.*, 2003). Intriguingly, clathrin-dependent endocytosis, lipid raft/caveolin-dependent endocytosis and macropinocytosis have all been associated as key mechanisms of CPP/cargo uptake by the cells (Fittipaldi *et al.*, 2003; Wadia *et al.*, 2004; Wender *et al.*, 2000).

The intracellular fate of the transduced CPP and its cargo depend on the internalisation pathway followed. If the CPP is transduced into the cytoplasm, it could possibly interact with its cytoplasmic target or undergo proteasomal degradation, interact with nuclear target following importation to the nucleus (Patel *et al.*, 2007). Alternatively, if the CPPs are internalised by endocytosis and taking into account the type of endocytosis, it may enter the cytoplasm or the nucleus after escaping lysosomal entrapment, which results in degradation, or be carried to the Golgi apparatus or the endoplasmic

reticulum. Once again, the type of CPP and cargo, the cell type under investigation and the nature of linkage between the CPP and cargo governs which transduction pathway will be followed.

1.6.2.3 Membrane Interaction

The interaction between the CPP and the surface of the cell has been firmly established as the first step in cellular internalisation initiation, whether it is through endocytosis or transduction (Patel *et al.*, 2007). It is believed that the cellular uptake of cationic peptides does not involve cognate receptors. Furthermore, the role of negatively charged cell surface proteoglycans in the electrostatic membrane interaction of peptides has been emphasised by several studies (Tyagi *et al.*, 2001; Rusnati *et al.*, 1999; Rusnati *et al.*, 1998). Proteoglycans are glycoproteins which consist of one or more glycosaminoglycan chains (GAGs) linked to the core protein covalently. The GAGs are long linear polysaccharides that bear a negative charge at physiological pH mainly attributed to the presence of polysulphates such as chondroitin sulphate, dermatan sulphate and heparan sulphate (Richard *et al.*, 2005). The ubiquitously expressed heparan sulphate proteoglycans have been associated with translocation of full length Tat protein with high binding affinity as compared to the truncated Tat peptide which interacts with lower affinity (Goncalves *et al.*, 2005; Sandgren *et al.*, 2002; Ziegler & Seelig, 2004).

It is clear that cationic macromolecules such as peptides possess huge potential as delivery vehicles by virtue of electrostatic interaction which facilitates internalisation through adsorptive endocytosis. Moreover, the proteoglycans internalised by endocytosis are subjected to subsequent lysosomal degradation as a resource of their

turnover (Patel *et al.*, 2007). Thus, the cargo molecules electrostatically bound to the proteoglycans are likely to be endocytosed and degraded if they do not dissociate before vesicle fusion.

1.6.2.4 Endocytotic pathways: Macropinocytosis

Endocytosis can be defined as the energy-dependent uptake of macromolecules and is characterised by vesicle formation (Patel *et al.*, 2007). They can be categorised into two types namely, phagocytosis for internalisation of large molecules, and pinocytosis for uptake of fluids and solutes. Although, phagocytosis can only occur in specialised cells of the immune system, pinocytosis can occur in all the cells through at least four different endocytosis pathways; caveolin mediated, clathrin mediated, caveolin and clathrin independent and macropinocytosis, with all four pathways associated with cellular internalisation of CPPs and cargos (Drin *et al.*, 2003; Ferrari *et al.*, 2003; Kaplan *et al.*, 2005; Richard *et al.*, 2005). The specific pathway of CPP-cargo uptake will depend on the size of the endocytic vesicles formed and intracellular trafficking of the vesicles. For example, caveolin pits are ~50-80 nm in diameter, clathrin vesicles are ~120 nm in diameter, caveolin and clathrin independent endocytic vesicles are ~90 nm in diameter. The macropinosomes arising from macropinocytosis are 1-5 µm in diameter (Conner & Schmid, 2003).

Being an actin-dependent form of endocytosis, macropinocytosis has been suggested as the major route of cellular internalisation of cationic CPPs (Khalil *et al.*, 2006; Nakase *et al.*, 2004; Wadia *et al.*, 2004). This could be attributed to the fact that uptake by macropinocytosis involves internalisation of significant volumes of extracellular fluids including CPPs which are mainly concentrated on the surface of the cell. However,

whether macropinocytosis is the only pathway of CPP uptake into the cell is debatable. For instance, Tat coated liposomes (200 nm) were shown to penetrate into cells without loss of integrity, taking into consideration the size of the liposomes, entry into cells is precluded by uptake mechanisms other than macropinocytosis since the vesicle sizes are considerably smaller than liposomes (Torchilin *et al.*, 2001). In addition, liposomes modified with a high density of octaarginine were preferentially internalised by macropinocytosis in contrast to liposomes modified with low density of oligoarginine which resulted in uptake by clathrin-mediated endocytosis (Khalil *et al.*, 2006). Although they suggested that the high density of oligoarginine is required to stimulate macropinocytosis, a similar concentration of free peptide did not stimulate macropinocytosis. On the contrary, Dowdy *et al.* showed that Tat peptide was not only internalised by macropinocytosis but was essential in inducing macropinocytosis and that uptake of Tat-Cre fusion protein was inhibited by amiloride which is a macropinocytosis inhibitor (Kaplan *et al.*, 2005; Wadia *et al.*, 2004). Interestingly, in HeLa, HepG2 and Chinese hamster ovary (CHO) cells fluorescently labelled Tat peptide was shown to be internalised via the clathrin-dependent endocytosis, whereby inhibiting clathrin-dependent endocytosis was shown to reduce Tat uptake by ~50% and inhibited transferrin which is a classical marker of clathrin-dependent endocytosis by 85% (Potocky *et al.*, 2003; Richard *et al.*, 2005).

1.6.2.5 Non-endocytotic uptake

The uptake of CPPs occurs not only through energy-dependent endocytotic pathways but via a non-endocytotic/transduction pathway (Patel *et al.*, 2007). This energy- and receptor-independent uptake mechanism has been shown to be the primary uptake

mechanism for the Tat peptide in CHO and HeLa cells (Zaro & Shen, 2005). Furthermore, the physiological relevance of the transduction pathway is illustrated by uptake of functionally intact transcription factors from which CPPs such as Tat are derived. With most studies focusing on endocytotic internalisation of CPPs, few efforts have concentrated on understanding the transduction mechanism which have led to suggest two hypothetical models with minimal experimental evidence, namely direct membrane penetration and inverted micelle (Patel *et al.,* 2007). Both uptake mechanisms follow a 3-step process of internalisation: (a) membrane interaction, (b) membrane permeation and (c) release of CPP into the cytosol. Steps 2 and 3 are where the main differences between endocytosis and transduction exists, wherein endocytosed CPPs are confined in vesicles and may be released into the cytosol, however, transduced CPPs directly localise in the cytoplasm following membrane permeation.

1.6.2.6 Endosomal escape of macromolecules internalised by endocytosis

During endocytosis, the macromolecules are compartmentalised after vesicle fusion and budding events. The vesicle content is then targeted to different parts of the cell depending on the different endocytotic pathways. For instance, caveolin-mediated endocytosed vesicles are targeted to the golgi apparatus or to the endoplasmic reticulum by retrograde transport mechanism (Fischer *et al.,* 2004). In clathrin-mediated endocytosis, some vesicles are recycled to the plasma membrane while others are directed to the lysosomes (Conner & Schmid, 2003; Richard *et al.,* 2005). Macropinosomes resulting from macropinocytosis have different intracellular fates which vary with cell type. In macrophages they have been shown to shrink and merge

with lysosomes but in the human epithelial carcinoma cell line (A431) and HeLa cells they are mainly recycled back to the extracellular space (Conner & Schmid, 2003).

Few reports have suggested the inefficient escape of fluorescently labelled CPPs from endosomal compartments due to being confined in vesicles, verified by punctate staining patterns with confocal laser scanning microscopy (Fuchs & Raines, 2004). A report by Potocky *et al*. demonstrated punctate as well as diffuse staining of Tat-derived CPPs in the cytoplasm and the nucleus, that could be attributed to pH change in the endosomes which alters CPP conformation, subsequently facilitating endosomal escape (Potocky *et al.*, 2003). Biologically active cargos, when entrapped in endosomes are ineffective and therefore endosomal escape and retention of functional activity of the cargo is vital. In order to instigate endosomolysis, lysosomotropic agents such as chloroquine and HA2 fusion peptides have been utilized to enhance peptide delivery of oligonucleotides and proteins (Lundberg *et al.*, 2007). The N-terminal domain of influenza virus hemagglutinin-2 (HA2) induces pH-dependent lysis of the membrane at low pH and has been shown to stimulate the escape of Tat-Cre fusion protein and p53 conjugated to oligoarginine (Michiue *et al.*, 2005). In addition to lysosomotropic agents, photochemical internalisation (PCI) which involves disruption of the endosomes by reactive oxygen species generated by photosensitizers upon irradiation, enhance release of peptide nucleic acid (PNA)-CPP and fluorescently labelled CPP entrapped in endosomes (Maiolo, III *et al.*, 2004; Shiraishi & Nielsen, 2006).

1.6.3 CPP-mediated siRNA delivery

The therapeutic applications of non-covalently linked carrier peptide/siRNA complexes have been recently reported *in vitro* and *in vivo* by several studies (Crombez *et al.*,

2009a; Eguchi *et al.*, 2009; Han *et al.*, 2010; Kim *et al.*, 2010b; Kumar *et al.*, 2007). The Tat_{48-60} peptide is a short cationic peptide derived from the human immunodeficiency virus type 1 (HIV-1) Tat transcriptional activator protein which has been widely employed for intracellular delivery of oligonucleotides (Shim & Kwon, 2010). Although the actual Tat protein is 101-amino acids in length, the laboratory version of the Tat protein is the 86-amino acids derived during tissue culture passaging (Jeang *et al.*, 1999). The Tat protein consists of five domains of which domain four is the most significant because it contains the basic RKKRRQRRR motif responsible for direct RNA binding and nuclear localisation of the protein (Ruben *et al.*, 1989; Weeks *et al.*, 1990).

The utility of Tat peptide for intracellular delivery of various cargos including β-galactosidase, horseradish peroxidase, RNase A *in vitro* was first performed in 1994 (Fawell *et al.*, 1994). They showed that the 36 amino acid long Tat_{37-72} fragment promoted uptake of the 177 kDa β-galactosidase protein in mammalian cells. With respect to delivery, two interesting domains included in this segment of the peptides were the basic domain and the adjacent α-helix (Loret *et al.*, 1991). To identify the domains responsible for peptide internalisation, synthetic Tat peptides with deletions in the α-helical and the basic cluster domain were prepared (Vives *et al.*, 1997). The α-helical domain which was previously thought to mediate transduction was found to be discrete to the cellular uptake of the cargos. The whole basic cluster domain (48-60 residues), however, was found to be responsible for the ability of Tat to internalise cargos since deletions in this domain resulted in reduced Tat uptake by the cells.

Polyamidoamine dendrimer-Tat conjugated with bacterial magnetic nanoparticles has been shown to deliver EGFR siRNA to human glioblastoma cells *in vitro* and xenograft models (Han *et al.*, 2010). A study by Chiu *et al.* demonstrated a clear correlation

between the siRNA localisation, cellular uptake and RNAi efficiency using siRNA-Tat_{47-57} conjugates in HeLa cells which represent a collective criteria required for siRNA delivery and effective gene silencing (Chiu *et al.*, 2004). Consequently, higher concentrations of the conjugates resulted in further increase in cellular uptake and RNAi activity. In addition, modification to the peptide backbone structure of the siRNA-Tat_{47-57} conjugate did not inhibit siRNA uptake neither did it influence the RNAi efficacy (Chiu *et al.*, 2004). The siRNA localisation pattern observed using unmodified and modified peptide conjugates were identical suggesting that the siRNA localisation was dictated by interaction with RISC and not the Tat_{47-57} peptide. Furthermore, the siRNA-Tat_{47-57} conjugate localisation to the cytoplasm was a decisive factor for efficient RNAi activity, mainly attributed to the localisation of the dicer enzyme to the cytoplasm and restriction of RNAi in human cells to the cytoplasm (Billy *et al.*, 2001; Zeng & Cullen, 2002).

The use of RNAi has been suggested as a therapeutic alternative to small-molecule inhibitors for the treatment of human diseases. A report by Moschos *et al.*, showed that lung delivery of target-specific siRNA using Tat_{48-60} peptide induced gene knockdown of p38 MAP kinase mRNA by 20-36% *in vitro* and 20-30% *in vivo* (Moschos *et al.*, 2007a). Interestingly, Tat_{48-60} peptide alone was shown to significantly downregulate p38 MAP kinase mRNA expression *in vivo* which may suggest a regulatory role of Tat_{48-60} on the p38 MAP kinase expression. This could be attributed to the uptake of TNFα and EGF receptors through clathrin-dependent endocytosis without their activation (Fotin-Mleczek *et al.*, 2005). In addition, since DNA-binding domain of the transcription factors form major component of cationic CPPs, it can be anticipated to interfere with host gene transcription (Moschos *et al.*, 2007b). A study by Baker *et al.* utilized Tat_{48-60} to deliver a cytotoxic peptide mimic of the cyclin-dependent kinase

inhibitor, $p21^{WAF1/CIP1}$ in glioma cell lines and showed significant reduction in cell viability after 24 h (Baker *et al.*, 2007). In the event of DNA damage, the cell responds by upregulation of p53 and $p21^{WAF1/CIP1}$ expression which inhibits cyclin-dependent kinases and cell replication. The proliferating cell nuclear antigen (PCNA) is a 36 kDa polypeptide which has a critical role in DNA replication, repair and protein-protein interaction (Cazzalini *et al.*, 2003). The authors showed that $Tat_{(48-60)}$-$p21^{WAF1/CIP1}$ peptide which contains the PCNA interacting protein (PIP) sequence blocks PCNA-dependent DNA replication and subsequently induced apoptosis in glioblastoma cells (Baker *et al.*, 2007).

In some cases, CPP-mediated siRNA delivery requires additional molecules to facilitate siRNA/CCP dissociation in the cell cytoplasm. A study by Endoh *et al.* reported that Tat conjugated siRNA showed no gene silencing due to entrapment of the conjugates in the endosomes following efficient internalisation (Endoh *et al.*, 2008). However, photostimulating fluorescently labelled Tat resulted in its release from the endosome subsequently increasing the gene silencing efficiency. Other agents which have been frequently used to destabilize endosomal membranes and improve cytosolic release of CPP-siRNA include chloroquine and influenza virus-derived hemagglutinin peptide (Shim & Kwon, 2010).

The CPPs have tremendous potential in biotechnology attributed mainly to their ability to increase uptake of biologically active proteins or macromolecules into the cells. To achieve this potential it is of utmost importance to understand the pathway of CPP entry into the cell and subsequent localisation to intracellular compartments (Wadia & Dowdy, 2002). A study by Rhee and Davis used a small peptide called C105Y, covalently attached to poly-L-lysine (polyK) condensed DNA complexes to increase cellular uptake both *in vitro* and *in vivo* (Rhee & Davis, 2006). C105Y was found to

translocate through the membrane and to the nucleus in an energy-independent manner, however, nucleolar localisation was energy-dependent. The internalisation of C105Y was suggested to be via a caveolin- and clathrin-independent pathway. The synthetic peptide C105Y which averages 25 nm in diameter, provides gene transfer of cystic fibrosis transmembrane regulator (CFTR) gene, to the airway epithelial cells in CFTR-deficient mice which was sufficient to partially correct the chloride transport defect with concomitant reversion of down-regulated NOS-2, a characteristic of cystic fibrosis mouse nasal epithelium (Ziady *et al.*, 2002). C105Y has also been demonstrated to enhance gene transfer in the liver, lung and spleen *in vivo* and increase the intensity and duration of reporter gene expression *in vitro* (Ziady *et al.*, 2004).

Interestingly, there are peptides which have the ability to recognise molecular targets that can influence several aspects of cellular physiology and pathology. Mimetic peptides including the sequence derived from functional protein domains can potentially make multiple contacts with target proteins once delivered to appropriate intracellular compartments. A recent report used bioactive CPPs from the human cytochrome c as prediction template to identify CPPs that imitate the apoptogenic activity of the native protein (Jones *et al.*, 2010). Two sequences namely, Cyt $c^{77\text{-}101}$ and Cyt $c^{86\text{-}101}$ (Figure 1.6.4) were observed to induce tumour cell apoptosis *in vitro*. Quantitative analysis confirmed Cyt $c^{77\text{-}101}$ as an extremely efficient CPP with enhanced propensity for cellular penetration and was selected for modification and development of chimeric apoptogenic agent targeting the nuclear pore complex (NPC), specifically the FG nucleoporins (FG Nups) which facilitates redistribution of NPC proteins, significantly enhancing its apoptogenic potency (Jones *et al.*, 2010). Utilisation of mimetic peptides such as Cyt $c^{77\text{-}101}$ with high translocation efficacy for siRNA delivery may enhance

cytotoxicity that combines the apoptogenic properties of the CPP and a bioactive target-specific siRNA.

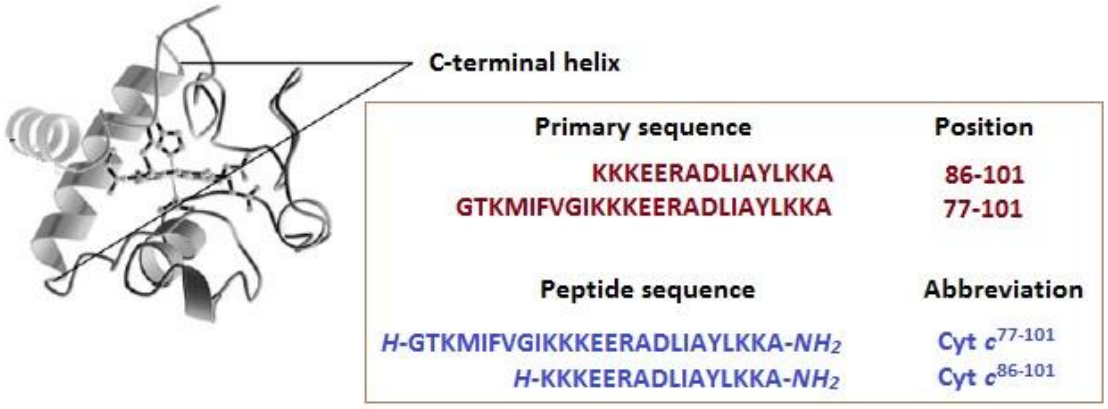

Figure 1.6.4: Cryptic CPP sequence of Cyt *c*. The quaternary structure of Cyt *c* and the distribution of highly probable CPP sequences are mainly located in the C-terminal helix. The primary sequence, peptide sequences and abbreviations of cryptic CPPs have been illustrated. Figure modified from (Jones *et al.*, 2010).

Although, CPPs have been proved to translocate across the plasma membrane of eukaryotic cells, they have been found to be toxic when used at high concentrations which could be due to lytic properties or membrane perturbation (Hallbrink *et al.*, 2001; Saar *et al.*, 2005). Studies on CPP-mediated uptake of cargo have focused on achieving high delivery yields with few studies aimed towards the classification of toxicity status of the peptides. The toxicity results of single CPPs and different cargos are divergent which makes comparison between studies rather challenging. Likewise, various studies use different cell lines, cell passages, incubation times and concentrations etc. making comparisons even more complicated (El-Andaloussi *et al.*, 2007). The effects of CPPs on membrane integrity can be measured as a function of cytoplasmic lactate dehydrogenase (LDH) released into the medium utilizing LDH leakage assays.

Previous reports have shown that Tat_{48-60} has no influence on membrane integrity even at higher concentrations (20 µM) in Bowes human melanoma cells (Hallbrink *et al.*, 2001). In addition, Tat_{48-60} at 50 µM concentration was shown to be non-cytotoxic in glioblastoma, astrocytoma, colorectal adenocarcinoma and breast carcinoma cells *in vitro* (Baker *et al.*, 2007). Tat_{47-57} together with dsDNA has been shown to be non-toxic in HeLa cells at concentrations up to 50 µM (El-Andaloussi *et al.*, 2007). In contrast, Tat_{47-57} showed higher membrane disturbance at the same concentration as a free peptide and drastically reduced the cell viability as a fluoresceinylated Tat_{47-57} at 20 µM, but not as free peptide. This highlights the importance of measuring both membrane disturbance and long-term cytotoxicity when studying CPPs since they do not necessarily correlate (El-Andaloussi *et al.*, 2007). Thus, it is clear that the toxicity of CPPs is heavily dependent on the cargo molecule, coupling strategy, peptide concentration and the cell line investigated.

1.7 Gene silencing and protein inhibition of cancer molecular targets and its implications *in vivo*

The structurally rigid and anionic nature of the siRNA molecule confer the cell membrane as an impermeable barrier and remains a major hurdle for using RNAi *in vivo* without delivery vectors (Gondi & Rao, 2009). Several techniques have been implicated to address this issue, including electroporation, encapsulation in liposomes and viral delivery systems. However, these approaches lack real potential for clinical use due to severe drawbacks such as limited efficiencies in *in vitro* and *in vivo* systems, cytotoxicity, cell damage and undesired immunogenic effects (Suhorutsenko *et al.*, 2011). In contrast, synthetic CPPs have shown an ability to deliver various cargos, for example, DNA, RNA and proteins *in vitro* (Lindberg *et al.*, 2011).

CPPs have been extensively employed for intracellular delivery of siRNA (Chiu *et al.*, 2004; Han *et al.*, 2010; Moschos *et al.*, 2007a). The concept of target-specific killing of glioblastomas by inducing synthetic RNAi response using CPPs has shown particular promise *in vivo*. A study by Michiue and co-workers, used Tat peptide to deliver sequence-specific siRNAs to knockdown EGFR and Akt, both oncogenic clientele of Hsp90, as a combinatorial approach to induce tumour cell specific apoptosis and significantly increased survival in intracerebral glioblastoma mouse models (Michiue *et al.*, 2009). For siRNA delivery, a dsRNA-binding domain (not gene specific) was fused on to the Tat peptide which masks the anionic charge of the siRNA and allows efficient siRNA delivery into the entire cell population by improving the stoichiometric ratio between the peptide and siRNA cargo which enhances cellular uptake and biological activity of the cargo as well as providing greater protection from serum during systemic passage (Coursindel *et al.*, 2012).

Another study utilized an improved variant of the amphipathic peptide MPG consisting of hydrophobic and hydrophilic domains derived from HIV gp41 and SV40 T-antigen respectively, a 21 amino acid peptide known as MPG-8 was shown to form nanoparticles with siRNA target specific to cyclin B1, promote its efficient delivery into primary cell lines and prevents tumour growth in tumour mouse models following i.v. injection (Crombez *et al.*, 2009b). Subsequently, a third 20-mer peptide, known as CADY, has also shown anti-cancer activity in prostate carcinoma when complexed with siRNA following entry into the cells by direct translocation (Divita *et al*., 2009).

An added benefit of CPPs is that these vectors enter the entire cell populations in a non-toxic fashion and as most CPPs are synthesised, the addition of predesigned structures and modification with different chemical entities is relatively straightforward widening their possible applications (Andaloussi *et al.*, 2011). Theoretically, the RNAi response utilizing siRNAs that can be readily redesigned could selectively target oncogenic pathways to induce a lethal RNAi response which could evolve as rapidly as the tumour genetics evolves and could thereby allow treatment of recurrent tumours.

The RNAi knockdown efficiency using sihsp90α/Tat complexes in combination with 17-AAG will be examined in intracranial glioblastoma mouse models. Following tumour implantation, the tumour growth will be monitored by measuring the weight of the mice, histological staining as well as by luciferase quantitation in tissue specimens. The Akt kinase activity will be quantitated to determine whether loss of Akt activity was subsequent to Hsp90α inhibition *in vivo*. These efforts will highlight whether the novel approach to dual targeting of Hsp90α possesses therapeutic potential in GBM.

Due to the limited resources and expertise to conduct intracranial surgery at UCLan, the experimental procedures presented in this chapter were performed at the Institute of

Technology, University of Tartu, Estonia, in collaboration with the research group of Professor Ulo Langel and under the supervision of Dr Kaido Kurrikoff. The procedures involving gene expression and Akt kinase activity were performed at the UCLan, UK. The research group at Tartu specializes in the development and utility of peptide cellular transporters *in vitro* and *in vivo* (Andaloussi *et al.*, 2011; Suhorutsenko *et al.*, 2011).

1.8 Summary

1. GBM is one of the most devastating cancers with poor prognosis and lack effective treatment therapies (Balducci *et al.*, 2012). The present standard treatment for GBM involves surgical resection of the tumour followed up with radiotherapy and concomitant chemotherapy associated with modest survival benefits (Thumma *et al.*, 2012).
2. The Hsp90 is highly abundant molecular chaperone and constitutes 1-2% of total cellular proteins under normal conditions (Workman *et al.*, 2007). Hsp90 has emerged as an important biomolecule that chaperones cancer survival under obnoxious conditions by regulating stability and activity of its oncogenic client proteins including key proteins involved in signal transduction, cell cycle control and transcriptional regulators, and contributes to tumour growth and progression (Zhu *et al.*, 2010).
3. The highly inducible isoform Hsp90α is highly expressed in brain tumours and is known to be involved in cell cycle progression, apoptosis and metastasis (Shervington *et al.*, 2008; Gaspar *et al.*, 2009). Hsp90α gene and protein expression levels in glioma cell lines and tissue specimens was highly induced as compared to normal brain cell lines and brain tissue (Shervington *et al.*, 2008), which serve as a rationale for targeting Hsp90α.
4. Benzoquinone ansamycin 17-AAG has demonstrated potent anti-cancer effects *in vitro* and *in vivo* (Li *et al.*, 2009). 17-AAG binds to the N-terminal nucleotide binding pocket of Hsp90 and subsequently prevents its stabilizing interactions with client proteins thereby preventing tumour growth.

5. RNA interference is the mechanism of inducing sequence-specific post-transcriptional gene silencing initially observed in invertebrate nematode but later encountered in plants and vertebrates (Fire *et al.*, 1998; Kim *et al.*, 2009). Exogenously administered siRNAs associate with protein complex known as RISC to drive the sequence-specific degradation of target mRNA. *Hsp90α*-specific siRNA exogenously introduced into glioblastoma cells was shown to significantly reduced Hsp90α gene and protein expression *in vitro* consequently inducing chemosensitivity to TMZ (Cruickshanks *et al.*, 2010).
6. The blood brain barrier confers an impermeable barrier to toxic molecules circulating in the blood including molecules of therapeutic activity which largely attributes to poor prognosis in patients with malignant gliomas (Patel *et al.*, 2009). The cell-penetrating peptides (CPPs) are short cationic peptides that have been widely used for the intracellular delivery of various cargos (Meade & Dowdy, 2007). The therapeutic applications of CPP/siRNA complexes have been widely reported *in vitro* and *in vivo* (Eguchi *et al.*, 2009; Kim *et al.*, 2010b;Han *et al.*, 2010).
7. The structurally rigid nature and the anionic charge of the siRNA molecule confer the cell membrane as an impervious barrier for RNAi therapy *in vivo*. Several studies have demonstrated the induced synthetic RNAi response utilizing CPPs *in vivo* (Crombez *et al.*, 2009b; Divita *et al.*, 2009; Michiue *et al.*, 2009).

1.9 Aims and objectives of this study

Hsp90α has been identified as a potential anti-glioma target according to recent findings from our laboratory. This novel investigation aims to target Hsp90α using a chemical approach (17-AAG) as well as molecular approach (siRNA) in GBM. Furthermore, this study will utilise cell-penetrating peptides for siRNA transfection/delivery and investigates its treatment efficacy and toxicity profile *in vitro* with a view to examine treatment effects in xenograft models.

The overall objective is to provide proof of concept for a new therapeutic strategy for treating glioblastomas.

This study aims;

1. To assess Hsp90α gene and protein expression profile in glioblastoma and non-tumourigenic cells after treatment with 17-AAG and siRNA.
2. To evaluate potential benefits of 17-AAG and sihsp90α as a therapeutic strategy.
3. To optimise a validated siRNA/CPP strategy.
4. To assess pharmacological stability of neat siRNA and siRNA/CPP complexes.
5. To evaluate the treatment efficacy of peptide-delivered siRNA combined with 17-AAG in GBM *in vitro* and *in vivo*.

CHAPTER 2

MATERIALS AND METHODS

2.1 Cell Culture

2.1.1 Cell line description

The cell lines used in this study were purchased from the European Collection of Cell Cultures (ECACC) and the American Type Culture Collection (ATCC) with no evidence of the presence of infectious viruses or toxic products. The normal human glial cell line was purchased from ATCC. The cells were handled according to the recommendations by the Advisory Committee on Dangerous Pathogens (ACDP) for Category 2 containment. Mycoplasma testing was performed on all the cell lines used in this study. A detailed cell line description and their source have been listed in Table 2.1.1.

The cells were received as frozen ampoules in 1 ml plastic cryotubes containing the cells with the appropriate freezing medium supplemented with 10% Foetal bovine serum (FBS), 2 mM L-glutamine and 10% (v/v) Dimethyl sulfoxide (DMSO).

2.1.2 Media and reagents

Media preparations for cell growth were carried out under aseptic conditions by the addition of required supplements as recommended by the ECACC/ATCC specific to the cell line (Table 2.1.1). Both DMEM and EMEM were supplied in 500 ml bottles, to which 50 ml of FBS and 5 ml of L-glutamine (200 mM) were aseptically added to achieve a final concentration of 10% FBS and 2 mM L-glutamine, respectively. The prepared medium was correctly labelled with the date of preparation and stored at $4^{\circ}C$

for up to 4 weeks. The media formulations, reagents and chemicals used in tissue have been listed in the appendix (Table 7.1.1).

The volume of the supplements added to the medium was calculated using the formula:

$$x = \frac{a \times b}{c}$$

Where, a = final concentration, b = final volume, c = stock concentration and x = required volume.

This formula has been utilized in most calculations to determine the volume and concentration of the reagents and chemicals used throughout the study.

Table 2.1.1: Cell lines used in cell culture and their media supplements.

Cell lines	**1321N1**	**GOS-3**	**U87-MG**	**SVGp12**
Description	Human astrocytoma	Human brain mixed astro-oligodendroglioma	Human glioblastoma-astrocytoma Epithelial-like cell line	Human non-tumourigenic cell line
Grade	I	II/III	IV	N/A
Supplier	ECACC, UK	DSMZ, Germany	ECACC, UK	ATCC, UK
Culture media and supplements	DMEM, 10% FBS and 2mM L-glutamine	DMEM, 10% FBS and 4 mM L-glutamine	EMEM, 10% FBS, 2mM L-glutamine, 1% (v/v) non-essential amino acids, and 1mM sodium pyruvate	EMEM, 10% FBS, 2mM L-glutamine, 1% (v/v) non-essential amino acids, and 1mM sodium pyruvate

2.1.3 Resuscitation of frozen cells

The cell lines supplied in cryotubes were immediately stored in liquid nitrogen on arrival. The cell medium was pre-warmed to 37°C before the frozen ampoules with the cells were thawed. Resuscitation of cells was carried out as recommended by ECACC/ATCC. The frozen cryotubes stored in liquid nitrogen were removed and thawed at 37°C in a water bath for 1-2 min. The cells were resuspended in 1 ml of medium in a 15 ml centrifuge tube and centrifuged at 1000 rpm for 5 min at room temperature. The supernatant medium was discarded and the cells were resuspended in 1 ml of fresh pre-warmed medium and aliquoted into 25 cm^2 flasks already containing 5 ml of pre-warmed medium. The flasks were labelled with the name of the cell line, passage number and date and gently rocked to ensure even distribution of cells in the medium. The cells were incubated at 37°C with 5% CO_2 in filtered air. For slow growing cells, the medium was changed after every 48 h of incubation to maintain sufficient nutrient levels for the cells. All the cell lines used were restricted to 5-7 passages to perform all the experiments.

2.1.4 Subculture and cell library maintenance

The cells were observed under a light microscope after overnight incubation. The cell growth was monitored daily until a mono-layer of cells up to 75-80% confluence was obtained. The cell culture medium was removed and the cells were washed with pre-warmed PBS (1X) pH 7.4 to remove any remaining culture medium. Trypsin EDTA was added (1 ml/25 cm^2) into each flask and incubated at room temperature for 2 - 4 min. The flasks were rocked to ensure maximum cell detachment and examined using a light microscope. The cells were then resuspended in 2 ml of fresh medium to inactivate

the trypsin EDTA. A small aliquot (20 µl) of resuspended cells was transferred to an eppendorf tube for cell counting and the remaining cells were subjected to centrifugation at 1000 rpm for 5 min. To maintain growth, cells (~2 x 10^4 cells/cm^2) were subcultured into a 75 cm^2 flask. The flask was labelled with cell line, passage number and date and incubated under standard cell culture conditions. To maintain cell library, approximately 1 x 10^6 cells were re-suspended in a cell freezing medium (culture medium with 10% DMSO) in 1 ml aliquots and transferred into cryoprotective ampoules labelled with cell line name, passage number and date. The ampoules were placed in Mr Frosty passive freezer (Nalgene, UK) filled with isopropanol and placed in -80°C overnight. Following the overnight storage, the ampoules were then transferred into liquid nitrogen. The cell information was entered in the data entry log book, stating the position of storage in liquid nitrogen. This simplifies tracing cells at a later date for further use. While 1 x 10^6 cells were frozen for stock maintenance, 2 x 10^6 cells were frozen at -80°C without freezing medium for mRNA isolation.

2.1.5 Quantification of cells

The 20 µl aliquot in the eppendorf tube was diluted by adding Trypan Blue to determine the total number of cells, viable (glowing cells) and dead (stained cells). To count cells a haemocytometer was prepared by attaching a cover slip using applied pressure to create Newton's refraction rings. Both sides of the chamber were filled with the stained cell suspension and the cells were counted under a light microscope using ×20 magnification. The cell count from only the middle square was used for cell quantification.

2.2 Cell treatment with Temozolomide and 17-allylamino-17-demethoxygeldanamycin (17-AAG)

Temozolomide was kindly provided by Katherine Ashton (Royal Preston Hospital, Preston, UK). It was then dissolved in DMSO to achieve a stock concentration of 100 mM. Cell culture media was used to make up a final concentration of 1.05 mM, in which cells were incubated for 48 h. 17-AAG was obtained from InvivoGen (UK) and was reconstituted in DMSO to give a stock concentration of 2 mM. The stock was then diluted in culture medium to achieve a final working concentration of 0.225 µM which was added to the cells followed by incubation for 48 or 72 h. The final concentration of DMSO in the control cells did not exceed 1%.

2.3 Oligonucleotide sequence and electroporation conditions

2.3.1 siRNA sequence/target gene alignment

The siRNA used in this study to target *hsp90α* gene has previously been shown to promote RNAi in glioblastoma cells (Cruickshanks *et al.*, 2010). Three sets of pre-designed *hsp90α* siRNA duplexes were purchased from Ambion (Life Technologies, UK). The siRNA were designed for maximum potency and specificity using a highly effective and extensively tested algorithm which guarantees a minimum of 70% reduction of the targeted mRNA. The *hsp90α* specific siRNAs have been listed and the target exon depicted in Figure 2.3.1.

The sihsp90α oligo 2 was used for gene silencing in this study mainly ascribed to its ability to induce chemosensitivity in glioblastoma as previously established in our laboratory (Cruickshanks *et al.*, 2010). A standard nucleotide BLAST (Altschul *et al.*, 1990) was performed using this siRNA sequence and the Human genomic + transcript nucleotide database available from BLAST, that showed only 2 hits for transcripts. These were Hsp90α [transcript variant 1 (NM_001017963.2) and 2 (NM_005348.3)] showing a 100% identity demonstrating high specificity for Hsp90α.

Additionally, a BLAST2SEQ was performed with the same siRNA sequence against all the variants of the isoform Hsp90β (NM_001271971.1, NM_001271970.1, NM_001271972.1, NM_007355.3, NM_001271969.1), showing less than 50% match for all the variants indicating no specificity for Hsp90β.

A

sihsp90α	Sequence	Target exon
Oligo 1	Sense: 5'GCAGGAAGAGAAAAAAACAtt3' Antisense: 5'UGUUUUUUUCUCUUCCUGCtt3'	5
Oligo 2	Sense: 5'CGUGAUAAAGAAGUAAGCGtt3' Antisense: 5'CGCUUACUUCUUUAUCACGtt3'	5
Oligo 3	Sense: 5'GCGAUGAUGAGGCUGAAGAtt3' Antisense: 5'UCUUCAGCCUCAUCAUCGCtt3'	9

B

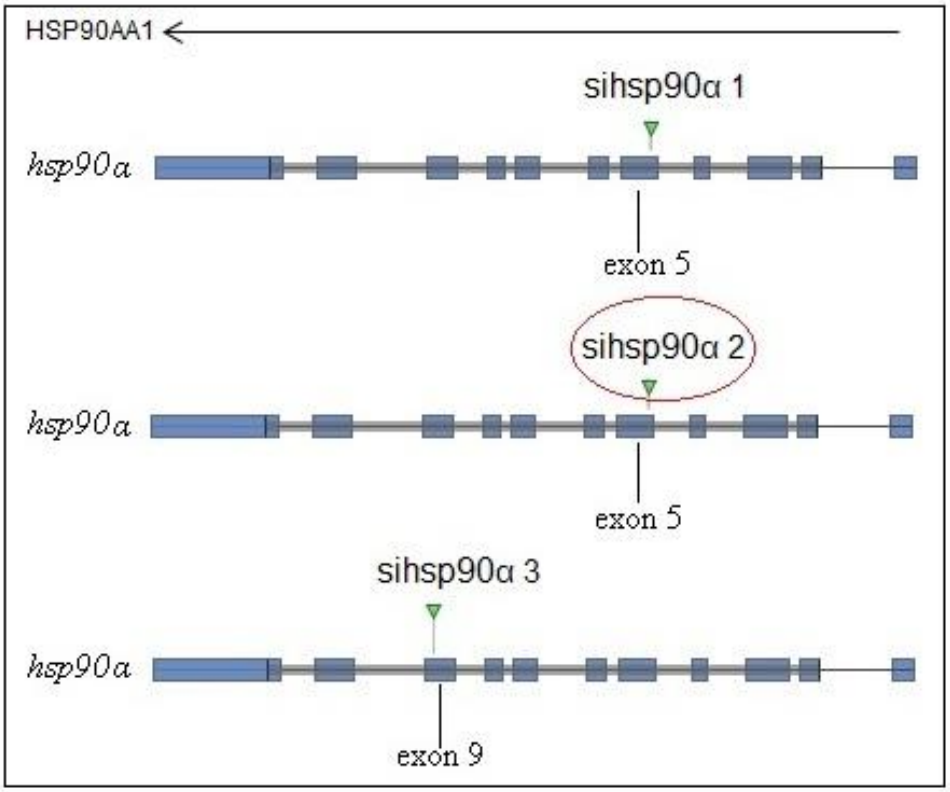

Figure 2.3.1: The sihsp90α sequences and depiction of target exon location. The different sihsp90α oligos previously used have been shown with the highlighted sihsp90α oligo utilized in this study (modified from Ambion, UK).

2.3.2 Cell electroporation and transfection with siRNA

The *Silencer*® Pre-designed siRNA used for transfections were obtained from Ambion (Life Technologies, UK). The siRNA sequences consisted of 21-nt and targets Hsp90AA1 gene with sense strand: 5'CGUGAUAAAGAAGUAAGCGtt3' and antisense: 5'CGCUUACUUCUUUAUCACGtt3'. The annealed siRNA was resuspended in nuclease-free water (400 µl) to achieve a stock concentration of 100µM which was further diluted to 50 µM working concentration prior to use.

2.3.2.1 siRNA electroporation

Electroporation is a method used to introduce siRNA into mammalian cells. The procedure involves the use of electric pulse which temporarily disturbs the phospholipid bilayer, thus allowing molecules like DNA/RNA to pass into the cell (Chen *et al.*, 2007). Recent work from our laboratory optimised and validated electroporation conditions for siRNA transfection targeting *hsp90α* mRNA (Cruickshanks *et al.*, 2010). The current study focuses on the use of sihsp90α oligo 2 to target *hsp90α* mRNA and further aims to determine its anti-tumour efficacy when used alone or as a combination with Hsp90-inhibitor.

The electroporation conditions vary according to the cell types. Factors that influence the electroporation efficiency are pulse length, number of pulses and concentration of siRNA. The siRNA transfections were carried out using the siPORT™ siRNA Electroporation Kit according to the manufacturer's instructions (Ambion, UK). Bio-Rad gene pulser Xcell was used for electroporation. Electroporation parameters

used in this study were: 3 pulses (square wave type pulse) at 400 V for 100 µsec with 0.1 sec intervals between the pulses.

2.3.2.2 si-FAM control siRNA transfection procedure

To evaluate whether the electroporation parameters described above translate into efficient siRNA transfection *in vitro*, U87-MG and SVGp12 cells were transfected with *Silencer*® FAM labelled Negative Control siRNA (si-FAM; Ambion, UK). For transfection, U87-MG cells and SVGp12 cells (7.5×10^5 cells/electroporation sample) were centrifuged at 1000 rpm for 5 min at room temperature. The cells were resuspended in 75 µl of siPORT™ siRNA electroporation buffer (designed to help the cells recover after electroporation) and then transferred to 1 mm electroporation cuvette and 1.5 µg of si-FAM was added to the cuvette. The cells in the cuvette were electroporated using parameters: 3 pulses (square wave type pulse) at 400 V for 100 µsec with 0.1 sec intervals between the pulses. The cuvette was then incubated for 10 min at 37°C and the cells were transferred to chamber slides containing pre-warmed culture medium. The cells were incubated overnight under normal cell culture conditions. The transfection of siRNA into the cells was visualised using the Axiovert 200 LSM 510 laser scanning confocal microscope (Carl Zeiss, UK) which showed that the siRNA was efficiently delivered to the cells (Figure 2.3.2).

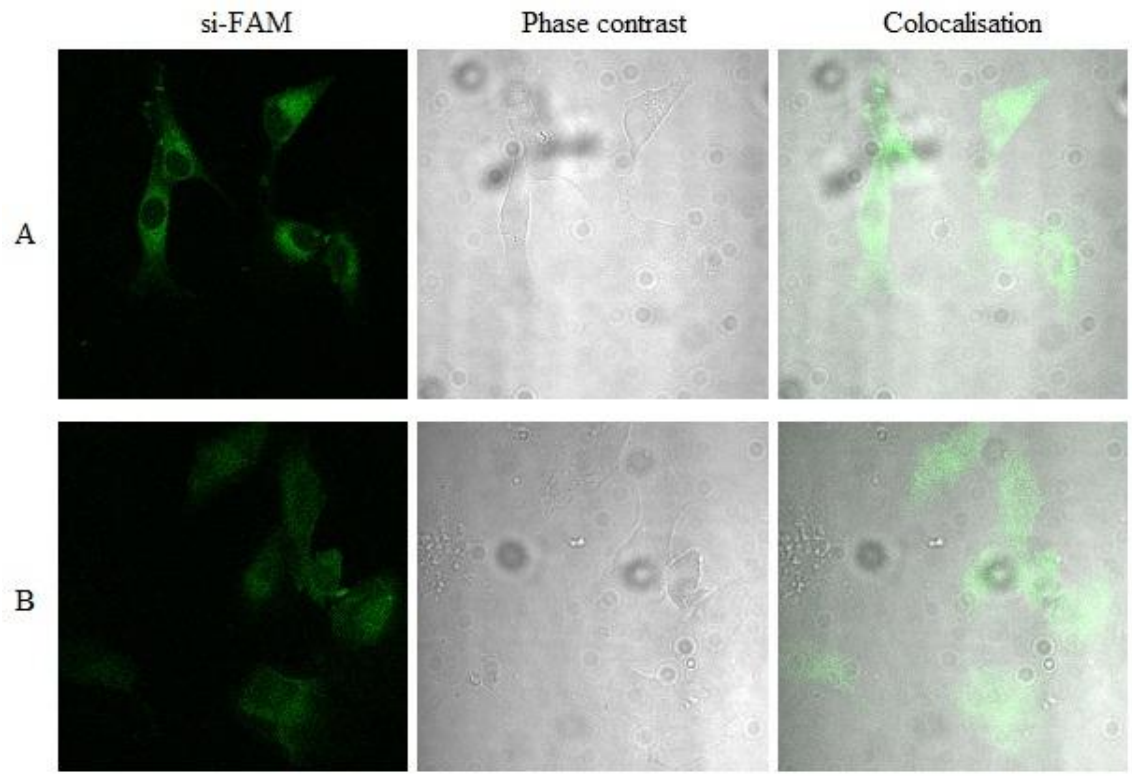

Figure 2.3.2: Uptake of si-FAM in U87-MG and SVGp12 cells. The U87-MG (A) and SVGp12 (B) cells show uptake of si-FAM (green fluorescence) as confirmed by colocalisation with phase contrast.

2.3.2.3 sihsp90α and 17-AAG treatment

The sihsp90α treatment procedure is the same as above only the si-FAM control siRNA was replaced with sihsp90α and the cells were transferred to a 25 cm^2 tissue culture flasks containing pre-warmed medium. The cells were incubated for either 48 or 72 h after which the cells were harvested for qRT-PCR analysis to assess *hsp90α* expression and Hsp90α protein levels. For concurrent combinatorial assays involving sihsp90α and 17-AAG, 17-AAG (0.225 μM) was added to the pre-warmed medium prior to transferring cells into the flask.

2.4 Cell viability assay

The cell viability was assessed using CellTiter-Glo® Luminescent cell viability assay (Promega, UK) according to the manufacturer's protocol. This assay determines the number of viable cells based on the quantitation of ATP present signalling the presence of metabolically active cells. The addition of the reagent results in cell lysis and generation of luminescent signal proportional to the amount of the ATP present and the amount of ATP is directly proportional to the number of cells present in each well (Crouch *et al.*, 1993).

2.4.1 Protocol for cell viability assay

Briefly, cultured cells were seeded (1×10^3 cells/well) in a white flat-bottom 96-well plate. A control well containing only the culture medium without cells was used to obtain a value for background luminescence. After 24 h, the test compound (TMZ and 17-AAG) was added to the wells and incubated at standard cell culture conditions. Following incubation with the drug, the 96-well plate was equilibrated to room temperature for 30 min. The CellTiter-Glo reagent was prepared by mixing the CellTiter-Glo buffer and CellTiter-Glo substrate (1:1). A working stock was prepared by mixing appropriate volume (depending on the number of wells used) of CellTiter-Glo reagent with culture media (1:1). The contents of the 96-well plate were emptied by gently tapping on a clean paper towel and washed twice with PBS. From the working stock prepared, 200 µl was added to the appropriate wells of the 96-well plate. The contents of the 96-well plate were mixed for 2 min on a shaker to induce cell lysis and

the plate was subsequently incubated at room temperature for 10 min to stabilize luminescent signal. The luminescent signal was recorded using Tecan GENios Pro® (Tecan, Austria).

2.4.2 Cell line growth curves

The growth curve of the three glioma cell lines and non-tumourigenic cells was generated to evaluate the growth characteristics of each cell line. Three glioma cell lines and non-tumourigenic cell line were seeded in a 96-well plate and the cell growth was monitored for 6 days using the CellTiter-Glo reagent as described in section 2.4.1. The growth curves have been shown in Figure 2.4.1.

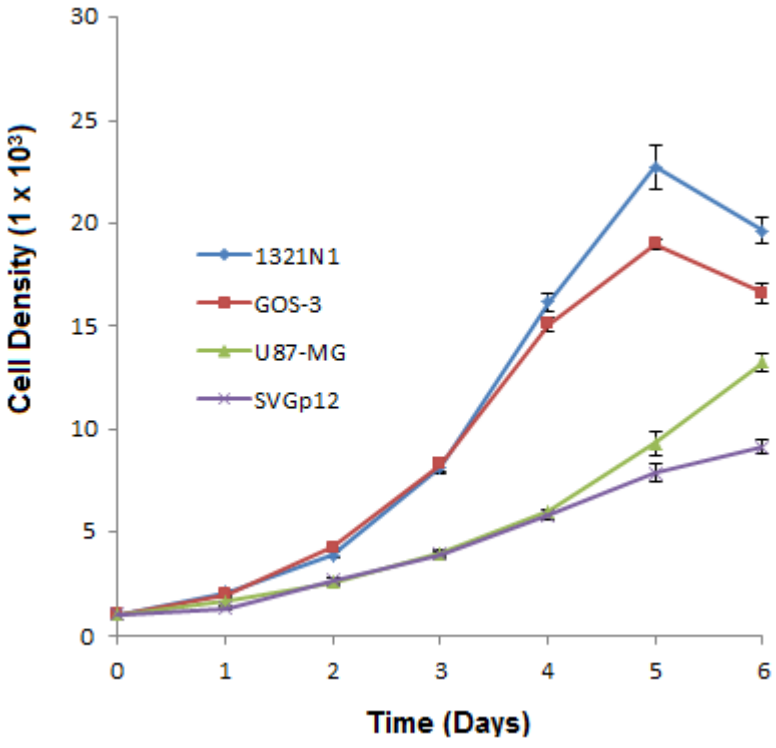

Figure 2.4.1: Growth curves of all the cell lines used in this study. The values shown are mean ±SD, n = 3.

2.5 Isolation of mRNA

The mRNA isolation procedure was performed using a commercially available mRNA isolation kit (Roche Applied Science, UK). The kit is safe to use as no aggressive organic reagents were used and the mRNA isolated using this kit was of the highest purity.

The principle of this kit is that the poly $(A)^+$ tail of the mRNA hybridizes to a Biotin-labelled Oligo$(dT)_{20}$ probe provided with the kit. These biotin labelled probes are in turn captured by streptavidin-coated magnetic particles which are then separated from the cell lysate using a magnetic separator (Figure 2.5.1). The excess fluid is removed using PBS buffer and the mRNA is eluted from the particles by incubating with redistilled water.

All the components of the kit and composition of all reagents used and the volume of reagents and buffers used to conduct this investigation are listed in the appendix (Table 7.1.2 & 7.1.3).

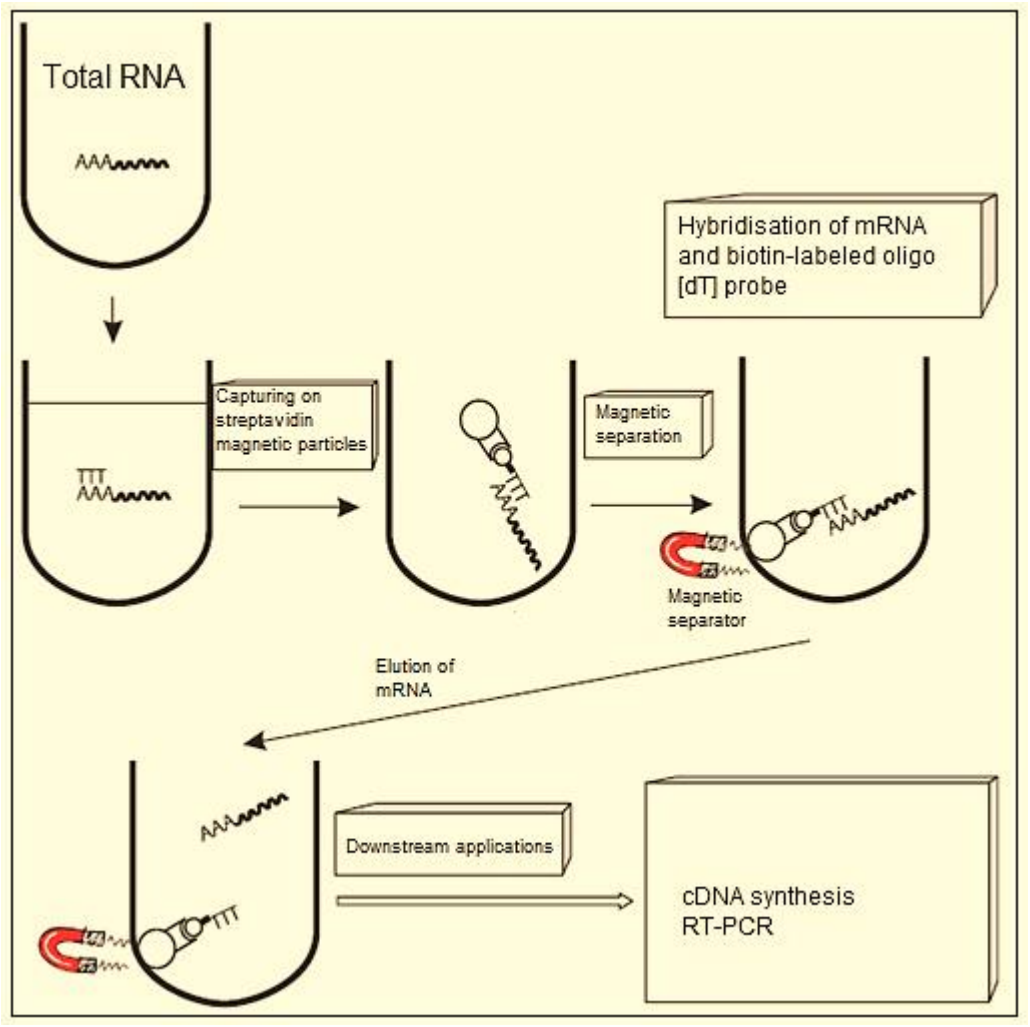

Figure 2.5.1: Experimental overview of the method of mRNA isolation technique (Roche Applied Science, UK). Figure modified from the mRNA isolation kit instruction manual.

2.5.1 Procedure

The cells were washed twice with cold PBS, lysed using lysis buffer and were mechanically sheared six times using 21-gauge needle. The Biotin-labelled Oligo$(dT)_{20}$ probe was added to the sample and mixed to form the hybridization mix. Simultaneously, the Streptavidin-coated Magnetic Particles aliquoted in an eppendorf were immobilized using a Magnetic Particle Separator and rinsed in lysis buffer to remove any excess storage buffer. The Biotinylated dT-A hybrids were immobilized

with the SMPs by resuspending the SMPs in the hybridization mix followed by incubation at 37°C for 5 min. After incubation, the hybrid-linked SMPs were separated from the fluid with a Magnetic Particle Separator and the fluid was discarded. The SMPs were washed with Wash Buffer (thrice) and the mRNA was eluted from the SMPs with redistilled water following incubation at 65°C for 2 min. The eluted mRNA was transferred to a fresh eppendorf and stored at -20°C for various downstream applications.

2.5.2 Analysis of nucleic acid by alkaline gel electrophoresis

The isolated mRNA was analysed on an alkaline gel to determine whether the RNA remained intact or had been degraded. A 2% gel was prepared by dissolving 0.6 g of agarose (Geneflow, UK) in 30 ml of distilled water utilizing a microwave. The gel was heated until a transparent molten solution had formed. The molten gel was then allowed to cool down to 50°C prior to the addition of NaOH (stock 10 M) and EDTA (stock 0.5 M) to achieve a final concentration of 50 mM and 1 mM, respectively. The solution was poured into a gel cast and left undisturbed for 30-45 min to solidify. Once solidified, running buffer with a final concentration of 50 mM NaOH and 1 mM EDTA prepared in distilled water was poured into the gel tank. The mRNA samples with the loading dye at 1:4 (dye:sample) were run at 50 V for 1-2 h. The gel was stained with freshly made ethidium bromide (0.5 µg/ml) for ~10 min and destained in distilled water before gel analysis by GENE GENIUS bioimaging system (Syngene, UK).

2.5.3 Quantifying the isolated mRNA using NanoDrop™ Spectrophotometer

The isolated mRNA was quantified using a NanoDrop™ 1000 Spectrophotometer (Thermo Scientific, UK) which measures the optical density of 1 µl of the sample with high accuracy and reproducibility. The full spectrum (220-750 nm) spectrophotometer uses a patented sample retention technology that employs surface tension alone to hold the sample in place. mRNA sample (1 µl) is pipetted onto the end of a fiber optic cable and a second fiber optic cable is then brought into contact with the liquid sample causing the liquid to bridge the gap between the two fiber optic cables. A pulsed xenon flash lamp provides the light source and a spectrophotometer utilizing a linear CCD array is used to analyse the light after passing through the mRNA sample. The instrument is connected to computer based software and controlled through the computer. The software calculates and displays A_{260}, A_{280}, A_{260}/A_{280} and concentration in ng/µl.

2.6. cDNA synthesis

The mRNA isolated previously was reverse transcribed into cDNA using First Strand cDNA Synthesis Kit (Roche Applied Science, UK). The Master Mix was prepared by adding the components listed in Table 2.6.1. Avian Myeloblastosis Virus (AMV) reverse transcriptase is the enzyme which synthesizes the cDNA strand at the 3'end of the poly (A) mRNA where oligo dT is used as a primer. All the reagents were thawed on ice. A sterile microfuge tube was used to pipette specified volumes of Reaction Buffer (10X), $MgCl_2$ (25 mM), Deoxynucleotide Mix, Oligo-$p(dT)_{15}$ Primer, RNase Inhibitor, AMV Reverse Transcriptase, sterile water and finally the RNA sample isolated previously. The mixture was vortexed, centrifuged and incubated at 25°C for 10 min to allow annealing of the primer to the mRNA template. The mixture was then incubated at 42°C for 1 h which allows cDNA formation via reverse transcription. Subsequently, the AMV reverse transcriptase in the mixture was denatured by incubating at 99°C for 5 min and cooling to 4°C for 5 min. The isolated cDNA was then used as template for qRT-PCR.

Table 2.6.1: The following components were used in the order of listing for cDNA synthesis.

Reagents	Volumes	Final concentration
Reaction buffer (10X)	2.0 µl	1X
25mM $MgCl_2$	4.0 µl	5 mM
Deoxynucleotide Mix	2.0 µl	1 mM
Oligo-p$(dT)_{15}$ Primer	2.0 µl	1.6 µg
RNase Inhibitor	1.0 µl	50 units
AMV Reverse Transcriptase	0.8 µl	20 units
Sterile Water	variable	-
RNA sample	variable	100 ng
Total volume	20 µl	-

2.7 Bioinformatics: Gene sequence and Primer design

Bioinformatics is the application of statistics and computer science to the field of molecular biology that enables us to congregate, analyse and represent biological information in order to comprehend various processes involved in healthy and diseased states. The field of bioinformatics has rapidly expanded with progress in full genome sequencing, functional genomics, pharmacogenomics, proteomics and biopathway modelling (Curioso *et al.*, 2008).

Ensembl and NCBI allow users to assess the nucleotide sequence of the genes of interest. NCBI provides genomic databases, sequence identification tools and genome specific resources. NCBI provides verification for genes that have been found through computational techniques. The sequence obtained from NCBI can then be exported to a software application called Primer 3, which designs a left and right primer for that particular gene. The gene sequence for *GAPDH* and *hsp90α* were obtained from NCBI (See appendix Figure 7.2.1 and 7.2.2). The primers for *hsp90α* and the control *GAPDH* were designed using Primer 3 (Figure 2.7.1 & 2.7.2).

There are two major isoforms of Hsp90, namely Hsp90α and Hsp90β (Sreedhar *et al.*, 2004). This study focuses on downregulation of *hsp90α* gene expression due to its induced levels in glioma cell lines and tissues (Shervington *et al.*, 2008). The *hsp90α* and *GAPDH* gene locations were found using public databases, namely

1. Genecards at (http://genome-www.stanford.edu/genecards/index.shtml)
2. NCBI at (http://www.ncbi.nlm.nih.gov/entrez/query.fcgi?db=nucleotide&cmd=search&term)

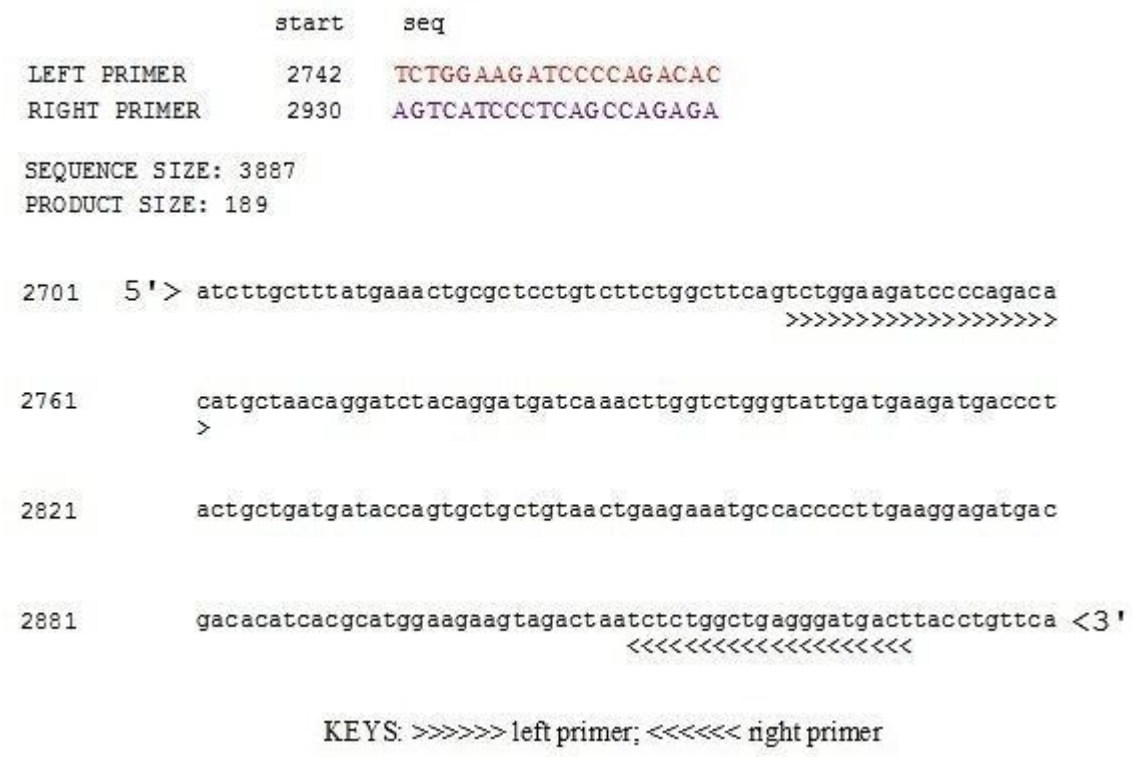

Figure 2.7.1: Primers for *hsp90α*. The output page of Primer 3 provides the right and the left primers.

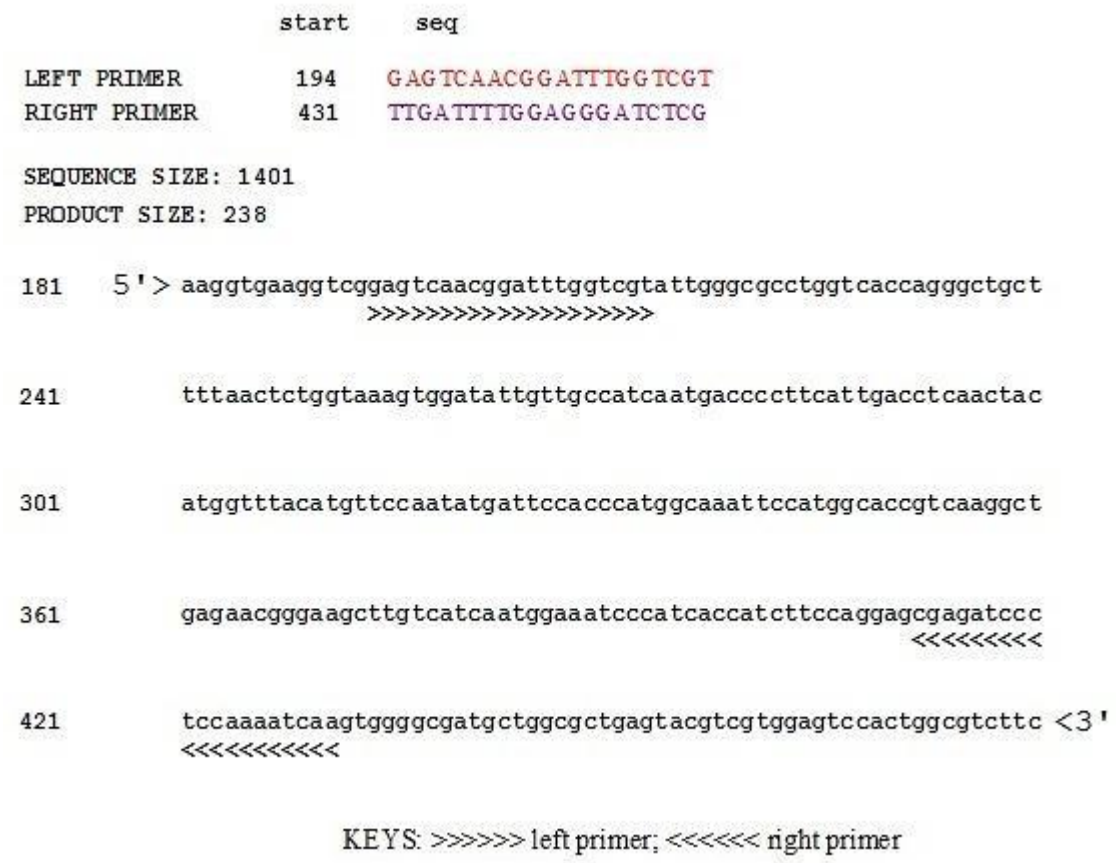

Figure 2.7.2: Primers for *GAPDH*. The output page of Primer 3 provides the right and the left primers.

2.8 Quantitative Real Time Polymerase Chain Reaction (qRT-PCR)

Polymerase chain reaction (PCR) is a method that allows logarithmic amplification of short DNA sequences usually 100 to 600 bases long allowing quantification of very low copies of mRNA that would otherwise not show up if other analytical techniques such as northern blotting was used. qRT-PCR was performed to amplify the *hsp90α* and Glyceraldehyde-3-phosphate dehydrogenase (*GAPDH,* as a control) using LightCycler® FastStart DNA Master^{PLUS} SYBR Green I (Roche Applied Science, UK). The samples along with a negative sample (no cDNA) were run on the LightCycler real-time PCR detecting system (Roche Diagnostics, Grenzach-Wyhlen, Germany). The composition of the reagents provided within the LightCycler FastStart DNA Master^{PLUS} SYBR Green I kit has been listed in the appendix (Table 7.1.4). The quantities of the reagents required for each RT-PCR reaction are listed in Table 2.8.1.

Table 2.8.1: The quantities of reagents required of each RT-PCR reaction.

Reagents	Quantity
Molecular biology-grade H_2O	12 µl
Enzyme Master Mix	4 µl
PCR primer mix (1µl left + 1µl right)	2 µl
Single-stranded cDNA template	2 µl
Total	20 µl

Each qRT-PCR capillary contained the volumes of reagents as listed above and the negative sample contained 2 µl of PCR-grade water instead of cDNA. The PCR protocol considered consist of pre incubation, amplification, melting and cooling steps which took approximately 50 min to complete and the various steps included are listed in Table 2.8.2. To confirm the amplification specificity of the RT-PCR run, the PCR products were subjected to a melting curve analysis and agarose gel electrophoresis. The primers for the genes were prepared by TIB MOLBIOL (Berlin, Germany). Different annealing temperatures derived, calculated or optimised are listed in Table 2.8.3.

Table 2.8.2: LightCycler program for qRT-PCR utilizing FastStart DNA Master^{PLUS} SYBR Green I kit.

Analysis mode	Cycles	Segment	Target Temperature (°C)	Hold Time (sec)
Pre incubation	1		95	600
Amplification	35	Denaturation	95	15
		Annealing	Variable (Table 2.8)	15
		Extension	72	9
Melting	1	Denaturation	95	0
		Annealing	10 higher than amplification	40
		Extension	95	0
Cooling	1		40	30

Table 2.8.3: Primer sequences used to amplify target genes, specifying expected amplicon size and annealing temperature.

Gene	Primer sequence	Expected amplicon (bp)	Primer Annealing Temperatures (°C)			
			Primer 3	GC/AT rule *	TIB MOLBIOL	Experimental Temperature
hsp90α	Sense: 5'–TCTGGAAGATCCCCAGACAC–3' Antisense: 5'–AGTCATCCCTCAGCCAGAGA–3'	189	60 59.9	62 62	55.4 55.6	63
GAPDH	Sense: 5'–GAGTCAACGGATTTGGTCGT–3' Antisense: 5'–TTGATTTTGGAGGGATCTCG–3'	238	59.97 60.01	60 58	56.2 54.8	56

* GC / AT rule: A method of calculating the primer annealing temperature using the formula: T = 2° (A + T) + 4° (G + C), where A, C, G and T represent the number of adenine, cytosine, guanine and thymine bases respectively in the primer sequence concerned.

2.8.1 Agarose Gel Electrophoresis

The amplified PCR products were run on 2% agarose prepared by dissolving 0.8 g of agarose in 40 ml of TAE buffer (1X). Once the solution had been micro-waved, which ensures that the agarose particles have completely dissolved, the solution was poured into a casting tray that had previously been prepared by the insertion of the sample comb. Once the gel had solidified, 300 ml of TAE buffer was added to the electrophoresis apparatus and then the comb was removed. 8 µl of sample and 2 µl of loading buffer were loaded into each of the wells. The loading buffer consisted of 25 mg bromophenol blue, 25 mg xylene and 4 g sucrose in 10 ml of distilled water. AGE was run at 50 V and the gels were stained in ethidium bromide (0.5 µg/ml). The materials and reagents used for gel electrophoresis are listed in Table 7.1.5.

2.8.2 Copy number calculation

The quantification of the target amplicon was expressed as a copy number. In real time PCR, a positive reaction is detected by the accumulation of a fluorescent signal defined as the cycle threshold (Ct) which reflects the number of cycles required for the fluorescent signal to cross the threshold. The Ct levels are inversely proportional to the amount of target nucleic acid in the sample. Genomic DNA was used as an external standard to demonstrate that 1 µg corresponds to 3.4 x 10^5 copies of a single gene (Wittwer *et al*., 2004). Previously in our laboratory (Mohammed & Shervington, 2008; Shervington *et al.*, 2007), genomic DNA of known concentrations were used as a standard to amplify GAPDH gene using the LighCycler instrument. The Ct which serves as a tool for calculating the starting template amount was used to plot a standard curve to determine the copy number in unknown samples. A standard curve was generated with different concentrations of genomic DNA in duplicate: 0.005, 0.05, 0.5, 5 and 50 ng (known copy numbers) and their corresponding average Ct's (Table 2.8.4 and Figure 2.8.1). The equation generated (y=-1.3124Ln(x) + 32.058) was rearranged to (=EXP((Ct value-32.058)/-1.3124)) and used to determine copy numbers of the mRNA expression of all the genes used throughout this study.

Table 2.8.4: Different concentrations and dilutions of DNA with known copy numbers used for quantitative PCR amplification and the corresponding crossing points.

Concentration of Genomic DNA (ng)	Average Ct	Copy number
0.005	30.15	1.7
0.05	29.10	17
0.5	26.42	170
5	22.60	1700
50	18.30	17000

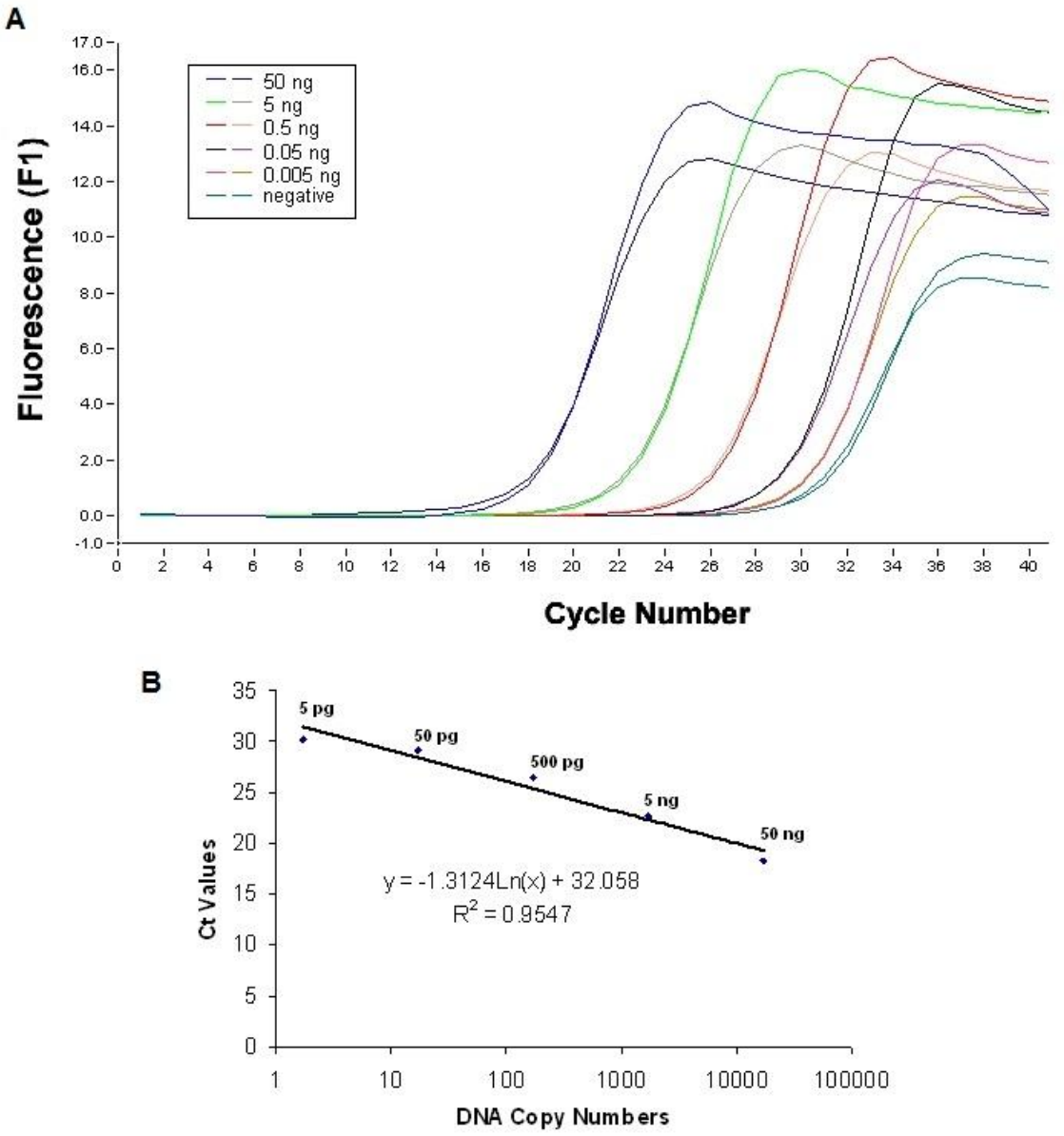

Figure 2.8.1: Standards used to generate the copy numbers for each gene. LightCycler quantification curve generated by known concentrations of genomic DNA was amplified, which shows that the higher the concentration of DNA the lower the Ct value (A). The negative control (primer alone) shows no fluorescence acquisition until after 30 Ct. (B) The standard generated from the crossing points shows the relationship between the Ct values and the copy numbers of the amplified genomic DNA using *GAPDH* reference gene (Figure adapted from Mohammed, 2007).

2.9 Laser Scanning Confocal Imaging Microscopy

Cells were seeded (1 x 10^5 cells/well) on culture slides in 6 well plates 24 h prior to treatment. Following treatment with sihsp90α and 17-AAG, the cells were fixed with 4% paraformaldehyde, washed three times with warm PBS and subsequently permeabilized with 0.3% Triton X-100 at room temperature for 7 min. The cells were then washed three times with warm PBS and incubated in blocking solution followed by 1 h of incubating in the primary monoclonal antibody against Hsp90α antigen (Cambridge Bioscience, UK). After the incubation, the cells were washed thrice with PBS and exposed to a light sensitive fluorescein isothiocyanate secondary antibody (goat anti-rat IgG FITC) for 1 h with gentle agitation. Finally, cells were washed three times with PBS in the dark and counter stained with PI (Vectashield, UK), mounted and fixed on slides for analysis. For each sample, a total of 150 cells were counted using Axiovert 200M LSM 510 laser scanning confocal microscope (Carl Zeiss Ltd, UK). A typical example of fluorescent staining is shown in Figure 2.9.1.

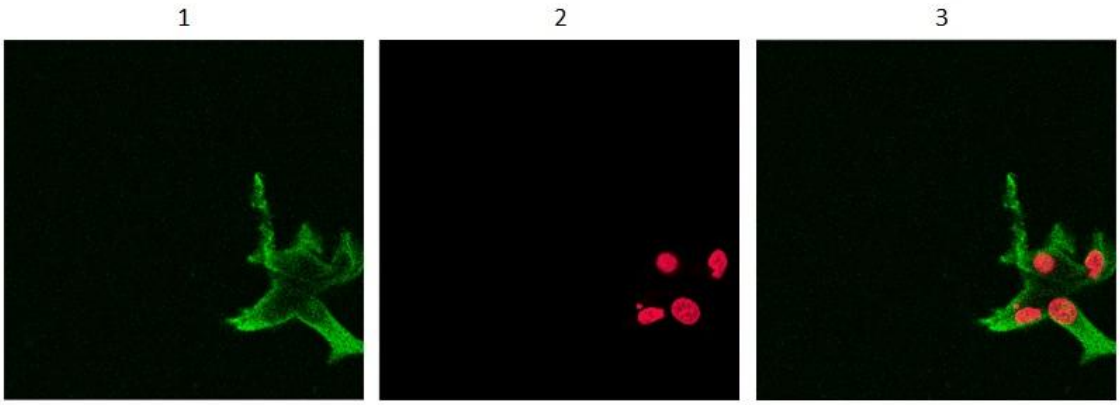

Figure 2.9.1: A typical example of Hsp90α staining in U87-MG cells. Column 1 represents Hsp90α staining with FITC-conjugated secondary antibody, 2 shows the nuclei staining with PI and 3 shows the colocalisation of Hsp90α and nuclei staining.

2.10 Protein extraction and quantitation

After the treatment, cells were spun down at 1200 rpm for 5 min to give a cell pellet. The cells were washed with ice-cold PBS and lysed using CelLytic M Cell Lysis Reagent (Sigma, UK). For every 1 x 10^6 cells, 50 µl of CelLytic M lysis buffer was added ensuring complete suspension. The cells were centrifuged at 13000 rpm and 4 $^{\circ}$C for 15 min. The supernatant was transferred to a fresh pre-chilled microcentrifuge tube. Protease inhibitor (1µl) was added to inhibit protease activity. Protein concentration was calculated using the Bradford protein assay, a spectroscopic analytical method to determine the protein concentration in the sample solution utilizing Coomassie Blue dye. The presence of protein molecules in a solution causes the Coomassie Blue dye to undergo an absorbance shift as a result of the colour transformation where red form of the dye is converted into a blue form when bound to protein. The increase of absorbance reading is proportional to the amount of bound dye and to the concentration of protein present in a sample.

The unknown protein concentrations were calculated using the standard curve (Figure 2.10.1). Increasing concentration of bovine serum albumin (BSA) ranging between 1-8 µg/µl prepared in PBS (1X) was used to derive a standard curve. A small aliquot of BSA/sample (1 µl) was added to 1 ml of Coomassie Blue Reagent (1:10 dilution in distilled water) and the absorbance was measured in a cuvette at 595 nm. The spectrophotometer was blanked using 1 ml of Coomassie Blue Reagent without the sample.

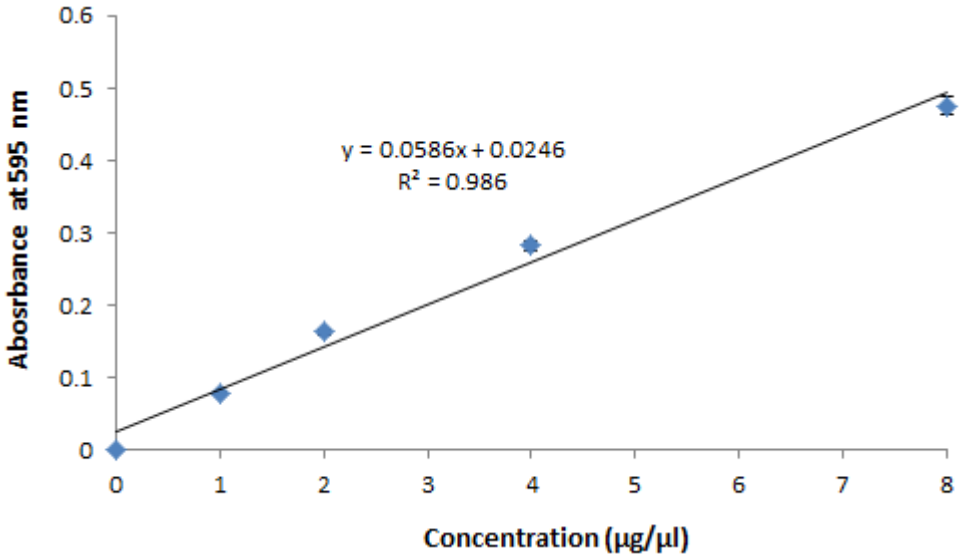

Figure 2.10.1: Protein quantitation standard curve derived using BSA. The equation was used to calculate the concentration of protein in test samples. The values shown are mean ± SD, n = 3.

2.11 Akt/PKB kinase activity quantitation

Akt/PKB activity was measured using the non-radioactive Akt/PKB Kinase Activity Assay (Enzo Life Sciences, UK). The assay is based on a solid phase enzyme-linked immuno-absorbent assay (ELISA) which utilizes synthetic peptide (Tetramethyl-benzidine, TMB) as a substrate readily phosphorylated by PKB, pre-coated on the wells of the microtiter plate and a polyclonal antibody which binds specifically to the phosphorylated form of the substrate to produce colour intensity in proportion to the phosphorylated TMB. Once the samples are added, the addition of ATP to the wells initiates the reaction. The colour intensity is measured at 450 nm using a microplate reader. The assay procedure is summarised in Figure 2.11.1 and the components of the kit are listed in the appendix (Table 7.1.6). The assay was performed as per manufacturer's instructions.

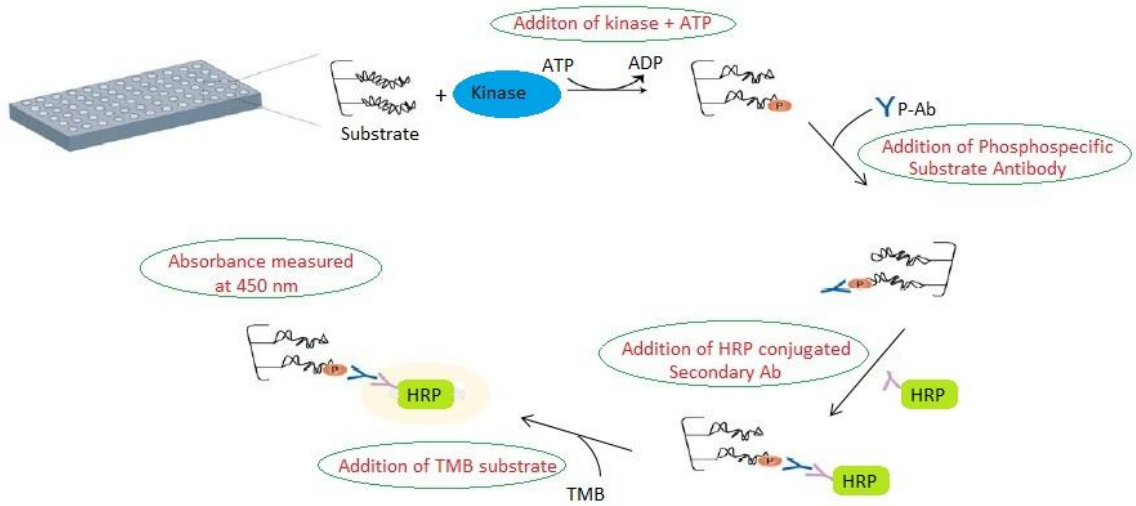

Figure 2.11.1: A summary of the steps involved in the Akt/PKB Kinase Assay. Figure modified from the manufacturer's instruction manual.

2.11.1 Standard curve using purified recombinant active PKB/Akt

1. Initially PKB Substrate Microtiter Plate, Antibody Dilution Buffer, Kinase Assay Dilution Buffer, 20X Wash Buffer, TMB Substrate and Stop Solution 2 were brought to room temperature prior to use. The Microtiter plates were soaked with Kinase Assay Dilution Buffer (50 µl) at room temperature for 10 min. The liquid was carefully aspirated from each well and varying quantities of purified Active PKB (30 µl) were added to the wells at this point. Kinase Assay Dilution Buffer with no kinase was used as a blank. The reaction was initiated by addition of diluted ATP (10 µl) to each well, except the blank. The wells were covered with plate sealer and incubated at 30°C for 60 min on a shaker with rotate angle at 60 rpm. The reaction was stopped by emptying the contents of the wells followed by the addition of Phosphospecific Substrate Antibody (40 µl to each well except the blank) and incubated at room temperature for 1 h. At this point the liquid was aspirated and the wells were washed four times with 1X Wash Buffer (100 µl). Anti-Rabbit IgG: HRP Conjugate was diluted to 1 µg/ml and 40 µl was added to each well except the blank and further incubated at room temperature for 30 min. The washing step was repeated as described above. Once the liquid was carefully aspirated, TMB Substrate (60 µl) was added to each well and incubated at room temperature until colour development. Stop Solution 2 (20 µl) was added to each well and the intensity of the colour was measured at a wavelength of 450 nm and the standard curve has been shown below (Figure 2.11.2). To determine the Akt kinase activity in treated and untreated samples, protein samples (10 µg) were added to the Microtiter plate. The equation generated was rearranged to ($x = y + 0.182/0.475$) and used to determine the Akt levels in the samples.

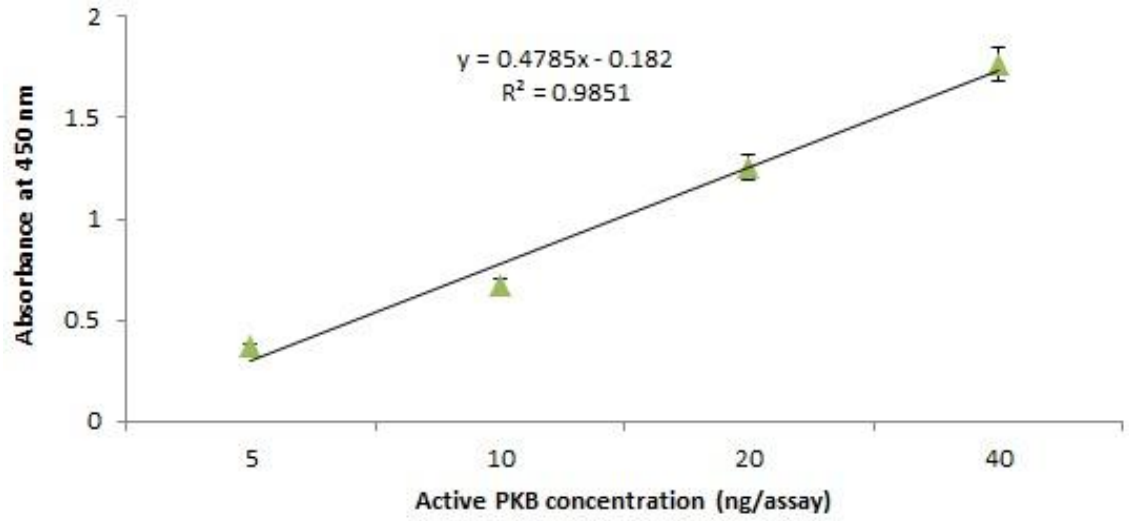

Figure 2.11.2: Standard curve for Akt kinase activity assay obtained using purified recombinant active Akt. The provided recombinant active Akt was diluted in Kinase Assay Dilution Buffer to give final concentration from 5-40 ng/assay. The equation derived from the curve was then used to calculate the Akt activity in treated and untreated samples based on the absorbance readings. This graph is typical of three independent experiments. Data values are mean ± SD, n = 3.

2.12 Peptide synthesis

The peptides Tat, Cyt $c^{77\text{-}101}$ and C105Y were prepared by solid phase using a standard N_{α}–Fmoc(N-(9-fluorenyl)methoxycarbonyl) protection strategy on Rink amide methylbenzhydrylamine (MBHA) resin (NocaBiochem, UK) with O-(6-Chloro-1-hydrocibenzotriazol-1-yl)- 1,1,3,3-tetramethyluronium hexafluorophosphate (HCTU; AGTC Bioproduts Ltd.)/HoBt (Advanced ChemTech) activation on a 0.2 mmol scale with Kaiser tests performed at each step to confirm coupling and/or deprotection (Baker *et al.,* 2007). The peptides were purified to apparent homogeneity by high-performance liquid chromatography (Genesis C_{18} column) and predicted masses of all the peptides (average $M + H^{+}$) were validated by matrix-assisted laser desorption ionisation-time of flight spectrometry (MALD-TOF) operated in positive ion mode using Kratos Analytic Kompact probe. All the peptides were supplied by Professor John Howl (University of Wolverhampton) (Table 2.12.1).

Table 2.12.1: The amino acid sequence of the cell penetrating peptides used in this study.

Name	Peptide sequence	Molecular weight
$Tat_{48\text{-}60}$	*H*-GRKKRRQRRRPPQ-NH_2	1718.06
C105Y	*H*-CSIPPEVKFNKPFVYLI-NH_2	1993.46
Cyt $c^{77\text{-}101}$	*H*-GTKMIFVGIKKKEERADLIAYLKKA-NH_2	2850.52

2.13 Gel mobility assay

To examine whether the peptides successfully bind to and form complexes with the siRNA, gel mobility assay was performed. sihsp90α (200 nM) was mixed with increasing concentration of Tat, Cyt $c^{77\text{-}101}$ and C105Y CPPs at different molar concentrations ranging from 1:1 to 1:50 (sihsp90α:peptide) in serum-free medium for 30 min at 37°C. The siRNA/peptide complexes were then subjected to electrophoresis on 15% TBE polyacrylamide gel (Bio-Rad Laboratories, UK) in TBE buffer at 100 V under non-denaturing conditions and stained with ethidium bromide (0.5 µg/ml) and analysed by UV-transilluminator GENE GENIUS bioimaging system (Syngene, UK).

2.14 Serum stability of sihsp90α

Neat sihsp90α (200 nM) or Tat peptide complexed sihsp90α were incubated in EMEM with human serum (50%) at 37°C. Aliquots (20 µl) were taken from neat sihsp90α samples at 1, 3, 6 and 24 h, and immediately stored at -80°C. All samples were analysed on 15% TBE polyacrylamide gel in TBE buffer at 100 V under non-denaturing conditions and stained with ethidium bromide (0.5 µg/ml) and detected by UV-transilluminator GENE GENIUS Bioimaging system. Aliquots (20 µl) were taken from sihsp90α/Tat samples at 1, 3, 6, 24 and 36 h, to which Proteinase K (200 µg/ml; Sigma, UK) and SDS (0.5% w/v) was added and incubated for 1 h at 37°C which allows segregation and digestion of Tat peptide. The sihsp90α was subsequently extracted from the samples using phenol:chloroform extraction and analysed on 15% TBE polyacrylamide gel and stained with ethidium bromide.

2.14.1 Phenol:chloroform extraction

To each sample equal volume of water-saturated phenol:cholorform:isolamyl alcohol (25:24:1; Sigma-Aldrich, UK) was added. The tubes were inverted to mix the samples and then centrifuged at 4°C and 13,000 rpm for 10 min. The aqueous phase was transferred to fresh eppendorfs tubes and particular care was taken not to disturb the interphase. At this point, to each sample 3 M NaOAc (one-tenth of the total volume), 1 mM EDTA (one-tenth of the total volume) and cold 100% ethanol (2.5X total volume) was added. The samples were mixed and incubated at -80°C for 20 min before centrifugation at 4°C and 13,000 rpm for 10 min. The ethanol was decanted from the

pellets and discarded, 80% ethanol (300 µl) was used to wash the pellets. The pellets (siRNA) were dried for 20-30 min and resuspended in 15 µl of nuclease-free water ready for electrophoresis analysis.

2.15 Membrane Disturbance analysis

An *In Vitro* Toxicology Assay Kit was used to measure the membrane integrity as a function of the amount of cytoplasmic LDH released into the medium (Sigma, UK). This assay is based on the reduction of NAD to NADH by LDH resulting in the stoichiometric conversion of a tetrazolium dye. The resulting coloured compound is measured spectrophotometrically to evaluate the degree of membrane disturbance.

Both U87-MG and SVGp12 cells were seeded (1 x 10^4 cells/well) in 96-well plate 24 h prior to treatment with Tat alone or sihsp90α/Tat complexes (50 µl) at concentrations ranging from 1:15-1:100 (siRNA:peptide molar ratio) in serum-free medium for 30 min at 37°C. Following incubation, the cells were centrifuged at 250 x g for 4 min and 25 µl was transferred to a clean 96-well flat bottom plate. Lactate Dehydrogenase Assay mixture was prepared by mixing equal volume of LDH assay substrate, LDH assay dye solution, and 1X LDH assay cofactor preparation. Lactate dehydrogenase assay mixture (50 µl) was added to the samples and incubated at room temperature for 25 min. The reaction was quenched by the addition of 1 N HCl (1/10 total volume) to each well. The absorbance was measured spectrophotometrically at 490 nm. Serum-free medium without cells was used as a blank, untreated cells lysed with LDH assay lysis solution (1/10 total volume) was used as a control.

2.16 Cellular uptake of si-FAM complexed with Tat peptide

To examine whether the Tat peptide interacts efficiently with siRNA and is able to transfect cells, *Silencer*® FAM™-labelled Negative Control siRNA (si-FAM; Ambion, UK) was incubated with various concentrations of Tat, from 15-fold molar excess of the peptide compared with siRNA to a 50-fold molar excess for 30 min at 37°C in serum-free medium. Glioblastoma and non-tumourigenic cells were seeded (3×10^4 cells /well) in a chamber slide (Lab-Tek®, Thermo Scientific, UK) 24 h prior to treatment with the complexes. On the day of treatment, the cells were washed with serum-free medium prior to incubation with the si-FAM/Tat complexes for 1 h followed by the addition of fresh serum-supplemented medium for 1 h. The cells were washed three times with PBS followed by fixation using 4% (w/v) paraformaldehyde. The cells were washed 3 times with PBS and the si-FAM uptake by the cells was observed using Axiovert 200M LSM 510 laser scanning confocal microscope (Carl Zeiss Ltd, UK). For observation of si-FAM a fluorescein isothiocyanate (FITC) filter was used. To determine whether the Tat peptide interacts efficiently with the si-FAM, a gel shift assay was performed at molar ratios ranging from 15 to 50 and the si-FAM/Tat complexes were assessed on 15% polyacrylamide gel.

2.17 Long-term toxicity of the Tat peptide in glioblastoma and non-tumourigenic cells

The long-term toxicity of the sihsp90α/Tat complexes was quantified by CellTiter-Glo® Luminescent cell viability assay as described in section 2.4.1. Briefly, U87-MG and SVGp12 cells were seeded (1 x 10^3 cells/well) 24 h prior to treatment with the complexes. Following treatment with sihsp90α/Tat complexes for 24, 48 and 72 h, CellTiter-Glo reagent prepared with culture media (1:1) was added to each well. The contents of each well were mixed for 2 min on a shaker to induce cell lysis and the plate was incubated at room temperature for 10 min. The luminescent signal was recorded using Tecan GENios Pro®.

2.18 Tat-mediated *hsp90α* knockdown in combination with 17-AAG

Glioblastoma or non-tumourigenic cells were seeded in either 96-well plate or 25 cm^2 tissue culture flasks 24 h prior to treatment. The sihsp90α/Tat peptide complexes formed by mixing increasing concentrations of Tat at molar ratios ranging from 1:15 to 1:50 in serum-free medium for 30 min, were added to the cells and incubated at 37°C for 4 h. At this point, fresh serum-supplemented medium was added to the cells and further incubated for 24, 48 and 72 h. After incubation, the cells were washed and cell viability, gene and protein expression profiles, and Akt activity was assessed as described previously. For combinational treatment, 17-AAG was added after the transfection, with fresh medium to achieve a final concentration of 0.225 μM and incubated for upto 72 h.

2.19 RNAi experiments *in vivo*

2.19.1 Cell culture

Glioblastoma U87-MG-luc2 (source of parental cell line, ATCC) is a luciferase expressing cell line that was stably transfected with firefly luciferase gene (luc2) established by lentiviral transduction, a commonly used method to express reporter transgenes (Kim *et al.*, 2010a), to achieve high levels of homogenous luciferase expression and an *in vitro* phenotype similar to the parental cell line (Caliper Life Sciences). U87-MG-luc2 cells were grown in EMEM supplemented with 2 mM L-glutamine, 10% FBS, 1% (v/v) non-essential amino acids and 1 mM sodium pyruvate and were cultured at 37˚C in a humidified 5% CO_2 incubator. For the tumour implantation and luciferase experiments, cells were trypsinized and counted using Countess® automated cell counter (Invitrogen) and resuspended in media according to experimental requirements.

2.19.2 Intracranial tumour implantation and treatment with sihsp90α/Tat complexes and 17-AAG

All the procedures for animal care and tumour cell implantation followed approved animal protocols and guidelines of the Estonian Laboratory Animal Ethics Committee (approval number 19 dated 25th September 2009, number 69 and 70 dated 9th Febuary 2011). The intracranial implantation of U87-MG-luc2 cells into one of the striatums of 22 homozygous female nude mice (C.Cg/AaNTac-Foxn1nu, Taconic) was performed while the animals were under anaesthesia (a mixture of ketamine 75 mg/kg (Bioketan,

Vetoquinol) and dexmedetomidine 1 mg/kg (Dorbene, Laboratorios SYBA) i.p. in saline) utilizing a stereotaxic frame (Figure 2.19.1). U87-MG-luc2 cells (1 x 10^6 cells/5 µl of fresh media without serum) were injected into the right striatum using a syringe at stereotaxic coordinates Anterior = +1, Lateral = +2, Vertical = +3.5 from the reference point Bregma (+ indicates forward movement of the syringe from the point of reference as shown in Figure 2.19.1). Following surgery, the anaesthesia was blocked using the α2-adrenergic antagonist atipamezole hydrochloride (Antisedan) at 1mg/kg subcutaneously.

The tumour growth was monitored by measuring the weight, post tumour implantation. At the time of tumour implantation the weight of the animals ranged between 11.9-18.8 g. The first sign of tumour growth in intracranial tumour models is usually after reaching weight losses (~5-10%) at which point the mice (n = 3) were injected with sihsp90α/Tat complexes (i.v., 5 mg/kg) and 17-AAG (i.p., 80 mg/kg), and tumour tissues were harvested after 24 h and stored immediately at -80˚C. The sihsp90α/Tat complexes were formed in nuclease-free water in half the injection volume (100 µl) using 0.5 mM sihsp90α and 10 mM Tat peptide stock solutions, at 50-fold peptide molar excess to sihsp90α. Following 30 min incubation at 37˚C, 100 µl of 10.8% mannitol solution was added to the complexes and the complexes were injected into the tail-vein of mice. Subsequently, the mice were injected with 17-AAG (stock concentration 25 mg/300 µl in DMSO) intraperitoneally. As the tumours were implanted in the right striatum of the mice, the left striatum was used as normal brain tissue. Mice (n = 2) treated with siluc/Tat nanoparticles (siRNA targeting luciferase) and 17-AAG were used as a negative control for gene expression and Akt kinase activity experiments.

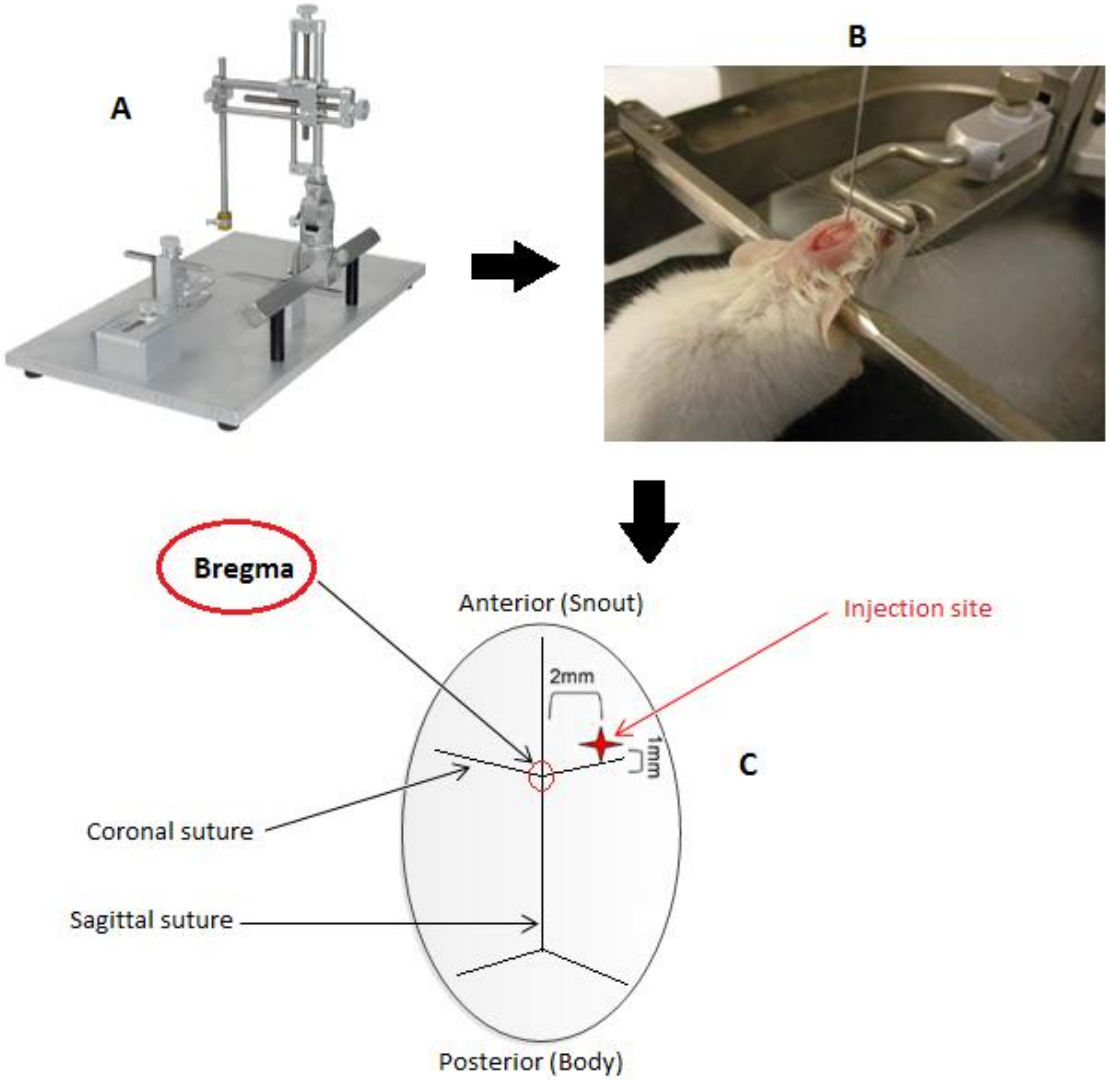

Figure 2.19.1: Intracranial surgery in mouse. A typical stereotaxic frame utilized for intracranial surgery (A). After sedation, the mouse skull was firmly fixed on the frame using ear bars and nose clamp (B, for representation only). The stereotaxic coordinates for the injection site were measured from the reference point Bregma (C). Figure modified from (Serwer *et al.*, 2010).

2.19.3 Determination of luciferase activity

For *in vitro* luciferase experiments, U87-MG-luc2 cells (5 x 10^4) were seeded in a 24-well plate 24 h prior to treatment with siluc/Tat complexes. The siluc/Tat complexes were prepared using siluc (0.1 mM stock solution) and Tat peptide in serum-free EMEM as previously described. Briefly, siluc (200 nM) was added to 1 ml of EMEM with increasing concentrations of Tat peptide ranging from 15 to 50-fold peptide molar excess to siluc. Tat peptide alone (3, 6 and 10 μM) served as a negative control. After 30 min incubation, the complexes were added to the cells and incubated for 4 h at 37˚C, at which point 1 ml of fresh growth media was added and cells were incubated for 24 h.

The luciferase gene was downregulated with siluc. The sequence of siluc was: sense 5'ACGCCAAAAACAUAAAGAAAG3' and antisense 5'UUCUUUAUGUUUUUGG-CGUCU3'. The cells were lysed using 0.1% Triton X-100 in Hepes Krebbs Ringer buffer (100 μl) on ice for 30 min and the luciferase expression was measured using Luciferase Assay System (Promega, Sweden) according to manufacturer's instructions on Glomax luminometer (Promega, Sweden). For luciferase quantitation, protein was extracted from the tissue specimens using the Reporter Lysis Buffer (Promega, Sweden). The procedure involved taking 1 ml of Reporter Lysis Buffer (1X in PBS) and adding it to the ground tissue and subsequently vortexing for 10 min to ensure complete suspension of tissue in lysis buffer. The samples were then subjected to repeated freeze-thaw cycles (to increase protein yield) and centrifuged at 13,000 rpm and 4˚C for 30 min. The supernatant was transferred to fresh eppendorfs and luciferase activity was quantitated using the Luciferase Assay System. After protein extraction, the protein levels were quantitated using DC Protein Assay (Bio-Rad) according to manufacturer's instructions to accurately determine luciferase activity.

2.19.4 H&E staining

For H&E staining, mice brain tumour and normal tissue specimens collected were frozen immediately in isobutanol bath on dry ice, a freezing method which maintains the structural integrity of soft tissues such as the brain tissue. Tissue sectioning was performed using a cryotome with a tissue thickness of 15 µm and were mounted on a glass slides. The tissue sections were stained with Haematoxylin (0.1%) for 10 min, rinsed in deionised water for 5 min and counterstained with Eosin (0.5%) for 30 sec. The sections were rinsed in deionised water, dehydrated in 50, 70, 95 and 100% ethanol for 1 min each and immersed in xylene for 10 min before mounting the slides for analysis. The stained tissue sections were processed using light microscopy.

2.19.5 qRT-PCR and Akt kinase activity analysis

The frozen tumour and normal brain tissue specimens were ground using a pestle and mortar in a cold room and transferred to fresh eppendorfs. For the gene expression experiments, mRNA isolation, cDNA synthesis and qRT-PCR were performed as described previously (Sections 2.5, 2.6 and 2.8). For the Akt kinase activity assessment, protein extraction was performed using Reporter Lysis Buffer as described above. The quantitation of protein was performed using Bradford protein assay as described previously in section 2.10. Subsequently, the Akt kinase activity in normal and tumour tissue specimens were quantitated using Akt/PKB Kinase Activity Assay as described in section 2.11.

2.20 Statistical analysis

In this study, data have been analysed using the PASW Statistics 18 package using the One-Sample Students T-test and Paired-Sample T-test. A p value of * $\leq$ 0.05 and ** $\leq$ 0.001 was considered as statistically significant.

CHAPTER 3

RESULTS

3.1 mRNA isolation, *q*RT-PCR and IC_{50} analysis of glioma cell lines and non-tumourigenic cells

3.1.1 mRNA isolation, *q*RT-PCR: Gene expression evaluation

After extraction of mRNA from the cell lines, the purity of mRNA was checked using a spectrophotometer. The absorbance values measured at 260 nm and 280 nm and the concentration of mRNA isolated are listed in the Table 3.1.1. The isolated mRNA was further analysed using an agarose gel electrophoresis as shown in Figure 3.1.1.

Table 3.1.1: An example of the obtained spectrophotometry reading for glioma and normal cell lines and the mRNA concentrations. Data values are mean ± SD, n = 3.

Cell Lines	Ratio (A_{260}/A_{280})	mRNA concentrations (µg/ml)
1321N1	1.91 ± 0.03	78 ± 5
GOS-3	2.05 ± 0.04	151.7 ± 9.7
U87-MG	2.04 ± 0.04	61.2 ± 7.4
SVGp12	1.88 ± 02	44 ± 3.2

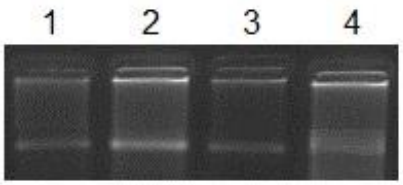

Figure 3.1.1: Agarose gel electrophoresis of mRNA isolated from glioma cell lines. Lanes 1-4 represent mRNA isolated from 1321N1, GOS-3, U87-MG and SVGp12 (Control). Isolated mRNA is distinctly visible.

The isolated mRNA (100 ng) was reverse transcribed into cDNA and real time PCR was performed to measure the *hsp90α* and *GAPDH* gene expression. *hsp90α* expression was found to be highly expressed in all the glioma cell lines (*$p < 0.05$). The median increase in mRNA transcription in glioma cells was 1.85×10^2-fold compared to the normal cell line. Although *hsp90α* was detected in non-tumourigenic cells which was used as a control, the expression levels were negligible compared to the glioma cell lines (Figure 3.1.2). *GAPDH* is a housekeeping gene and its expression was used as a control throughout all qRT-PCR experiments (Barber *et al.*, 2005).

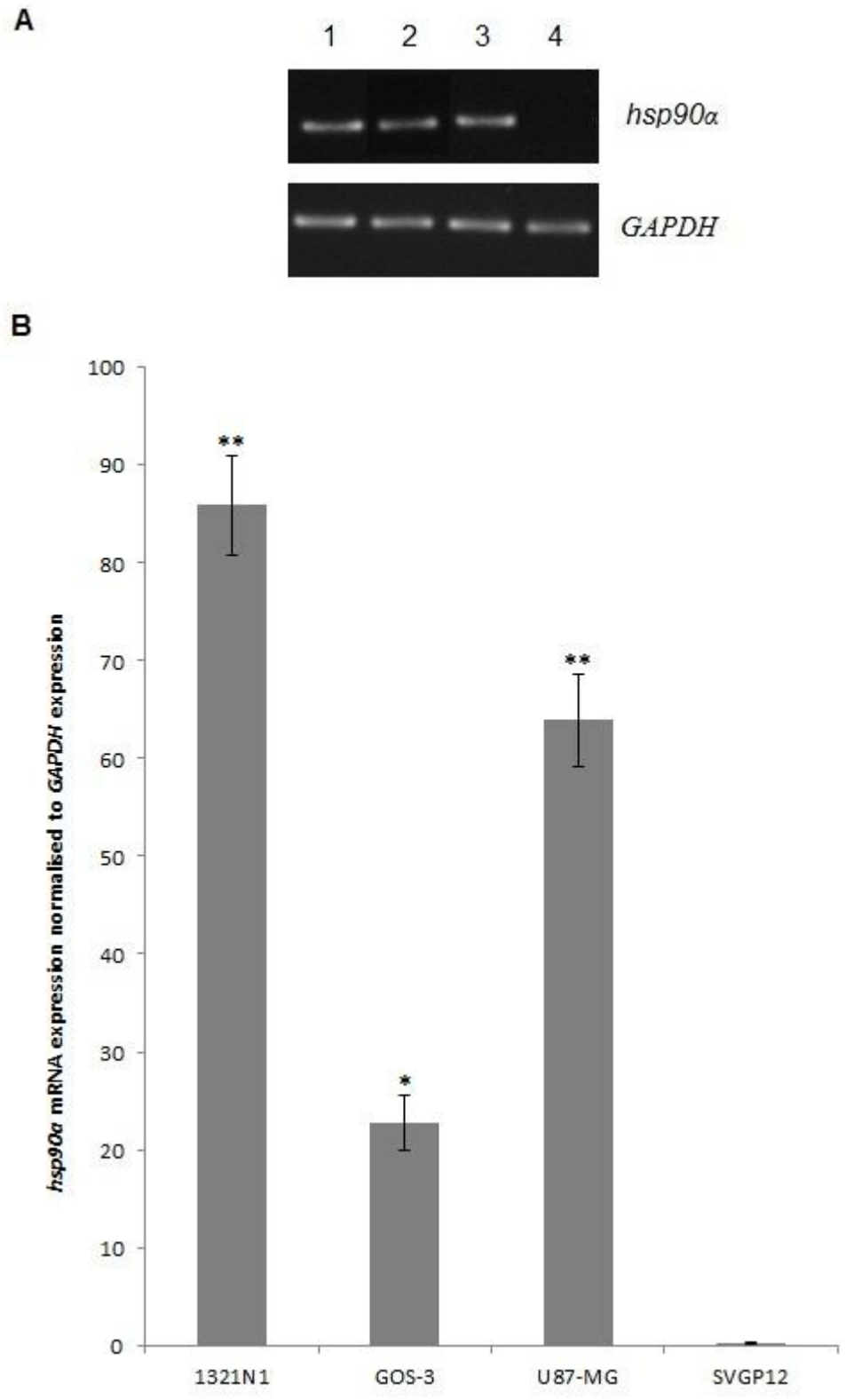

Figure 3.1.2: Gene expressions of *hsp90α* in glioma cell lines. A) Agarose gel electrophoresis: lane 1-4 represents 1321N1, GOS-3, U87-MG and SVGp12 respectively. B) The expression levels of *hsp90α* mRNA relative to *GAPDH* expression in glioma cell lines and non-tumourigenic cells have been shown. Data values are mean ± SD, n = 3. *$p \leq 0.05$ and **$p \leq 0.001$ were considered statistically significant.

3.1.2 IC_{50} derivation in glioma cell lines and non-tumourigenic cells

The three glioma cell lines and one non-tumourigenic cell line were treated with increasing concentrations of TMZ and 17-AAG for 48 h and the cell viability was analysed using *CellTiter-Glo*® Luminescent cell viability assay. The IC_{50} results show reduced glioma cell viability with increase in the drug dose (Figure 3.1.3A & B). The 50% inhibition concentrations (IC_{50}) for glioma cell lines are listed in Table 3.1.2.

Table 3.1.2: The IC_{50} of the chemotherapeutic drug TMZ and Hsp90 inhibitor 17-AAG. The values are mean ± SD, n = 3.

IC_{50} values (μM)	**1321N1 (Grade I)**	**GOS-3 (Grade II/III)**	**U87-MG (Grade IV)**	**SVGp12 (Control)**
TMZ	750 ± 25	600 ± 33	1050 ± 38	850 ± 8
17-AAG	0.38 ± 0.03	0.43 ± 0.05	0.225 ± 0.03	N/A

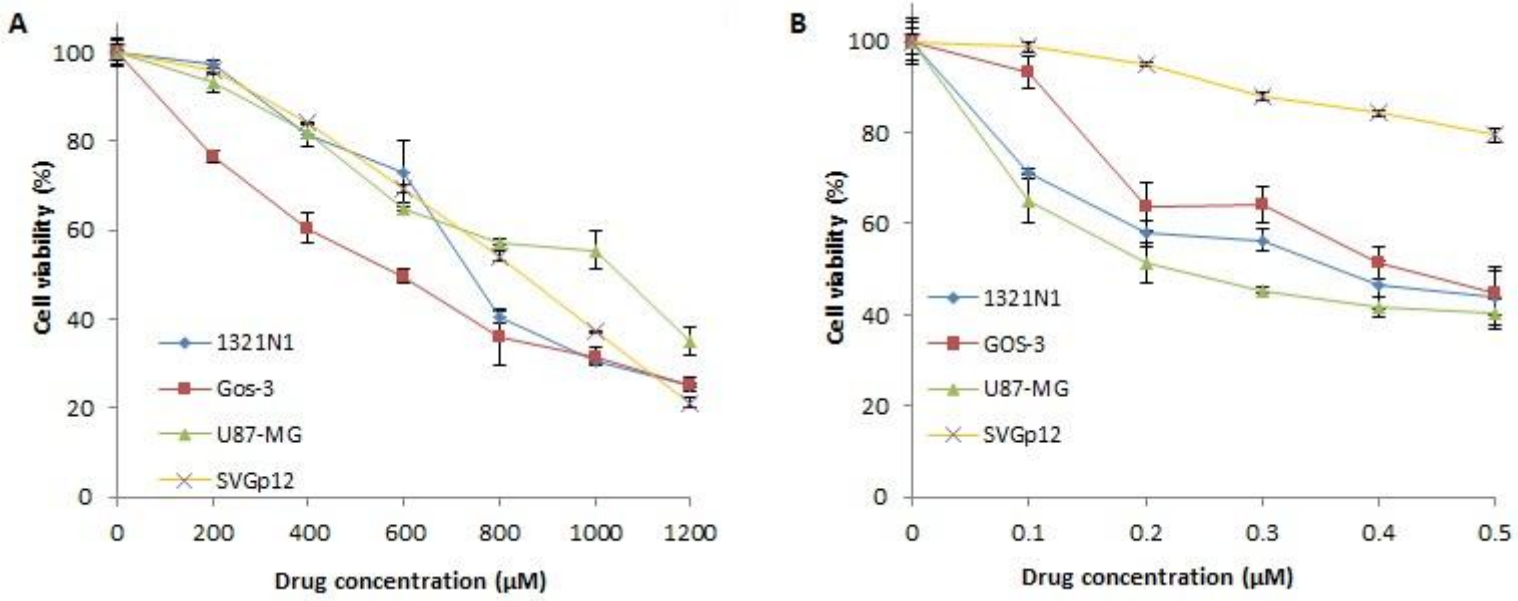

Figure 3.1.3: IC_{50} evaluation of TMZ and 17-AAG. TMZ (0-1200 µM) inhibits the growth of glioma as well as non-tumourigenic cells (A). Hsp90 inhibitor 17-AAG (0-0.5 µM) inhibits the growth of glioma cell lines but not normal human astrocyte cells (B). The data values are mean ± SD, n = 3.

3.2 Hsp90α inhibition combining chemical and molecular approach

3.2.1 Silencing *hsp90α in vitro* with sihsp90α

In order to assess the efficiency of silencing *hsp90α*, U87-MG cells were treated with 17-AAG, sihsp90α or a combination of sihsp90α/17-AAG to quantitate *hsp90α* and *GAPDH* mRNA expression by qRT-PCR. Cells transfected with sihsp90α alone reduced the mRNA copy number by 96% after 48 h, however, the mRNA copy number recovered to 55% after 72 h (Figure 3.2.1). 17-AAG demonstrated a successful downregulation of *hsp90α* expression and reduced mRNA copy numbers by 94 and 86% after 48 and 72 h, respectively. A combinatorial treatment with sihsp90α and 17-AAG together silenced *hsp90α* by 99% after 48 and 72 h. The qRT-PCR results were also validated by agarose gel electrophoresis. The level of *hsp90α* and *GAPDH* was also quantitated in the non-tumourigenic cells SVGp12 to validate targeting *hsp90α,* a therapeutic candidate in this study (Figure 3.2.2). The *hsp90α* levels in SVGp12 demonstrated negligible though detectable levels of mRNA. The different treatments did not have significant effect on transcriptional regulation of *hsp90α*. The *hsp90α* expression levels showed are relative to *GAPDH* levels.

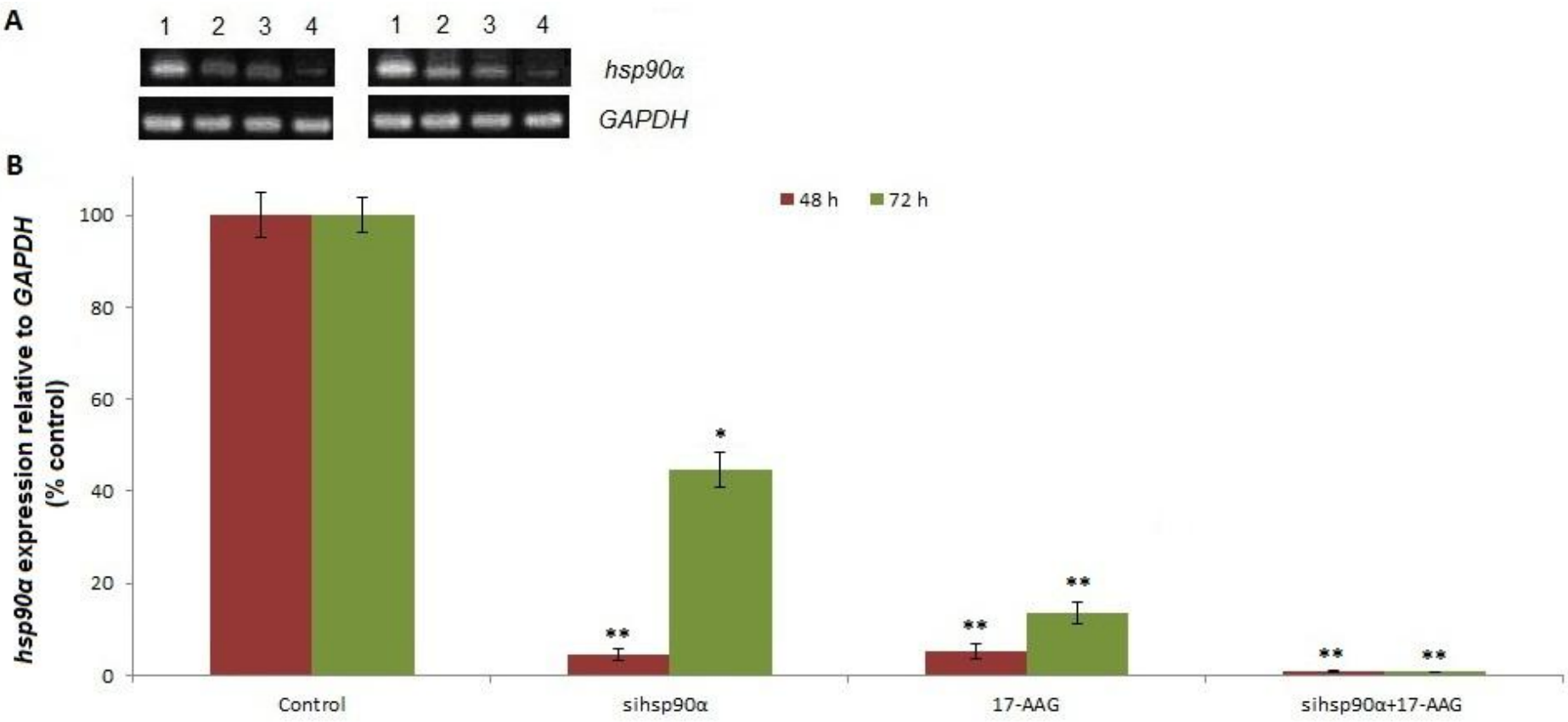

Figure 3.2.1: The effects of 17-AAG and sihsp90α on *hsp90α* expression in glioblastoma. mRNA expression levels of *hsp90α* was relative to *GAPDH* in U87-MG cells treated with Hsp90 inhibitor 17-AAG and/or sihsp90α which targets exon 5 on the *hsp90α* gene were assessed by agarose gel electrophoresis (A) and qRT-PCR (B) 72 h. Lane (1) control, (2) sihsp90α, (3) 17-AAG, (4) sihsp90α+17-AAG. sihsp90α represents cells treated with *hsp90α* specific siRNA. sihsp90α+17-AAG represent concurrent assays where the cells were treated with 17-AAG and *sihsp90α* for either 48 or 72 h. *$p \leq 0.05$ and **$p \leq 0.001$ were considered statistically significant (Data values are mean ± SD, n = 3).

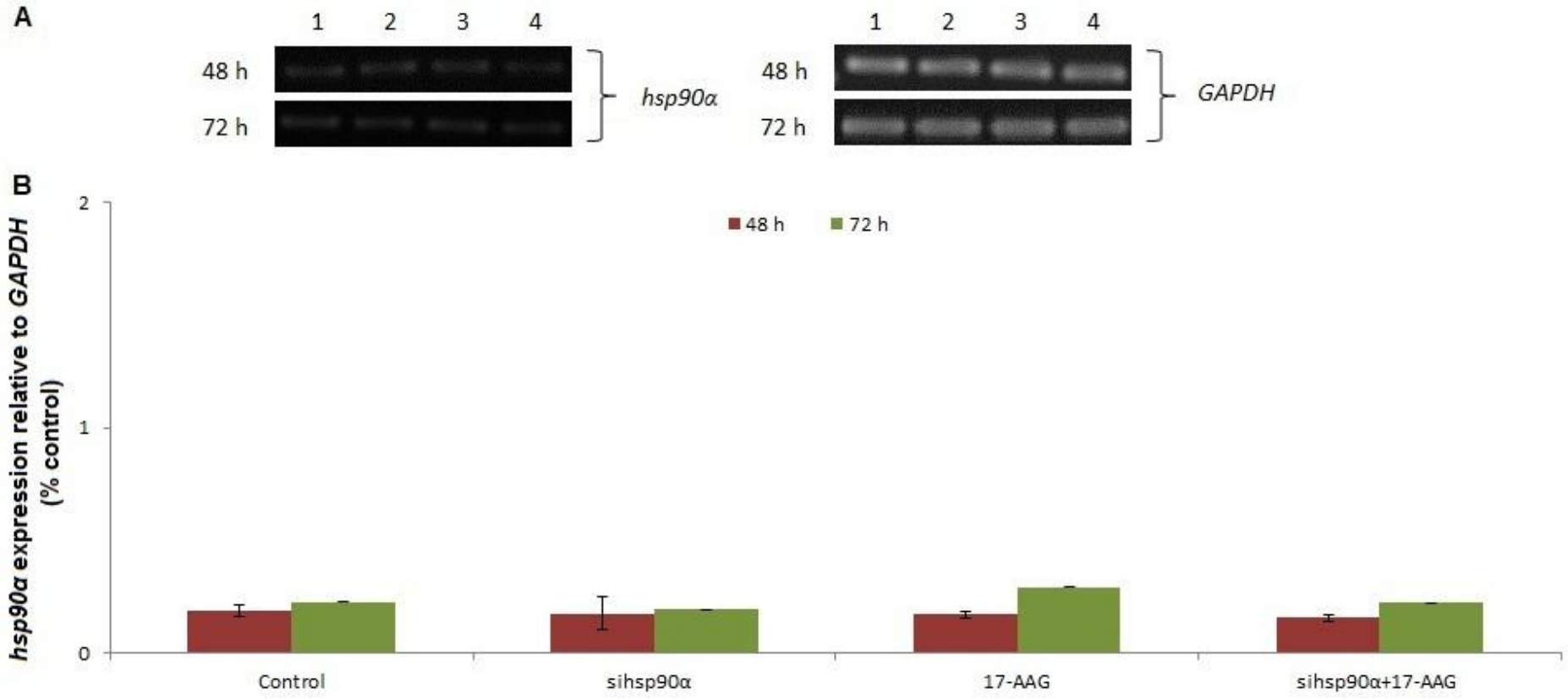

Figure 3.2.2: *hsp90α* mRNA level in SVGp12 cells. mRNA expression levels of *hsp90α* was relative to *GAPDH* in SVGp12 cells treated with Hsp90 inhibitor 17-AAG and/or sihsp90α were assessed for 48 h and 72 h by agarose gel electrophoresis (A) and qRT-PCR (B). Lane (1) control, (2) sihsp90α, (3) 17-AAG, (4) sihsp90α+17-AAG. Data values are mean ± SD, n = 3.

3.2.2 17-AAG and sihsp90α exposure promotes Hsp90α protein degradation in U87-MG cell line

Hsp90α protein levels were monitored by immunocytochemistry to correlate the transcription to the protein levels following sihsp90α and 17-AAG treatment. Figure 3.2.3 represents a sample of the stained cells showing a positive staining for Hsp90α. Hsp90α protein levels were significantly reduced following independent treatment with 17-AAG and sihsp90α. Most degradation of Hsp90α protein was observed after combinatorial treatment using 17-AAG and sihsp90α simultaneously, whereby approximately 4% of the cells strongly expressed Hsp90α after 48 and 72 h (Table 3.2.1). When used as individual agents, sihsp90α and 17-AAG reduced Hsp90α protein levels by 66 and 82%, respectively. Based on the qRT-PCR and Hsp90α protein expression data, there was a clear correlation between the Hsp90α mRNA and protein expression levels.

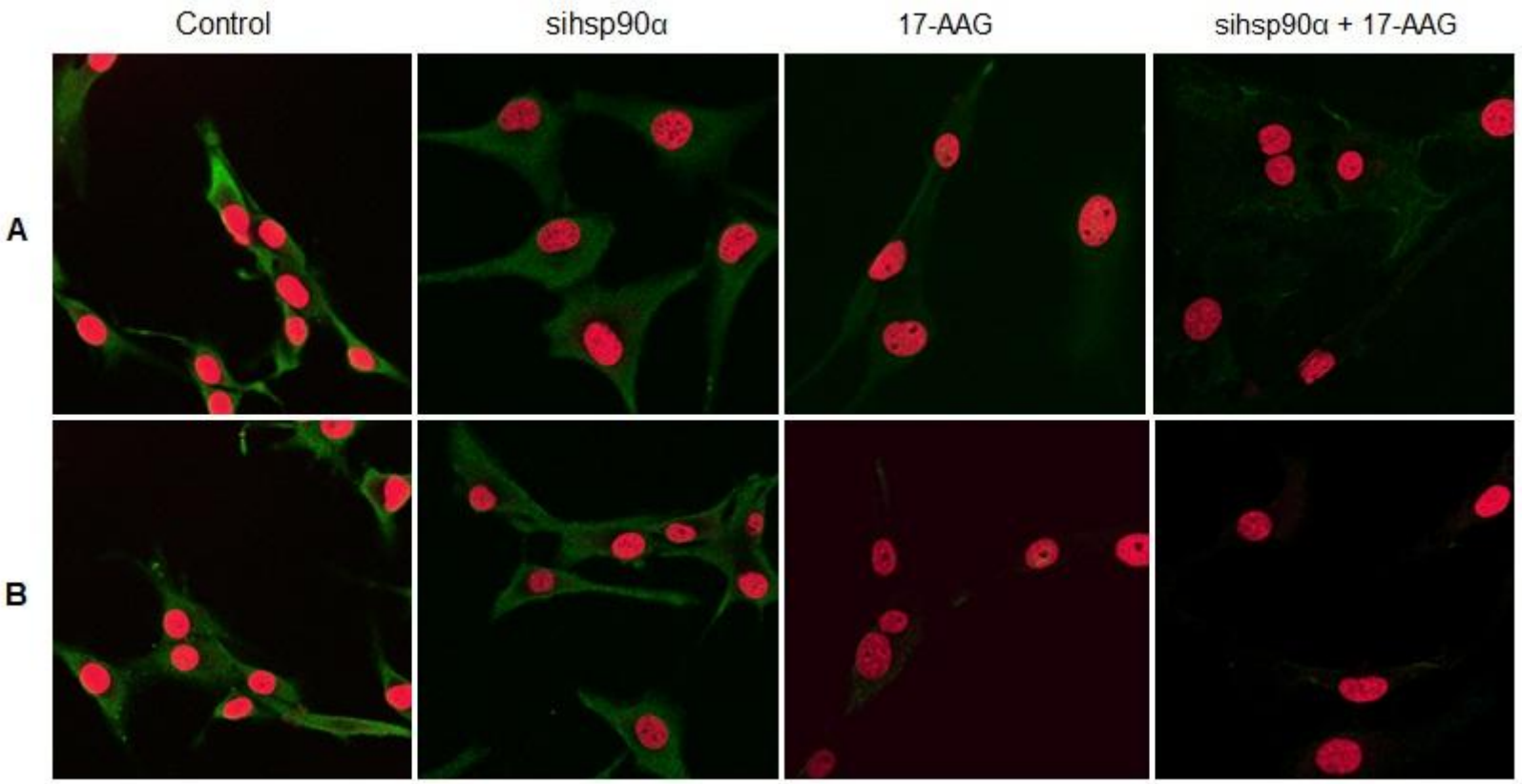

Figure 3.2.3: Hsp90α protein level in U87-MG assessed using immunohistochemistry. Hsp90α protein expression in glioblastoma after 48 h (A) and 72 h (B). The cells were stained with FITC conjugate secondary antibody bound to Hsp90α antigen (green) and propidium iodide (PI) to detect nucleus (red) at ×40 objective magnifications. Hsp90α was mainly located in the cell cytoplasm. This data is representative of three independent experiments.

Table 3.2.1: Hsp90α expression in U87-MG post 17-AAG and sihsp90α treatment. The Hsp90α levels were deduced as the fraction of the observed Hsp90α levels in treated samples relative to the total Hsp90α levels in the untreated sample using immunofluorescence after 48 and 72 h. Hsp90α expression analysis using immunofluorescence was performed by counting 150 cells in triplicates. sihsp90α represent cells treated with *hsp90α* specific siRNA. sihsp90α+17-AAG represent concurrent assays where the cells were treated with 17-AAG and sihsp90α for either 48 or 72 h. This data is typical of three independent experiments. *$p \leq 0.05$ and **$p \leq 0.001$ were considered statistically significant.

Incubation Time (h)	Hsp90α protein expression (%)	Control	sihsp90α	17-AAG	sihsp90α + 17-AAG
48	Strong (++)	71.7 ± 1.8	33.9 ± 2.3 **	18.7 ± 1.2 **	3.5 ± 1.0 **
	Weak (+)	23.0 ± 2.0	43.4 ± 1.3 **	35.2 ± 2.7 **	37.6 ± 2.6 **
	Absent (–)	5.4 ± 0.2	22.7 ± 0.9 **	46.2 ± 1.5 **	59.2 ± 2.2 **
72	Strong (++)	72.1 ± 3.6	40.3 ± 0.6 *	16.7 ± 1.7 **	4.3 ± 1.5 **
	Weak (+)	26.5 ± 2.3	42.6 ± 1.5 **	53.4 ± 3.1 **	25.8 ± 0.9
	Absent (–)	1.5 ± 1.4	17.2 ± 2.1 **	28.3 ± 3.1 **	69.9 ± 0.5 **

3.2.3 Hsp90α inhibition promotes degradation of Hsp90 client Akt/PKB kinase in U87-MG cells

Hsp90 protein regulates conformation, stability and function of many client proteins including Akt. Akt is a signalling protein kinase and is a vital component of the PI3K/Akt signalling pathway known to be abnormally activated in glioblastoma (Zhu *et al.*, 2010). Exposure to Hsp90 inhibitors results in Akt destabilisation and subsequently undergoes proteasomal degradation.

A standard curve was plotted to determine the Akt activity in unknown treated and untreated samples. The equation in the graph was utilized to calculate the active Akt levels in the samples (refer Figure 2.9). To examine whether sihsp90α and 17-AAG affects inhibition of Hsp90α, activity levels of Akt protein, client protein of Hsp90, was investigated in control and treated U87-MG cells using 10 µg of total protein. A

combination of sihsp90α and 17-AAG reduced Akt activity to 47.3 and 43% after 48 and 72 h, respectively (Figure 3.2.4). When only 17-AAG was used, it was found to reduce Akt levels to 63 and 61% after 48 and 72 h treatments. Silencing *hsp90α* with siRNA inactivated Akt activity by 41% after 48 h. However, after 72 h the Akt activity was upregulated to over 100%. The expression profile of Akt emulates that of Hsp90α mRNA and the protein level following sihsp90α and 17-AAG treatments (Figure 3.2.1 & Table 3.2.1).

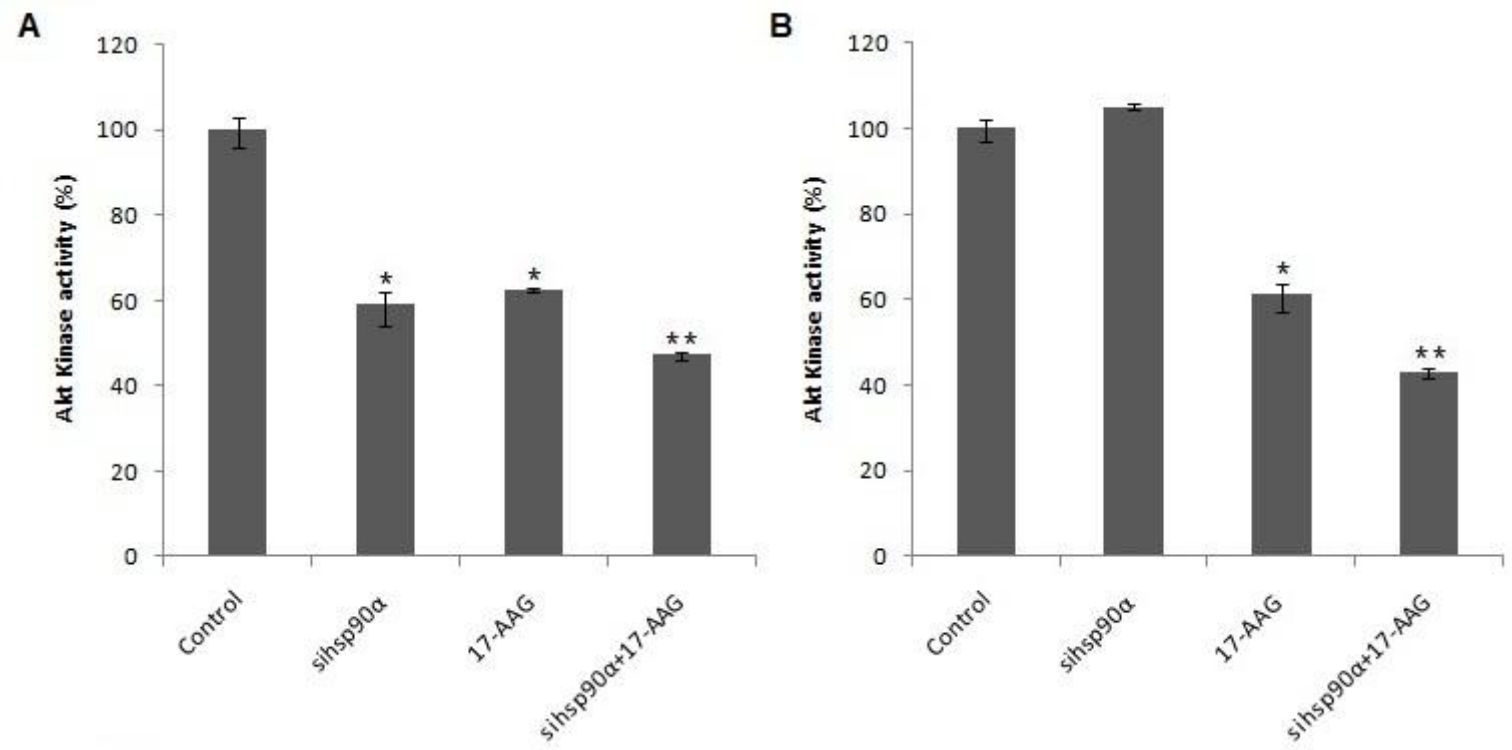

Figure 3.2.4: Hsp90α inhibition results in loss of Akt activity in U87-MG cells. The Akt activity was deduced as the fraction of the observed Akt activity in treated samples relative to the total Akt activity in the untreated sample after 48 h (A) and 72 h (B). sihsp90α represent cells treated with *hsp90α* specific siRNA. sihsp90α+17-AAG represent concurrent assays where the cells were treated with sihsp90α and 17-AAG for either 48 or 72 h. *$p \leq 0.05$ and **$p \leq 0.001$ were considered statistically significant (Data values are mean ± SD, n = 3).

3.2.4 Combinatorial assays with 17-AAG and sihsp90α inhibits tumour growth in U87-MG but does not affect SVGp12 cell viability

To determine the cell viability, U87-MG and SVGp12 cells were treated with 17-AAG and sihsp90α simultaneously for concurrent combinatorial assay. Both gene silencing and protein inhibitor approaches showed dramatic reduction in cell viability in U87-MG (Figure 3.2.5A). Data showed that sihsp90α, 17-AAG and a combination of sihsp90α/ 17-AAG reduced cell viability by 27, 75 and 88% after 72 h, respectively. Cytotoxic effects of 17-AAG, as a single agent, far exceeded the cytotoxic effects shown by sihsp90α at either 48 or 72 h. 17-AAG restricted tumour growth to 51 and 25% and sihsp90α treatment impaired tumour growth to 89 and 73% after 48 and 72 h, respectively. To determine the therapeutic potential of this combination treatment, non-tumourigenic cell line SVGp12 was treated with sihsp90α and 17-AAG for 48 and 72 h (Figure 3.2.5B). Neither of the treatments significantly reduced SVGp12 cell viability after 48 or 72 h, thus demonstrating the tumour-specific targeting of this combination treatment.

To assess whether there was significant difference between sequential and concurrent assays using sihsp90α and 17-AAG on growth inhibition, the cytotoxic effects of U87-MG cells treated sequentially with sihsp90α and 17-AAG were compared to cells that received concurrent administration. No significant difference was observed on the cell viability as well as the gene knockdown (Figure 3.2.6A & B).

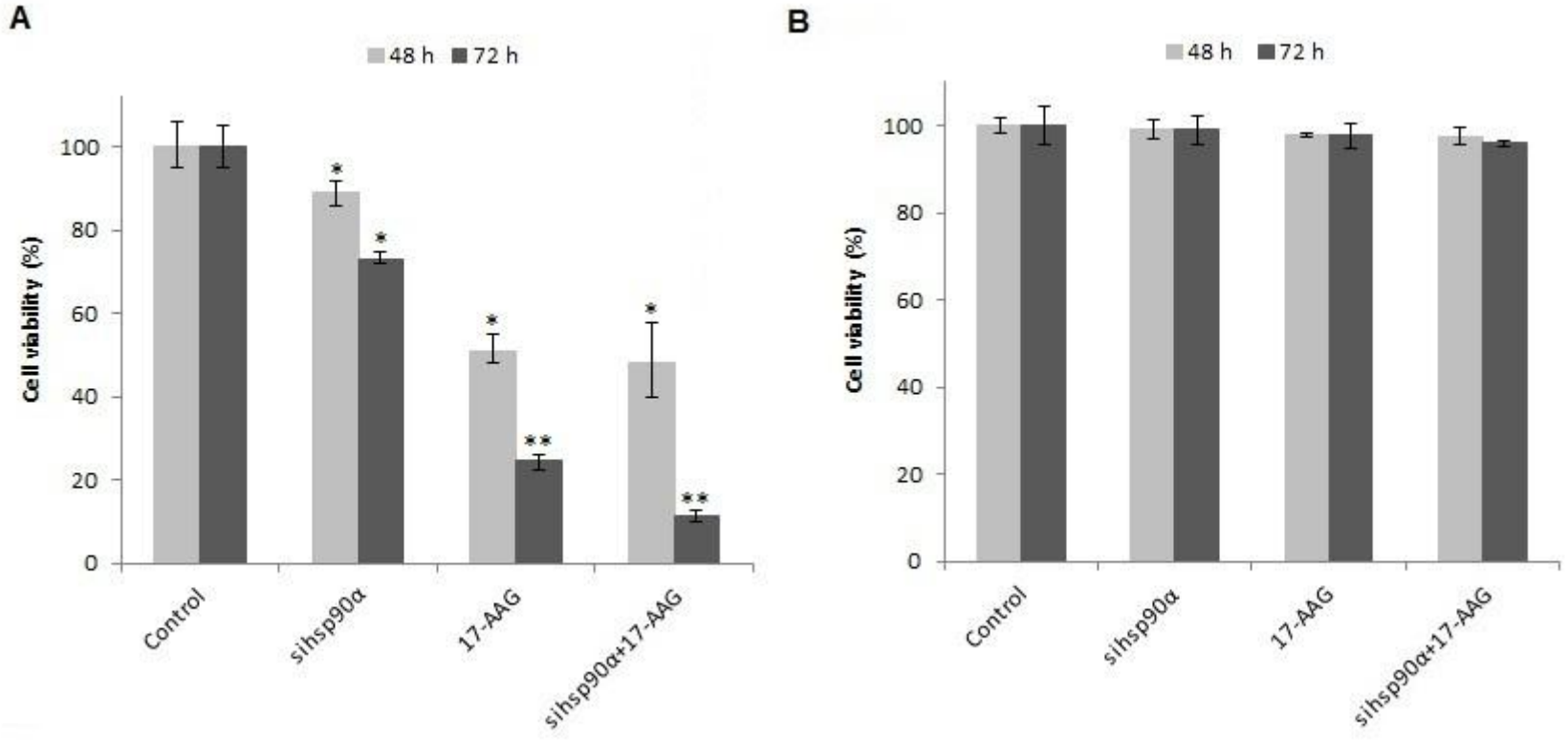

Figure 3.2.5: 17-AAG and sihsp90α effect on cell viability *in vitro*. Cell viability was monitored after cells treated with 17-AAG and sihsp90α after 48 h and 72 h in (A) U87-MG and (B) SVGp12. Control represent untreated cells, sihsp90α represent cells treated with *hsp90α* specific siRNA. sihsp90α+17-AAG represent concurrent assays where the cells were treated with 17-AAG and sihsp90α for either 48 or 72 h. *$p \leq 0.05$ and **$p \leq 0.001$ were considered statistically significant (Data values are mean ± SD, n = 3).

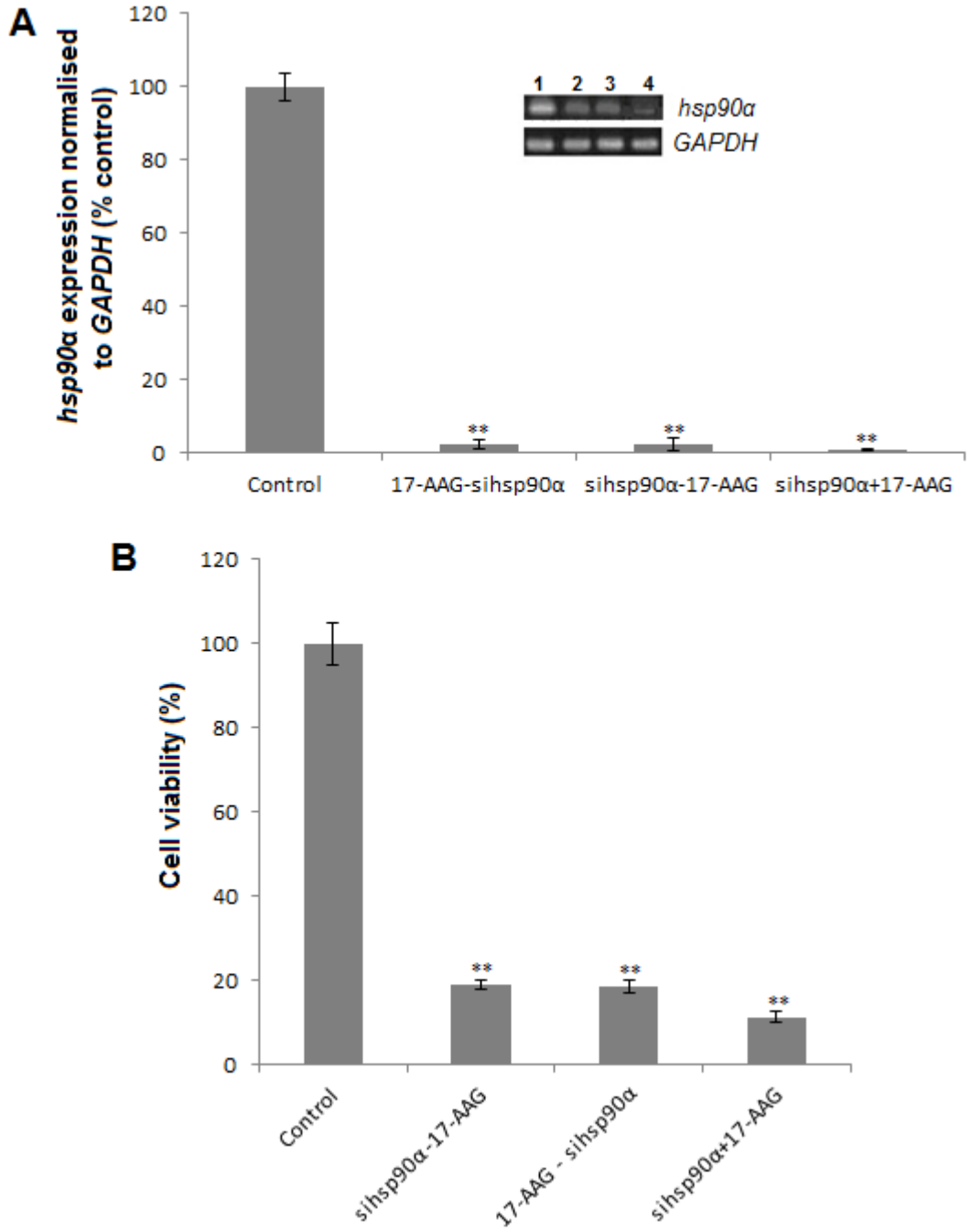

Figure 3.2.6: There is no significant difference between concurrent and sequential assays. sihsp90α-17-AAG represent sequential assays where the cells were treated with sihsp90α for 24 h followed by 17-AAG for 48 h and vice versa in case of 17-AAG-sihsp90α. 17+si represent concurrent assays where the cells were treated with 17-AAG and sihsp90α for 72 h. Lane (1) represents Control, (2-3) 17-AAG-sihsp90α and sihsp90α-17-AAG and (4) sihsp90α+17-AAG. *$p \leq 0.05$ and **$p \leq 0.001$ were considered statistically significant (Data values are mean ± SD, n = 3).

3.2.5 sihsp90α does not synergize with 17-AAG treatment in U87-MG cell line

The ability of sihsp90α to synergize with 17-AAG in U87-MG was examined. The efficacy of the concurrent assay with 17-AAG and sihsp90α was assessed using interaction ratios generated by a ratio of the observed growth inhibition following treatment with both compounds versus growth inhibition using either compound independently. A ratio of 1 indicates additive growth inhibition, a ratio greater than 1 demonstrates synergistic growth inhibition, while a ratio less than 1 suggests sub-additive effects on growth inhibition (Sauvageot *et al.*, 2009). The interaction ratio calculated for concurrent treatments in this study are listed in Table 3.2.2. The results indicate that the addition of sihsp90α to 17-AAG does not provide additional efficacy on growth inhibition in glioblastoma. However, the data indicates a strong correlation between Hsp90α mRNA and protein expression, Akt expression levels and cell viability in GBM (Table 3.2.3).

Table 3.2.2: sihsp90α does not synergize with 17-AAG treatment in U87-MG. The efficacy of the concurrent assay with 17-AAG and sihsp90α was assessed using interaction ratios generated by a ratio of the observed growth inhibition following treatment with both compounds versus growth inhibition using either compound independently. The data values are mean, ± SD, n = 3. *$p \leq 0.05$ was considered statistically significant.

Interaction ratio after	sihsp90α alone	17-AAG alone
48 h	4.62 ± 1.35 *	1.05 ± 0.11
72 h	3.28 ± 0.19 *	1.18 ± 0.29

Table 3.2.3: There was a strong correlation between Hsp90α mRNA expression levels, Akt activity and cell viability in GBM.

	hsp90α **mRNA expression normalised to *GAPDH* (%)**	**% Akt/PKB kinase activity**	**% Cell viability**
Control			
48 h	100 ± 4.78	100 ± 3.5	100 ± 5
72 h	100 ± 3.78	100 ± 2.5	100 ± 4.5
sihsp90α			
48 h	4.4 ± 1.29	59.3 ± 3.8	89 ± 3
72 h	44.6 ± 3.79	105.1 ± 0.79	73 ± 1.5
17-AAG			
48 h	5.3 ± 1.47	62.7 ± 0.48	51 ± 3.5
72 h	13.6 ± 2.25	61.1 ± 3.4	24.8 ± 1.9
sihsp90α+17AAG			
48 h	0.9 ± 0.07	47.3 ± 0.91	48 ± 9
72 h	0.8 ± 0.05	43 ± 1.28	11.3 ± 1.5

3.3 The Effects of Tat-delivered sihsp90α in combination with 17-AAG in GBM

3.3.1 Tat peptide effectively binds to sihsp90α but Cyt $c^{77\text{-}101}$ and C105Y peptides do not

To determine whether the CPPs interact efficiently with sihsp90α, a gel shift assay was performed. Increasing concentrations of the CPPs ranging from 0.2 µM to 4 µM for Tat and 0.2 µM to 10 µM for Cyt $c^{77\text{-}101}$ and C105Y were incubated with sihsp90α (200 nM) for 30 min. Tat peptide was able to bind to the sihsp90α in a dose-dependent manner and was observed to be completely retarded at 15-fold Tat molar excess compared to sihsp90α, characterised by movement of the band up on the gel (Figure 3.3.1A). Both Cyt $c^{77\text{-}101}$ and C105Y peptide did not completely retard sihsp90α at concentrations up to 50-fold peptide molar excess with 30 min incubations (Figure 3.3.1B). To determine whether increasing concentration and incubation time facilitated effective siRNA/peptide complex formation, sihsp90α was incubated with Cyt $c^{77\text{-}101}$ and C105Y at concentrations up to 100-fold peptide molar excess for 1 and 2 h at 37°C. Figure 3.3.1B showed that higher peptide concentrations of Cyt $c^{77\text{-}101}$ and C105Y had no significant effect on siRNA/peptide complex formation since no gel shift was observed. Subsequently, Cyt $c^{77\text{-}101}$ and C105Y peptide were considered redundant for this particular study and were discontinued from further analysis.

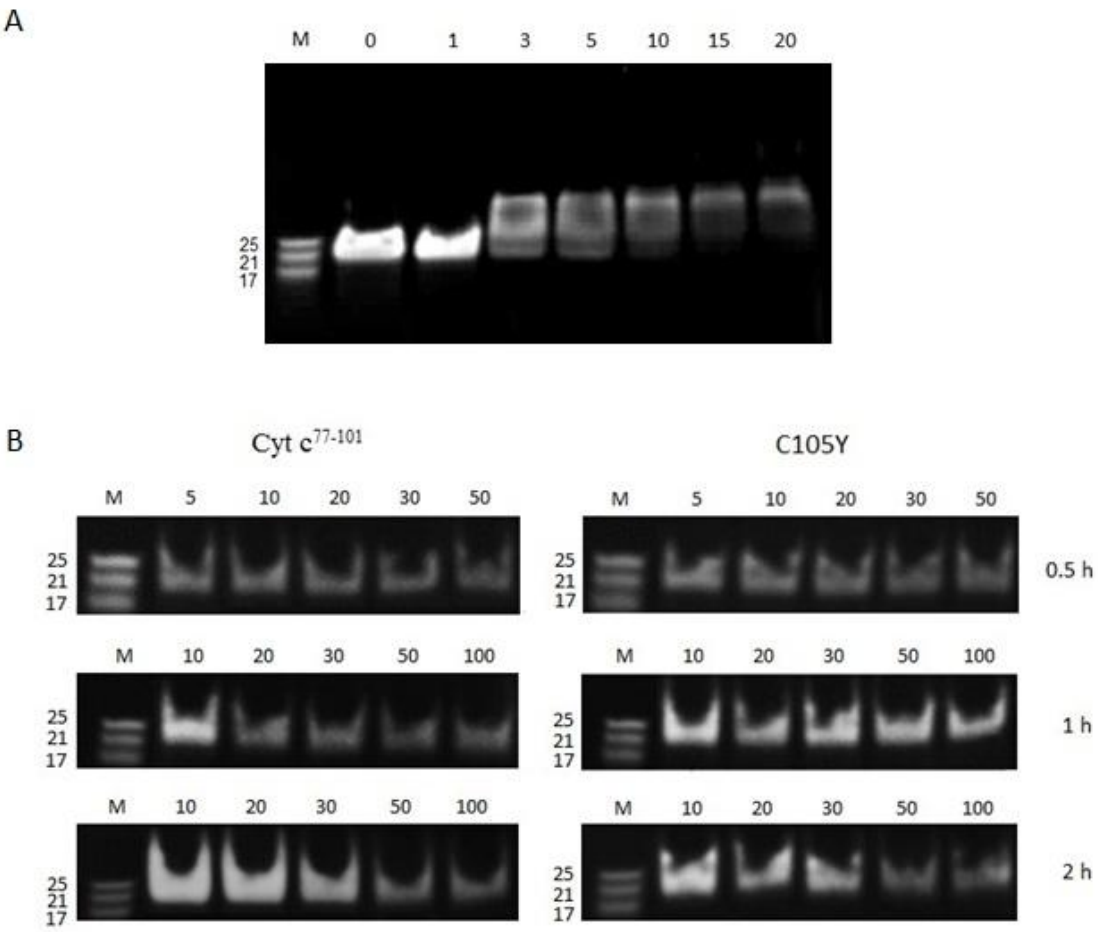

Figure 3.3.1: PAGE gel shift assay to assess the ability of Tat, Cyt $c^{77\text{-}101}$ and C105Y peptides to form complexes with sihsp90α. Increasing concentrations of the Tat peptides were added ranging from equimolar peptide compared with the siRNA to a 20-fold molar excess (A). As the peptide concentration increases the siRNA retardation increases and at 15-fold Tat molar excess almost all siRNA was completely retarded. Cyt $c^{77\text{-}101}$ and C105Y were incubated with increasing concentrations of peptide ranging from 5- to 100-fold peptide molar excess to siRNA at three different incubations 30 min, 1 h and 2 h (B). Lane M represents siRNA marker and 0 represents siRNA alone. This is representative of three independent experiments.

3.3.2 Serum stability of siRNA *in vitro*

Stability studies were performed to characterise the susceptibility of the aqueous and complexed siRNA used in this study to human serum as examined by polyacrylamide gel electrophoresis. When incubated with human serum (50%) aqueous siRNA was unstable in serum after 1 h and exhibits complete degradation after 6 h (Figure 3.3.2A). A control without any serum shows presence of siRNA after 24 h which also confirms that the oligonucleotide is 21 bp long. In an attempt to improve sihsp90α stability in serum, sihsp90α/Tat complexes were formed for 30 min as described previously and incubated in 50% human serum for up to 36 h. The sihsp90α integrity was analysed on 15% TBE polyacrylamide gel. At 15-fold Tat molar excess sihsp90α was stable for 6 h which is similar to stability of aqueous sihsp90α. However, 30-fold Tat excess improved the sihsp90α stability as stable sihsp90α was observed after 24 h (Figure 3.3.2B). Further increasing the concentration of Tat peptide to 50-fold excess of sihsp90α was associated with sihsp90α remaining intact after 36 h (Figure 3.3.2B).

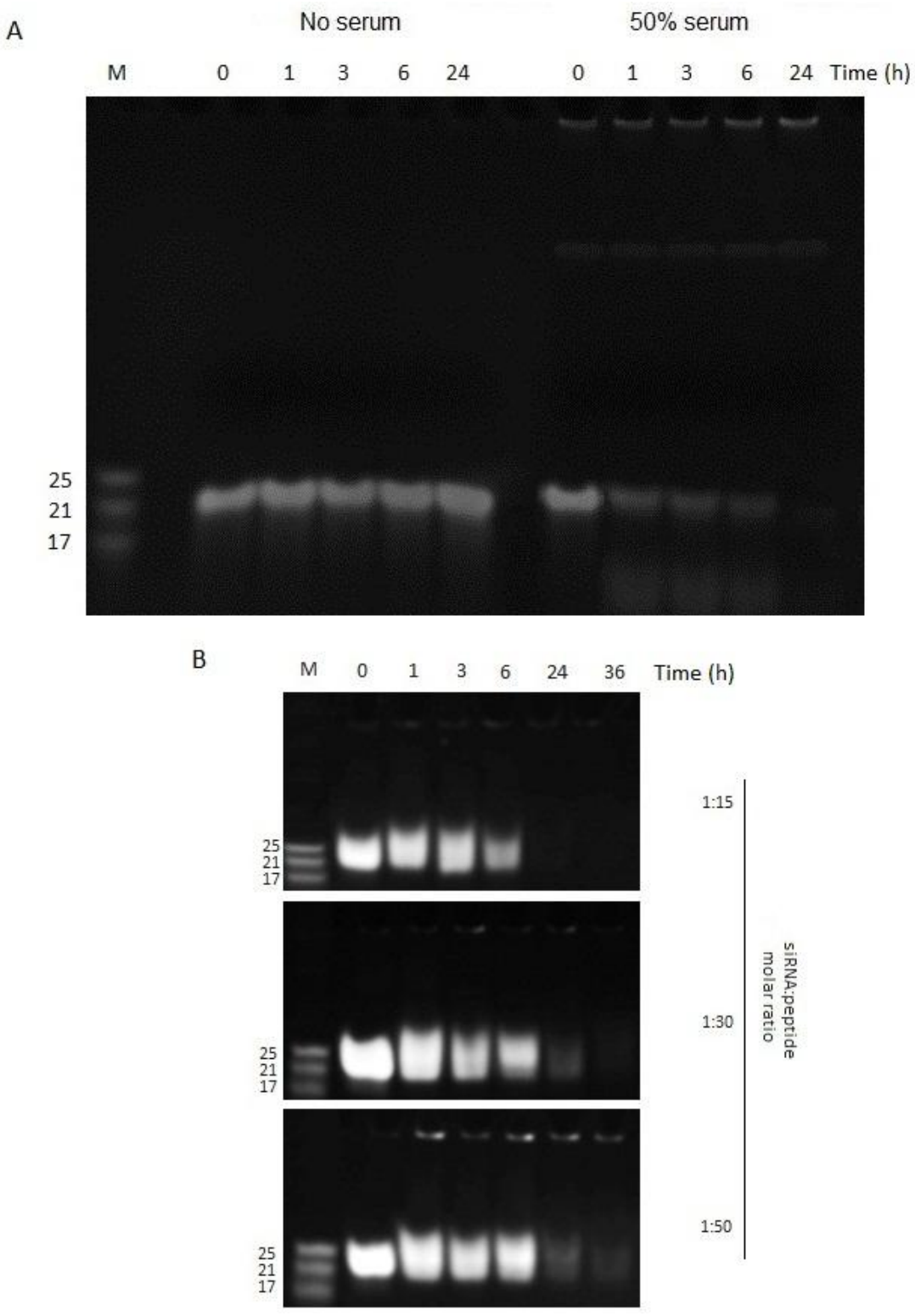

Figure 3.3.2: Stability of aqueous sihsp90α and sihsp90α/Tat complexes in 50% human serum. Serum stability of aqueous sihsp90α was assessed in 50% human serum (A). sihsp90α incubated without serum was used as control. sihsp90α/Tat complexes were incubated in 50% human serum for up to 36 h and stability of sihsp90α assessed on 15% polyacrylamide gel (B). At 15-fold peptide molar excess, sihsp90α was stable for 6 h, at 30-fold peptide molar excess stable sihsp90α was noted after 24 h. At 50-fold peptide molar excess, sihsp90α was stable after 36 h.

3.3.3 sihsp90α/Tat complexes did not induce membrane leakage in U87-MG or SVGp12 cells

To determine whether Tat peptide alone or complexed to sihsp90α exhibited potential toxic side effects, membrane disturbance was studied in U87-MG and SVGp12 cells. An LDH leakage assay was used to measure the acute membrane disturbance 30 min after treatment with Tat alone or sihsp90α/Tat complexes. Tat did not significantly affect membrane integrity up to 10 µM after which approximately 15% membrane leakage was induced at 20 µM rendering Tat redundant at concentrations higher than 10 µM (Figure 3.3.3A & B). Moreover, Tat demonstrates slightly higher LDH leakage as a multi-peptide complexed with sihsp90α compared to when used independently. In non-tumourigenic cells (SVGp12), Tat showed no significant effect on membrane integrity at concentrations up to 20 µM when used alone or at 100-fold Tat excess to sihsp90α.

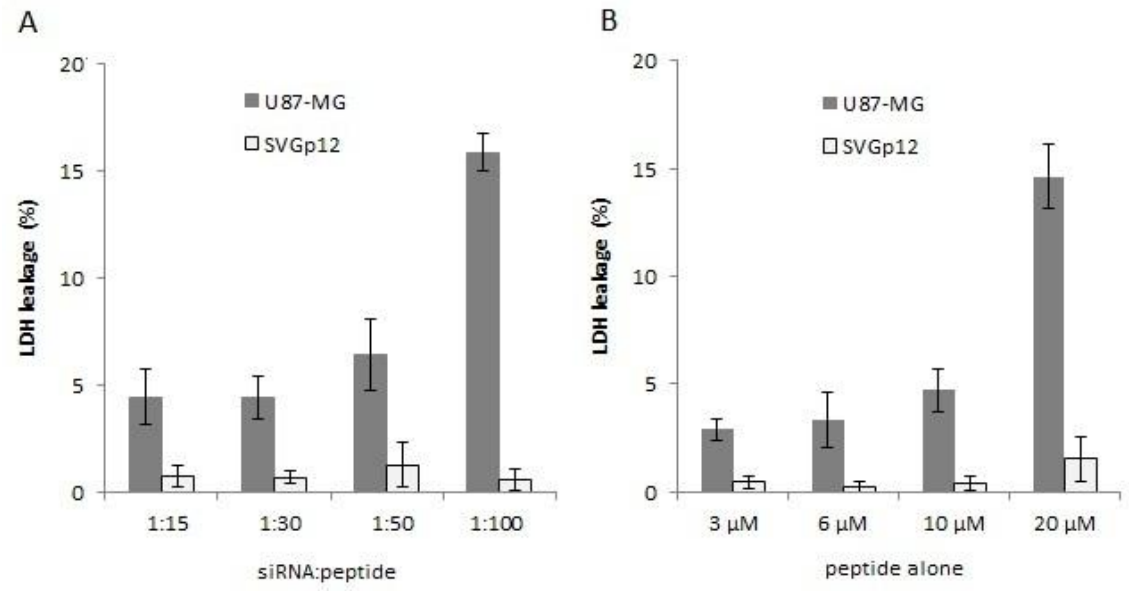

Figure 3.3.3: Membrane integrity analysis using Tat peptide with or without sihsp90α. Both U87-MG and SVGp12 cells were incubated with Tat at 15-, 30-, 50- and 100-fold peptide molar excess to sihsp90α (A), which corresponds to final peptide concentration of 3, 6, 10 and 20 µM when used without siRNA (B). Tat induced LDH leakage (~15%) only at 100-fold peptide excess to siRNA or 20 µM when used alone in U87-MG; LDH leakage in SVGp12 was negligible. Untreated cells were defined as control and LDH was released using Lysis solution to yield 100% LDH leakage. This is representative of three such independent experiments, data values are mean ± SD.

3.3.4 Tat mediated si-FAM delivery *in vitro* increases with peptide concentration

To examine whether the siRNA/Tat complexes increased cellular siRNA uptake *in vitro*, fluorescently labelled siRNA (si-FAM) was utilized for uptake and localisation studies. Firstly, the ability of Tat to form complexes with si-FAM was assessed by gel shift assay. The lowest molar ratio (siRNA:peptide) used for this assay, predetermined by complete complex formation using gel shift, was 15-fold peptide molar excess compared to sihsp90α (Figure 3.3.1A). All si-FAM (200 nM) formed complexes with Tat peptide at 15-fold peptide molar excess demonstrating corresponding retardation

efficiency for both sihsp90α and si-FAM (Figure 3.3.4). si-FAM/Tat complexes were then used for uptake study at increasing concentrations of up to 50-fold peptide molar excess compared to si-FAM. Cells transfected with si-FAM/Tat complexes exhibited efficient si-FAM cellular uptake in a concentration-dependent manner. Cellular uptake of si-FAM/Tat complexes by U87-MG and SVGp12 cells using 15-, 30- and 50-fold peptide molar excess are listed in Table 3.3.1. High si-FAM uptake was noted in U87-MG as compared to SVGp12 cells. Free si-FAM was not internalised by U87-MG or SVGp12 cells as seen by confocal microscopy (Figure 3.3.5 & 3.3.6).

3.3.5 Localisation of si-FAM/Tat complexes in glioblastoma and non-tumourigenic cells

The ability of Tat peptide to efficiently transfect U87-MG and SVGp12 cells with si-FAM was examined utilizing confocal microscopy. Increasing concentrations of Tat peptide were used with si-FAM and its effects on intracellular localisation and distribution of siRNA was assessed. In U87-MG cells, at 15-fold peptide molar excess to si-FAM, siRNA was mainly located in the cytoplasm though nuclear localisation of si-FAM was also detected (Figure 3.3.5). Both cytoplasmic as well as nuclear localisation of si-FAM was observed at 30-fold peptide molar excess to si-FAM. At 50-fold Tat peptide molar excess, although si-FAM was observed to localize to the cytoplasm, substantial accumulation of siRNA was noted in the nucleus (Figure 3.3.5). A diffused cytoplasmic uptake of si-FAM by SVGp12 cells (Figure 3.3.6) was noted at all si-FAM/peptide molar ratios indicating that cellular localisation of si-FAM was cell line dependent, however, the si-FAM uptake was dose-dependent and the si-FAM

uptake efficiency in SVGp12 cells was low in comparison to U87-MG cells (Table 3.3.1).

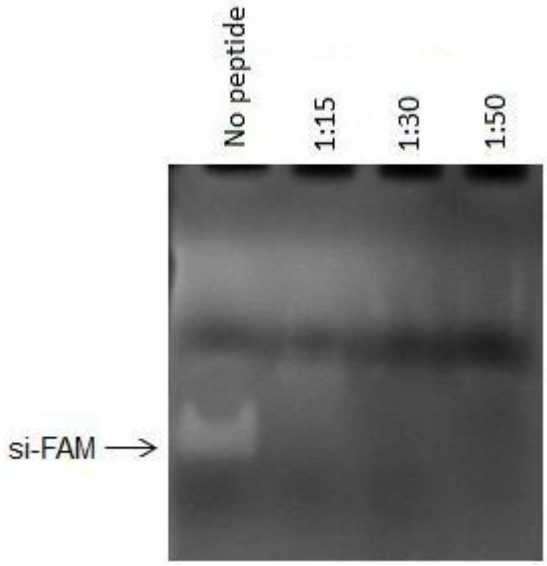

Figure 3.3.4: PAGE gel shift analysis using Tat peptide and si-FAM. The Tat peptide was used to assess whether si-FAM formed complexes with the peptide. The siRNA was completely retarded at 15-fold peptide molar excess. These preliminary results will allow the use of the si-FAM for siRNA uptake studies. This is typical of three such independent experiments.

Table 3.3.1: Tat efficiently delivers siRNA in U87-MG and SVGp12 cells in a dose-dependent manner. The siRNA/Tat complex uptake in U87-MG and SVGp12 cells was performed by counting 150 cells. The data is typical of three independent experiments, ± SD.

siRNA:Tat molar ratio	1:15	1:30	1:50	Free siRNA
si-FAM uptake in U87-MG (%)	48.1 ± 3.6	64.9 ± 6.0	73.9 ± 6.4	0
si-FAM uptake in SVGp12 (%)	32.8 ± 2.3	43.1 ± 3.1	46.0 ± 3.4	0

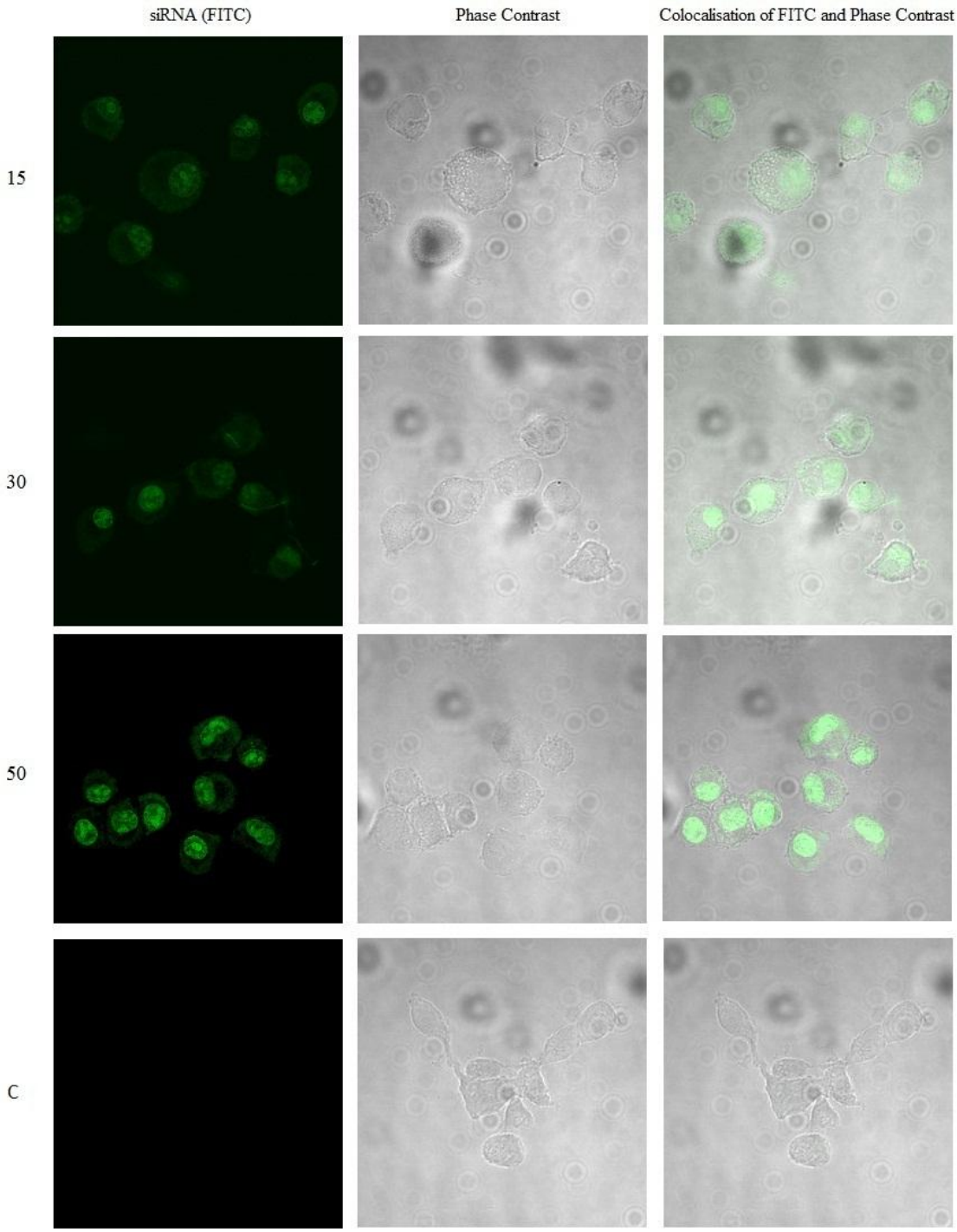

Figure 3.3.5: Uptake of si-FAM in U87-MG glioblastoma. si-FAM (200 nm) was mixed with increasing concentrations of Tat peptide giving rise to si-FAM/Tat molar ratios ranging from 1:15 to 1:50. Following 2 h incubation, the si-FAM uptake was assessed by confocal imaging. 15, 30 and 50 represents 15-, 30- and 50-fold peptide molar excess to siRNA, respectively. (C) represents control without peptide. This is typical of three such independent experiments.

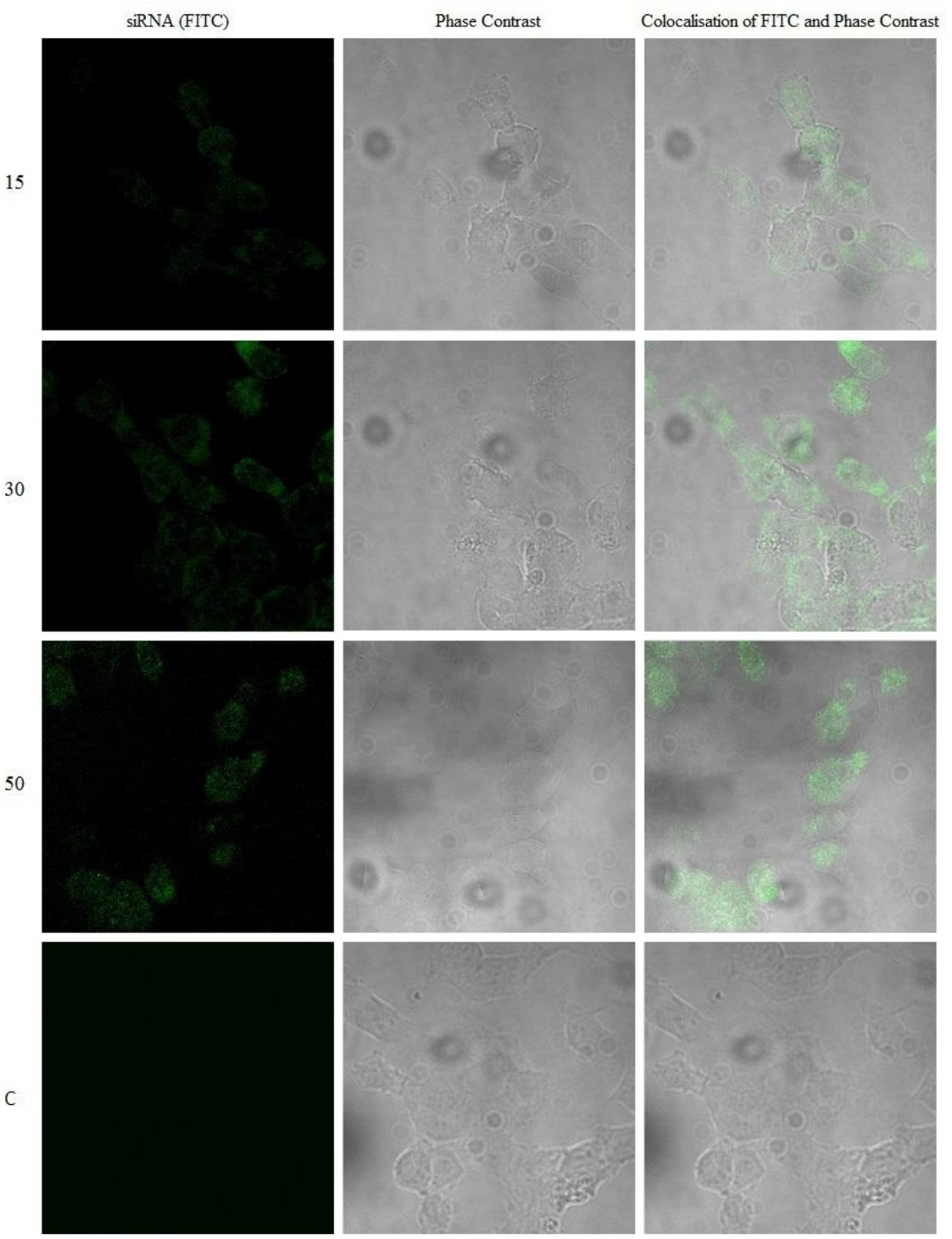

Figure 3.3.6: Uptake of si-FAM in SVGp12 cells. si-FAM (200 nm) was mixed with increasing concentrations of Tat peptide giving rise to si-FAM/Tat molar ratios ranging from 1:15 to 1:50. Following 2 h incubation, the si-FAM uptake was assessed by confocal microscopy. 15, 30 and 50 represents 15-, 30- and 50-fold peptide molar excess to siRNA, respectively. (C) represents control without peptide. This data is representative of three independent experiments.

3.3.6 sihsp90α–mediated *hsp90α* knockdown in glioblastoma and non-tumourigenic cells

The *hsp90α* and *GAPDH* gene expression levels were monitored to examine the gene silencing efficacy of sihsp90α/Tat complexes in glioblastoma U87-MG *in vitro*. The *hsp90α* mRNA levels showed are relative to *GAPDH* levels. The sihsp90α/Tat complexes showed significant *hsp90α* downregulation using 15, 30 and 50-fold Tat peptide molar excess to sihsp90α resulting in 75, 83 and 87% and 2, 12 and 10% gene knockdown after 24 and 48 h, respectively (Figure 3.3.7B). At 72 h post treatment, *hsp90α* silencing efficiency of sihsp90α/Tat complexes was 25 and 17% at 1:15 and 1:30.

The *hsp90α* gene expression was also investigated after treating cells with both sihsp90α/Tat complexes and 17-AAG *in vitro*, to assess whether the duration and magnitude of *hsp90α* mRNA knockdown was influenced. After 24 h, a combination of sihsp90α/Tat complexes and 17-AAG produced statistically significant *hsp90α* knockdown of 91, 93 and 95% at 15, 30 and 50-fold Tat peptide molar excess to sihsp90α, respectively ($p \leq 0.001$; Figure 3.3.7B). At 48 and 72 h, the combination treatment prompted significant *hsp90α* mRNA downregulation resulting in 33, 84 and 93% and 50, 65 and 78% mRNA knockdown after 48 and 72 h at 15, 30 and 50-fold Tat peptide molar excess to sihsp90α, respectively. All the qRT-PCR results were also validated by agarose gel electrophoresis (Figure 3.3.7A). The mRNA expression level of *GAPDH* was used as an internal standard for quantification in U87-MG cells and monitored to accurately determine the degree of downregulation. To examine whether Tat peptide itself attenuated RNAi efficacy, increasing concentrations of Tat peptide

were used (3, 6 and 10 μM). Intriguingly, cells treated with Tat exhibited a dose-dependent increase in *hsp90α* expression after 24, 48 and 72 h in U87-MG.

The *hsp90α* mRNA levels in non-tumourigenic cell line SVGp12 were quantitated to validate targeting *hsp90α* as a therapeutic approach. As seen in Figure 3.3.8B, negligible levels of *hsp90α* were detected at all time points in control as well as treated cells. The *hsp90α* expression in SVGp12 cells were expressed as relative to *GAPDH* expression. All the qRT-PCR results were validated using agarose gel electrophoresis (Figure 3.3.8A).

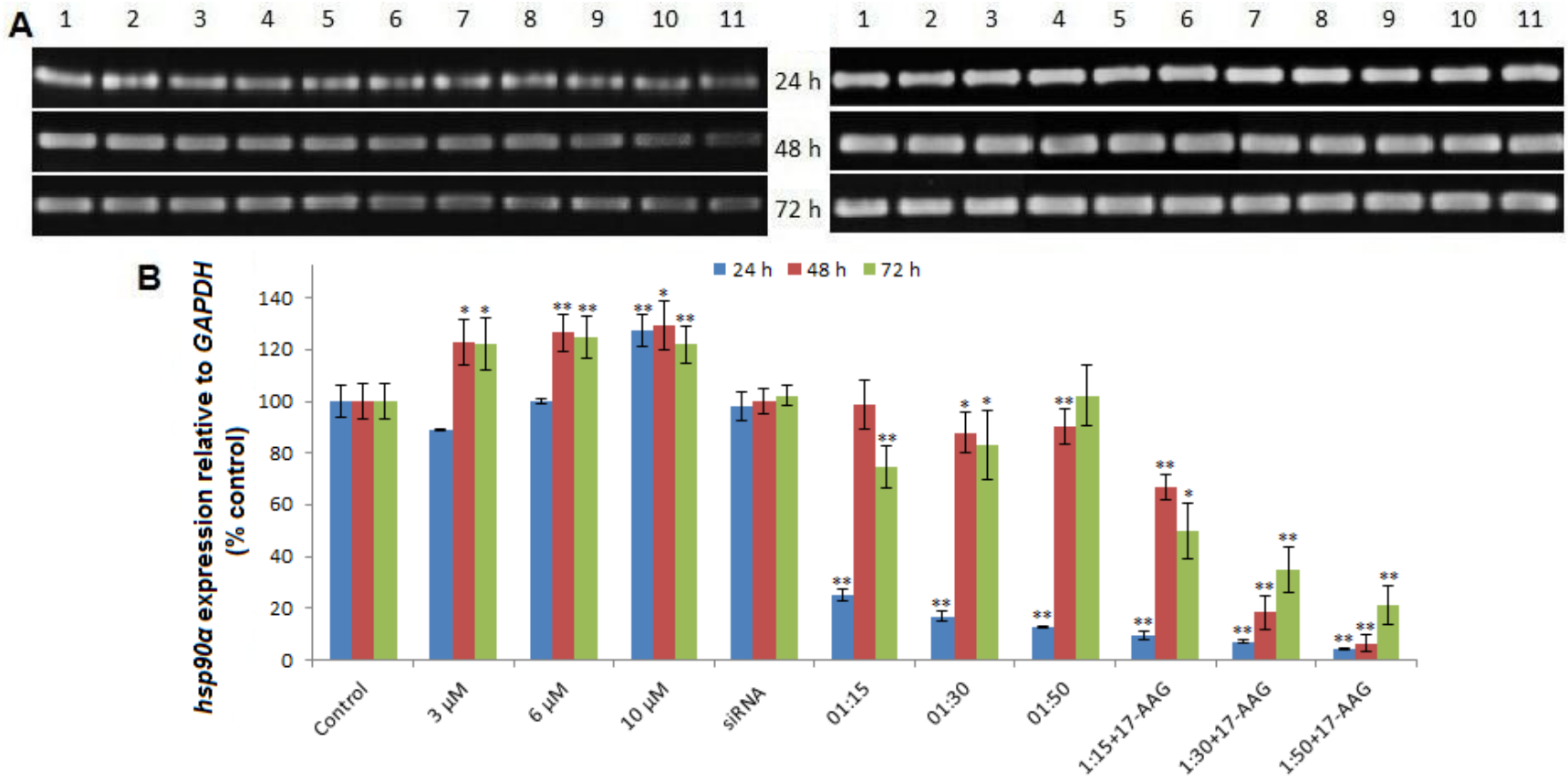

Figure 3.3.7: Effects of sihsp90α-mediated RNAi on *hsp90α* knockdown in U87-MG cells. mRNA expression levels of *hsp90α* and G*APDH* in U87-MG cells treated with sihsp90α and Hsp90 inhibitor 17-AAG were assessed by agarose gel electrophoresis (A) [*hsp90α* (left) and *GAPDH* (right)] and qRT-PCR (B) for *hsp90α* gene expression relative to *GAPDH* expression after 24, 48 and 72 h. Lane (1) Control; (2) 3 μM; (3) 6 μM; (4) 10 μM; (5) sihsp90α; (6) 1:15; (7) 1:30, (8) 1:50; (9) 1:15+17-AAG; (10) 1:30+17-AAG; (11) 1:50+17-AAG. 1:15-1:50+17-AAG represent combinatorial treatment where cells were transfected with sihsp90α and subsequently treated with 17-AAG (Data values are mean ± SD, n = 3). *$p \leq 0.05$ and **$p \leq 0.001$ were considered statistically significant.

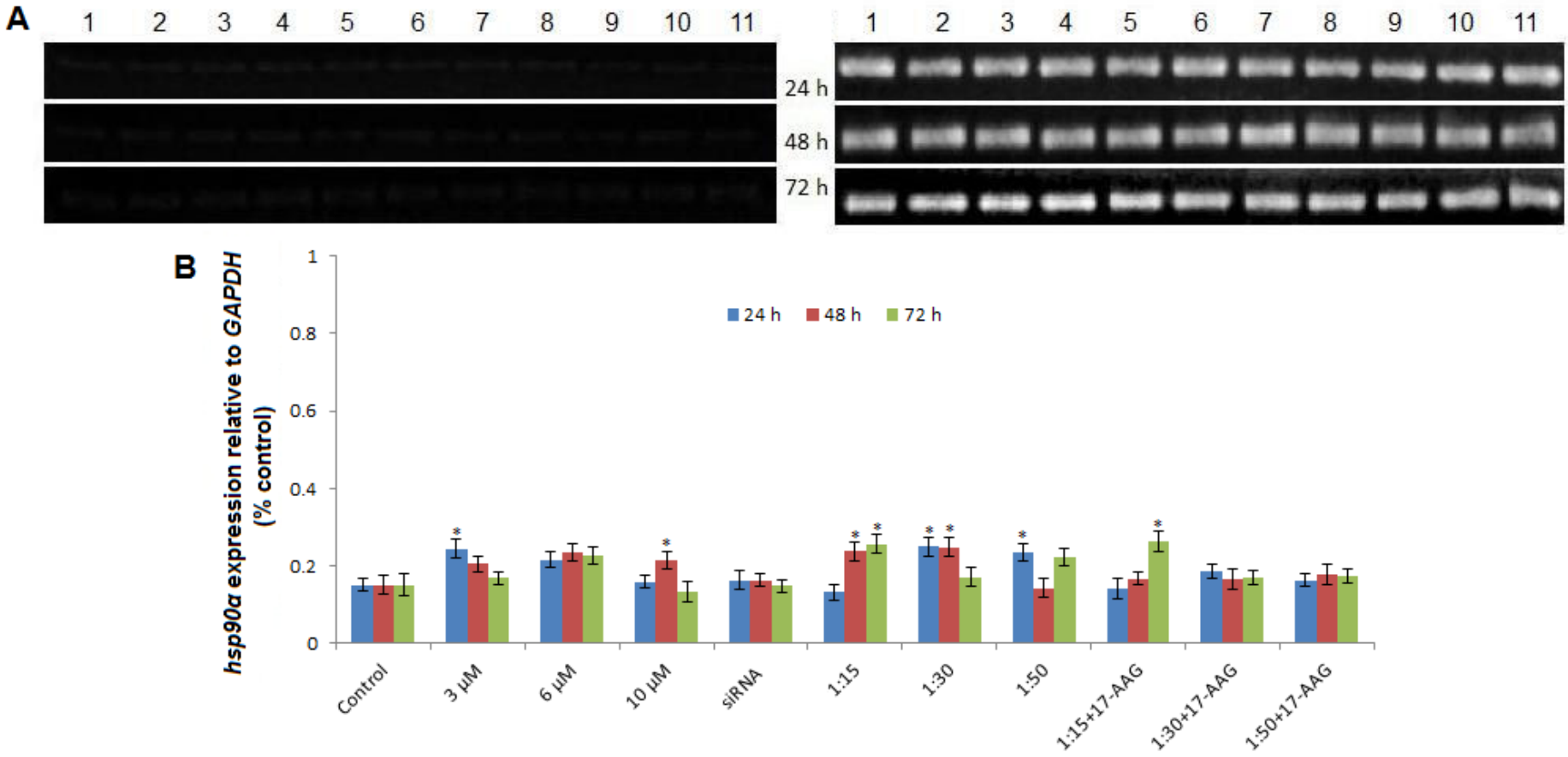

Figure 3.3.8: *hsp90α* mRNA expression levels in SVGp12 cells. mRNA expression levels of *hsp90α* and *GAPDH* in SVGp12 cells transfected with sihsp90α/Tat complexes and Hsp90 inhibitor 17-AAG were assessed by agarose gel electrophoresis (A) [*hsp90α* (left) and *GAPDH* (right)] and qRT-PCR (B), for *hsp90α* gene expression relative to *GAPDH* expression after 24, 48 and 72 h. Lane (1) Control; (2) 3 µM; (3) 6 µM; (4) 10 µM; (5) sihsp90α; (6) 1:15; (7) 1:30, (8) 1:50; (9) 1:15+17-AAG; (10) 1:30+17-AAG; (11) 1:50+17-AAG. 1:15-1:50+17-AAG represent combinatorial treatment where cells were transfected with sihsp90α and subsequently treated with 17-AAG (Data values are mean ± SD, n = 3). *$p \leq 0.05$ was considered statistically significant.

3.3.7 Hsp90α depletion in glioblastoma cells was subsequent to treatment with sihsp90α/Tat complexes and 17-AAG

Treatment with sihsp90α and 17-AAG showed significant effect on the transcriptional regulation *hsp90α* as shown previously. To determine whether the Hsp90α protein levels were influenced after the treatment, glioblastoma cells treated with sihsp90α and 17-AAG were analysed by immunocytochemistry. The cells were stained with fluorescently-labelled secondary antibody (FITC) specific to Hsp90α as shown in Figure 3.3.9. sihsp90α/Tat complexes significantly reduced Hsp90α protein levels after 24 and 48 h (Figure 3.3.9A & B) with significant Hsp90α downregulation achieved after 48 h, whereby Hsp90α expression was reduced by 84% (Table 3.3.2). The RNAi efficiency of sihsp90α diminished after 72 h post treatment as evident by the recurrence of Hsp90α expression in glioblastoma (Figure 3.3.9C). When sihsp90α transfection was accompanied with 17-AAG treatment, the cells exhibited significant reduction of Hsp90α levels after 24, 48 and 72 h. The combination treatment significantly reduced Hsp90α expression by 98, 99 and 95% after 24, 48 and 72 h, respectively. Glioblastoma cells treated with increasing concentrations of Tat alone showed no significant variation in Hsp90α expression after 24, 48 or 72 h.

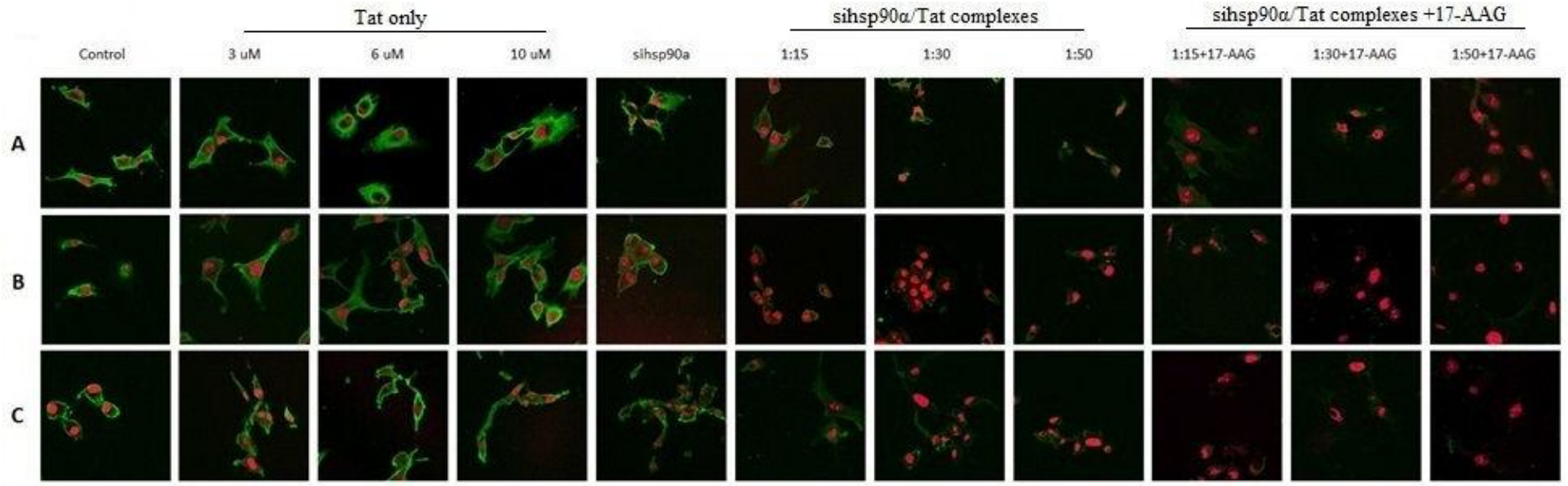

Figure 3.3.9: Hsp90α protein expression levels in U87-MG cells after treatment with sihsp90α and 17-AAG. The cells were stained with FITC conjugate secondary antibody bound to Hsp90α antigen (green) and propidium iodide (PI) to detect nucleus (red) at ×40 objective magnifications. A: 24 h; B: 48 h; C: 72 h. Hsp90α protein levels in U87-MG cells post treatment with sihsp90α/Tat complexes and 17-AAG after 24, 48 and 72 h has been listed (D). Hsp90α expression analysis using immunofluorescence was performed by counting 150 cells. 1:15-1:50+17-AAG represent combinatorial treatment where cells were transfected with sihsp90α and subsequently treated with 17-AAG. This data is representative of three independent experiments. *$p \leq 0.05$ was considered statistically significant.

Table 3.3.2 Treatment with sihsp90α/Tat complexes and 17-AAG reduces Hsp90α protein expression in U87-MG cells. This data is representative of three independent experiments. *$p \leq 0.05$ and **$p \leq 0.001$ were considered statistically significant.

Incubation period (h)	**24**			**48**			**72**		
Hsp90α expression (%)	Strong (++)	Weak (+)	Absent (–)	Strong (++)	Weak (+)	Absent (–)	Strong (++)	Weak (+)	Absent (–)
Control	71.7 ± 1.7	22.1 ± 2.7	6.3 ± 1.1	74.5 ± 2.3	23.2 ± 1.6	4.4 ± 1.3	73.2 ± 1.8	24.1 ± 0.6	2.8 ± 1.3
3 µM	76.6 ± 0.9*	16.5 ± 2.0*	7.4 ± 0.8*	74.0 ± 2.0	21.3 ± 0.7	5.4 ± 0.6	73.1 ± 1.1	24.7 ± 0.3*	2.8 ± 0.3
6 µM	76.0 ± 0.5*	18.7 ± 1.0	6.3 ± 0.4	74.1 ± 0.8	23.1 ± 0.7	5.2 ± 1.1*	72.0 ± 0.8	27.1 ± 0.9*	2.8 ± 0.2
10 µM	71.7 ± 2.5	22.3 ± 0.8	8.0 ± 0.2	74.8 ± 1.7	19.9 ± 0.2	5.3 ± 1.9	72.7 ± 2.9	26.5 ± 2.7	2.9 ± 0.2
sihsp90α	72.6 ± 1.4	19.3 ± 0.4	8.2 ± 0.9*	72.8 ± 2.7*	23.0 ± 1.2	4.3 ± 1.6	72.7 ± 0.7	25.2 ± 1.5	2.2 ± 0.8
1:15	40.2 ± 2.5**	34.9 ± 3.6*	25.0 ± 1.2**	27.3 ± 7.3*	43.6 ± 3.2*	29.2 ± 4.2*	30.8 ± 4.6**	58.7 ± 5.6*	10.5 ± 1.0**
1:30	34.9 ± 4.8*	37.1 ± 0.4*	27.9 ± 4.1*	22.2 ± 1.2**	44.5 ± 1.2**	33.9 ± 0.5**	33.2 ± 4.4**	57.2 ± 1.4**	9.8 ± 2.8*
1:50	38.2 ± 1.8**	37.0 ± 2.0**	24.9 ± 0.2**	16.0 ± 4.0**	45.9 ± 0.5**	38.2 ± 3.5**	26.0 ± 0.4**	57.2 ± 2.9*	11.8 ± 7.5
1:15 + 17-AAG	1.3 ± 1.1**	58.0 ± 1.3**	40.8 ± 2.6**	1.4 ± 0.7**	43.1 ± 4.8*	55.5 ± 4.1**	5.4 ± 2.7**	35.1 ± 3.2*	59.6 ± 5.9*
1:30 + 17-AAG	0.9 ± 0.8**	49.8 ± 2.0**	49.4 ± 2.8**	2.6 ± 2.3**	36.7 ± 0.1*	60.6 ± 2.7**	4.6 ± 3.7**	34.2 ± 3.2*	61.2 ± 6.9*
1:50 + 17-AAG	2.0 ± 1.8**	39.9 ± 1.4*	58.4 ± 3.5**	1.2 ± 1.0**	36.6 ± 3.8*	62.4 ± 4.9**	4.3 ± 2.2**	37.8 ± 2.2*	58.0 ± 6.5*

3.3.8 Effect of Hsp90α inhibition using sihsp90α and 17-AAG on Akt kinase activity in glioblastoma U87-MG cells

The Akt kinase activity, a Hsp90 client protein, was investigated to address whether sihsp90α and 17-AAG treatment altered the Akt kinase activity. Transfection of sihsp90α with Tat peptide reduced Akt activity to 58.1 and 69.9% after 24 and 48 h but the Akt activity was induced after 72 h (Figure 3.3.10). Combination treatment with sihsp90α and 17-AAG reduced Akt kinase levels to 49.7% at 50-fold Tat molar excess after 24 h ($p \leq 0.05$). Similarly, significant reduction in Akt kinase activity was noted after 48 and 72 h, as treated cells exhibit loss of Akt activity by 72.3 and 82.9% at 1:50 sihsp90α:peptide molar ratio ($p \leq 0.001$). Even at lower peptide concentrations (i.e. 1:15 and 1:30), a comparable and statistically significant reduction in Akt activity was produced after 48 and 72 h ($p \leq 0.05$). Interestingly, although uncomplexed Tat peptides were observed to reduce Akt activity after 24 h, Tat induced Akt activity to some extent after 48 and 72 h.

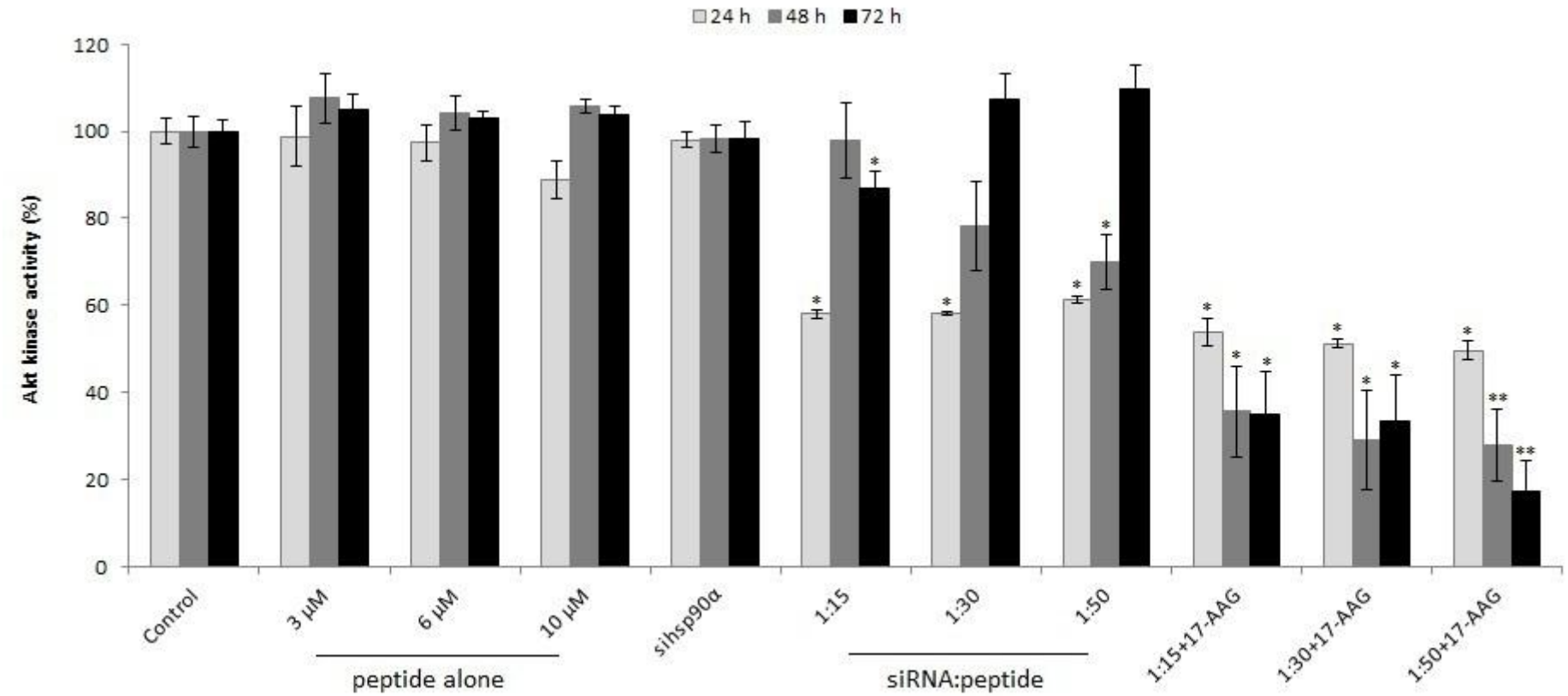

Figure 3.3.10: Hsp90α inhibition leads to loss of Akt/PKB kinase activity in glioblastoma. The Akt activity was deduced as the fraction of the observed Akt activity in treated samples relative to the total Akt activity in the untreated sample after 24, 48 and 72 h. 1:15-1:50+17-AAG represent combinatorial treatment where cells were transfected with sihsp90α and subsequently treated with 17-AAG. This data is typical of three independent experiments. Data values are mean ± SD, n = 3. *$p \leq 0.05$ and **$p \leq 0.001$ were considered statistically significant.

3.3.9 The effect of sihsp90α/Tat complexes on glioblastoma cell viability in combination with 17-AAG

To examine whether transfected cells exert a biological effect, U87-MG and SVGp12 cells were treated with increasing concentrations of sihsp90α/Tat complexes ranging from 1:15-1:50 (mol sihsp90α:mol peptide) and 17-AAG (0.225 μM) as established previously. sihsp90α/Tat complexes, even at the highest concentration was found not to be cytotoxic to glioblastoma cells at 24 h and 72 h post treatment. In contrast, after 48 h the sihsp90α/Tat complexes showed a dose-dependent reduction in U87-MG cell viability with significant cytotoxic effects achieved at 1:30 and 1:50 sihsp90α:peptide molar ratio whereby up to 20% tumour cell growth inhibition was recorded ($p \leq 0.05$). sihsp90α/Tat complexes together with 17-AAG significantly reduced tumour growth by 41.2, 88.2 and 83.2% after 24, 48 and 72 h, respectively ($p \leq 0.001$; Figure 3.3.11). To examine whether Tat peptide itself influenced sihsp90α-mediated cytotoxicity in glioblastoma, increasing concentrations of Tat peptide were used (3, 6 and 10 μM), which corresponded to 1:15, 1:30 and 1:50 when complexed with sihsp90α (sihsp90α:peptide). Tat peptide demonstrated no long-term toxic side effects in U87-MG cells at all time points examined. sihsp90α/Tat complexes demonstrated no significant cytotoxic effects in SVGp12 cells (Figure 3.3.12). A combination of sihsp90α/Tat complexes and 17-AAG was found to induce no more than 9.3% cell death at any of the time points examined, although this was not significant. In addition, Tat peptide did not exhibit long-term toxicity in SVGp12 cells after 24, 48 or 72 h. Based on the findings from this study, a clear correlation between the Hsp90α mRNA and protein expression profiles, Akt activity and cell viability was observed in glioblastoma (Table 3.3.2 and 3.3.3).

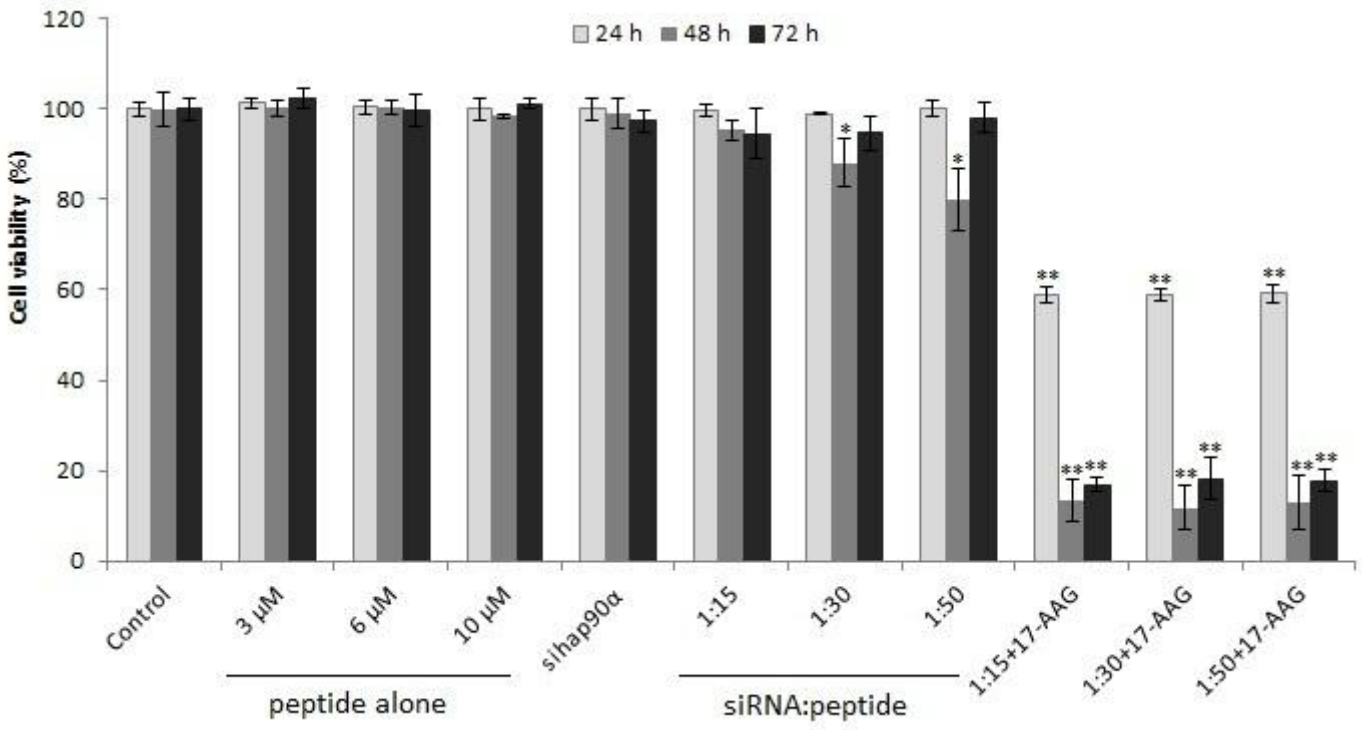

Figure 3.3.11: Cytotoxicity associated with sihsp90α/Tat and 17-AAG in U87-MG. 1:15-1:50+17-AAG represent combinatorial treatment where cells were transfected with sihsp90α and subsequently treated with 17-AAG. sihsp90α represent cells treated with sihsp90α alone without delivery vector. This data is typical of three independent experiments, the values are mean ± SD. *$p \leq 0.05$ and **$p \leq 0.001$ were considered statistically significant.

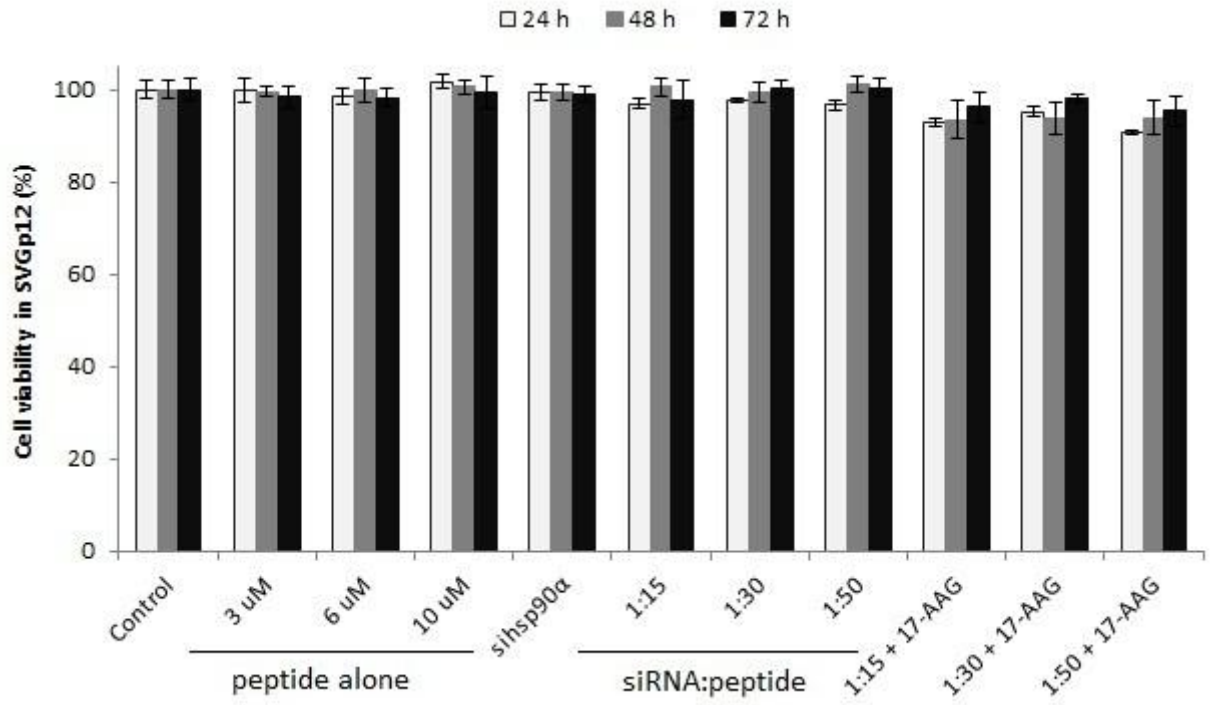

Figure 3.3.12: The effect of sihsp90α/Tat peptide complexes and 17-AAG on non-tumourigenic cell viability. 1:15-1:50+17-AAG represent combinatorial treatment where cells were transfected with sihsp90α and subsequently treated with 17-AAG. sihsp90α represent cells treated with sihsp90α alone without delivery vector. This data is typical of three independent experiments, the values are mean ± SD.

Table 3.3.3: The correlation profile between Hsp90α mRNA and protein expression levels compared to the Akt kinase activity and cell viability in glioblastoma. The data values are mean, ± SD, n = 3.

	sihsp90α:Tat molar ratio	*hsp90α* mRNA/100 ng Cells Extract (1 x 10^6 cells)			% Akt/PKB Kinase Activity			% Cell Viability		
		24 h	48 h	72 h	24 h	48 h	72 h	24 h	48 h	72 h
Control		8093 ± 770	7915 ± 763	7709 ± 767	100.0 ± 3.0	100.0 ± 3.5	100.0 ± 2.7	100.0 ± 1.7	100.0 ± 3.9	100.0 ± 2.6
Tat peptide alone	3 µM	6719 ± 51	10357 ± 2393	10197 ± 2752	98.7 ± 6.8	107.6 ± 5.5	104.9 ± 3.6	101.4 ± 1.2	100.2 ± 1.7	102.4 ± 2.4
	6 µM	7874 ± 118	10768 ± 2356	10546 ± 2112	97.3 ± 4.2	104.2 ± 3.9	103.0 ± 1.5	100.4 ± 1.7	100.3 ± 1.5	99.8 ± 3.6
	10 µM	7696 ± 656	11245 ± 2745	10198 ± 1987	88.9 ± 4.3	105.6 ± 1.6	103.6 ± 2.3	100.1 ± 2.4	98.4 ± 0.2	101.2 ± 1.3
sihsp90α alone		7525 ± 747	7891 ± 689	7855 ± 712	98.1 ± 1.7	98.2 ± 3.2	98.4± 3.7	100.0 ± 2.4	99.2 ± 3.4	97.3 ± 2.4
sihsp90α/Tat complexes	1:15	1781 ± 240	7095 ± 891	6275 ± 1038	58.1 ± 0.9	97.8 ± 7.7	86.6 ± 3.7	99.7 ± 1.4	95.3 ± 2.2	94.4 ± 5.6
	1:30	1216 ± 222	6907 ± 980	7014 ± 1362	58.2 ± 0.4	78.3 ± 8.5	106.0 ± 5.9	98.9 ± 0.3	88.1 ± 5.4	94.7 ± 3.9
	1:50	1156 ± 60	6639 ± 832	8120 ± 1522	61.3 ± 0.9	69.9 ± 6.3	109.5 ± 5.8	100.2 ± 1.7	80.0 ± 6.8	98.0 ± 3.2
sihsp90α/Tat + 17-AAG	1:15	723 ± 191	5177 ± 603	4082 ± 983	53.7 ± 3.1	35.5 ± 8.3	34.9 ± 8.1	59.1 ± 1.8	13.3 ± 4.7	16.8 ± 1.5
	1:30	488 ± 70	1594 ± 686	2939 ± 910	51.2 ± 1.1	29.0 ± 8.6	33.3 ± 8.6	58.8 ± 1.3	11.8 ±4.9	18.2 ± 4.8
	1:50	352 ± 77	577 ± 479	1930 ± 931	49.7 ± 2.2	27.7 ± 7.3	17.1 ± 7.2	59.2 ± 2.1	13.0 ± 6.0	17.7 ± 2.4

3.4 Gene silencing and protein inhibition of Hsp90α and its implications *in vivo*

3.4.1 Weight loss assessment in mice surgically implanted with tumour cells

After surgery, the mice (n = 22) were weighed on a frequent basis to monitor tumour growth. The first sign of tumour growth in mice is usually indicated by weight loss as shown in Figure 3.4.1. However, the initial dip in weight loss observed is due to anaesthesia. Recovery in weight was observed within 10 days, after that time the loss in weight was permanent indicating tumour growth.

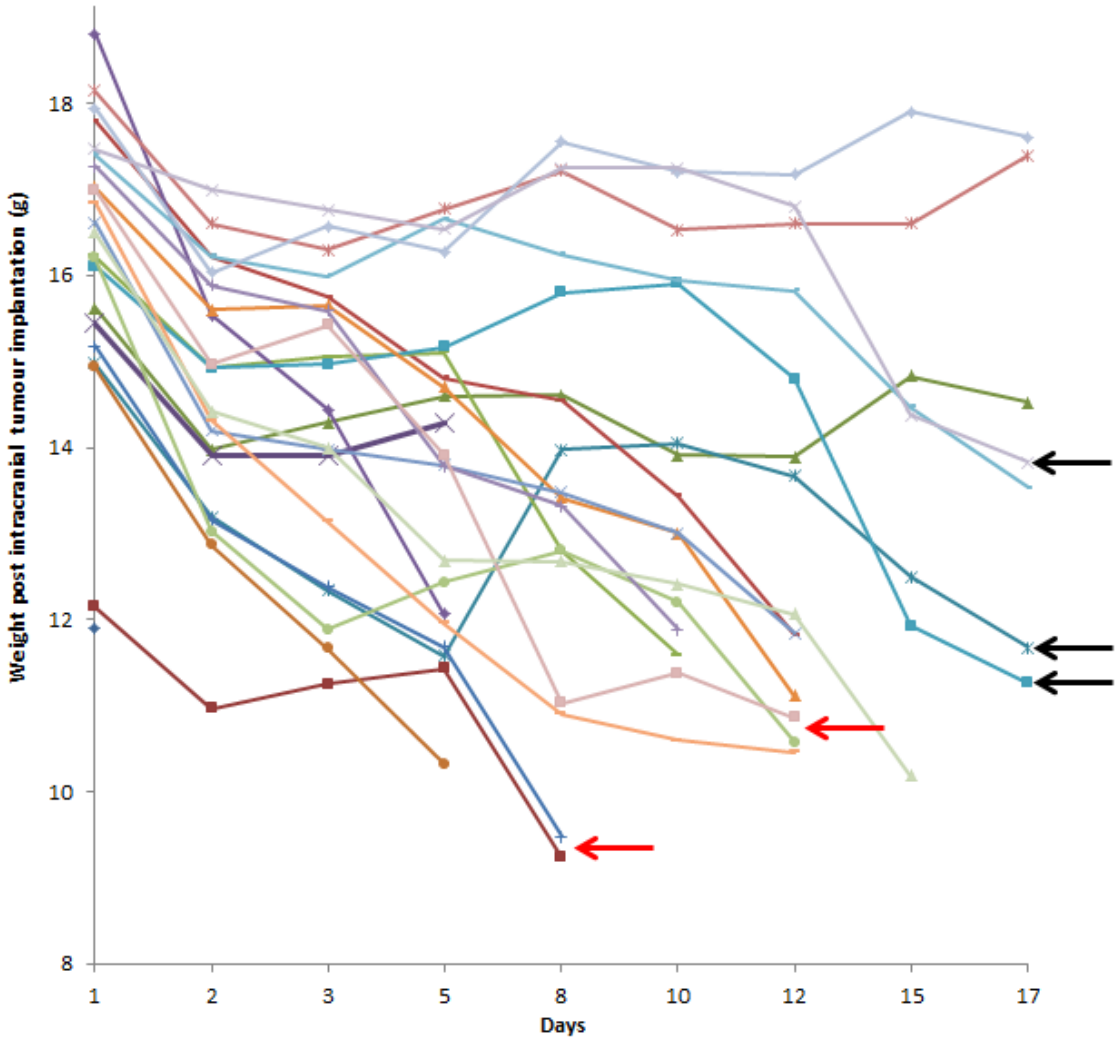

Figure 3.4.1: Weight loss assessment in mice implanted with U87-MG-luc2 cells. Each curve represents weight loss pattern in each of the 22 mice implanted with tumour cells. A typical weight loss profile in mice is characterised by two dips indicated by black arrows, the first dip is the effect of anaesthesia and the second dip observed after 10 days post tumour implantation indicates tumour growth. The red arrows indicate mice that died before the treatment with siRNA and 17-AAG on day 17.

3.4.2 siluc/Tat complexes reduce luciferase activity *in vitro*

To determine whether Tat peptide effectively binds and delivers siluc into U87-MG-luc2 cells *in vitro*, siluc/Tat complexes were formed in serum-free EMEM with increasing concentration of Tat peptide at siluc:Tat molar ratios ranging from 1:15 to

1:50 and added to U87-MG-luc2 cells seeded 24 h prior to treatment. The luciferase activity in treated samples was reduced in a dose-dependent manner with upto 73% luciferase knockdown achieved after 24 h (Figure 3.4.2).

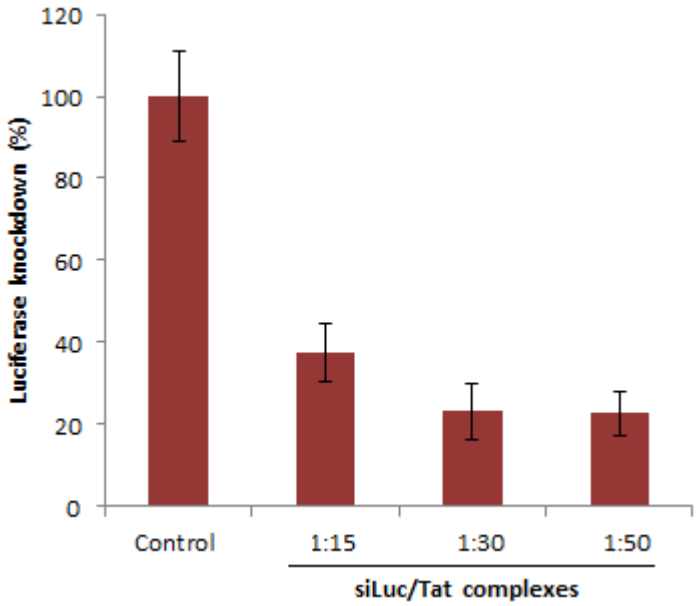

Figure 3.4.2: Luciferase activity in U87-MG-luc2 cells treated with siluc/Tat nanoparticles *in vitro*. The siluc/Tat complexes reduced luciferase expression in treated cells in a dose-dependent manner. This experiment was performed once in triplicate. The values represented are mean ± SD.

3.4.3 Luciferase quantitation and H&E staining confirm the presence of tumour growth *in vivo*

Following tumour implantation, the mice were weighed on a regular basis to study the weight loss pattern that indicates the presence of proliferating tumour. In addition, brain tissue specimens were collected on day 8 (n = 2) and 12 (n = 2) to further validate the presence of a tumour by H&E staining and luciferase quantitation. Stained sections of tumour specimen clearly showed the presence of a tumour resulting in distortion of the surrounding tissue (Figure 3.4.3A Left) in comparison to the normal brain specimen whereby the integrity was intact. Furthermore, luciferase expression in tumour and normal tissue was quantitated using Luciferase Assay System to confirm presence of tumour. Tumour tissue display high levels of luciferase activity as compared to normal tissue where negligible luciferase expression was detected (Figure 3.4.3B).

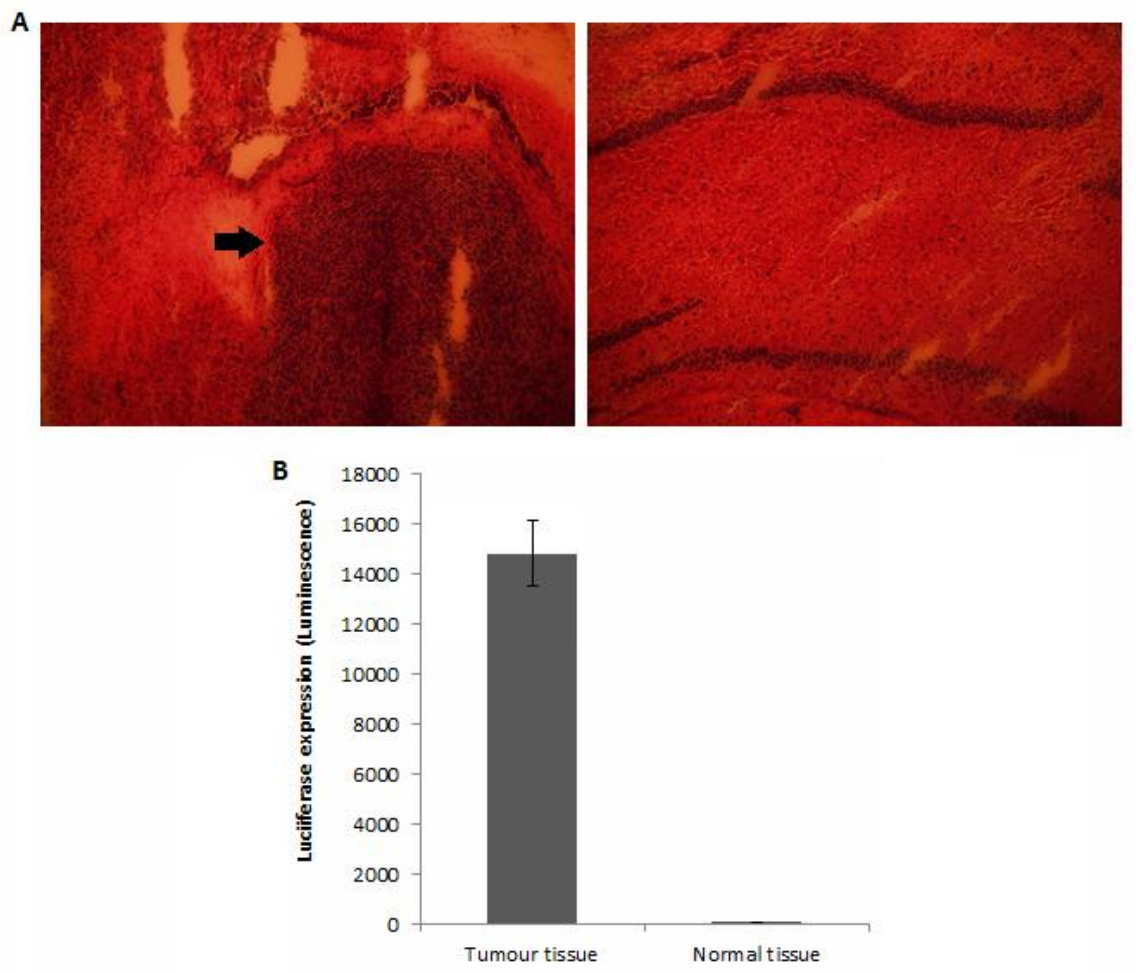

Figure 3.4.3: H&E staining and luciferase quantitation show presence of tumour in mice striatum. Tumour and normal tissue were stained with Haematoxylin and Eosin to study the tissue composition, structure and integrity (n = 2) (A). Tumour tissue lacks tissue integrity mainly attributed to tumour expansion indicated by the arrow. Normal tissue displayed intact tissue integrity. Luciferase quantitation validates tumour presence in mice, since tumour tissue display high levels of luciferase activity compared to normal tissue (B). The values are mean (n = 2).

3.4.4 Hsp90α gene expression and Akt kinase activity in mice treated with sihsp90α/Tat complexes and 17-AAG

The *hsp90α* gene expression in tumour tissue specimens was quantitated by qRT-PCR to determine whether the dual targeting of Hsp90α using sihsp90α and 17-AAG holds

anti-cancer activity *in vivo*. The tumour mice models (n = 3) treated with sihsp90α/Tat nanoparticles in combination with 17-AAG for 24 h exhibited 73% *hsp90α* knockdown. Mouse bearing tumour (n = 1) treated with siluc/Tat complexes and 17-AAG for 24 h was used as negative control (Figure 3.4.4A). The *hsp90α* expression in tumour tissue was normalised to *GAPDH* expression as well as normal brain tissue within each sample to accurately quantitate gene expression. Tat-mediated sihsp90α delivery induces chemosensitivity to 17-AAG *in vivo* and correlates well with findings *in vitro*. The Akt kinase activity was quantitated using Akt/PKB Kinase Activity Assay to examine the effects of Hsp90α inhibition on Akt activity *in vivo*. In xenograft models, Hsp90α inhibition exhibited 75% reduction in Akt kinase activity compared to the negative control (Figure 3.4.4B). The Akt activity in tumour specimens was normalised to normal brain tissue within each sample to accurately quantitate Akt expression. Furthermore, the qRT-PCR and Akt kinase activity result demonstrates a strong correlation.

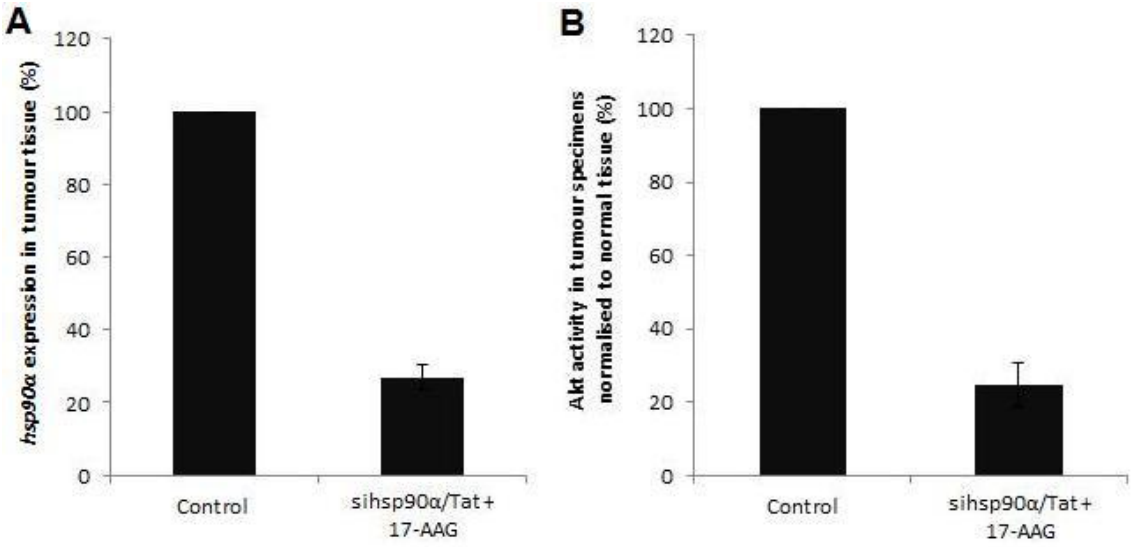

Figure 3.4.4: sihsp90α/Tat complexes in combination with 17-AAG exhibit *hsp90α* gene and Akt kinase activity knockdown. Xenograft models (n = 3) treated with sihsp90α and 17-AAG exhibit *hsp90α* downregulation (A) parallel to reduced Akt activity (B) compared to the negative control (n = 1).

CHAPTER 4

DISCUSSION

4.1 Discussion

Gliomas are generally not curable surgically, thus there is a high demand for effective adjuvant therapies such as chemotherapy and radiotherapy. Temozolomide, a DNA methylating agent commonly used as a chemotherapeutic agent has limitations due to drug resistance mainly attributed to the DNA repair enzyme MGMT which irreversibly transfers the methyl group of O^6-methylguanine (formed by TMZ treatment) in DNA to a cysteine in its active state (Ohba *et al.*, 2010). The molecular chaperone Hsp90 is of major interest as an anticancer drug target (Gaspar *et al.*, 2009; Ohba *et al.*, 2010; Sauvageot *et al.*, 2009; Siegelin *et al.*, 2009). In tumours, the induced Hsp90 expression is responsible for the dependence of tumour cells to multiple signalling pathways where Hsp90 clients play an oncogenic role (Karkoulis *et al.*, 2010). Hsp90 is essential for regulating the conformation, stability and function of several oncogenic client proteins involved in cell cycle regulation, anti-apoptotic mechanisms and oncogenesis (Gaspar *et al.*, 2009). These client proteins contribute extensively to malignant transformation, survival and the metastatic potential of cancer cells. Subsequently, the responsibility of the Hsp90 in tumorigenesis (Eustace *et al.*, 2004) justifies investigating its expression profiles in a set of glioma and control cell lines. There are two main cytoplasmic isoforms of the Hsp90 namely, the inducible Hsp90α and the constitutive Hsp90β (Sreedhar *et al.*, 2004). Hsp90 is mainly a constitutive dimer (αα or ββ), however, monomers and heterodimers also exist. High expression levels of Hsp90α were found in three glioma cell lines, confirmed by qRT-PCR, compared to normal cell line which is in agreement with previous findings from our laboratory (Shervington *et al.*, 2008), and the induced chemosensitivity to Hsp90α inhibition observed in glioblastoma

(Cruickshanks *et al.*, 2010) elucidates the importance of Hsp90α in the survival of gliomas. Hsp90α was therefore considered as an anti-cancer target for glioma therapy in this study.

Initially the *hsp90α* expression levels were quantitated in glioma and normal cell lines to study the expression pattern of *hsp90α*. Results indicated the enhanced *hsp90α* levels in glioma cells compared to the normal cell line. Although, normal proteins have limited requirement for Hsp90 assistance, tumours are highly dependent on molecular chaperone activity to cope with the lethal conditions prevalent in tumours and to regulate mutated and functionally deregulated proteins (Luo *et al.*, 2007). This could be an attribute to the increased transcriptional regulation of *hsp90α* in glioma cell lines. Due to the short blood half-life, increased side effects and modest survival time of the conventional chemotherapy (TMZ), there is an urgent need for novel treatment therapies for malignant gliomas with low side effects. 17-AAG was one of the few Hsp90 inhibitors to enter clinical trials and has since shown positive clinical activity in various types of tumours. An IC_{50} analysis was performed using 17-AAG, whereby a comparison between the Hsp90 inhibitor and the conventional therapeutic drug TMZ in glioma cell lines (Table 3.1.2) showed >1000-fold reduction in IC_{50} dose suggesting Hsp90 as an anti-cancer target in glioma. The high efficacy of Hsp90 inhibitors can be attributed to the higher binding affinity of Hsp90 expressed in tumour cells (100-fold higher) to 17-AAG relative to Hsp90 present in normal cells, that results in client protein degradation and ultimately cell death (Sauvageot *et al.*, 2009). Moreover, the IC_{50} concentration of Hsp90 inhibitors in U87-MG cells was almost half that observed in low grade gliomas (i.e. 1321N1 and GOS-3) which may imply that U87-MG cells contain Hsp90 in an activated, multi-chaperone complex which facilitates malignant progression (Kamal *et al.*, 2003). Therefore a series of experiments were performed

using only the U87-MG glioblastoma cell line in this study. TMZ was found to be cytotoxic to non-tumourigenic cells SVGp12 at concentrations utilized, however, 17-AAG illustrated selectivity towards glioma cells as the toxic effects exhibited on SVGp12 cells were considerably lower.

The present study showed that *hsp90α* levels in glioma cell lines are significantly higher (mean increase of 160-fold) than non-tumourigenic cell line (SVGp12) which agrees with a previous study within our laboratory that revealed the presence of Hsp90α mRNA and protein level at a highly induced state in glioma cell lines compared to normal counterparts (Shervington *et al.*, 2008). In a follow up study, the *hsp90α* was silenced in glioma cell lines using sihsp90α and not only was the *hsp90α* mRNA significantly down-regulated but sihsp90α also induced chemosensitivity to TMZ (Cruickshanks *et al.*, 2010). Silencing *hsp90α* using sihsp90α could thus, be a favorable therapeutic approach due to enhanced target specificity and reduced toxicity. The benzoquinone ansamycin 17-AAG has previously been shown to inhibit tumour growth in human glioma cell lines (Sauvageot *et al.*, 2009). This study investigated anti-tumour effects of Hsp90α inhibition using two approaches, using chemical agent 17-AAG (protein inhibition) and molecular approach using *hsp90α* target-specific siRNA (gene silencing) with the aim of achieving maximum Hsp90α downregulation.

Three sets of pre-designed sihsp90α oligos (as described in Figure 2.3.1) were previously used in our laboratory to downregulate *hsp90α* expression in glioblastoma (Cruickshanks *et al.*, 2010). Although, sihsp90α oligo 3 that targets exon 9 of the *hsp90α* showed significant *hsp90α* downregulation, sihsp90α oligos 2 that targets exon 5 was observed to increase chemosensitivity in glioblastoma after 24 and 48 h, suggesting that proximity of the oligo to the initiation site for translation enhances the

efficiency of RNAi (Cruickshanks *et al.*, 2010). Consequently, sihsp90α oligo 2 was utilized to perform the entire gene silencing experiments in this study.

In order to assess quantitative gene silencing in GBM using sihsp90α and 17-AAG, *hsp90α* and *GAPDH* (control) mRNA expressions were measured using qRT-PCR. Results showed that a combination of 17-AAG and sihsp90α significantly reduced *hsp90α* copy numbers by 99% in GBM after 48 and 72 h. Sequence specific interactions between the siRNA and target mRNA are essential for RNAi functionality, and the target site recognition relies on the molecular mechanism of RNA-RNA interactions (Elbashir *et al.*, 2001). The target-sequence specificity of sihsp90α was unprecedented since the housekeeping gene *GAPDH* mRNA expression was unaffected. To further support our findings, the cytotoxic effects of sihsp90α and 17-AAG on non-tumourigenic cells SVGp12 was investigated. The SVGp12 cell viability was not significantly affected with no more than 5% reduction in viable cells after 48 and 72 h which clearly demonstrates selective tumour cell targeting over normal cells. These findings correspond to a previous study in our laboratory showing that *hsp90α* expression is highly induced in U87-MG as compared to normal counterpart (Shervington *et al.*, 2008). Since *hsp90α* was transcribed at basal level in SVGp12 and other normal brain cell lines as reported previously (Shervington *et al.*, 2008), there was no need for further investigation to be carried out on this cell line.

The concurrent and sequential assays with 17-AAG and sihsp90α were statistically analysed to determine which one of the two assays showed significant effects on cell viability and gene silencing. Paired-Sample T-test carried out between concurrent and sequential assays showed a p-value between 0.227 and 0.177. It was clear that both concurrent and sequential assays with 17-AAG and sihsp90α had a similar effect on cell viability and mRNA down regulation. However, the results demonstrate that the

combination treatment with sihsp90α and 17-AAG had higher efficacy than sihsp90α alone. Subsequently, only the concurrent combinatorial assay was utilized to investigate Hsp90α protein expression and Akt kinase activity.

The transcription of human *hsp90α* gene is regulated by the 5' upstream promoter sequences bearing the heat shock elements (HSEs) known to regulate gene expression of *hsp90α* (Sreedhar *et al.,* 2004). The heat shock factor 1 (HSF1) binds to the HSEs and marks the initiation of *hsp90α* gene transcription. Under normal conditions, HSF1 is bound to cytosolic Hsp90 and Hsp70 and hence avoids transcription of heat shock genes. However, under stress, or upon inhibition of Hsp90, the Hsp90 chaperone refolds partially denatured client proteins which liberates HSF1 consequently resulting in its translocation to the nucleus where it initiates transcription of *hsp90* gene (Kamal *et al.*, 2004). This negative feedback mechanism may be the continued source of Hsp90 in tumour cells treated with 17-AAG or sihsp90α, which may be responsible for tumour survival even after 72 h. In this study, we targeted the inducible isoform *hsp90α* mRNA using sihsp90α and Hsp90 protein using 17-AAG with an aim to achieve maximum Hsp90 inhibition. The results from this study indicate that the induced cytotoxicity observed in glioblastoma U87-MG and not in non-tumourigenic cell line SVGp12, using combination treatment with sihsp90α and17-AAG, may be due to a greater degree of Hsp90 inhibition. The results also indicate that SVGp12 cells are not dependent on Hsp90 for cell growth and survival. Although, the interaction ratios generated reveal that there is no synergistic relationship between sihsp90α treatment and 17-AAG, optimising certain variables could provide additional efficacy on growth inhibition of glioblastomas. For instance, longer incubations with sihsp90α as well as 17-AAG, and using sihsp90α with increasing drug doses could improve the therapeutic value of this combination regimen.

The fundamental role of Hsp90α in tumour invasion and cell cycle has been previously investigated (Eustace *et al.*, 2004). However, altered *hsp90α* expression post 17-AAG treatment has not been studied in glioma. Nevertheless, a study by Clarke *et al.* investigating *hsp90α* gene expression in colon adenocarcinoma cell lines showed that the *hsp90α* expression in HCT116 (human colon cancer cells) following 17-AAG treatment was induced (Clarke *et al.*, 2000). The same treatment on HT29 (human colon cancer grade II cell line) had no influence on *hsp90α* mRNA levels, suggesting that the post-transcriptional regulation of *hsp90α* after 17-AAG treatment was cell line dependent (Clarke *et al.*, 2000). In GBM, 17-AAG was observed to downregulate *hsp90α* mRNA expression after 48 and 72 h which correlates with its cytotoxic effects *in vitro*. Numerous studies have been conducted involving the use of 17-AAG, however, it is still not clear as to whether the Hsp90 affinity binding of 17-AAG is isoform specific or not (Clarke *et al.*, 2000). The present study demonstrates the ability of 17-AAG to inhibit Hsp90α expression and subsequently reduces Akt kinase activity in glioblastoma.

Hsp90 expression in tumours is 2 to 10-fold higher as compared to its basal expression in normal counterparts (Isaacs *et al.*, 2003). In addition to chaperoning mutated and deregulated client proteins, Hsp90 is of critical importance in tumour survival and progression. Theoretically, silencing *hsp90α* gene with sihsp90α should lead to tumour demise. The overall results from this study reveal non-complementarity between the cell viability and qRT-PCR data after sihsp90α treatment. Although, *hsp90α* mRNA expression was reduced by 96%, the cell viability was barely affected at 90%. *hsp90α* gene silencing was effective up to 48 h using sihsp90α, however, sihsp90α vulnerability to metabolism within the cell and its inability to duplicate (McAnuff *et al.*, 2007), ultimately lead to *hsp90α* resurgence after 72 h. In contrast, the Hsp90 protein half-life

of 36 h may suggest that the efficacy of *hsp90α* silencing on cell viability was modest after 48 and 72 h, owing to the downstream regulation of anti-apoptotic clientele by Hsp90 (Basso *et al.*, 2002). The half-life of *hsp90α* mRNA is 6 h under normal conditions but is reduced to 3 h post Hsp90 inhibition using geldanamycin in rat gliosarcoma cells (Chang *et al.*, 2006). This suggested that the translational efficiency of *hsp90α* mRNA (i.e. protein synthesis per mRNA) was high in treated cells owing to the dependence of malignant cells to Hsp90. Thus, it was reasonable to speculate that *hsp90α* mRNA in glioblastomas were more effectively translated which could be responsible for the lack of anti-cancer activity observed post sihsp90α treatment.

The Hsp90α expression after treatment with 17-AAG and sihsp90α were measured by immunocytochemistry. The Hsp90α protein was detected using FITC-conjugated secondary antibodies, taking into consideration the intensity, contrast and sharpness of the image. The Hsp90α protein expression profiles showed a distinct correlation with the *hsp90α* mRNA expression in U87-MG which strongly suggests that the regulation of Hsp90 occurs not only at the post-translational level as proposed by previous observations (Karkoulis *et al.*, 2010), but also under transcriptional control.

The Hsp90 chaperone plays a vital role at maintaining Akt stability (Basso *et al.*, 2002). The involvement of Akt kinase in deregulated signalling pathways which facilitates tumour progression, survival and invasion, has been well documented (Brader & Eccles, 2004). Previous studies have demonstrated severe inhibition of Akt-dependent anti-apoptotic signalling pathways upon the administration of 17-AAG in gastric cancers, urinary bladder cancer and osteosarcoma (Gazitt *et al.*, 2009; Karkoulis *et al.*, 2010; Lang *et al.*, 2007). To determine whether Hsp90α inhibition/silencing disturbed Akt levels in U87-MG, Akt kinase activity was measured using a Akt/PKB Kinase Activity Assay. The present study showed downregulation of Akt kinase levels post 17-AAG

and sihsp90α treatment which decisively contributes to the cytotoxic potencies of 17-AAG and sihsp90α after 48 and 72 h. The decrease in cell viability observed in U87-MG cells may be attributed to the 17-AAG-dependent inhibition of Akt activity in addition to the sihsp90α-mediated *hsp90α* downregulation which counteracts the tumour survival response of *hsp90α* upregulation (Chang *et al.*, 2006), eventually leading to Hsp90 depletion and apoptosis. It has been previously demonstrated that depletion of *hsp90β* by siRNA can induce apoptosis in multiple myeloma (Chatterjee *et al.*, 2007), which may suggest cooperating anti-apoptotic properties for Hsp90α and Hsp90β. In this study, downregulation of Hsp90α with sihsp90α was insufficient in suppressing Akt activity in U87-MG after 72 h, possibly due to the anti-apoptotic role of Hsp90β via association with Bcl-2 leading to caspase inactivation and to cell survival (Cohen-Saidon *et al.*, 2006). In addition, it could be attributed to the inability of siRNA to duplicate, reducing silencing efficacy through cell division (McAnuff *et al.*, 2007). This may suggest why Akt levels recovered after 72 h following sihsp90α treatment.

Although, 17-AAG and sihsp90α triggered Akt degradation, interestingly, the most significant Akt suppression achieved was relatively higher than the corresponding Hsp90α levels. This may suggest that crucial components of the growth and survival signalling pathways, such as the Akt kinase, are not regulated by only Hsp90 chaperone. Indeed, upregulation of Hsp70 following Hsp90 inhibition using 17-AAG has been previously reported in prostate, cervical, and human colon tumours (Clarke *et al.*, 2000; McCollum *et al.*, 2006). Furthermore, a recent proteomic study from our laboratory showed induced Hsp70 levels post 17-AAG exposure in glioblastoma cells (data unpublished). Thus, even though 17-AAG and sihsp90α inhibited Hsp90α levels in GBM, compensatory upregulation of Hsp70 may have proven to exhibit regulatory effects on Akt (Koren, III *et al.*, 2010). The Akt activity was reduced by 2.3-fold with

the dual combination treatment after 72 h despite the Hsp70 compensation. This reduction of Akt activity demonstrates induced chemosensitivity in GBM since Hsp90 binds and protects Akt from dephosphorylation which is responsible for inactivation of Bcl-2 family protein Bad and caspase-9, known to be inducers of the intrinsic apoptosis pathway (Lanneau *et al.*, 2007). Thus, targeting Hsp70 in addition to Hsp90 could be of therapeutic importance for the treatment of glioblastoma.

For the first time a combination of 17-AAG and siRNA targeting *hsp90α* has been shown to significantly suppress GBM growth after 48 and 72 h *in vitro* (Mehta *et al.*, 2011), clearly evident from the reduced Akt activity. This may suggest that mutated proteins in GBM may have enhanced Hsp90α binding affinity and are more sensitive to Hsp90α inhibition (Cruickshanks *et al.*, 2010). Despite its anti-tumour activity in GBM, RNAi efficiency using siRNA is very limited *in vivo*, mainly due to siRNA degradation by nucleases, non-specific immune stimulation and poor cellular uptake (Shim & Kwon, 2010; Boado, 2005; Schiffelers *et al.*, 2004). However, intracellular delivery of biologically active siRNA has been successfully achieved using delivery systems (Han *et al.*, 2010; Kumar *et al.*, 2007). Accordingly, these limitations were addressed by enhancing cellular siRNA uptake, serum stability and pharmacokinetics using cell-penetrating peptides.

Hsp90 has been considered as a vital molecular chaperone for regulating protein maturation and function of its voluminous and highly diverse clientele of cancer-related proteins (Karkoulis *et al.*, 2010). Through this Hsp90 seems to be crucial for malignant transformation, progression and increasing invasive potential of tumour cells (Workman *et al.*, 2007). In glioblastoma, Hsp90 levels are highly induced to support a range of activated oncoproteins and signalling pathways that glioblastomas are dependent on (Collins, 2004). The benzoquinone antibiotic 17-AAG has previously shown anti-

tumour effects in a number of tumour cell lines and in preclinical models mainly attributed to the higher binding affinity of 17-AAG to Hsp90 in tumour cells as compared to the native Hsp90 in normal cells and inducing proteasomal degradation of its client proteins (Sauvageot *et al.*, 2009). The anti-tumour efficacy of 17-AAG and sihsp90α has been shown previously in U87-MG glioblastoma cells *in vitro* (Mehta *et al.*, 2011). Furthermore, Hsp90α, one of the two major isoforms of Hsp90, known to have inducible expression and play an important role in cell cycle progression and apoptosis exhibits high expression at both mRNA and protein levels in glioma cell lines and tissues but not in normal cell lines and tissues (Shervington *et al.*, 2008). This corroborated Hsp90α as an anti-glioma target and inhibition of Hsp90α as an approach to glioma treatment. A study by Cruickshanks *et al.* targeted *hsp90α* by RNAi using siRNA in glioblastoma and demonstrated significant *hsp90α* silencing after 48 h and subsequently inducing chemosensitivity to TMZ in glioblastoma *in vitro* (Cruickshanks *et al.*, 2010). The ability of sihsp90α/Tat complexes combined with 17-AAG to induce Hsp90α gene and protein knockdown and inhibit tumour growth was evaluated *in vitro*.

Efficient delivery of siRNAs to their RNA targets in the cytoplasm is desired for regulating gene expression and the activity of certain proteins. However, the major issue in gene therapy is the poor bioavailability of the negatively charged siRNA. Commonly used transfection systems such as cationic lipids or viruses have several disadvantages; the use of cationic lipids is restricted *in vitro*, and viruses have the tendency to initiate immunogenic responses *in vivo* (Mae & Langel, 2006). Often the complexes formed between the siRNA and the carrier are too large for *in vivo* utilization due to the rapid clearance by phagocytes present in the liver and spleen (Astriab-Fisher *et al.*, 2002). On the other hand, the effectiveness of many delivery systems is compromised by the presence of serum proteins. For efficient translocation of the Tat peptide and a given

cargo into the cell, an appropriate number of arginines are required; hence the optimal number of Tat peptides required for efficient internalisation of sihsp90α by the cells was investigated by gel shift assay (Brooks *et al.*, 2005). The present study evaluated the ability of Tat, Cyt $c^{77\text{-}101}$ and C105Y to form complexes with sihsp90α, enhance its serum stability and transport it through the plasma membrane into the cells. Although, Tat efficiently formed complexes with sihsp90α; Cyt $c^{77\text{-}101}$ and C105Y failed to show complete retardation of sihsp90α as examined by gel shift assay using PAGE. This was confirmed by the upward shift of the band compared to noncomplexed sihsp90α. Furthermore, in addition to a standard incubation time of 30 min at 37°C, Cyt $c^{77\text{-}101}$ and C105Y peptides were incubated with sihsp90α for longer incubations periods of 1 and 2 h, and two-fold the concentration initially used (100-fold peptide molar excess to sihsp90α) to assess their ability to form complexes with sihsp90α. Even though the incubation time and peptide concentration were increased, the ability of Cyt $c^{77\text{-}101}$ and C105Y peptides to form complexes with sihsp90α was unaltered since sihsp90α was not completely retarded. The use of Cyt $c^{77\text{-}101}$ and C105Y peptides for additional analysis was therefore considered redundant and was discontinued from further studies.

A major limitation of siRNA use *in vitro* and *in vivo* is the inability of naked siRNA to translocate through the cell membrane due to both the size of the siRNA molecule (~14 kDa) (Michiue *et al.*, 2009), and the strong anionic charge of the phosphate backbone, and low serum stability owing to rapid degradation by the nucleases (Meade & Dowdy, 2007; Shim & Kwon, 2010). The Tat CPP has previously been used for delivery of oligonucleotides such as siRNA *in vitro* and *in vivo* (Chiu *et al.*, 2004; Endoh *et al.*, 2008; Moschos *et al.*, 2007a). These CPPs have a high density of positively charged amino acids such as arginine and lysine which have been suggested to enhance its internalisation potential by interacting with the anionic surface of the

plasma membrane (Endoh & Ohtsuki, 2009). As described in this study, sihsp90α/Tat complexes were observed to enhance sihsp90α stability significantly in human serum (50%) where sihsp90α integrity was maintained up to 36 h. This could be attributed to the ability of Tat CPP to form macro-complexes with sihsp90α thus covering the siRNA surface with CPPs subsequently reducing susceptibility to serum nucleases. In contrast, aqueous sihsp90α was unstable in human serum and exhibited complete degradation after 6 h which was in agreement with results reported elsewhere (Schiffelers *et al.*, 2004).

Once it was established that sihsp90α/Tat complexes were relatively stable in human serum as compared to aqueous sihsp90α, an LDH leakage assay (LLA) was used. LLA measures the acute membrane disturbance reportedly caused by peptides at high concentrations (El-Andaloussi *et al.*, 2007; Endoh & Ohtsuki, 2009; Hallbrink *et al.*, 2001). In glioblastoma, Tat either alone or complexed with sihsp90α did not display membrane perturbations up to 50-fold peptide molar excess to sihsp90α or 10 μM final concentration when used independently. Tat induced membrane disturbance (~15%) at 100-fold peptide molar excess to sihsp90α or concentration of 20 μM when used independently, the peptide concentrations in this study were accordingly restricted to 1:50 (sihsp90α:Tat ratio) or 10 μM free peptide prevent non-specific interference in the observed gene silencing, since CPPs have been suggested to influence the observed gene silencing when utilised at high concentrations (Lundberg *et al.*, 2007; Moschos *et al.*, 2007a). Interestingly, the non-tumourigenic cells showed negligible LDH leakage at concentrations up to 100-fold peptide molar excess to sihsp90α or 20 μM concentration (free peptide). The LDH leakage measurements for SVGp12 cells from this study complements the acute toxicity profile displayed by Tat peptide in tumour cell lines and in immortalised aortic endothelial cells where no significant LDH leakage was reported

(Hallbrink *et al.*, 2001; Saar *et al.*, 2005). Although, the acute toxicity profiles of free Tat and sihsp90α/Tat complexes did not display any variance in U87-MG or SVGp12 cells, a comparison of the toxicity profiles between the cell lines is difficult due to the lack of a comprehensive study with findings that are consistent because the toxicity of peptides is not only dependent on peptide concentrations and the cargo molecule utilized but also on the different cell lines and cell passages used (El-Andaloussi *et al.*, 2007).

The long term toxicity of Tat was investigated by measuring cell proliferation after 24, 48 and 72 h in both glioblastoma and non-tumourigenic cells. Tat peptide exhibited no long term toxicity at concentrations 3, 6 and 10 μM in U87-MG or SVGp12 cells; however, Tat complexed with sihsp90α significantly reduced cell viability in glioblastoma. This may suggest that Tat efficiently transports sihsp90α into the cells which consequently downregulates *hsp90α* expression resulting in reduced cell viability. On the other hand, it cannot be disputed that cytotoxic effects exhibited could in fact be due to Tat itself, but cargo-dependent. Similar findings have been reported previously whereby the addition of cargo to the Tat peptide induced its toxicity profile *in vitro* (El-Andaloussi *et al.*, 2007). The data from this study implies that Tat uptake is a one-way process resulting in entrapment of the fragment within the cell as free Tat or Tat in complex with sihsp90α induces minimal LDH leakage in either U87-MG or SVGp12 cells (Baker *et al.*, 2007). In contrast, sihsp90α/Tat significantly reduced cell viability in glioblastoma, but not in non-tumourigenic cells. This difference in short- and long-term toxicity of Tat peptide highlights the significance of measuring both the acute membrane disturbance as well as the long-term toxic effects of Tat because the two do not necessarily correlate. The LDH leakage profiles in U87-MG cells demonstrated a slightly higher membrane disturbance exhibited by sihsp90α/Tat

complexes as compared to the free Tat which indicates that strong interaction between peptide and siRNA does not essentially reduce the peptide toxicity as previously reported (Lundberg *et al.*, 2007). This difference further elaborates the disparity shared by these peptides when complexed with siRNA suggesting that the toxicity of peptides is siRNA-dependent.

Moreover, the membrane perturbation effects of Tat were more pronounced in glioblastoma cells as compared to non-tumourigenic cells which may suggest that Tat could possess selectivity towards malignant cell membranes. Indeed, previous reports have demonstrated the inherent selective toxicity of cationic CPPs for the membranes of malignant cells, although the exact mechanism of this anti-tumour activity is not fully understood (Johnstone *et al.*, 2000; Leuschner & Hansel, 2004). Nonetheless, certain features of malignant cell membranes such as varying composition and fluidity, higher transmembrane potential, greater negative charge and increased levels of acidic components on the cell surface have been ascribed as possible reasons for the selectivity of CPPs towards malignant cell membranes (Saar *et al.*, 2005). This could be a possible reason as to why Tat did not influence *hsp90α* gene expression in SVGp12 cells.

In order to investigate whether the ability of the complex formation of siRNA and Tat promotes cellular internalisation, si-FAM/Tat complexes were formed as confirmed by gel shift assay, and the cellular uptake of si-FAM/Tat was quantitated using confocal microscopy taking into consideration the intensity, contrast and sharpness of the image. si-FAM/Tat complexes were internalized by U87-MG cells and SVGp12 cells, however, uptake efficiency in SVGp12 cells was low compared to U87-MG cells at high peptide concentrations. In addition, the cellular localisation profiles of the transfected si-FAM were divergent between the two cell lines. A plausible explanation for this behaviour could be that Tat utilizes different internalisation mechanisms in

different cell lines depending on the hydrophobicity and electrostatic interaction between the arginine residues of the Tat transduction domain and anionic cell membrane through transduction and/or macropinocytosis (Patel *et al.*, 2007; Wadia & Dowdy, 2005). Thus, it is not surprising that Tat has been simply considered to be an opportunistic peptide that interacts with the negative environment of the cell surface, initiating cellular internalisation (Brooks *et al.*, 2005).

The cell plasma membrane is renewed constitutively at an estimated rate of ~2%/min (Kilic *et al.*, 2001; Mellman *et al.*, 1986), hence 50-200% of the cell surface can be predicted to be internalised per hour suggesting that the higher dose-dependent si-FAM uptake efficiency observed in malignant U87-MG cells compared to normal human astrocyte cell line SVGp12, could be due to the specific selectivity of cationic peptides, in this case Tat, towards malignant cell membranes probably to ubiquitously expressed proteoglycans including chondroitin sulfate, dermatan sulfate and heparan sulfate (Mai *et al.*, 2002; Richard *et al.*, 2005; Saar *et al.*, 2005). This interaction between si-FAM /Tat complexes and the negatively charged cell surface proteoglycans may be the first step in cellular internalisation either through transduction or endocytosis, and has previously been implicated in translocation of Tat peptide (Sandgren *et al.*, 2002). Following membrane interaction, vesicle fusion and budding events occur which lead to vesicle formation of the internalised peptide complexes from which they must escape to reach the target sites of their cargo. The si-FAM localisation in SVGp12 cells is mainly cytoplasmic which may suggest that endosomal escape is efficient, attributed mainly to the diffused staining observed since endosomal entrapment of si-FAM causes punctate staining patterns as evidenced by confocal microscopy (Fischer *et al.*, 2004), a result corroborated when inhibition of endosome acidification displayed only punctate staining (Potocky *et al.*, 2003). In U87-MG cells, si-FAM was noted to localise

primarily in the nucleus as well as diffused staining in the cytoplasm. This diffused staining pattern exhibited by si-FAM may be the effect of pH change in the endosomes which may alter Tat conformation subsequently facilitating its escape from the endosomes. However, another conceivable explanation could be that the si-FAM/Tat complexes are degraded within the endosomes and the diffused staining observed is the outcome of the endosomal escape of smaller metabolites with the fluorescent tag (Patel *et al.*, 2007).

The nuclear accumulation of oligonucleotides complexed with CPPs has been suggested to occur through different pathways in different cell models. The si-FAM/Tat complexes would be expected to exceed size limits for free diffusion of macromolecules across the nuclear envelope, thereby requiring active transport mediated by nuclear pore complex (NPC) when accompanied by nuclear localisation signal (NLS) (Patel *et al.*, 2007). Tat peptide, being a derivative of a transcription factor, has the NLS embedded in its sequence which may facilitate active transport of si-FAM/Tat complexes into the nucleus, but the uptake was not high enough to be visualised in SVGp12 cells. In contrast, si-FAM/Tat complexes in rapidly proliferating malignant cells have an extra entry point to the nucleus owing to the nuclear envelop break down during mitosis, which could be accountable for the higher nuclear localisation of the si-FAM in U87-MG cells as compared to normal counterpart. Although evidence suggests that cell fixation can lead to artificial uptake and redistribution of Tat (Baker *et al.*, 2007), optical and biophysical analysis of live fibroblast uptake of the Tat peptide previously reported has essentially confirmed the nuclear penetrating properties of the peptide (Ziegler *et al.*, 2005). Additionally, the differences in the si-FAM localisation pattern observed between the two cell lines and ability of Tat to efficiently deliver sihsp90α with subsequent RNAi activity as well as specific cytotoxicity associated with

sihsp90α/Tat suggest that the localisation of si-FAM/Tat complexes in this study is unlikely to be a fixation-associated artefact.

The ability of Tat to effectively deliver sihsp90α and induce anti-cancer activity *in vitro* was assessed using cell viability assay. To confirm whether the observed tumour inhibition effects were not due to the intrinsic toxicity of Tat, both U87-MG and SVGp12 cells were incubated with increasing concentrations of the peptide and the long-term toxicity was examined. Tat peptide exhibited no long-term toxicity after 24, 48 or 72 h at concentrations up to 10 μM in either of the cell lines used which correlates with data reported elsewhere (El-Andaloussi *et al.*, 2007). This suggests that the short- or long-term toxicity of Tat peptide may not influence the gene silencing potential of its cargo, sihsp90α. However, Tat peptide has been well documented to possess uncharacterised bioactivity (Moschos *et al.*, 2007a), in addition to integral roles of chaperones in refolding of Tat protein following entry into the cell (Patel *et al.*, 2007). It thus seemed reasonable to speculate that Tat may display bioactivity *in vitro* when used at high concentrations. It was for this reason that long-term toxicity analysis was performed after 24, 48 as well as 72 h post treatment. Surprisingly, Tat peptide alone induced *hsp90α* levels in U87-MG cells after 48 and 72 h, however, the mechanism underlying this response is currently unknown. Previous studies have illustrated uncharacterised regulatory activity of Tat on signalling pathways (Fotin-Mleczek *et al.*, 2005), furthermore, the fact that Tat is derived from the DNA binding domain of HIV-1 *trans*-activator protein with high positive charge which at high concentrations has been suggested to directly interfere with the gene transcription (Moschos *et al.*, 2007a), could be a possible reason for this observation.

The sihsp90α/Tat complexes did not exhibit cytotoxic effects after 24 or 72 h, but significantly reduced U87-MG cell viability after 48 h by 12 and 20% at 1:30 and 1:50

sihsp90α:Tat molar ratio, respectively, indicating a dose-dependent response ($p \leq 0.05$). This may suggest that Tat delivers functional sihsp90α since cells transfected with free sihsp90α did not show significant anti-tumour activity. Likewise, the *hsp90α* and *GAPDH* (control) gene expression levels were monitored by performing *q*RT-PCR to assess quantitative gene silencing, whereby the *hsp90α* mRNA expression was significantly reduced by 78, 85 and 86% after 24 h using 15, 30 and 50-fold Tat peptide molar excess to sihsp90α. After 48 and 72 h, the sihsp90α/Tat complexes produced mRNA knockdown but was insignificant at all peptide concentrations used. The cytotoxicity and *q*RT-PCR data do not display complementarity which could be attributed to the vulnerability of the siRNA to metabolism within the cell due to its inability to duplicate (McAnuff *et al.*, 2007); the siRNA integrity in the cells lasts for only 3-5 doubling times, therefore gradually reducing its efficacy through cell division (Kim, 2003), and the Hsp90 protein half-life of 36 h may suggest why sihsp90α/Tat complexes downregulated *hsp90α* but did not induce anti-cancer activity after 24 and 72 h owing to the downstream regulation of anti-apoptotic clientele by Hsp90 (Basso *et al.*, 2002). Tat-mediated *hsp90α* knockdown was only significant after 24 h post treatment despite significant gene knockdown after 48 and 72 h post sihsp90α treatment (Mehta *et al*., 2011). Revisiting the Tat-mediated siRNA delivery where the localisation pattern was predominantly in the nucleus along with diffused cytoplasmic staining in a dose-dependent manner, correlates well with the lower RNAi activity observed in this study indicating that cytoplasmic localisation of sihsp90α is critical for *hsp90α* gene knockdown (Chiu *et al.*, 2004). It should, however, be pointed out that the actual gene silencing efficiency of sihsp90α may be higher than the observed values owing to the biological activity of Tat peptide on *hsp90α* gene expression. The *hsp90α* mRNA downregulation did not correspond with Hsp90α protein expression levels with most

Hsp90α degradation observed after 48 h, however, these observations are consistent with *hsp90α* mRNA and protein expression profiles obtained previously (Mehta *et al*., 2011). In addition, Tat alone at 10 μM concentration did not show significant effects on Hsp90α regulation suggesting that Tat did not affect translational regulation of Hsp90α.

The ability of Tat-delivered sihsp90α to enhance anti-cancer activity of 17-AAG was assessed by measuring the Hsp90α gene and protein expression and cell viability after 24, 48 and 72 h. *hsp90α* gene expression was observed to be significantly reduced in a dose-dependent manner, though *hsp90α* levels gradually recovered after 48 and 72 h. Despite the reclamation of *hsp90α* levels, Hsp90α protein levels were significantly downregulated at 24, 48 and 72 h dose-dependently, which may imply that the gene silencing concomitant to protein inhibition approach applied in this study could be an effective method for downregulation of Hsp90, whose activity is absolutely essential for oncogenic transformation (Brown *et al.*, 2007; Neckers & Workman, 2012). The requirement of Hsp90 chaperone for glioblastoma growth and survival was therefore validated, ascribed mainly to the reduced cell viability after 24, 48 and 72 h subsequent to Hsp90 inhibition. Hsp90α mRNA and protein expression profiles clearly correlates with result from a previous study (Mehta *et al*., 2011), thus implying that the Tat peptide did not significantly influence Hsp90α expression or associated regulatory processes in glioblastoma.

The Akt activity was used to quantitate the extent of Hsp90 inhibition as functional Hsp90 is critical for stability and activity of Akt (Liao & Hung, 2010). Hsp90 inhibition was tightly associated with loss of Akt activity, most likely responsible for the reduced cell viability owing to the role of Akt in anti-apoptotic signalling pathways prevalent in glioblastomas (Sauvageot *et al.*, 2009). Tat peptide alone did not display significant regulatory effects on Akt activity at concentrations up to 10 μM at all time points

examined which corresponds with the cell viability data where no long-term toxicity of the peptides was observed. It is noteworthy to mention that the reduced Akt activity noted at 10 μM peptide concentration could possibly suggest a modulatory role of Tat on Akt kinase since Tat has previously been reported as a regulator of MAP kinase (Moschos *et al.*, 2007a), though this response was not significant and did not influence U87-MG cell viability. Interestingly, sihsp90α/Tat complexes reduced Akt activity after 24 and 48 h but Akt levels were observed to recuperate after 72 h in a dose-dependent manner which correlates with *hsp90α* mRNA expression levels, once again suggesting that cytoplasmic localisation of sihsp90α is crucial for RNAi. Although one cannot rule out the possibility that vital components of the survival signalling pathway, such as the Akt kinase, may be regulated by other chaperones, post Hsp90 inhibition. A combination of Tat delivered sihsp90α and 17-AAG significantly reduced Akt levels especially after 48 and 72 h with subsequent anti-cancer effects in glioblastoma, further confirming the association with Hsp90 is vital for Akt activity in glioblastoma. Although, Hsp90 inhibition significantly reduced glioblastoma growth *in vitro*, persistent Akt levels may suggest a rescindable effect of this treatment. Most kinases have conventionally been considered as Hsp90 clients, however, recent studies have suggested the inducible isoform of Hsp70 (Hsp72) as well as the constitutive variant Hsc70 to influence Akt levels due to the induced Hsp70 levels subsequent to 17-AAG exposure in several tumours including glioblastomas (Koren, III *et al.*, 2010). Therefore, targeting Hsp90 may not be sufficient to cause glioblastoma demise.

The treatment of Tat alone or in complex with sihsp90α did not affect non-tumourigenic cell viability even when used together with 17-AAG at all time points examined. The lack of *hsp90α* expression suggests that Hsp90 in SVGp12 cells is in latent/uncomplexed state along with low transcriptional regulation. The negligible

levels of *hsp90α* mRNA levels quantitated in SVGp12 cells indicates that glioblastomas are more reliant on molecular chaperones for stabilising oncogenic clientele responsible for malignant transformation. Moreover, the dual combination treatment with sihsp90α and 17-AAG, at the doses utilized, may be critical in the clinical setting whereby a frame of dosing can be established such that only glioblastomas are primarily targeted.

The present study focused on inhibiting Hsp90α at both gene and protein levels that simultaneously target several signalling pathways involved in proliferation and survival through proteasomal degradation of its oncogenic client proteins. A combination of Tat-mediated sihsp90α delivery and 17-AAG showed reduced *hsp90α* expression as well as Akt kinase activity *in vivo*. For these experiments, U87-MG stably transfected with the firefly luciferase gene 2 was utilized for two reasons. Firstly, U87-MG-luc2 cells aid in the detection of tumours following tumour implantation into mice. Although, weight loss is an indication of tumour growth in mice glioblastoma models (Blouw *et al.*, 2003), quantification of luciferase in tumour tissue yielded a strong luminescence signal in comparison to the normal brain tissue confirming presence of a tumour *in vivo*. Secondly, the use of U87-MG-luc2 cells allows targeting of luciferase gene using siluc/Tat nanoparticles *in vitro*, and consequently highlights the versatile nature of the Tat-mediated delivery of various siRNA sequences used in this study including sihsp90α, siluc and si-FAM (Section 2.15).

Glioblastomas are at the core of brain tumour therapeutic studies due to several reasons, including limited clinical aid and known oncogene mutations (Aoki *et al.*, 2007). In addition, the intracranial Ommaya reservoir catheters are regularly placed on glioblastoma patients to deliver chemotherapy (Mason, 2008), similar to the stereotaxic delivery approach utilized here which could potentially allow the local intracranial delivery of the therapeutic siRNA. Thus, by means of synthetic RNAi response, the

genetic composition and oncogene addiction of glioblastoma tumours may be exploited to our benefit.

Here, nude mice were utilized as carriers of exogenously introduced human tumour and as a model system that closely simulates human disease. The immunodeficiency trait accommodates the xenografted tumours and permits growth and expansion *in vivo* which would otherwise not be possible in case of immunocompetent mice. However, the use of nude mice models makes it challenging to study the toxic effects that the peptide as well as the drug might exert such as the unwanted immune responses (Coursindel *et al.*, 2012). On a positive note, the small size of the peptide reduces the risk of triggering inflammation responses to certain extent. Whether sihsp90α/Tat complexes and 17-AAG stimulate inflammatory responses in *in vivo* setting requires further investigation.

For gene expression and Akt kinase study, 3 mice were treated with sihsp90α/Tat complexes in combination with 17-AAG and 2 mice (control) were treated with siluc/Tat complexes and 17-AAG, 17 days post tumour implantation. The siRNA:peptide molar ratio of 1:50 was utilized for *in vivo* siRNA delivery that complements the Hsp90α gene knockdown and protein downregulation results *in vitro*, since optimum efficacy was noted at 1:50. Initially, the experimental design included 3 control groups (1. No treatment; 2. 17-AAG alone (80 mg/kg); 3. siluc/Tat nanoparticles + 17-AAG (negative control)) and 3 treatment groups (sihsp90α/Tat complexes at 1, 2.5 and 5 mg/kg + 17-AAG) with three animals per group. However, some animals lost weight considerably after tumour implantation and showed no sign of recovery as seen with other animals with the tumour. These animals (n = 13) were considered redundant and were terminated from this study. As to what actually caused the acute weight loss is still unknown. Dr Kaido Kurrikoff supervised the *in vivo* experiments and has worked

with animal models for over 10 years but could not justify these as yet uncharacterised observations. Due to the unexpected drop of animal numbers to five, the experimental design was re-evaluated to comprise of one control group (n = 2) and one treatment group (n = 3). Over the period of 24 h when the animals were treated with siRNA and 17-AAG, unfortunately another animal died from the control group possibly due to the expanding tumour. The gene expression and Akt kinase activity results presented in this study are preliminary and requires additional repeats in order to validate the results. Nonetheless, the data is encouraging.

Due to the ability to redesign siRNAs complementary to virtually any oncogene mRNA target, synthetic RNAi responses can potentially target numerous pathways to induce tumour specific lethal responses. Target specific knockdown of oncoproteins by RNAi may have added benefit with regards to catalytic inhibition since protein-protein interactions are crucial for signal transduction (Michiue *et al.*, 2009). Likewise, the ability of RNAi to swiftly adapt to the changing genetic composition of tumours confers an extra advantage especially in recurrent tumours where drug resistance has been an issue. Here, Tat-mediated sihsp90α delivery demonstrates the chemosensitizing effect *in vivo* concomitant to reduced Akt kinase activity. In addition, the qRT-PCR and Akt kinase activity results demonstrate a strong correlation which correlates with the *in vitro* studies. Overall, targeting Hsp90α using molecular and chemical approaches may have an anti-tumour potential in the treatment of glioblastomas.

CHAPTER 5

CONCLUSION AND FUTURE WORK

5.1 Conclusion

In this study, the level of *hsp90α* mRNA expression in glioma cell lines was observed to be induced and is consistent with previous studies carried out in our laboratory. A combination therapy utilizing sihsp90α and 17-AAG significantly downregulated Hsp90α mRNA and protein levels in GBM whereby upto 99% and 95.7% knockdown was achieved, respectively. The Akt kinase activity, a major survival kinase, was significantly reduced following Hsp90α inhibition. In contrast, the combination treatment had no significant cytotoxic effect on SVGp12 cell viability and the transcriptional regulation of *hsp90α* was negligible in SVGp12. Given the role of Akt in growth signalling pathways, Hsp90α-dependent Akt downregulation was accompanied by reduced cell viability in glioblastoma. Thus, targeting Hsp90α using sihsp90α and 17-AAG may have a therapeutic prospect in the treatment of GBM ascribed to its tumour-specific activity.

The efficient complex formation between sihsp90α and Tat, as confirmed by a gel shift assay, effectively delivered functional sihsp90α yielding upto 96% *hsp90α* gene silencing in glioblastoma when combined with 17-AAG. The sihsp90α/Tat complexes improved stability of sihsp90α in human serum, although, results suggest uncharacterized bioactivity of Tat peptides on *hsp90α* gene expression in glioblastoma. Treatment with sihsp90α/Tat complexes and 17-AAG significantly reduced the Hsp90α protein level that was associated with loss of Akt activity and subsequent reduction in cell viability in glioblastoma. The same treatment showed no significant impact on non-tumourigenic cell viability with negligible *hsp90α* levels *in vitro* which further validates the dependence of glioblastomas on cancer chaperone Hsp90 for tumour progression and survival. Acute and long-term toxicity assessment revealed no significant intrinsic

toxicity in U87-MG or SVGp12 cells at Tat peptide concentrations used in this study. This novel approach of silencing *hsp90α* using a delivery vehicle concomitant to protein inhibition subsequently inducing chemosensitivity in glioblastoma shows great promise in *in vivo* models.

The effects of Tat-delivered sihsp90α combined with 17-AAG on *hsp90α* expression and the survival kinase Akt was examined in glioblastoma mouse models. The results demonstrated that the combined treatment induced a strong RNAi response concomitant to reducing Akt kinase activity *in vivo*. Although, these results are preliminary and requires further validation, the anti-cancer effects of targeting Hsp90α using Tat-mediated sihsp90α combined with 17-AAG is promising.

The main findings of this study include:

1. combination therapy using a molecular and chemical approach indicating a significant anti-tumour activity resulting in enhanced tumour specificity *in vitro*.
2. peptide based delivery vector Tat effectively transfects multiple siRNA sequences into mammalian cells which is decisive from a clinical perspective.
3. the efficient interaction between the peptide and siRNA improving serum stability of siRNA.
4. combination therapy utilizing sihsp90α and 17-AAG induced *hsp90α* gene knockdown with subsequent downregulation of Akt kinase levels *in vivo*.

5.2 Future Work

The molecular chaperone Hsp90 plays a critical role in glioblastoma tumourigenesis and has been considered as an ideal therapeutic target due to its versatile properties (Elstrand *et al.*, 2012). This study utilized the ansamycin benzoquinone 17-AAG as a protein inhibitor due to its positive clinical activity in adult and paediatric tumours. However, ansamycins present limitations including suboptimal solubility, cumbersome formulations and extensive metabolism (Menezes *et al.*, 2012). Taking this into consideration, further work could be carried out using other Hsp90 inhibitors with improved pharmacologic properties such as NVP-AUY922, NVP-HSP990, IPI-504, IPI-493 and 17-DMAG (Gaspar *et al.*, 2010; Stingl *et al.*, 2012). NVP-AUY922 and NVP-HSP990 are synthetic pyrazole/isoxazole resorcinol class of Hsp90 inhibitors possessing improved solubility, and IPI-504 and IPI-493 are the reduced forms and active metabolites. 17-DMAG has the added benefit of being water soluble, more potent, and has an improved oral bioavailability compared to its predecessor 17-AAG (Kobayashi *et al.*, 2012).

Although sihsp90α produced significant *hsp90α* knockdown *in vitro*, its vulnerability to metabolism within the cell and its inability to duplicate results in a temporary effect (McAnuff *et al.*, 2007). However, several reports have focused on the modification of the siRNA with a view to enhance its activity and stability *in vivo* (Bramsen *et al.*, 2009; Choung *et al.*, 2006; Haringsma *et al.*, 2012; Laursen *et al.*, 2010; Terrazas & Kool, 2009). A 2'-OMe and phosphorothioate substitutions at the 3' end exhibited increased siRNA stability in serum without compromising the knockdown efficiency (Choung *et al.*, 2006). Likewise, the incorporation of unlocked nucleic acid, an acyclic monomer that lack the C2'-C3'-bond of the RNA ribose ring, has been shown to

decrease nucleic acid duplex thermostability, increasing biostability and improving siRNA efficiency both *in vitro* and *in vivo* (Laursen *et al.*, 2010). In addition, a recent study showed that 2'F ribose modification coupled with 5'-end phosphorylation improves RNAi efficiency *in vitro* and *in vivo* (Haringsma *et al.*, 2012). The incorporation of chemical modifications in siRNA sequences could represent an effective strategy in enhancing siRNA stability without compromising the RNAi potency *in vitro* and *in vivo*.

The role of Hsp70 in cell survival pathways and its upregulation in several tumours such as prostate, cervical and colon tumours post Hsp90 inhibition (Mehta *et al.*, 2011), further supported by recent findings from our laboratory whereby Hsp70 levels were induced following 17-AAG treatment in glioblastomas (data unpublished), highlights the importance of understanding the anti-apoptotic role of Hsp90-Hsp70 and its implications in glioma therapy. Work is presently ongoing in our laboratory focusing at downregulating Hsp70 concomitant to Hsp90 using protein inhibitors and RNAi, and assessing its tumour inhibition potential which should enhance our understanding of the complex role played by these chaperones in tumour progression and survival.

A recent study by Andaloussi and co-workers, demonstrated the use of a novel CPP known as PepFect 6 (PF6), to promote robust RNAi response mainly attributed to its ability to facilitate endosomal escape (Andaloussi *et al.*, 2011). PF6-mediated siRNA delivery is not significantly hindered by serum proteins and induces a strong RNAi response *in vivo* without toxic side effects. Since PF6/siRNA complexes showed a strong gene knockdown effect in brain tissue specimens, future work could involve incorporating PF6 peptide along with Tat for systemic delivery of sihsp90α to compare the treatment efficacy and toxicity profiles *in vivo*.

The present study showed that the effects of Tat-delivered sihsp90α and 17-AAG on *hsp90α* knockdown and Akt kinase activity in xenograft models were encouraging. However, in order to validate these results further experimental repeats are required. The experimental design for further work could include 3 control groups (1. No treatment; 2. 17-AAG alone (80 mg/kg); 3. siluc/Tat nanoparticles + 17-AAG (negative control)) and 3 treatment groups (sihsp90α/Tat complexes at 1, 2.5 and 5 mg/kg combined with 17-AAG) with three animals per group. In addition, the toxicity profile of Tat could be investigated to determine whether CPPs really possess therapeutic implications.

CHAPTER 6

REFERENCES

Ali MM, Roe SM, Vaughan CK, Meyer P, Panaretou B, Piper PW, Prodromou C, & Pearl LH (2006). Crystal structure of an Hsp90-nucleotide-p23/Sba1 closed chaperone complex. *Nature* **440**, 1013-1017.

Altschul SF, Gish W, Miller W, Myers EW, & Lipman DJ (1990). Basic local alignment search tool. *J Mol Biol* **215**, 403-410.

Andaloussi SE, Lehto T, Mager I, Rosenthal-Aizman K, Oprea II, Simonson OE, Sork H, Ezzat K, Copolovici DM, Kurrikoff K, Viola JR, Zaghloul EM, Sillard R, Johansson HJ, Said HF, Guterstam P, Suhorutsenko J, Moreno PM, Oskolkov N, Halldin J, Tedebark U, Metspalu A, Lebleu B, Lehtio J, Smith CI, & Langel U (2011). Design of a peptide-based vector, PepFect6, for efficient delivery of siRNA in cell culture and systemically in vivo. *Nucleic Acids Res* **39**, 3972-3987.

Aoki T, Hashimoto N, & Matsutani M (2007). Management of glioblastoma. *Expert Opin Pharmacother* **8**, 3133-3146.

Arthanari Y, Pluen A, Rajendran R, Aojula H, & Demonacos C (2010). Delivery of therapeutic shRNA and siRNA by Tat fusion peptide targeting BCR-ABL fusion gene in Chronic Myeloid Leukemia cells. *J Control Release* **145**, 272-280.

Astriab-Fisher A, Sergueev D, Fisher M, Shaw BR, & Juliano RL (2002). Conjugates of antisense oligonucleotides with the Tat and antennapedia cell-penetrating peptides: effects on cellular uptake, binding to target sequences, and biologic actions. *Pharm Res* **19**, 744-754.

Bagatell R & Whitesell L (2004). Altered Hsp90 function in cancer: a unique therapeutic opportunity. *Mol Cancer Ther* **3**, 1021-1030.

Baker RD, Howl J, & Nicholl ID (2007). A sychnological cell penetrating peptide mimic of p21(WAF1/CIP1) is pro-apoptogenic. *Peptides* **28**, 731-740.

Balducci M, Chiesa S, Diletto B, D'Agostino GR, Mangiola A, Manfrida S, Mantini G, Albanese A, Fiorentino A, Frascino V, De BB, Micciche' F, De RF, Morganti AG, Anile C, & Valentini V (2012). Low-dose fractionated radiotherapy and concomitant chemotherapy in glioblastoma multiforme with poor prognosis: a feasibility study. *Neuro Oncol* **14**, 79-86.

Barber RD, Harmer DW, Coleman RA, & Clark BJ (2005). GAPDH as a housekeeping gene: analysis of GAPDH mRNA expression in a panel of 72 human tissues. *Physiol Genomics* **21**, 389-395.

Basso AD, Solit DB, Chiosis G, Giri B, Tsichlis P, & Rosen N (2002). Akt forms an intracellular complex with heat shock protein 90 (Hsp90) and Cdc37 and is destabilized by inhibitors of Hsp90 function. *J Biol Chem* **277**, 39858-39866.

Billy E, Brondani V, Zhang H, Muller U, & Filipowicz W (2001). Specific interference with gene expression induced by long, double-stranded RNA in mouse embryonal teratocarcinoma cell lines. *Proc Natl Acad Sci U S A* **98**, 14428-14433.

Blouw B, Song H, Tihan T, Bosze J, Ferrara N, Gerber HP, Johnson RS, & Bergers G (2003). The hypoxic response of tumors is dependent on their microenvironment. *Cancer Cell* **4**, 133-146.

Boado RJ (2005). RNA interference and nonviral targeted gene therapy of experimental brain cancer. *NeuroRx* **2**, 139-150.

Bock HC, Puchner MJ, Lohmann F, Schutze M, Koll S, Ketter R, Buchalla R, Rainov N, Kantelhardt SR, Rohde V, & Giese A (2010). First-line treatment of malignant glioma with carmustine implants followed by concomitant radiochemotherapy: a multicenter experience. *Neurosurg Rev* **33**, 441-449.

Brader S & Eccles SA (2004). Phosphoinositide 3-kinase signalling pathways in tumor progression, invasion and angiogenesis. *Tumori* **90**, 2-8.

Bramsen JB, Laursen MB, Nielsen AF, Hansen TB, Bus C, Langkjaer N, Babu BR, Hojland T, Abramov M, Van AA, Odadzic D, Smicius R, Haas J, Andree C, Barman J, Wenska M, Srivastava P, Zhou C, Honcharenko D, Hess S, Muller E, Bobkov GV, Mikhailov SN, Fava E, Meyer TF, Chattopadhyaya J, Zerial M, Engels JW, Herdewijn P, Wengel J, & Kjems J (2009). A large-scale chemical modification screen identifies design rules to generate siRNAs with high activity, high stability and low toxicity. *Nucleic Acids Res* **37**, 2867-2881.

Brooks H, Lebleu B, & Vives E (2005). Tat peptide-mediated cellular delivery: back to basics. *Adv Drug Deliv Rev* **57**, 559-577.

Brown MA, Zhu L, Schmidt C, & Tucker PW (2007). Hsp90--from signal transduction to cell transformation. *Biochem Biophys Res Commun* **363**, 241-246.

Cahill DP, Levine KK, Betensky RA, Codd PJ, Romany CA, Reavie LB, Batchelor TT, Futreal PA, Stratton MR, Curry WT, Iafrate AJ, & Louis DN (2007). Loss of the mismatch repair protein MSH6 in human glioblastomas is associated with tumor progression during temozolomide treatment. *Clin Cancer Res* **13**, 2038-2045.

Cazzalini O, Perucca P, Riva F, Stivala LA, Bianchi L, Vannini V, Ducommun B, & Prosperi E (2003). p21CDKN1A does not interfere with loading of PCNA at DNA replication sites, but inhibits subsequent binding of DNA polymerase delta at the G1/S phase transition. *Cell Cycle* **2**, 596-603.

Chang YS, Lo CW, Sun FC, Chang MD, & Lai YK (2006). Differential expression of Hsp90 isoforms in geldanamycin-treated 9L cells. *Biochem Biophys Res Commun* **344**, 37-44.

Chatterjee M, Jain S, Stuhmer T, Andrulis M, Ungethum U, Kuban RJ, Lorentz H, Bommert K, Topp M, Kramer D, Muller-Hermelink HK, Einsele H, Greiner A, & Bargou RC (2007). STAT3 and MAPK signaling maintain overexpression of heat shock proteins 90alpha and beta in multiple myeloma cells, which critically contribute to tumor-cell survival. *Blood* **109**, 720-728.

Chen X, Kang H, & Zou F (2009). Low concentration of GA activates a preconditioning response in HepG2 cells during oxidative stress-roles of Hsp90 and vimentin. *Cell Stress Chaperones* **14**, 381-389.

Chen Xs, Zhang Y, Wang Js, Li Xy, Cheng Xk, Zhang Y, Wu Nh, & Shen YF (2007). Diverse effects of Stat1 on the regulation of hsp90+¦ gene under heat shock. *J Cell Biochem* **102**, 1059-1066.

Chiu YL, Ali A, Chu CY, Cao H, & Rana TM (2004). Visualizing a correlation between siRNA localization, cellular uptake, and RNAi in living cells. *Chem Biol* **11**, 1165-1175.

Choung S, Kim YJ, Kim S, Park HO, & Choi YC (2006). Chemical modification of siRNAs to improve serum stability without loss of efficacy. *Biochem Biophys Res Commun* **342**, 919-927.

Clarke PA, Hostein I, Banerji U, Stefano FD, Maloney A, Walton M, Judson I, & Workman P (2000). Gene expression profiling of human colon cancer cells following inhibition of signal transduction by 17-allylamino-17-demethoxygeldanamycin, an inhibitor of the hsp90 molecular chaperone. *Oncogene* **19**, 4125-4133.

Cloughesy TF & Mischel PS (2011). New strategies in the molecular targeting of glioblastoma: how do you hit a moving target? *Clin Cancer Res* **17**, 6-11.

Cohen MH, Shen YL, Keegan P, & Pazdur R (2009). FDA drug approval summary: bevacizumab (Avastin) as treatment of recurrent glioblastoma multiforme. *Oncologist* **14**, 1131-1138.

Cohen-Saidon C, Carmi I, Keren A, & Razin E (2006). Antiapoptotic function of Bcl-2 in mast cells is dependent on its association with heat shock protein 90beta. *Blood* **107**, 1413-1420.

Collins VP (2004). Brain tumours: classification and genes. *J Neurol Neurosurg Psychiatry* **75 Suppl 2**, ii2-11.

Conner SD & Schmid SL (2003). Regulated portals of entry into the cell. *Nature* **422**, 37-44.

Console S, Marty C, Garcia-Echeverria C, Schwendener R, & Ballmer-Hofer K (2003). Antennapedia and HIV transactivator of transcription (TAT) "protein transduction

domains" promote endocytosis of high molecular weight cargo upon binding to cell surface glycosaminoglycans. *J Biol Chem* **278**, 35109-35114.

Coursindel T, Jarver P, & Gait MJ (2012). Peptide-based in vivo delivery agents for oligonucleotides and siRNA. *Nucleic Acid Ther* **22**, 71-76.

Crombez L, Aldrian-Herrada G, Konate K, Nguyen QN, McMaster GK, Brasseur R, Heitz F, & Divita G (2009a). A new potent secondary amphipathic cell-penetrating peptide for siRNA delivery into mammalian cells. *Mol Ther* **17**, 95-103.

Crombez L, Morris MC, Dufort S, Aldrian-Herrada G, Nguyen Q, Mc MG, Coll JL, Heitz F, & Divita G (2009b). Targeting cyclin B1 through peptide-based delivery of siRNA prevents tumour growth. *Nucleic Acids Res* **37**, 4559-4569.

Crouch SP, Kozlowski R, Slater KJ, & Fletcher J (1993). The use of ATP bioluminescence as a measure of cell proliferation and cytotoxicity. *J Immunol Methods* **160**, 81-88.

Cruickshanks N, Shervington L, Patel R, Munje C, Thakkar D, & Shervington A (2010). Can hsp90alpha-targeted siRNA combined with TMZ be a future therapy for glioma? *Cancer Investigation* **28**, 608-614.

Curioso WH, Hansen JR, Centurion-Lara A, Garcia PJ, Wolf FM, Fuller S, Holmes KK, & Kimball AM (2008). Evaluation of a joint Bioinformatics and Medical Informatics international course in Peru. *BMC Med Educ* **8**, 1.

de Groot JF & Gilbert MR (2007). New molecular targets in malignant gliomas. *Curr Opin Neurol* **20**, 712-718.

Drin G, Cottin S, Blanc E, Rees AR, & Temsamani J (2003). Studies on the internalization mechanism of cationic cell-penetrating peptides. *J Biol Chem* **278**, 31192-31201.

Duerfeldt AS & Blagg BS (2010). Hsp90 inhibition: elimination of shock and stress. *Bioorg Med Chem Lett* **20**, 4983-4987.

Eguchi A, Meade BR, Chang YC, Fredrickson CT, Willert K, Puri N, & Dowdy SF (2009). Efficient siRNA delivery into primary cells by a peptide transduction domain-dsRNA binding domain fusion protein. *Nat Biotechnol* **27**, 567-571.

Ekeblad S, Sundin A, Janson ET, Welin S, Granberg D, Kindmark H, Dunder K, Kozlovacki G, Orlefors H, Sigurd M, Oberg K, Eriksson B, & Skogseid B (2007). Temozolomide as monotherapy is effective in treatment of advanced malignant neuroendocrine tumors. *Clin Cancer Res* **13**, 2986-2991.

El-Andaloussi S, Holm T, & Langel U (2005). Cell-penetrating peptides: mechanisms and applications. *Curr Pharm Des* **11**, 3597-3611.

El-Andaloussi S, Jarver P, Johansson HJ, & Langel U (2007). Cargo-dependent cytotoxicity and delivery efficacy of cell-penetrating peptides: a comparative study. *Biochem J* **407**, 285-292.

Elbashir SM, Martinez J, Patkaniowska A, Lendeckel W, & Tuschl T (2001). Functional anatomy of siRNAs for mediating efficient RNAi in Drosophila melanogaster embryo lysate. *EMBO J* **20**, 6877-6888.

Elstrand MB, Stavnes HT, Trope CG, & Davidson B (2012). Heat shock protein 90 is a putative therapeutic target in patients with recurrent advanced-stage ovarian carcinoma with serous effusions. *Hum Pathol* **43**, 529-535.

Endoh T & Ohtsuki T (2009). Cellular siRNA delivery using cell-penetrating peptides modified for endosomal escape. *Adv Drug Deliv Rev* **61**, 704-709.

Endoh T, Sisido M, & Ohtsuki T (2008). Cellular siRNA delivery mediated by a cell-permeant RNA-binding protein and photoinduced RNA interference. *Bioconjug Chem* **19**, 1017-1024.

Esteller M, Garcia-Foncillas J, Andion E, Goodman SN, Hidalgo OF, Vanaclocha V, Baylin SB, & Herman JG (2000). Inactivation of the DNA-repair gene MGMT and the clinical response of gliomas to alkylating agents. *N Engl J Med* **343**, 1350-1354.

Eustace BK, Sakurai T, Stewart JK, Yimlamai D, Unger C, Zehetmeier C, Lain B, Torella C, Henning SW, Beste G, Scroggins BT, Neckers L, Ilag LL, & Jay DG (2004). Functional proteomic screens reveal an essential extracellular role for hsp90 alpha in cancer cell invasiveness. *Nat Cell Biol* **6**, 507-514.

Fawell S, Seery J, Daikh Y, Moore C, Chen LL, Pepinsky B, & Barsoum J (1994). Tat-mediated delivery of heterologous proteins into cells. *Proc Natl Acad Sci U S A* **91**, 664-668.

Ferrari A, Pellegrini V, Arcangeli C, Fittipaldi A, Giacca M, & Beltram F (2003). Caveolae-mediated internalization of extracellular HIV-1 tat fusion proteins visualized in real time. *Mol Ther* **8**, 284-294.

Fire A, Xu S, Montgomery MK, Kostas SA, Driver SE, & Mello CC (1998). Potent and specific genetic interference by double-stranded RNA in Caenorhabditis elegans. *Nature* **391**, 806-811.

Fischer R, Kohler K, Fotin-Mleczek M, & Brock R (2004). A stepwise dissection of the intracellular fate of cationic cell-penetrating peptides. *J Biol Chem* **279**, 12625-12635.

Fittipaldi A, Ferrari A, Zoppe M, Arcangeli C, Pellegrini V, Beltram F, & Giacca M (2003). Cell membrane lipid rafts mediate caveolar endocytosis of HIV-1 Tat fusion proteins. *J Biol Chem* **278**, 34141-34149.

Fontana J, Fulton D, Chen Y, Fairchild TA, McCabe TJ, Fujita N, Tsuruo T, & Sessa WC (2002). Domain mapping studies reveal that the M domain of hsp90 serves as a molecular scaffold to regulate Akt-dependent phosphorylation of endothelial nitric oxide synthase and NO release. *Circ Res* **90**, 866-873.

Fotin-Mleczek M, Welte S, Mader O, Duchardt F, Fischer R, Hufnagel H, Scheurich P, & Brock R (2005). Cationic cell-penetrating peptides interfere with TNF signalling by induction of TNF receptor internalization. *J Cell Sci* **118**, 3339-3351.

Friedman HS, Kerby T, & Calvert H (2000). Temozolomide and treatment of malignant glioma. *Clin Cancer Res* **6**, 2585-2597.

Fuchs SM & Raines RT (2004). Pathway for polyarginine entry into mammalian cells. *Biochemistry* **43**, 2438-2444.

Fukushima T, Takeshima H, & Kataoka H (2009). Anti-glioma therapy with temozolomide and status of the DNA-repair gene MGMT. *Anticancer Res* **29**, 4845-4854.

Fukuyo Y, Hunt CR, & Horikoshi N (2010). Geldanamycin and its anti-cancer activities. *Cancer Lett* **290**, 24-35.

Gaspar N, Sharp SY, Eccles SA, Gowan S, Popov S, Jones C, Pearson A, Vassal G, & Workman P (2010). Mechanistic evaluation of the novel HSP90 inhibitor NVP-AUY922 in adult and pediatric glioblastoma. *Mol Cancer Ther* **9**, 1219-1233.

Gaspar N, Sharp SY, Pacey S, Jones C, Walton M, Vassal G, Eccles S, Pearson A, & Workman P (2009). Acquired resistance to 17-allylamino-17-demethoxygeldanamycin (17-AAG, tanespimycin) in glioblastoma cells. *Cancer Res* **69**, 1966-1975.

Gazitt Y, Kolaparthi V, Moncada K, Thomas C, & Freeman J (2009). Targeted therapy of human osteosarcoma with 17AAG or rapamycin: characterization of induced apoptosis and inhibition of mTOR and Akt/MAPK/Wnt pathways. *Int J Oncol* **34**, 551-561.

Gerstein J, Franz K, Steinbach JP, Seifert V, Fraunholz I, Weiss C, & Rodel C (2010). Postoperative radiotherapy and concomitant temozolomide for elderly patients with glioblastoma. *Radiother Oncol* **97**, 382-386.

Goetz MP, Toft DO, Ames MM, & Erlichman C (2003). The Hsp90 chaperone complex as a novel target for cancer therapy. *Ann Oncol* **14**, 1169-1176.

Goncalves E, Kitas E, & Seelig J (2005). Binding of oligoarginine to membrane lipids and heparan sulfate: structural and thermodynamic characterization of a cell-penetrating peptide. *Biochemistry* **44**, 2692-2702.

Gondi CS & Rao JS (2009). Concepts in in vivo siRNA delivery for cancer therapy. *J Cell Physiol* **220**, 285-291.

Grammatikakis N, Vultur A, Ramana CV, Siganou A, Schweinfest CW, Watson DK, & Raptis L (2002). The role of Hsp90N, a new member of the Hsp90 family, in signal transduction and neoplastic transformation. *J Biol Chem* **277**, 8312-8320.

Graner MW & Bigner DD (2005). Chaperone proteins and brain tumors: potential targets and possible therapeutics. *Neuro Oncol* **7**, 260-278.

Grunweller A, Wyszko E, Bieber B, Jahnel R, Erdmann VA, & Kurreck J (2003). Comparison of different antisense strategies in mammalian cells using locked nucleic acids, 2'-O-methyl RNA, phosphorothioates and small interfering RNA. *Nucleic Acids Res* **31**, 3185-3193.

Hallbrink M, Floren A, Elmquist A, Pooga M, Bartfai T, & Langel U (2001). Cargo delivery kinetics of cell-penetrating peptides. *Biochim Biophys Acta* **1515**, 101-109.

Han L, Zhang A, Wang H, Pu P, Jiang X, Kang C, & Chang J (2010). Tat-BMPs-PAMAM conjugates enhance therapeutic effect of small interference RNA on U251 glioma cells in vitro and in vivo. *Hum Gene Ther* **21**, 417-426.

Hanahan D & Weinberg RA (2011). Hallmarks of cancer: the next generation. *Cell* **144**, 646-674.

Harada H, Nakagawa K, Saito M, Kohno S, Nagato S, Furukawa K, Kumon Y, Hamada K, & Ohnishi T (2003). Introduction of wild-type p53 enhances thrombospondin-1 expression in human glioma cells. *Cancer Letters* **191**, 109-119.

Haringsma HJ, Li JJ, Soriano F, Kenski DM, Flanagan WM, & Willingham AT (2012). mRNA knockdown by single strand RNA is improved by chemical modifications. *Nucleic Acids Res* **40**, 4125-4136.

Hegi ME, Diserens AC, Gorlia T, Hamou MF, de TN, Weller M, Kros JM, Hainfellner JA, Mason W, Mariani L, Bromberg JE, Hau P, Mirimanoff RO, Cairncross JG, Janzer RC, & Stupp R (2005). MGMT gene silencing and benefit from temozolomide in glioblastoma. *N Engl J Med* **352**, 997-1003.

Holdhoff M, Supko JG, Gallia GL, Hann CL, Bonekamp D, Ye X, Cao B, Olivi A, & Grossman SA (2010). Intratumoral concentrations of imatinib after oral administration in patients with glioblastoma multiforme. *J Neurooncol* **97**, 241-245.

Holmes JL, Sharp SY, Hobbs S, & Workman P (2008). Silencing of HSP90 Cochaperone AHA1 Expression Decreases Client Protein Activation and Increases Cellular Sensitivity to the HSP90 Inhibitor 17-Allylamino-17-Demethoxygeldanamycin. *Cancer Res* **68**, 1188-1197.

Holsken A, Gebhardt M, Buchfelder M, Fahlbusch R, Blumcke I, & Buslei R (2011). EGFR signaling regulates tumor cell migration in craniopharyngiomas. *Clin Cancer Res* **17**, 4367-4377.

Holzbeierlein JM, Windsperger A, & Vielhauer G (2010). Hsp90: a drug target? *Curr Oncol Rep* **12**, 95-101.

Hubbard J, Erlichman C, Toft DO, Qin R, Stensgard BA, Felten S, Ten EC, Batzel G, Ivy SP, & Haluska P (2011). Phase I study of 17-allylamino-17 demethoxygeldanamycin, gemcitabine and/or cisplatin in patients with refractory solid tumors. *Invest New Drugs* **29**, 473-480.

Isaacs JS, Xu W, & Neckers L (2003). Heat shock protein 90 as a molecular target for cancer therapeutics. *Cancer Cell* **3**, 213-217.

Iyer G, Morris MJ, Rathkopf D, Slovin SF, Steers M, Larson SM, Schwartz LH, Curley T, DeLaCruz A, Ye Q, Heller G, Egorin MJ, Ivy SP, Rosen N, Scher HI, & Solit DB (2012). A phase I trial of docetaxel and pulse-dose 17-allylamino-17-demethoxygeldanamycin in adult patients with solid tumors. *Cancer Chemother Pharmacol* **69**, 1089-1097.

Jaeckle KA, Ballman KV, Giannini C, Schomberg PJ, Ames MM, Reid JM, McGovern RM, Safgren SL, Galanis E, Uhm JH, Brown PD, Hammack JE, Arusell R, Nikcevich DA, Morton RF, Wender DB, & Buckner JC (2010). Phase II NCCTG trial of RT + irinotecan and adjuvant BCNU plus irinotecan for newly diagnosed GBM. *J Neurooncol* **99**, 73-80.

Jarver P & Langel U (2004). The use of cell-penetrating peptides as a tool for gene regulation. *Drug Discov Today* **9**, 395-402.

Jeang KT, Xiao H, & Rich EA (1999). Multifaceted activities of the HIV-1 transactivator of transcription, Tat. *J Biol Chem* **274**, 28837-28840.

Johnstone SA, Gelmon K, Mayer LD, Hancock RE, & Bally MB (2000). In vitro characterization of the anticancer activity of membrane-active cationic peptides. I. Peptide-mediated cytotoxicity and peptide-enhanced cytotoxic activity of doxorubicin against wild-type and p-glycoprotein over-expressing tumor cell lines. *Anticancer Drug Des* **15**, 151-160.

Jones S, Holm T, Mager I, Langel U, & Howl J (2010). Characterization of bioactive cell penetrating peptides from human cytochrome c: protein mimicry and the development of a novel apoptogenic agent. *Chem Biol* **17**, 735-744.

Kamal A, Boehm MF, & Burrows FJ (2004). Therapeutic and diagnostic implications of Hsp90 activation. *Trends Mol Med* **10**, 283-290.

Kamal A, Thao L, Sensintaffar J, Zhang L, Boehm MF, Fritz LC, & Burrows FJ (2003). A high-affinity conformation of Hsp90 confers tumour selectivity on Hsp90 inhibitors. *Nature* **425**, 407-410.

Kang BH, Tavecchio M, Goel HL, Hsieh CC, Garlick DS, Raskett CM, Lian JB, Stein GS, Languino LR, & Altieri DC (2011). Targeted inhibition of mitochondrial Hsp90 suppresses localised and metastatic prostate cancer growth in a genetic mouse model of disease. *Br J Cancer* **104**, 629-634.

Kang TY, Jin T, Elinzano H, & Peereboom D (2008). Irinotecan and bevacizumab in progressive primary brain tumors, an evaluation of efficacy and safety. *J Neurooncol* **89**, 113-118.

Kanzawa T, Germano IM, Komata T, Ito H, Kondo Y, & Kondo S (2004). Role of autophagy in temozolomide-induced cytotoxicity for malignant glioma cells. *Cell Death Differ* **11**, 448-457.

Kaplan IM, Wadia JS, & Dowdy SF (2005). Cationic TAT peptide transduction domain enters cells by macropinocytosis. *J Control Release* **102**, 247-253.

Karagiannis TC & El-Osta A (2005). RNA interference and potential therapeutic applications of short interfering RNAs. *Cancer Gene Ther* **12**, 787-795.

Karkoulis PK, Stravopodis DJ, Margaritis LH, & Voutsinas GE (2010). 17-Allylamino-17-demethoxygeldanamycin induces downregulation of critical Hsp90 protein clients

and results in cell cycle arrest and apoptosis of human urinary bladder cancer cells. *BMC Cancer* **10**, 481.

Khalil IA, Kogure K, Futaki S, & Harashima H (2006). High density of octaarginine stimulates macropinocytosis leading to efficient intracellular trafficking for gene expression. *J Biol Chem* **281**, 3544-3551.

Kilic G, Doctor RB, & Fitz JG (2001). Insulin stimulates membrane conductance in a liver cell line: evidence for insertion of ion channels through a phosphoinositide 3-kinase-dependent mechanism. *J Biol Chem* **276**, 26762-26768.

Kim JB, Urban K, Cochran E, Lee S, Ang A, Rice B, Bata A, Campbell K, Coffee R, Gorodinsky A, Lu Z, Zhou H, Kishimoto TK, & Lassota P (2010a). Non-invasive detection of a small number of bioluminescent cancer cells in vivo. *PLoS One* **5**, e9364.

Kim SS, Garg H, Joshi A, & Manjunath N (2009). Strategies for targeted nonviral delivery of siRNAs in vivo. *Trends Mol Med* **15**, 491-500.

Kim SW, Kim NY, Choi YB, Park SH, Yang JM, & Shin S (2010b). RNA interference in vitro and in vivo using an arginine peptide/siRNA complex system. *J Control Release* **143**, 335-343.

Kim VN (2003). RNA interference in functional genomics and medicine. *J Korean Med Sci* **18**, 309-318.

Kobayashi N, Toyooka S, Soh J, Yamamoto H, Dote H, Kawasaki K, Otani H, Kubo T, Jida M, Ueno T, Ando M, Ogino A, Kiura K, & Miyoshi S (2012). The anti-proliferative effect of heat shock protein 90 inhibitor, 17-DMAG, on non-small-cell

lung cancers being resistant to EGFR tyrosine kinase inhibitor. *Lung Cancer* **75**, 161-166.

Koren J, III, Jinwal UK, Jin Y, O'Leary J, Jones JR, Johnson AG, Blair LJ, Abisambra JF, Chang L, Miyata Y, Cheng AM, Guo J, Cheng JQ, Gestwicki JE, & Dickey CA (2010). Facilitating Akt clearance via manipulation of Hsp70 activity and levels. *J Biol Chem* **285**, 2498-2505.

Kumar P, Wu H, McBride JL, Jung KE, Kim MH, Davidson BL, Lee SK, Shankar P, & Manjunath N (2007). Transvascular delivery of small interfering RNA to the central nervous system. *Nature* **448**, 39-43.

Lai A, Tran A, Nghiemphu PL, Pope WB, Solis OE, Selch M, Filka E, Yong WH, Mischel PS, Liau LM, Phuphanich S, Black K, Peak S, Green RM, Spier CE, Kolevska T, Polikoff J, Fehrenbacher L, Elashoff R, & Cloughesy T (2011). Phase II study of bevacizumab plus temozolomide during and after radiation therapy for patients with newly diagnosed glioblastoma multiforme. *J Clin Oncol* **29**, 142-148.

Lamers LM, Stupp R, van den Bent MJ, Al MJ, Gorlia T, Wasserfallen JB, Mittmann N, Jin SS, Crott R, & Uyl-de Groot CA (2008). Cost-effectiveness of temozolomide for the treatment of newly diagnosed glioblastoma multiforme: a report from the EORTC 26981/22981 NCI-C CE3 Intergroup Study. *Cancer* **112**, 1337-1344.

Lang SA, Klein D, Moser C, Gaumann A, Glockzin G, Dahlke MH, Dietmaier W, Bolder U, Schlitt HJ, Geissler EK, & Stoeltzing O (2007). Inhibition of heat shock protein 90 impairs epidermal growth factor-mediated signaling in gastric cancer cells and reduces tumor growth and vascularization in vivo. *Mol Cancer Ther* **6**, 1123-1132.

Lanneau D, De TA, Maurel S, Didelot C, & Garrido C (2007). Apoptosis versus cell differentiation: role of heat shock proteins HSP90, HSP70 and HSP27. *Prion* **1**, 53-60.

Lanzetta G & Minniti G (2010). Treatment of glioblastoma in elderly patients: an overview of current treatments and future perspective. *Tumori* **96**, 650-658.

Laursen MB, Pakula MM, Gao S, Fluiter K, Mook OR, Baas F, Langklaer N, Wengel SL, Wengel J, Kjems J, & Bramsen JB (2010). Utilization of unlocked nucleic acid (UNA) to enhance siRNA performance in vitro and in vivo. *Mol Biosyst* **6**, 862-870.

Lee SK & Kumar P (2009). Conditional RNAi: towards a silent gene therapy. *Adv Drug Deliv Rev* **61**, 650-664.

Leuschner C & Hansel W (2004). Membrane disrupting lytic peptides for cancer treatments. *Curr Pharm Des* **10**, 2299-2310.

Li Y, Zhang T, Schwartz SJ, & Sun D (2009). New developments in Hsp90 inhibitors as anti-cancer therapeutics: mechanisms, clinical perspective and more potential. *Drug Resist Updat* **12**, 17-27.

Liao Y & Hung MC (2010). Physiological regulation of Akt activity and stability. *Am J Transl Res* **2**, 19-42.

Lindberg S, Copolovici DM, & Langel U (2011). Therapeutic delivery opportunities, obstacles and applications for cell-penetrating peptides. *Ther Deliv* **2**, 71-82.

Linz U (2008). Chemotherapy for glioblastoma: is costly better? *Cancer* **113**, 2617-2622.

Liu HL, Yang HW, Hua MY, & Wei KC (2012). Enhanced therapeutic agent delivery through magnetic resonance imaging-monitored focused ultrasound blood-brain barrier disruption for brain tumor treatment: an overview of the current preclinical status. *Neurosurg Focus* **32**, E4.

Loret EP, Vives E, Ho PS, Rochat H, Van RJ, & Johnson WC, Jr. (1991). Activating region of HIV-1 Tat protein: vacuum UV circular dichroism and energy minimization. *Biochemistry* **30**, 6013-6023.

Lundberg P, El-Andaloussi S, Sutlu T, Johansson H, & Langel U (2007). Delivery of short interfering RNA using endosomolytic cell-penetrating peptides. *FASEB J* **21**, 2664-2671.

Luo W, Dou F, Rodina A, Chip S, Kim J, Zhao Q, Moulick K, Aguirre J, Wu N, Greengard P, & Chiosis G (2007). Roles of heat-shock protein 90 in maintaining and facilitating the neurodegenerative phenotype in tauopathies. *Proc Natl Acad Sci U S A* **104**, 9511-9516.

Mabasa VH & Taylor SC (2006). Re-evaluation of the cost effectiveness of temozolomide for malignant gliomas in British Columbia. *J Oncol Pharm Pract* **12**, 105-111.

Mabeta P & Pepper MS (2009). A comparative study on the anti-angiogenic effects of DNA-damaging and cytoskeletal-disrupting agents. *Angiogenesis* **12**, 81-90.

Mae M & Langel U (2006). Cell-penetrating peptides as vectors for peptide, protein and oligonucleotide delivery. *Curr Opin Pharmacol* **6**, 509-514.

Mahanthappa N (2005). Translating RNA interference into therapies for human disease. *Pharmacogenomics* **6**, 879-883.

Mai JC, Shen H, Watkins SC, Cheng T, & Robbins PD (2002). Efficiency of protein transduction is cell type-dependent and is enhanced by dextran sulfate. *J Biol Chem* **277**, 30208-30218.

Maiolo JR, III, Ottinger EA, & Ferrer M (2004). Specific redistribution of cell-penetrating peptides from endosomes to the cytoplasm and nucleus upon laser illumination. *J Am Chem Soc* **126**, 15376-15377.

Mason WP (2008). Emerging drugs for malignant glioma. *Expert Opin Emerg Drugs* **13**, 81-94.

McAnuff MA, Rettig GR, & Rice KG (2007). Potency of siRNA versus shRNA mediated knockdown in vivo. *J Pharm Sci* **96**, 2922-2930.

McCollum AK, Teneyck CJ, Sauer BM, Toft DO, & Erlichman C (2006). Up-regulation of heat shock protein 27 induces resistance to 17-allylamino-demethoxygeldanamycin through a glutathione-mediated mechanism. *Cancer Res* **66**, 10967-10975.

Meade BR & Dowdy SF (2007). Exogenous siRNA delivery using peptide transduction domains/cell penetrating peptides. *Adv Drug Deliv Rev* **59**, 134-140.

Meade BR & Dowdy SF (2008). Enhancing the cellular uptake of siRNA duplexes following noncovalent packaging with protein transduction domain peptides. *Adv Drug Deliv Rev* **60**, 530-536.

Mellman I, Fuchs R, & Helenius A (1986). Acidification of the endocytic and exocytic pathways. *Annu Rev Biochem* **55**, 663-700.

Menezes DL, Taverna P, Jensen MR, Abrams T, Stuart D, Yu GK, Duhl D, Machajewski T, Sellers WR, Pryer NK, & Gao Z (2012). The novel oral Hsp90 inhibitor NVP-HSP990 exhibits potent and broad-spectrum antitumor activities in vitro and in vivo. *Mol Cancer Ther* **11**, 730-739.

Meng S, Wei B, Xu R, Zhang K, Wang L, Zhang R, & Li J (2009). TAT peptides mediated small interfering RNA delivery to Huh-7 cells and efficiently inhibited hepatitis C virus RNA replication. *Intervirology* **52**, 135-140.

Mercer RW, Tyler MA, Ulasov IV, & Lesniak MS (2009). Targeted therapies for malignant glioma: progress and potential. *BioDrugs* **23**, 25-35.

Meyer P, Prodromou C, Liao C, Hu B, Roe SM, Vaughan CK, Vlasic I, Panaretou B, Piper PW, & Pearl LH (2004). Structural basis for recruitment of the ATPase activator Aha1 to the Hsp90 chaperone machinery. *EMBO J* **23**, 1402-1410.

Michiue H, Eguchi A, Scadeng M, & Dowdy SF (2009). Induction of in vivo synthetic lethal RNAi responses to treat glioblastoma. *Cancer Biol Ther* **8**, 2306-2313.

Michiue H, Tomizawa K, Wei FY, Matsushita M, Lu YF, Ichikawa T, Tamiya T, Date I, & Matsui H (2005). The NH2 terminus of influenza virus hemagglutinin-2 subunit peptides enhances the antitumor potency of polyarginine-mediated p53 protein transduction. *J Biol Chem* **280**, 8285-8289.

Minniti G, Muni R, Lanzetta G, Marchetti P, & Enrici RM (2009). Chemotherapy for glioblastoma: current treatment and future perspectives for cytotoxic and targeted agents. *Anticancer Res* **29**, 5171-5184.

Miyata Y (2005). Hsp90 inhibitor geldanamycin and its derivatives as novel cancer chemotherapeutic agents. *Curr Pharm Des* **11**, 1131-1138.

Modi S, Stopeck AT, Gordon MS, Mendelson D, Solit DB, Bagatell R, Ma W, Wheler J, Rosen N, Norton L, Cropp GF, Johnson RG, Hannah AL, & Hudis CA (2007). Combination of trastuzumab and tanespimycin (17-AAG, KOS-953) is safe and active in trastuzumab-refractory HER-2 overexpressing breast cancer: a phase I dose-escalation study. *J Clin Oncol* **25**, 5410-5417.

Mohammed K & Shervington A (2008). Can CYP1A1 siRNA be an effective treatment for lung cancer? *Cell Mol Biol Lett* **13**, 240-249.

Morris MC, Deshayes S, Heitz F, & Divita G (2008). Cell-penetrating peptides: from molecular mechanisms to therapeutics. *Biol Cell* **100**, 201-217.

Moschos SA, Jones SW, Perry MM, Williams AE, Erjefalt JS, Turner JJ, Barnes PJ, Sproat BS, Gait MJ, & Lindsay MA (2007a). Lung delivery studies using siRNA conjugated to TAT(48-60) and penetratin reveal peptide induced reduction in gene expression and induction of innate immunity. *Bioconjug Chem* **18**, 1450-1459.

Moschos SA, Williams AE, & Lindsay MA (2007b). Cell-penetrating-peptide-mediated siRNA lung delivery. *Biochem Soc Trans* **35**, 807-810.

Mueller S & Chang S (2009). Pediatric brain tumors: current treatment strategies and future therapeutic approaches. *Neurotherapeutics* **6**, 570-586.

Muller L, Schaupp A, Walerych D, Wegele H, & Buchner J (2004). Hsp90 regulates the activity of wild type p53 under physiological and elevated temperatures. *J Biol Chem* **279**, 48846-48854.

Nakase I, Niwa M, Takeuchi T, Sonomura K, Kawabata N, Koike Y, Takehashi M, Tanaka S, Ueda K, Simpson JC, Jones AT, Sugiura Y, & Futaki S (2004). Cellular uptake of arginine-rich peptides: roles for macropinocytosis and actin rearrangement. *Mol Ther* **10**, 1011-1022.

Narayana A, Gruber D, Kunnakkat S, Golfinos JG, Parker E, Raza S, Zagzag D, Eagan P, & Gruber ML (2012). A clinical trial of bevacizumab, temozolomide, and radiation for newly diagnosed glioblastoma. *J Neurosurg* **116**, 341-345.

Neckers L & Workman P (2012). Hsp90 molecular chaperone inhibitors: are we there yet? *Clin Cancer Res* **18**, 64-76.

Ohba S, Hirose Y, Yoshida K, Yazaki T, & Kawase T (2010). Inhibition of 90-kD heat shock protein potentiates the cytotoxicity of chemotherapeutic agents in human glioma cells. *J Neurosurg* **112**, 33-42.

Ohgaki H, Dessen P, Jourde B, Horstmann S, Nishikawa T, Di Patre PL, Burkhard C, Schuler D, Probst-Hensch NM, Maiorka PC, Baeza N, Pisani P, Yonekawa Y, Yasargil MG, Lutolf UM, & Kleihues P (2004). Genetic pathways to glioblastoma: a population-based study. *Cancer Res* **64**, 6892-6899.

Ohgaki H & Kleihues P (2005). Epidemiology and etiology of gliomas. *Acta Neuropathol* **109**, 93-108.

Patel LN, Zaro JL, & Shen WC (2007). Cell penetrating peptides: intracellular pathways and pharmaceutical perspectives. *Pharm Res* **24**, 1977-1992.

Patel MM, Goyal BR, Bhadada SV, Bhatt JS, & Amin AF (2009). Getting into the brain: approaches to enhance brain drug delivery. *CNS Drugs* **23**, 35-58.

Patel R, Shervington L, Lea R, & Shervington A (2008). Epigenetic silencing of telomerase and a non-alkylating agent as a novel therapeutic approach for glioma. *Brain Res* **1188**, 173-181.

Pope WB, Lai A, Mehta R, Kim HJ, Qiao J, Young JR, Xue X, Goldin J, Brown MS, Nghiemphu PL, Tran A, & Cloughesy TF (2011). Apparent diffusion coefficient histogram analysis stratifies progression-free survival in newly diagnosed bevacizumab-treated glioblastoma. *AJNR Am J Neuroradiol* **32**, 882-889.

Porter JR, Fritz CC, & Depew KM (2010). Discovery and development of Hsp90 inhibitors: a promising pathway for cancer therapy. *Curr Opin Chem Biol* **14**, 412-420.

Potocky TB, Menon AK, & Gellman SH (2003). Cytoplasmic and nuclear delivery of a TAT-derived peptide and a beta-peptide after endocytic uptake into HeLa cells. *J Biol Chem* **278**, 50188-50194.

Powers MV & Workman P (2006). Targeting of multiple signalling pathways by heat shock protein 90 molecular chaperone inhibitors. *Endocr Relat Cancer* **13 Suppl 1**, S125-S135.

Powers MV & Workman P (2007). Inhibitors of the heat shock response: biology and pharmacology. *FEBS Lett* **581**, 3758-3769.

Prados MD, Yung WK, Wen PY, Junck L, Cloughesy T, Fink K, Chang S, Robins HI, Dancey J, & Kuhn J (2008). Phase-1 trial of gefitinib and temozolomide in patients with malignant glioma: a North American brain tumor consortium study. *Cancer Chemother Pharmacol* **61**, 1059-1067.

Pratt WB & Toft DO (2003). Regulation of signaling protein function and trafficking by the hsp90/hsp70-based chaperone machinery. *Exp Biol Med (Maywood)* **228**, 111-133.

Premkumar DR, Arnold B, Jane EP, & Pollack IF (2006). Synergistic interaction between 17-AAG and phosphatidylinositol 3-kinase inhibition in human malignant glioma cells. *Molecular Carcinogenesis* **45**, 47-59.

Price JT, Quinn JM, Sims NA, Vieusseux J, Waldeck K, Docherty SE, Myers D, Nakamura A, Waltham MC, Gillespie MT, & Thompson EW (2005). The heat shock protein 90 inhibitor, 17-allylamino-17-demethoxygeldanamycin, enhances osteoclast formation and potentiates bone metastasis of a human breast cancer cell line. *Cancer Res* **65**, 4929-4938.

Prodromou C, Panaretou B, Chohan S, Siligardi G, O'Brien R, Ladbury JE, Roe SM, Piper PW, & Pearl LH (2000). The ATPase cycle of Hsp90 drives a molecular 'clamp' via transient dimerization of the N-terminal domains. *EMBO J* **19**, 4383-4392.

Pu PY, Kang CS, Zhang ZY, Liu XZ, & Jiang H (2006). Downregulation of PIK3CB by siRNA suppresses malignant glioma cell growth in vitro and in vivo. *Technology in Cancer Research & Treatment* **5**, 271-280.

Quiros S, Roos WP, & Kaina B (2011). Rad51 and BRCA2--New molecular targets for sensitizing glioma cells to alkylating anticancer drugs. *PLoS One* **6**, e27183.

Reardon DA, Desjardins A, Peters KB, Gururangan S, Sampson JH, McLendon RE, Herndon JE, Bulusu A, Threatt S, Friedman AH, Vredenburgh JJ, & Friedman HS (2012). Phase II study of carboplatin, irinotecan, and bevacizumab for bevacizumab naive, recurrent glioblastoma. *J Neurooncol* **107**, 155-164.

Rhee M & Davis P (2006). Mechanism of uptake of C105Y, a novel cell-penetrating peptide. *J Biol Chem* **281**, 1233-1240.

Richard JP, Melikov K, Brooks H, Prevot P, Lebleu B, & Chernomordik LV (2005). Cellular uptake of unconjugated TAT peptide involves clathrin-dependent endocytosis and heparan sulfate receptors. *J Biol Chem* **280**, 15300-15306.

Roe SM, Prodromou C, O'Brien R, Ladbury JE, Piper PW, & Pearl LH (1999). Structural basis for inhibition of the Hsp90 molecular chaperone by the antitumor antibiotics radicicol and geldanamycin. *J Med Chem* **42**, 260-266.

Ruben S, Perkins A, Purcell R, Joung K, Sia R, Burghoff R, Haseltine WA, & Rosen CA (1989). Structural and functional characterization of human immunodeficiency virus tat protein. *J Virol* **63**, 1-8.

Rusnati M, Tulipano G, Spillmann D, Tanghetti E, Oreste P, Zoppetti G, Giacca M, & Presta M (1999). Multiple interactions of HIV-I Tat protein with size-defined heparin oligosaccharides. *J Biol Chem* **274**, 28198-28205.

Rusnati M, Tulipano G, Urbinati C, Tanghetti E, Giuliani R, Giacca M, Ciomei M, Corallini A, & Presta M (1998). The basic domain in HIV-1 Tat protein as a target for polysulfonated heparin-mimicking extracellular Tat antagonists. *J Biol Chem* **273**, 16027-16037.

Saar K, Lindgren M, Hansen M, Eiriksdottir E, Jiang Y, Rosenthal-Aizman K, Sassian M, & Langel U (2005). Cell-penetrating peptides: a comparative membrane toxicity study. *Anal Biochem* **345**, 55-65.

Sandgren S, Cheng F, & Belting M (2002). Nuclear targeting of macromolecular polyanions by an HIV-Tat derived peptide. Role for cell-surface proteoglycans. *J Biol Chem* **277**, 38877-38883.

Sansal I & Sellers WR (2004). The biology and clinical relevance of the PTEN tumor suppressor pathway. *J Clin Oncol* **22**, 2954-2963.

Sarin H, Kanevsky AS, Wu H, Brimacombe KR, Fung SH, Sousa AA, Auh S, Wilson CM, Sharma K, Aronova MA, Leapman RD, Griffiths GL, & Hall MD (2008). Effective transvascular delivery of nanoparticles across the blood-brain tumor barrier into malignant glioma cells. *J Transl Med* **6**, 80.

Sarkaria JN, Kitange GJ, James CD, Plummer R, Calvert H, Weller M, & Wick W (2008). Mechanisms of chemoresistance to alkylating agents in malignant glioma. *Clin Cancer Res* **14**, 2900-2908.

Sashital DG & Doudna JA (2010). Structural insights into RNA interference. *Curr Opin Struct Biol* **20**, 90-97.

Sathornsumetee S, Reardon DA, Desjardins A, Quinn JA, Vredenburgh JJ, & Rich JN (2007). Molecularly targeted therapy for malignant glioma. *Cancer* **110**, 13-24.

Sauvageot CM, Kesari S, & Stiles CD (2007). Molecular pathogenesis of adult brain tumors and the role of stem cells. *Neurol Clin* **25**, 891-924, vii.

Sauvageot CME, Weatherbee JL, Kesari S, Winters SE, Barnes J, Dellagatta J, Ramakrishna NR, Stiles CD, Kung ALJ, Kieran MW, & Wen PYC (2009). Efficacy of the HSP90 inhibitor 17-AAG in human glioma cell lines and tumorigenic glioma stem cells. *Neuro-Oncology* **11**, 109-121.

Scheufler C, Brinker A, Bourenkov G, Pegoraro S, Moroder L, Bartunik H, Hartl FU, & Moarefi I (2000). Structure of TPR domain-peptide complexes: critical elements in the assembly of the Hsp70-Hsp90 multichaperone machine. *Cell* **101**, 199-210.

Schiffelers RM, Ansari A, Xu J, Zhou Q, Tang Q, Storm G, Molema G, Lu PY, Scaria PV, & Woodle MC (2004). Cancer siRNA therapy by tumor selective delivery with ligand-targeted sterically stabilized nanoparticle. *Nucleic Acids Res* **32**, e149.

Schulte TW & Neckers LM (1998). The benzoquinone ansamycin 17-allylamino-17-demethoxygeldanamycin binds to HSP90 and shares important biologic activities with geldanamycin. *Cancer Chemother Pharmacol* **42**, 273-279.

Serwer L, Hashizume R, Ozawa T, & James CD (2010). Systemic and local drug delivery for treating diseases of the central nervous system in rodent models. *J Vis Exp*.

Shan G (2010). RNA interference as a gene knockdown technique. *Int J Biochem Cell Biol* **42**, 1243-1251.

Shervington A, Cruickshanks N, Lea R, Roberts G, Dawson T, & Shervington L (2008). Can The Lack of HSP90 Protein in Brain Normal Tissue and Cell Lines, Rationalise it as a Possible Therapeutic Target for Gliomas? *Cancer Investigation* **26**, 900-904.

Shervington A, Cruickshanks N, Wright H, Atkinson-Dell R, Lea R, Roberts G, & Shervington L (2006). Glioma: what is the role of c-Myc, hsp90 and telomerase? *Mol Cell Biochem* **283**, 1-9.

Shervington A, Mohammed K, Patel R, & Lea R (2007). Identification of a novel co-transcription of P450/1A1 with telomerase in A549. *Gene* **388**, 110-116.

Shim MS & Kwon YJ (2010). Efficient and targeted delivery of siRNA in vivo. *FEBS J* **277**, 4814-4827.

Shiraishi T & Nielsen PE (2006). Photochemically enhanced cellular delivery of cell penetrating peptide-PNA conjugates. *FEBS Lett* **580**, 1451-1456.

Siegel D, Yan C, & Ross D (2012). NAD(P)H:quinone oxidoreductase 1 (NQO1) in the sensitivity and resistance to antitumor quinones. *Biochem Pharmacol* **83**, 1033-1040.

Siegelin MD, Habel A, & Gaiser T (2009). 17-AAG sensitized malignant glioma cells to death-receptor mediated apoptosis. *Neurobiology of Disease* **33**, 243-249.

Siomi MC (2009). Short interfering RNA-mediated gene silencing; towards successful application in human patients. *Adv Drug Deliv Rev* **61**, 668-671.

Siu A, Wind JJ, Iorgulescu JB, Chan TA, Yamada Y, & Sherman JH (2012). Radiation necrosis following treatment of high grade glioma--a review of the literature and current understanding. *Acta Neurochir (Wien)* **154**, 191-201.

Sreedhar SA, Kalmar E, Csermely P, & Shen YF (2004). Hsp90 isoforms: functions, expression and clinical importance. *FEBS Letters* **562**, 11-15.

Stingl L, Niewidok N, Muller N, Selle M, Djuzenova CS, & Flentje M (2012). Radiosensitizing effect of the novel Hsp90 inhibitor NVP-AUY922 in human tumour cell lines silenced for Hsp90alpha. *Strahlenther Onkol* **188**, 507-515.

Stupp R & Baumert BG (2003). Promises and controversies in the management of low-grade glioma. *Annals of Oncology* **14**, 1695-1696.

Stupp R, Hegi ME, Mason WP, van den Bent MJ, Taphoorn MJ, Janzer RC, Ludwin SK, Allgeier A, Fisher B, Belanger K, Hau P, Brandes AA, Gijtenbeek J, Marosi C, Vecht CJ, Mokhtari K, Wesseling P, Villa S, Eisenhauer E, Gorlia T, Weller M, Lacombe D, Cairncross JG, & Mirimanoff RO (2009). Effects of radiotherapy with concomitant and adjuvant temozolomide versus radiotherapy alone on survival in glioblastoma in a randomised phase III study: 5-year analysis of the EORTC-NCIC trial. *Lancet Oncol* **10**, 459-466.

Stupp R, Mason WP, van den Bent MJ, Weller M, Fisher B, Taphoorn MJ, Belanger K, Brandes AA, Marosi C, Bogdahn U, Curschmann J, Janzer RC, Ludwin SK, Gorlia T, Allgeier A, Lacombe D, Cairncross JG, Eisenhauer E, & Mirimanoff RO (2005). Radiotherapy plus concomitant and adjuvant temozolomide for glioblastoma. *N Engl J Med* **352**, 987-996.

Suhorutsenko J, Oskolkov N, Arukuusk P, Kurrikoff K, Eriste E, Copolovici DM, & Langel U (2011). Cell-penetrating peptides, PepFects, show no evidence of toxicity and immunogenicity in vitro and in vivo. *Bioconjug Chem* **22**, 2255-2262.

Taipale M, Jarosz DF, & Lindquist S (2010). HSP90 at the hub of protein homeostasis: emerging mechanistic insights. *Nat Rev Mol Cell Biol* **11**, 515-528.

Taldone T, Gozman A, Maharaj R, & Chiosis G (2008). Targeting Hsp90: small-molecule inhibitors and their clinical development. *Curr Opin Pharmacol* **8**, 370-374.

Tallen UG, Truss M, Kunitz F, Wellmann S, Unryn B, Sinn B, Lass U, Krabbe S, Holtkamp N, Hagemeier C, Wurm R, Henze G, Riabowol KT, & von DA (2008). Down-regulation of the inhibitor of growth 1 (ING1) tumor suppressor sensitizes p53-deficient glioblastoma cells to cisplatin-induced cell death. *J Neurooncol* **86**, 23-30.

Terasawa K, Minami M, & Minami Y (2005). Constantly updated knowledge of Hsp90. *J Biochem* **137**, 443-447.

Terrazas M & Kool ET (2009). RNA major groove modifications improve siRNA stability and biological activity. *Nucleic Acids Res* **37**, 346-353.

Thumma SR, Elaimy AL, Daines N, Mackay AR, Lamoreaux WT, Fairbanks RK, Demakas JJ, Cooke BS, & Lee CM (2012). Long-term survival after gamma knife radiosurgery in a case of recurrent glioblastoma multiforme: a case report and review of the literature. *Case Report Med* **2012**, 545492.

Timotheadou E (2011). New agents targeting angiogenesis in glioblastoma. *Chemother Res Pract* **2011**, 878912.

Torchilin VP, Rammohan R, Weissig V, & Levchenko TS (2001). TAT peptide on the surface of liposomes affords their efficient intracellular delivery even at low temperature and in the presence of metabolic inhibitors. *Proc Natl Acad Sci U S A* **98**, 8786-8791.

Tran N, Cairns MJ, Dawes IW, & Arndt GM (2003). Expressing functional siRNAs in mammalian cells using convergent transcription. *BMC Biotechnol* **3**, 21.

Tyagi M, Rusnati M, Presta M, & Giacca M (2001). Internalization of HIV-1 tat requires cell surface heparan sulfate proteoglycans. *J Biol Chem* **276**, 3254-3261.

Uhm JH, Ballman KV, Wu W, Giannini C, Krauss JC, Buckner JC, James CD, Scheithauer BW, Behrens RJ, Flynn PJ, Schaefer PL, Dakhill SR, & Jaeckle KA (2011). Phase II evaluation of gefitinib in patients with newly diagnosed Grade 4 astrocytoma: Mayo/North Central Cancer Treatment Group Study N0074. *Int J Radiat Oncol Biol Phys* **80**, 347-353.

Vives E, Brodin P, & Lebleu B (1997). A truncated HIV-1 Tat protein basic domain rapidly translocates through the plasma membrane and accumulates in the cell nucleus. *J Biol Chem* **272**, 16010-16017.

Voellmy R & Boellmann F (2007). Chaperone regulation of the heat shock protein response. *Adv Exp Med Biol* **594**, 89-99.

Vredenburgh JJ, Desjardins A, Reardon DA, Peters KB, Herndon JE, Marcello J, Kirkpatrick JP, Sampson JH, Bailey L, Threatt S, Friedman AH, Bigner DD, & Friedman HS (2011). The addition of bevacizumab to standard radiation therapy and temozolomide followed by bevacizumab, temozolomide, and irinotecan for newly diagnosed glioblastoma. *Clin Cancer Res* **17**, 4119-4124.

Wadia JS & Dowdy SF (2002). Protein transduction technology. *Curr Opin Biotechnol* **13**, 52-56.

Wadia JS & Dowdy SF (2005). Transmembrane delivery of protein and peptide drugs by TAT-mediated transduction in the treatment of cancer. *Adv Drug Deliv Rev* **57**, 579-596.

Wadia JS, Stan RV, & Dowdy SF (2004). Transducible TAT-HA fusogenic peptide enhances escape of TAT-fusion proteins after lipid raft macropinocytosis. *Nat Med* **10**, 310-315.

Wang SI, Puc J, Li J, Bruce JN, Cairns P, Sidransky D, & Parsons R (1997). Somatic mutations of PTEN in glioblastoma multiforme. *Cancer Res* **57**, 4183-4186.

Weeks KM, Ampe C, Schultz SC, Steitz TA, & Crothers DM (1990). Fragments of the HIV-1 Tat protein specifically bind TAR RNA. *Science* **249**, 1281-1285.

Wender PA, Mitchell DJ, Pattabiraman K, Pelkey ET, Steinman L, & Rothbard JB (2000). The design, synthesis, and evaluation of molecules that enable or enhance cellular uptake: peptoid molecular transporters. *Proc Natl Acad Sci U S A* **97**, 13003-13008.

Wesolowski JR, Rajdev P, & Mukherji SK (2010). Temozolomide (Temodar). *AJNR Am J Neuroradiol* **31**, 1383-1384.

Westerheide SD & Morimoto RI (2005). Heat shock response modulators as therapeutic tools for diseases of protein conformation. *J Biol Chem* **280**, 33097-33100.

Whitesell L & Lindquist SL (2005). HSP90 and the chaperoning of cancer. *Nat Rev Cancer* **5**, 761-772.

Won MS, Im N, Park S, Boovanahalli SK, Jin Y, Jin X, Chung KS, Kang M, Lee K, Park SK, Kim HM, Kwon BM, Lee JJ, & Lee K (2009). A novel benzimidazole analogue inhibits the hypoxia-inducible factor (HIF)-1 pathway. *Biochem Biophys Res Commun* **385**, 16-21.

Wong ML, Kaye AH, & Hovens CM (2007). Targeting malignant glioma survival signalling to improve clinical outcomes. *J Clin Neurosci* **14**, 301-308.

Workman P, Burrows F, Neckers L, & Rosen N (2007). Drugging the cancer chaperone HSP90: combinatorial therapeutic exploitation of oncogene addiction and tumor stress. *Ann N Y Acad Sci* **1113**, 202-216.

Xiao L, Lu X, & Ruden DM (2006). Effectiveness of hsp90 inhibitors as anti-cancer drugs. *Mini Rev Med Chem* **6**, 1137-1143.

Zaro JL & Shen WC (2005). Evidence that membrane transduction of oligoarginine does not require vesicle formation. *Exp Cell Res* **307**, 164-173.

Zeng Y & Cullen BR (2002). RNA interference in human cells is restricted to the cytoplasm. *RNA* **8**, 855-860.

Zhu H, Woolfenden S, Bronson RT, Jaffer ZM, Barluenga S, Winssinger N, Rubenstein AE, Chen R, & Charest A (2010). The novel Hsp90 inhibitor NXD30001 induces tumor regression in a genetically engineered mouse model of glioblastoma multiforme. *Mol Cancer Ther* **9**, 2618-2626.

Ziady AG, Kelley TJ, Milliken E, Ferkol T, & Davis PB (2002). Functional evidence of CFTR gene transfer in nasal epithelium of cystic fibrosis mice in vivo following luminal application of DNA complexes targeted to the serpin-enzyme complex receptor. *Mol Ther* **5**, 413-419.

Ziady AG, Kim J, Colla J, & Davis PB (2004). Defining strategies to extend duration of gene expression from targeted compacted DNA vectors. *Gene Ther* **11**, 1378-1390.

Ziegler A, Nervi P, Durrenberger M, & Seelig J (2005). The cationic cell-penetrating peptide CPP(TAT) derived from the HIV-1 protein TAT is rapidly transported into living fibroblasts: optical, biophysical, and metabolic evidence. *Biochemistry* **44**, 138-148.

Ziegler A & Seelig J (2004). Interaction of the protein transduction domain of HIV-1 TAT with heparan sulfate: binding mechanism and thermodynamic parameters. *Biophys J* **86**, 254-263.

Ziegler DS, Wright RD, Kesari S, Lemieux ME, Tran MA, Jain M, Zawel L, & Kung AL (2008). Resistance of human glioblastoma multiforme cells to growth factor inhibitors is overcome by blockade of inhibitor of apoptosis proteins. *J Clin Invest* **118**, 3109-3122.

Zuehlke A & Johnson JL (2010). Hsp90 and co-chaperones twist the functions of diverse client proteins. *Biopolymers* **93**, 211-217.

CHAPTER 7

APPENDIX

7.1 Supplementary Tables

Table 7.1.1: Media formulation, reagents and chemicals used in cell culture.

Reagents	Formulation	Supplier
Dulbecco's modified eagle's medium	25 mM Hepes 1.0 g/l glucose 1.0 mM sodium bicarbonate 0.011 g/l phenol red	Sigma, UK
Eagle's minimum essential medium	2.2 g/l sodium bicarbonate 1 g/l glucose Earle's salt 0.0053 g/l phenol red	Sigma, UK
Foetal bovine serum (FBS)	Heat inactivated FBS	GIBCO, UK
Non-essential amino acid	100X non-essential amino acid	Sigma, UK
L-glutamine	200 mM L-glutamine	Sigma, UK
Phosphate buffer saline 0.1 M	8 g/l Sodium chloride 0.2 g/l Potassium chloride	Sigma, UK
Trypsin EDTA	0.25%, 2.5 g Porcine trypsin 0.2 g EDTA in 4Na per liter of Hanks' balanced salt solution with phenol red	Sigma, UK
Dimethyl sulfoxide (DMSO)	DMSO 99.5%	Sigma, UK
Trypan blue (0.4%)	0.81% Sodium chloride 0.06% Potassium phosphate dibasic	Sigma UK

Table 7.1.2: A list of reagents and buffers provided with the mRNA isolation kit (Roche Applied Science, UK).

Reagent	Components
Lysis Buffer	0.1 M Tris buffer, 0.3 M LiCl, 10 mM EDTA, 1% lithium dodecylsulfate, 5mM DTT (dithiothreitol), pH 7.5
Washing Buffer	10 mM Tris buffer, 0.2 M LiCl and 1 mM EDTA, pH 7.5
Streptavidin Magnetic Particles (SMPs)	(10 mg/ml) in 50 mM Hepes, 0.1% bovine serum albumin, 0.1% chloracetamide, 0.01% methylisothiazolone, pH 7.4
Biotin-labelled Oligo$(dT)_{20}$ probe	100 pmol biotin-labelled oligo$(dT)_{20}$ per µl of redistilled water
Double-distilled Water (PCR Grade)	RNAse free
Storage Buffer	10 mM Tris buffer, 0.1% chloracetamide, 0.01% methyliso-thiazolone, pH 7.5

Table 7.1.3: The volume of reagents and buffers used for isolation of mRNA from samples. The shaded column depicts the number of cells used and the volumes of the reagents and buffers used for mRNA isolation in this study.

Number of Cells	**2 x 10^6**
Lysing Buffer	0.5 ml
Volume of SMPs	50 µl (0.5 mg)
Lysing Buffer for preparation of SMPs	70 µl
Biotin-labelled Oligo$(dT)_{20}$	0.5 µl 50 pmol
Washing Buffer	3 x 200 µl
Redistilled Water	10 µl

Table 7.1.4: The composition and quantity of reagents provided with the LightCycler® FastStart DNA Master^{PLUS} SYBR Green I kit. The Enzyme master mix was prepared by transferring 14 µl of enzyme (1a) into vial of reaction mix (1b).

Reagents	**Reagent Compositions**	**Quantity**
LightCycler® FastStart Enzyme (1a)	FastStart *Taq* DNA Polymerase	1 vial
H_2O, PCR Grade	RNase-free H_2O	2 ml
LightCycler® FastStart Reaction Mix SYBR Green (1b)	Reaction buffer, dNTP mix (with dUTP instead of dTTP), SYBR Green I dye and 10 mM $MgCl_2$	3 vials

Table 7.1.5: A list of materials and reagents used for agarose gel electrophoresis in this study.

Reagents	Suppliers	Preparation	Working concentration
Ultrapure agarose	Gibco BRL, UK	0.6-2 g Agarose 30-100 ml TBE (1X). Solubilized by boiling in a microwave for 3-4 min.	2% weight/volume
10X TAE (Ultrapure 10X Tris Acetate EDTA electrophoresis buffer)	Sigma, UK	1 M Trizma base 0.9 M Acetic acid (1X) 0.01 M EDTA Diluted to 1X concentration with distilled water	1X
Alkaline buffer	BDH AnalaR, UK	10 N NaOH 0.5 M EDTA	1X
Gel loading dye	Sigma, UK	0.25% w/v Bromophenol blue 0.25% w/v Xylene cyanole 40% w/v Sucrose Supplied ready for use 4X concentration	1:4 (dye:sample)
100 base pair (bp) molecular marker	Sigma, UK	100 µg supplied ready for use	1 µg/ml
Ethidium bromide 10 mg/tablet	Amresco, UK	10 mg Ethidium bromide in 10 ml distilled water. Diluted to 0.5 µg/ml with distilled water	1:20

Table 7.1.6: The components of the Akt Kinase Activity Assay.

Components	Quantity/Description
PKB Substrate Microtiter Plate	96-well plate
Phosphospecific Substrate Antibody	5 ml (1 µg/ml)
Anti-Rabbit IgG: HRP conjugate	20 µl (1mg/ml)
Antibody Dilution Buffer	10 ml
Kinase Assay Dilution Buffer (KADB)	10 ml
ATP	2 mg, diluted with 2 ml of KADB
Purified recombinant active PKB/Akt	28 µl
Wash Buffer	30 ml
TMB Substrate	10 ml
Stop Solution 2	10 ml

7.2 Supplementary Figures

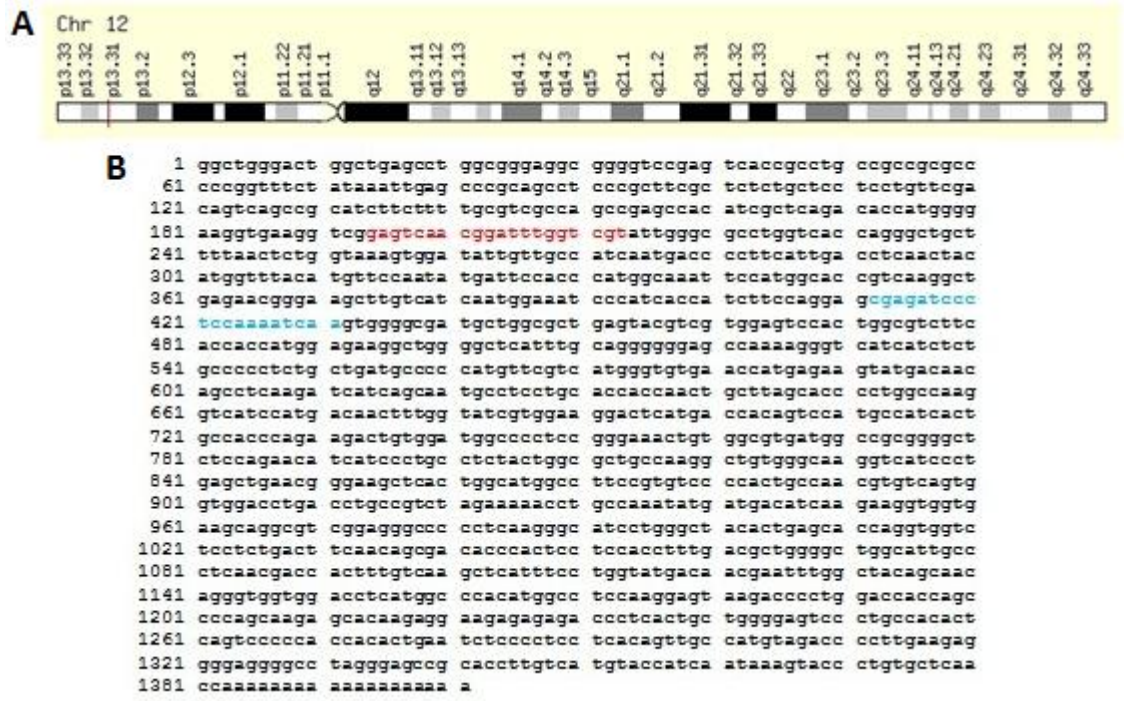

Figure 7.2.1: Gene location of *GAPDH* represented by the red bar (A) and *GAPDH* sequence obtained from NCBI (B). Primer locations have been highlighted in red and blue indicating sense and antisense right primers, respectively.

Figure 7.2.2: Gene location of *hsp90α* represented by the red bar (A) and *hsp90α* sequence obtained from NCBI (B). Primer locations have been highlighted in red and blue indicating sense and antisense primers, respectively.